NUREG/CR-1407
PNL-3345
RU

A Field and Modeling Study of Windblown Particles from a Uranium Mill Tailings Pile

Manuscript Completed: May 1980
Date Published: June 1980

Prepared by L.C. Schwendiman, G.A. Sehmel, T.W. Horst,
C.W. Thomas, R.W. Perkins

Pacific Northwest Laboratory
Richland, WA 99352

**Prepared for Division of Safeguards, Fuel Cycle and Environmental Research
Office of Nuclear Regulatory Research
U.S. Nuclear Regulatory Commission
Washington, D.C. 20555
NRC FIN No. B2095-9**

ACKNOWLEDGMENTS

This study was made possible only through the cooperation of management and other personnel of the three uranium mills in the Ambrosia Lake District of New Mexico. They provided us with unlimited access to their property and on occasion furnished us equipment and storage facilities. These services and access are greatly appreciated.

The NRC project manager at the initiation of the study was Dr. Harry H. Landon; more recently Ms. Laura Santos has been the project manager. Both have been most helpful in supporting this work through suggestions, reviews, and responses to our requests for equipment funds and support. We thank them for their constructive participation in these ways.

We further acknowledge the able assistance of Gregory Long, the editor for the interim report and this final report. He has worked diligently to prepare and perfect the final mats for the reports.

ABSTRACT

An extensive field study whose primary objective was to obtain knowledge and understanding of the nature and quantity of windblown particles from uranium mill tailings piles was conducted in the Ambrosia Lake District of New Mexico.

The following major field tasks were undertaken: determination of physical, chemical, and radioactivity characteristics of mill tailings particles; an investigation of the nature and quantity of tailings particles in soil in the vicinity of tailings piles; and the determination of the nature and flux of particles being transported by wind as a function of wind speed and height. Results of the field study are presented. Particle size distributions and associated radioactivity were measured. Radioactivity relationships showed uranium daughters in mill tailings to be in essential radioactive equilibrium for the carbonate leach process but thorium-230 tends to be leached into the slurry water for the acid process mill tailings. One objective of the study was to relate windblown particle concentrations, fluxes, and particle sizes to wind speed. Hundreds of samples were taken and analyses were performed, but relationships between wind speed, airborne particle sizes and concentrations were found to be vague and inconclusive. A resuspension, deposition, and transport model was developed and applied using site meteorology. Ground deposition patterns predicted were similar to those found.

SUMMARY

A research study was carried out whose primary objective was to obtain knowledge and understanding of the nature and behavior of uranium mill tailings particles when acted upon by wind stresses. The investigation consisted of field and modeling studies designed to develop data and relationships between particle suspension, wind speed and other important variables. The field study was conducted at three uranium mills in the Ambrosia Lake District of New Mexico, but with much of the study centered on an alkaline carbonate leach plant. Two other tailings piles investigated were at plants employing the acid leach processes. Four major tasks comprised the study. Following are brief descriptions with some of the highlight findings:

- Tailings particle characterization. Surface and core samples to 40 cm deep were taken from selected areas of the tailings piles, and the activity densities of uranium-235, uranium-238, lead-210, radium-226 and thorium-230 were determined as a function of depth. Considerable variation with depth was noted. For the alkaline leach plant generally, daughter radionuclides of uranium were in radioactive equilibrium. Acid leach tailings showed some depletion of ^{230}Th due to solubility in the acidic slurry which was confirmed by considerably higher levels in water samples. Particle size distributions and associated radioactivity distributions showed much higher activity density in the 7- to 20-μm fraction than for larger particles, but all size fractions had significant associated radioactivity. Relationships are presented in a series of graphs. A complete spectrum of elements taken through x-ray fluorescence showed uranium, selenium, and molybdenum prominently present above ambient levels.

- Tailings particles in the vicinity of the plant. Soil samples out to about 8 km taken from the surface and in some samples taken from depths showed the presence of tailings particles. Isopleths showed a general pattern similar to the pattern for prevailing winds. Activity density of ^{226}Ra and ^{210}Pb ranged from a few hundred dpm per g near the pile to background levels of a few dpm per g at distances several km from the pile. Estimates of radon release from deposited soil showed this deposited material to contribute radon to the

air roughly 20% that of the tailings pile itself. Association of radionuclides with particle size fractions was determined through particle size separations. Radioactivity with depth in the soil at various distances showed that mixing in the upper several cm had occurred such that roughly exponential decrease of radioactivity with depth occurs. At distances of a few miles, surface and subsurface concentrations reached ambient levels. In flood plain areas north of the tailings pile, solid particle size distributions showed much smaller sizes due to water classification.

- Characterization of airborne particles and measurement of fluxes. Many field experiments were carried out at the alkaline leach plant to characterize particles blowing from the tailings pile as a function of wind speed and height. The sampling array permitted samples to be taken on the pile and at various downwind points when wind was blowing within a given sector and at selected wind speeds. The expected general trend of very low upwind concentrations, increasing concentrations across the pile, and subsequent return to background levels at distances of a few km was found. Concentration changes as a function of wind speed and height up to 15 m showed no consistent pattern, demonstrating the very complex nature of the suspension process. The distribution of radionuclides on airborne particles was determined and showed the activity density of the smaller size fraction to be greater than for larger particles. Fluxes of particles as a function of wind speed could only be roughly bracketed because of wind variations among samples taken from crosswind points in the vicinity of the tailings pile and further downwind. Apparent anomalous concentrations with height from the ground could not be reconciled with present knowledge of wind character near the ground. Downwind concentrations were referenced to guidance levels in 10 CFR 20 with the conclusion that ^{230}Th likely represents the radionuclide of most interest. Elemental composition of airborne particles was reasonably consistent with that reported for the tailings material and showed selenium to be present in considerably greater abundance than in local virgin soil. The great complexity of the system studied emphasized the considerable uncertainties in applying simplistic models to suspension, deposition, and transport. Attention is called to the unrealism in considering only particle mass flux measurements for

modeling when both mass flux and associated radionuclide activity densities vary as a function of wind speed and height.

- Model development. A transport and deposition model was developed and applied to the alkaline leach tailings pile. Actual site meteorology was organized into joint frequency distributions of wind speed, direction, and stability for a 17-mo period. The model utilizes deposition velocities of each particle size and thus calculates net vertical fluxes to the ground as well as air concentrations at ground level. Relationships are presented in a series of curves showing relative air concentrations as a function of wind speed and distance. The model was applied using an actual size distribution of composited airborne particle samples from the alkaline leach tailings pile. A unit source term was input. Resulting vertical fluxes to the ground at various distances from the source were in reasonable agreement with relative surface concentrations measured. The model has not yet been exercised using experimentally derived source and wind-speed data. Additional work is recommended to exercise this and other models with the data available and to determine the sensitivities to the source term description of the resulting downwind airborne concentrations and deposition.

CONTENTS

FIGURES

TABLES

INTRODUCTION

Windblown solid wastes from a uranium mill tailings pile will result in airborne concentrations of particles containing uranium and daughter products, toxic elements in the original ore, and small amounts of residual chemicals used in the process. These particles do not remain airborne indefinitely but are deposited at various distances from the tailings pile. The airborne concentrations and deposition fluxes will be functions of wind speed, direction, distance, particle size, and nature of the surface. The characteristics of the tailings pile particles and their subsequent suspension, transport, and deposition determine the environmental significance whose evaluation is important in determining whether additional control measures should be instituted. Although radon gas emission from tailings has been given considerable attention in environmental assessment, windblown particles have received a rather small investigative effort. One reason for this situation is that usual measures to suppress radon emission will greatly reduce windblown particles; hence, once it is determined that radon release must be mitigated, airborne particles will also be reduced in significance or completely eliminated from consideration as an airborne source.

Active tailings piles provide a field laboratory and an opportunity for examining the influence of important variables on wind suspension, transport, and deposition of particles. The Nuclear Regulatory Commission's Office of Nuclear Regulatory Research recognized the need to determine how well modeling concepts could be used to predict airborne concentrations and surface deposition. Thus, this study was sponsored to develop an understanding of the problem and to determine the nature and quantity of airborne particles from an active tailings pile. Although the emphasis of the study was to be placed on investigating the influencing factors, the field measurements were expected to yield information at specific sites that could be useful in determining the radiological significance of operating a uranium mill over many years.

The study described here was initiated by Pacific Northwest Laboratory (PNL) for the Nuclear Regulatory Commission (NRC), Office of Nuclear Regulatory

Research in late 1976 at an alkaline leach process mill near Grants, New Mexico. The field sampling program was in place in late summer of 1977, and a large number of samples was taken and analyzed in 1978. This earlier work was reported in an interim report, A Field and Modeling Study of Windblown Particles from a Uranium Mill Tailings Pile, NUREG/CR-0629, PNL-2890 (Schwendiman et al. 1979). Much valuable data related to the flux of windblown particles and their deposition to surfaces around the tailings pile were reported in the interim report.

Since the publication of that report, the complexity of the system has become better known and the limitations of the early sampling arrays have been observed. Maintaining reliability of the sampling control system during heavy particle fluxes and severe weather continued to be a challenge.

This report presents the results of continuing experiments in 1979 and examines the application of a resuspension, transport, and deposition model to some of the results.

OBJECTIVES

A prime objective of this study was to achieve an understanding of the variables influencing airborne suspension of tailings particles from an active uranium mill tailings pile. Complete achievement of this objective would be a descriptive model that would permit reasonable estimates of downwind concentrations of airborne particles and ground contamination at various distances and azimuths from the tailings pile as a function of time, and that takes into account site meteorology and climatology. Supplemental objectives needed to fulfill the principal objectives were the following:

- Determine the chemical, radiochemical, and physical characteristics of the surface material on the tailings pile.
- Determine the nature and extent of tailings particles which have been deposited on soil in the vicinity of the mill during its operating life. This information would be used to estimate secondary sources of particle resuspension and radon emission. Model prediction could be compared with field measurement.
- Collect field data relating suspension flux of particles with wind speed and other variables.
- Investigate and apply transport and deposition models that take into account important variables and predict airborne concentration and ground deposition as a function of particle size.
- Make observations of concentrations of radionuclides in the environment and reference these concentrations to background levels or regulatory requirements. (The environmental monitoring aspects of the study, however, were of lesser importance than the other objectives.)

Although much of the experimental field work was focused on a large alkaline carbonate process tailings pile, the initial scope of the work was to include acid leach tailings piles. Some samples of acid leach process particles were collected; measurements were made and are reported in this document. However, insufficient data were collected to permit a good description of

airborne particles from acid leach mills. This study has been truncated before reaching several of the objectives, particularly in relationship to acid leach mill tailings piles.

To avoid repetition, much of the data reported in the 1979 report will not be repeated here. The reader is encouraged to refer to the earlier report for tables, figures, diagrams, and other data developed during 1977 and 1978.

Although intended to be a field study to demonstrate the practical feasibility of relating concentrations of airborne particles to a particular active tailings pile configuration and makeup, it was believed that the relationships might prove valuable generically. However, the early data obtained on airborne particles at the downwind boundary of the tailings pile and on the tailings pile proper proved to be almost intractable insofar as providing consistent relationships between composition and concentrations of airborne particles and the dominating variable, believed to be wind speed. The system under study is extremely complex, and the inability to adequately define the atmospheric processes and interactions at the surface has contributed materially to the lack of definition of relationships in the study.

A different approach was taken for the current phase of the study of airborne constituents from the tailings pile, and as described in the following section, the intention was to avoid some of the problems attending on-pile and close-in sampling.

EXPERIMENTAL STUDY APPROACH

SITE SELECTION AND DESCRIPTION

The Ambrosia Lake District in New Mexico was visited in the fall of 1976, and three tailings piles were investigated. Mill A was using the carbonate (alkaline) leach process, whereas mills B and C were using the acid leach process.

Since an extensive air sampling network was required, available electrical power was needed within a reasonable distance to operate a widespread array of air samplers. The principal site for the study, Site A, was selected not only on the basis of available power but also on the choice of a relatively unobstructed, flat terrain in all directions from the tailings pile. Although ideal conditions were not met by any of the three mill tailings piles, Site A was judged to have the most advantages for the objectives of the study.

An aerial photograph of the tailings pile at Site A is shown in Figure 1. The tailings pile at the time of our field studies was about 600 m wide and 1400 m long. The tailings pile is divided into two approximately equal halves by a north-south tailings dike. The tailings pile is formed by the delivery of water and the spent, finely ground ore to a point on the perimeter of the tailings dike. The slurry of sand and water is then discharged through a truck-mounted centrifugal (cyclone) separator which effects a partial separation of the water containing the finer material and the coarser particles. The slurry containing the finer particles is directed toward the center of the tailings pile. The cyclone separation vehicle is moved around the perimeter of the dike at a rate to keep the dike level with ample height above the water. The wetted surface area varies considerably, but during most of the 1978 to 1979 sampling period, much of the east half of the tailings pile was dry. In the 1979 period about 85% of the west area was dry (Silker and Heasler 1979).

A typical north-south section through the west tailings pile is shown roughly to scale in Figure 2. The crest of the dike is about 25 m above the level terrain. Water evaporates or seeps through the bottom of the tailings pile, some of which is collected in ditches at the toe of the perimeter dike.

FIGURE 1. Aerial Photograph of Mill A and Tailings Pile

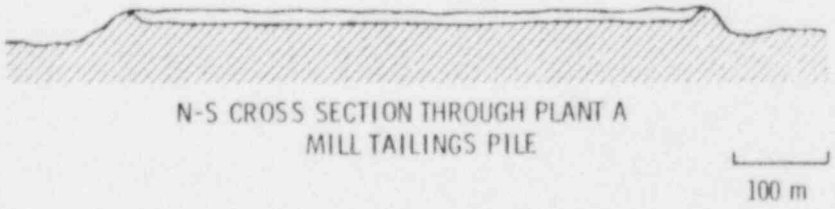

FIGURE 2. North-South Cross Section Through Tailings Pile, Site A

The profile shown in Figure 2, taken generally parallel to the prevailing wind, provides a long, relatively flat surface for suspension of particles. The profile of the dike also provides surfaces that produce flow patterns causing heavy erosion on the upwind site. In our 1978 study we attempted to evaluate the flux of particles from these bluff surfaces but were only partially successful.

The terrain to the north (downwind side) of the tailings pile is virtually flat for ~4 km. The flat terrain transforms into rolling hills and then into much more pronounced topography.

The climatology and meteorology of the site are described in detail in the section of the report dealing with atmospheric modeling.

GENERAL STUDY APPROACH

The field investigation was composed of four separate studies or tasks:

- Task A. Characterization of the physical and radiochemical properties of tailings sand.
- Task B. Determination of the windblown particles from the tailings pile that have been deposited on the soil in the vicinity of the site.
- Task C. Implementation of a study to determine the nature and quantity of windblown particles through an air sampling program designed to evaluate particle flux as a function of wind speed.
- Task D. Investigation and application of atmospheric dispersion and deposition models to the field experimental data.

Each task and its experimental methods, results, and conclusions will be discussed separately.

TASK A. CHARACTERIZATION OF TAILINGS

Principal Investigator: C. W. Thomas

The principal objective of this task was to determine the physical, chemical, and radiochemical nature of the tailings particles. General observations concerning the nature of the tailings at the carbonate leach plant, the experimental methods employed, and the results of these characterization studies are reported in the following sections.

GENERAL OBSERVATIONS

The development of the Site A tailings pile was described earlier. During the milling process the ore is crushed and then rod-milled to reduce the particle sizes to 5% +48 mesh, 38% -200 mesh.[a] After chemical separation of ~95% of the uranium, this finely ground depleted ore is slurried with a large volume of process water to the tailings pile and is discharged to the dike around the tailings pond. The active side of the tailings pile (about one half) stays relatively wet, although the dike and portions of the "beach" area can dry out on one side during the time the tailings slurry is being discharged to the opposite side. The inactive half of the tailings pile dries out to a much greater degree although the central portion remains wet. The slurried water passing through the cyclone separator carries many of the finer particles with it, and these are flushed out onto the "beach" area where they settle as the water seeps into the sand or flows to the center pool.

This continual building of the tailings pile, with the depleted ore sand experiencing various degrees of classification and wetting-drying cycles, results in highly variable surface conditions. Upon drying, residual chemicals in the process slurry water tend to cement the surface layer into a crust in places. Characterization of the deposited tailings sand in terms of the ease with which the particles may resuspend presented a difficulty which could not be completely resolved.

(a) 48 mesh = 297 μm, 200 mesh = 74 μm (1 μm = 10^{-4} cm).

The degree of solubility of uranium and daughter radionuclides also determines which nuclides remain with the sand grains and which move preferentially with the water. The geochemistry involved in the precipitation of uranium and daughter products on the surface of the sand grains results in higher radioactivity per unit weight of the very fine or "slime" fraction of the tailings particles. Properly characterizing the tailings material will require recognition of these many factors that affect the physical and chemical composition of the tailings material.

Other sites visited were acid leach plants with tailings impoundments generally consisting of an earth dam across a small valley. The tailings were slurried out to the tailings impoundment where a large fraction was maintained wet or underwater.

EXPERIMENTAL: MILL TAILINGS CHARACTERIZATION

The characterization of mill tailings was accomplished by: 1) sampling the tailings pile in a manner believed to insure representative samples; 2) determining particle size distributions; and 3) measuring radioactive and nonradioactive elemental constituents in the various particle fractions that dissolved in water by a "heap-leaching" process in the tailings pile.

Sampling locations for the two halves of the tailings pile at Site A are shown in Figure 3. Cores 5 cm and 40 cm in depth were collected as shown in the diagram. Analysis of sections of these cores indicated the degree to which various uranium daughters remained in solution or were held on particles.

The radionuclides of principal concern in the tailings material included ^{234}U, ^{238}U, ^{230}Th, ^{226}Ra, and ^{210}Pb. There was also interest in the trace element concentrations in the tailings material. Some samples were analyzed for potentially toxic materials, and results were compared with ambient soils in the area. All the measurements were made by nondestructive analyses; the techniques employed for these analyses are described in Appendix A.

In addition to the sampling and analysis at tailings pile A, some initial measurements of the material from tailings piles B and C were made. These

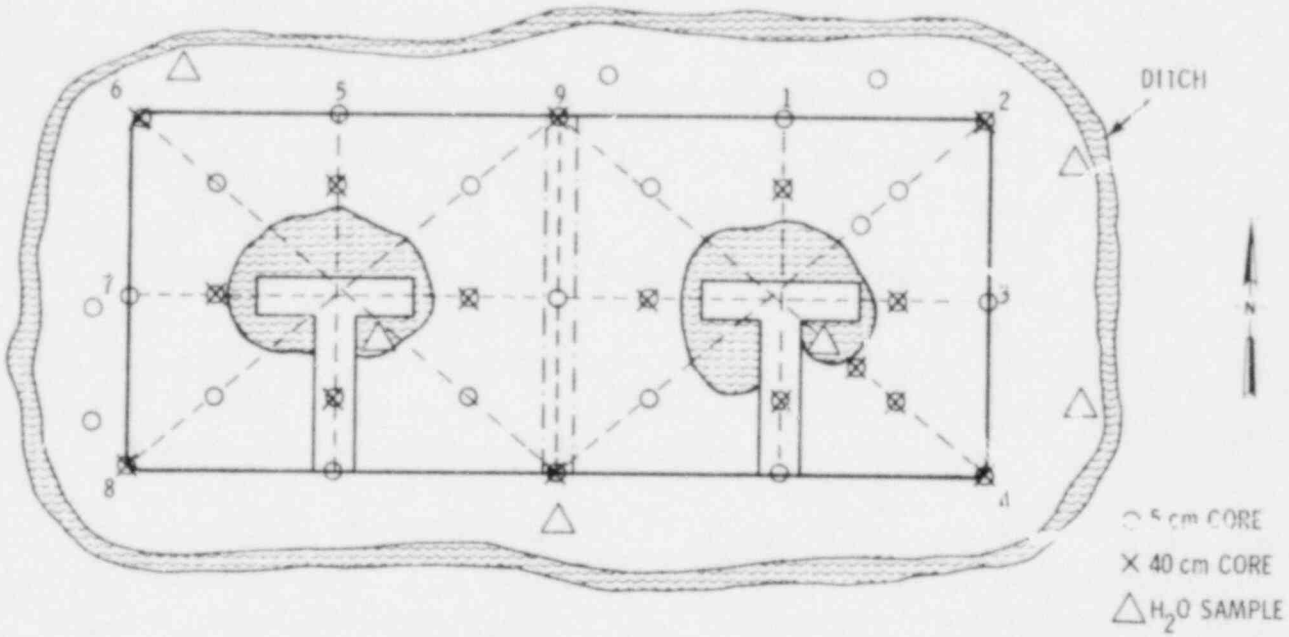

FIGURE 3. Sampling Locations on Tailings Pile A

acid leach tailings were expected to show differences in the uranium daughter ratios which reflected the chemical extraction process differences.

Samples of tailings sand were separated into particle size fractions and the various radionuclides present per unit weight in each particle size were determined.

To provide a sample for such an analysis, 1/2-cm-deep samples from several positions across the tailings pile A were collected. A portion of this collected material was dried in the laboratory under a heat lamp and subsequently pulverized and analyzed using an air elutriation procedure.

The results of initial measurements indicated that smaller particles were associated with larger particles, and the particle size distribution was not likely to be the same as the tailings materials themselves. Therefore, a particle size separation based on wet sieving and sedimentation rates was conducted. A slurry of the tailings material was wet-sieved through sieve sizes down to 44 μm. Smaller size fractions were separated using a sedimentation column, and the Stokes Law equations were applied to obtain size fractions down through less than 1.4 μm.

RESULTS AND DISCUSSION--MILL TAILINGS PARTICLES CHARACTERIZATION

Alkaline Leach Tailings Pile (Pile A)

The percent of material in each size fraction along with its radionuclide composition and the amounts of the radionuclides that were dissolved in the water are shown in Table 1.

To investigate further the distribution of radioactivity as a function of particle size, a second set of measurements was made in which the slurry material that comes to the tailings pile from the mill was collected and fractionated according to particle size as described above. These results are shown in Table 2.

Particle size distributions from these two samplings are shown in Figure 4 plotted as log-probability versus particle diameter. Size distributions frequently follow a normal distribution of the logarithm of diameters and thus show as a straight line on a log-probability plot. The two ways of obtaining

TABLE 1. Particle Size Versus Radionuclide Composition of Tailings from Top 0.5 cm of Tailings Pile A

Particle Size μm	Weight %	dpm/g and (%) activity							
		^{210}Pb	(%)	^{238}U	(%)	^{230}Th	(%)	^{226}Ra	(%)
>250	60.3	319	21.7	38.0	16.9	198	14.4	299	19.9
125-250	7.5	385	3.3	40.4	2.2	269	2.4	370	3.1
53-125	4.2	476	2.2	55.0	1.7	420	2.1	475	2.2
44-53	3.8	429	1.8	50.4	1.4	497	2.3	551	2.3
20-44	7.8	1527	13.5	230	13.2	1825	17.2	1785	15.4
7-20	7.2	2415	19.6	379	20.1	2616	22.8	2222	17.7
1.4-7	9.1	3663	37.6	653	43.8	3514	38.6	3876	39.0
<1.4	0.1	2703	0.3	755	0.6	1208	0.1	2991	0.3
			2.6(a)		15.9(a)		1.6(a)		10.0(a)

(a) Radionuclide radioactivity in the water used for sieving and sedimentation as a % of radioactivity associated with particles

TABLE 2. Particle Size Versus Radionuclide Composition of Tailings in Input Slurry to Tailings Pile A

Particle Size μm	Weight %	dpm/g and (%) activity							
		^{210}Pb	(%)	^{238}U	(%)	^{230}Th	(%)	^{226}Ra	(%)
>250	39.6	229	16.2	94	11.3	148	11.0	166	20.8
125-250	26.0	252	11.7	115	9.1	187	9.1	184	15.1
53-125	7.1	316	4.0	160	3.5	289	3.8	217	4.9
44-53	1.6	345	1.0	224	1.1	345	1.0	214	1.1
20-44	4.0	707	5.1	536	6.5	1053	7.9	364	4.6
7-20	14.5	1900	49.2	1362	59.9	2115	57.6	775	35.5
1.4-7	1.6	3119	8.9	1342	6.5	2448	7.4	2128	10.7
<1.4	0.9	2402	3.9	774	2.1	1269	2.1	2555	7.3
	0.8(a)	368(b)		228(b)		165(b)		826(b)	
	3.6(c)			397(d)		32(d)		693(c)	

(a) Residue from evaporation of slurry.
(b) Soluble radionuclide radioactivity in tailings slurry water.
(c) Soluble salts in water used for sieving and sedimentation.
(d) Soluble radionuclide radioactivity in the water used for sieving and sedimentation

samples gave a median size of greater than 200 μm. (We did not separate through sieving fractions greater than 250 μm and thus were not able to determine accurately the median diameter.) The two size distributions are similar but not identical. Radionuclide activity as a function of particle size is shown in Figure 5.

The sample from the tailings pile surface showed a larger fraction less than 10 μm than did the slurry sample taken from the discharge pipe. A considerably smaller fraction in the less than 1.4-μm range was found in the tailings surface sample than in the slurry sample. The surface tailings sample is more representative of the particles available for resuspension; however, the wet sieving and sedimentation methods would tend to emphasize the fraction in the small size range compared to the dry in situ particles.

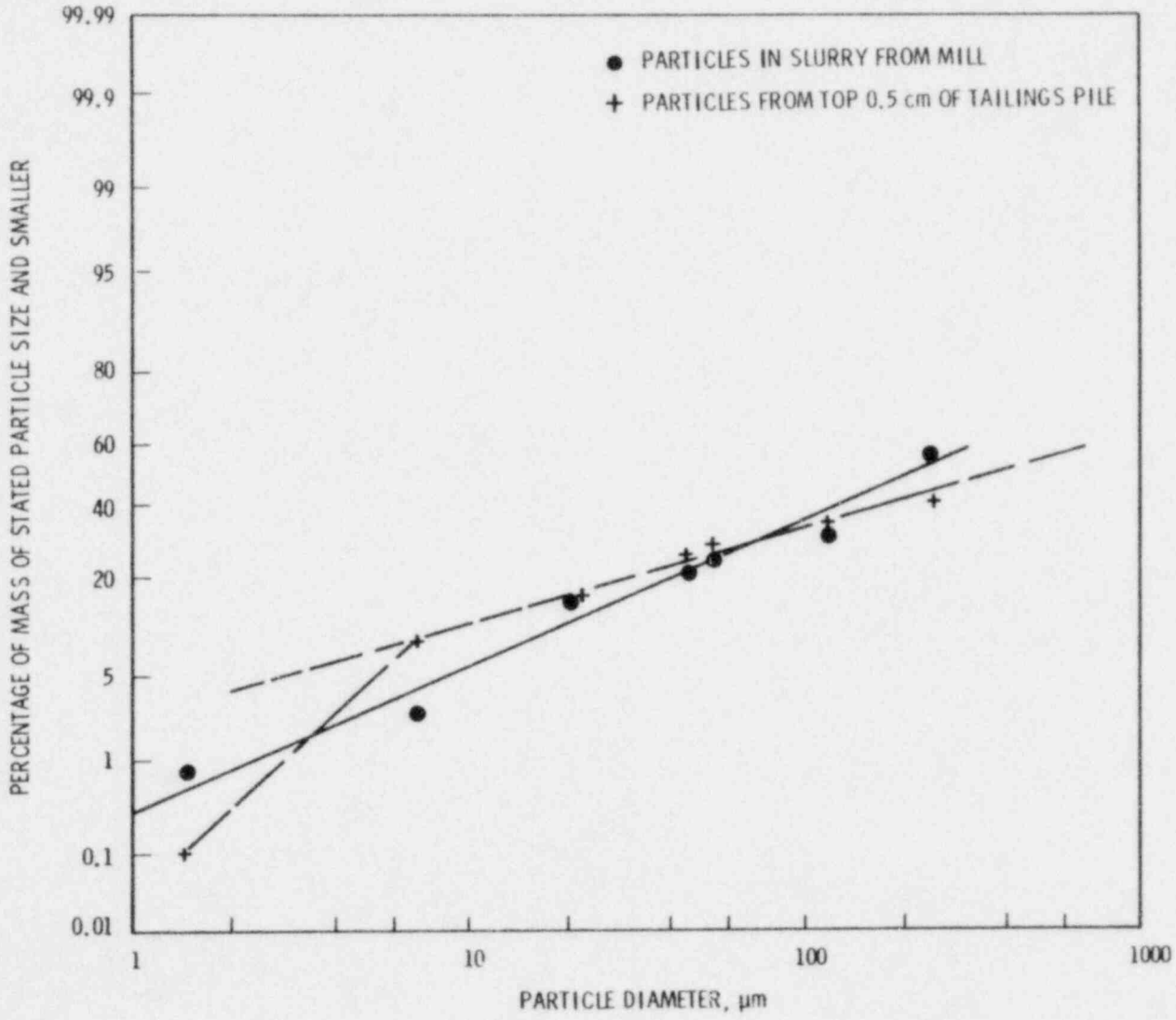

FIGURE 4. Tailings Particle Size Distributions Pile A

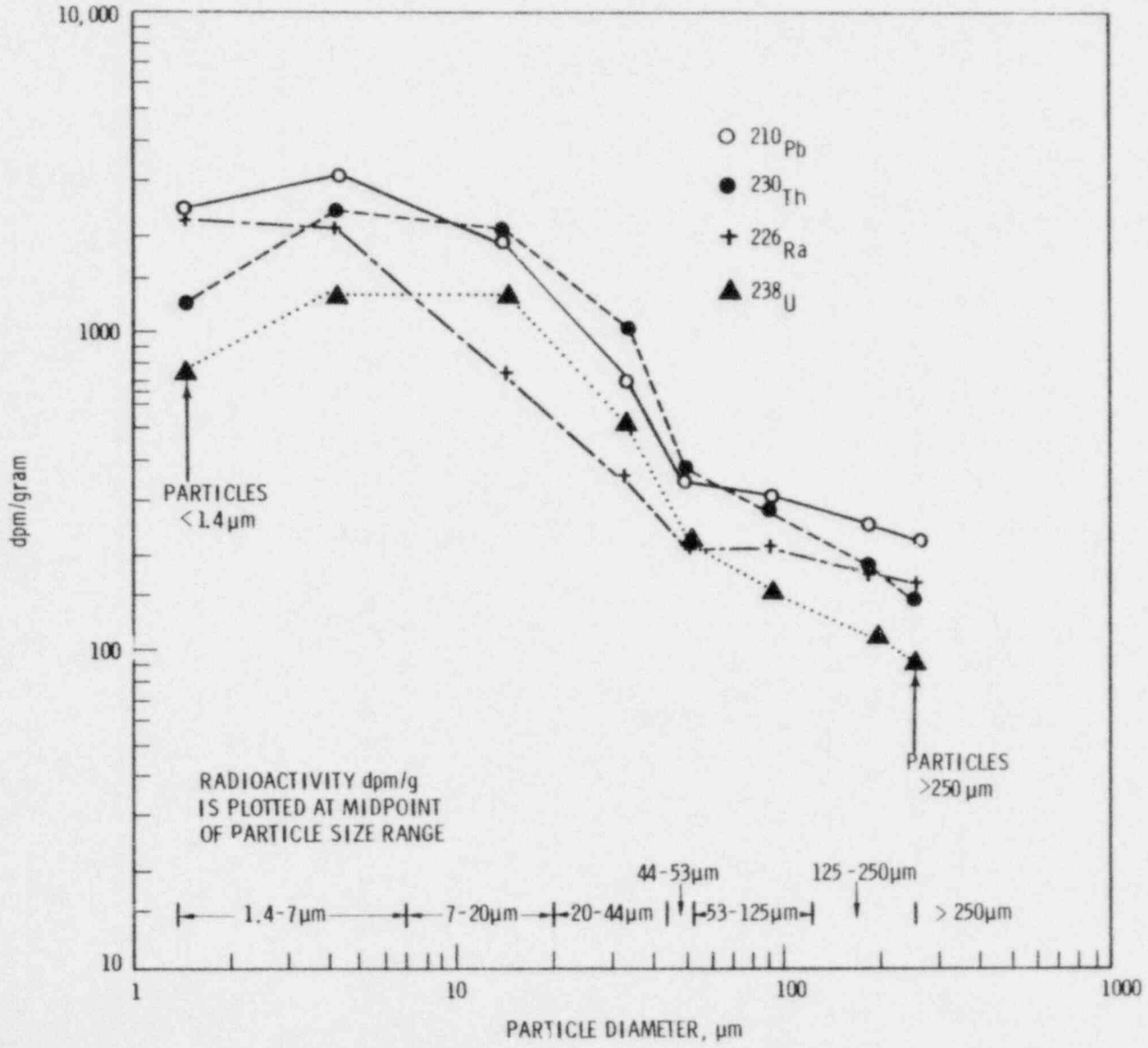

FIGURE 5. Radionuclides Associated with One Gram of Particles of Different Sizes

The data in Tables 1 and 2 show that a relatively large fraction of the radioactivity is associated with particles smaller than 7 μm in diameter. It is also apparent that activity density (dpm/g) of the smaller particles is about an order of magnitude greater than that of the large particles. The data also show that a significant amount of material is dissolved and on drying out could form an easily suspendable fine salt.

The distribution of radioactivity with respect to particle size is particularly important in drawing conclusions regarding the radiological significance of windblown particles. Particles smaller than about 10-μm aerodynamic equivalent diameter (AED)[(a)] are considered respirable; that is, a significant fraction of this size will deposit in sensitive regions of the lung or air passageways. A relatively small fraction of particles as large as 10-μm AED will be deposited in the pulmonary region of the lung since particles of this size and larger are preferentially retained in the naso-pharyngeal region (Mercer 1977).

The data in Tables 1 and 2 were converted to AED, and the fraction of radioactivity associated with a given AED and smaller was calculated. These data are shown in Table 3 for tailings sampled from two sources and sized using wet sieving and sedimentation.

Although there appears from Table 3 to be some systematic differences between the percent of radionuclide activity associated with AED fraction 11 μm and smaller taken from the pile itself and taken from the slurried tailings, differences appear to be of little significance for the two samples when particles larger than about 31-μm AED are examined. Although the cumulative activity on particles 31 μm (AED) and larger is not greatly different from one radionuclide to the other nor for the two sample sources, considerable differences are observed for the two smallest size fractions, < 2.2 and 11 μm. The

---

(a) Aerodynamic Equivalent Diameter (AED) is the diameter of a unit density particle having the same terminal settling velocity as the particle under consideration. Since the settling velocity is proportional to the density and to the diameter squared, the AED is obtained by multiplying the diameter of the particle considered by $\sqrt{\rho_p}$, where ρ_p is the density of the particle whose AED is to be determined. The density assumed for tailings sand was 2.4 g/cm^3.

TABLE 3. Aerodynamic Equivalent Particle Diameters and Associated Cumulative Radioactive Constituents

Particles from Surface of Pile A and from Slurry to Pile A

Particle AED μm	% of wt. represented by size and smaller		% of Radionuclide Activity Associated with Particles of Stated AED and Smaller							
			^{210}Pb		^{238}U		^{230}Th		^{226}Ra	
	0.5 cm[(a)]	Slurry	0.5 cm	Slurry	0.5 cm	Slurry	0.5 cm	Slurry	0.5 cm	Slurry
<2.2	0.1	0.9	0.3	3.9	0.6	2.1	0.1	2.1	0.3	7.3
11	9.2	2.5	37.9	12.8	44.4	8.6	38.7	9.5	39.3	18.0
31	16.4	7.0	57.5	62.0	64.5	68.5	61.5	67.1	57.0	53.5
68	24.2	21.0	71.0	67.1	77.7	75	78.7	75	72.4	58.1
82	28	22.6	72.8	68.1	79.1	76.1	81.0	76	74.8	59.2
194	32.2	29.7	75.0	72.1	80.8	79.6	83.2	79.9	76.9	64.1
387	39.7	55.7	78.3	83.8	83.1	88.7	85.5	88.9	80.0	79.2

(a) Samples were from surface down to 0.5 cm.

differences between sample sources are more significant than differences between fractional activity for different radionuclides.

Some difference between the slurry sample and the tailings surface sample is expected since the surface sample has doubtless been affected by the cyclone classification, interaction with atmospheric processes, and the degree to which all particles were truly dispersed in the sedimentation column.

Regarding the 11-μm and smaller particles as of greater interest from a radiological perspective, we make the following observations:

- For the tailings surface material, 40 ± 2.5% (σ) of the activity of the four radionuclides is associated with ≤11-μm (AED) particles. This radioactivity is associated with 9.2% of the total mass.
- For the sample taken from the discharge pipe slurry, 12.3 ± 3.7% (σ) of the activity of the four radionuclides is associated with ≤11 μm (AED) particles. This radioactivity is associated with 2.5% of the total mass.

The tailings sample as a composite taken from the top 0.5 cm represents more nearly the material "available" for wind suspension. Both samples, however, were water-dispersed, which would alter their suspension characteristics compared to the dry material on the tailings pile.

An indication of some possible differences in particle size available for wind suspension is shown in some earlier size distribution data included here as Table 4. The sample from the top 0.5 cm was dried under a heat lamp, then pulverized with enough mechanical working to break down obvious aggregates and separate particles from each other. The size distribution of the resulting particles was determined with a Bahco separator, which employs air elutriation and centrifugal forces to effect the classification. Particles smaller than 100 μm represented less than 3% of the mass. We acknowledge, however, the drying and mechanical pulverizing process was arbitrary and may not have produced a particle size spectrum the same as that available for suspension on the tailings pile.

The slurry sample and the sample taken from the top 0.5 cm of the tailings (and subsequently slurried with water for the particle size distribution

TABLE 4. Particle Size Distribution and ^{210}Pb Activity Density of Surface Tailings Pile Material[a]

Size Fractions, μm	Weight, gm	Weight, %	^{210}Pb dpm/g
>100	17,100	97.09	719
10 - 100	500	2.84	860
3 - 10	8	0.04	1,559
1 - 3	2	0.01	2,148
<1	2	0.01	1,556

(a) Tailings material from the top 0.5 cm was dried, pulverized, then separated by air elutriation using a Bahco particle separator. Since the pulverization process was arbitrary, the particle size may not be the same as in situ particles on the tailings pile subject to wind suspension.

measurement), better represent the true size distribution of the particles; however, the in situ particle size distribution would be more realistic as an index to resuspendability if the in situ particle size could be determined. Although the governing relationships between particle-surface characteristics and resuspension rate are ill-defined with the present state-of-the-art, the particle size characteristics of the surface material can be used in determining limiting concentrations when models are applied to describe the wind-blown soil.

The foregoing data represent characteristics of mill tailings particles from contemporary mill operations. The variation of radioactive constituents with depth representing earlier operating periods was determined for two locations on tailings pile A from the 40-cm core samples. The resulting data are shown in Table 5.

These data show that the ratios of uranium daughters are relatively close to unity but that their absolute concentrations as a function of depth vary considerably. These data indicate that there is a considerable degree of stratification of the tailings pile that apparently results as different fractions of the fine slurry material are deposited from the tailings pond water. Another possible explanation would be that some of the stratification may result

TABLE 5. Variation of Radionuclide Concentration with Increased Depth in Core Samples from Tailings Pile A

Sample No.[a]	Depth cm	Concentration, dpm/g			
		^{210}Pb	^{238}U	^{230}Th	^{226}Ra
A-1	4	493	78.3	294	435
2	8	568	38.8	363	512
3	12	466	39.8	344	494
4	16	571	52.2	581	649
5	20	491	57.4	540	602
6	24	449	47.6	452	508
7	28	462	37.0	352	461
8	32	512	50.9	373	473
9	36	902	28.8	746	941
10	40	623	59.1	597	677
Average		554	49.0	464	575
B-1	4	1149	103.0	1204	1387
2	8	987	53.0	1167	1215
3	12	686	37.0	637	745
4	16	3305	129.0	3182	4044
5	20	604	60.4	552	646
6	24	506	28.0	349	449
7	28	446	34.0	324	451
8	32	581	38.0	449	576
9	36	440	30.0	318	578
10	40	428	27.0	333	493
Average		913	53.9	851	1063

(a) Core A from north edge of evaporation pond shoreline in west half of tailings pile.

Core B from 100 m southeast of evaporation pond in eastern half of evaporation pond.

from changes in ore grade or mill processing variables from time to time. A much more intensive sampling and analysis study would have to be carried out to determine the cause(s) of this stratification. Because the windblown particles arise from the surface most recently deposited and dried, the variation with depth would also represent to a large degree the variability expected in the flux of particles during blowing.

The stable isotope compositions in tailings material from a selected core sample from mill A was determined by x-ray fluorescence analysis. These results are shown in Table 6.

It was possible in the characterization of tailings material to establish whether there were concentrations of trace elements in tailings material significantly above those in ambient soil. To explore this possibility, samples of ambient soil were collected at a distance of 8 km from the tailings pile and at a depth of 30 cm to ensure that no windblown tailings were present. The x-ray fluorescence spectra of this sample and of samples taken directly from the tailings pile are shown in Figures 6 and 7, respectively. From an examination of these spectra, it is evident that the elements in the tailings at substantially higher concentrations than in ambient soil were selenium, uranium, and molybdenum. The selenium concentrations were actually about 100 times those in ambient soil. The concentrations of selenium and uranium are compared in a core sample from the tailings pile in Table 7. The ratio of selenium to uranium varies by a factor of about 2.6 through the length of this 40-cm core. One could, therefore, possibly use environmental measurements of selenium as an indication of the presence of tailings material.

Acid Leach Tailings Piles (Piles B and C)

Table 8 shows the radionuclide concentrations in material from tailings pile B. In this case, materials from the tailings pile that were obviously fine, obviously coarse, or about average were collected. It is evident that there is a very much higher concentration of uranium daughters in the fine material and that this concentration is an order of magnitude higher than that of the coarse material for most of the radionuclides. In addition, the ^{230}Th is present in lower concentrations than ^{226}Ra or ^{210}Pb in both the fine and coarse material from this acid leach mill.

TABLE 6. Elements in Mill A Tailings (ppm) (X-ray Fluorescence Analysis)

Depth cm	K	Ca	Ti	V	Cr	Th	Mn	Fe	Co	Ni	Cu	Zn	Ga	Hg
4	<217	2790	355	234	<63	<9.0	239	24700	<144	<21	53	62	11	<28
8	<225	3396	172	311	<60	<9.0	211	17770	111	<22	45	42	19	<29
12	260	1649	302	216	61	<9.2	191	21400	<107	<23	47	49	17	<28
16	244	1470	441	266	<66	<9.4	318	30570	<126	<24	51	71	20	<30
20	<227	985	300	350	<64	<9.3	259	29320	<134	<23	68	71	17	>29
24	266	896	328	239	<64	<9.1	245	28310	128	<23	55	68	21	>29
28	225	3177	282	250	91	<9.2	219	25600	<118	<22	59	50	15	>29
32	358	3183	292	<80	<62	<8.7	184	11440	< 81	<22	47	33	16	>30
36	<231	3524	142	151	<59	<8.5	160	6336	< 63	<21	46	16	9.6	>29
40	<230	2892	122	<75	<62	<8.5	170	5899	< 60	<20	32	31	<8.8	>29

	Se	Pb	As	Rn	Rb	U	Sr	Y	Zr	Cl	Nb	Mo
4	197	70	37	<4.0	64	148	246	32	114	92410	10.8	112
8	195	47	39	<4.0	60	213	244	30	91	90360	9.3	56
12	207	53	18	<4.1	74	174	243	31	115	87140	11.9	58
16	234	44	31	<4.2	81	112	340	34	116	92960	15.4	68
20	224	34	34	<4.2	79	95	284	30	116	89390	15.2	70
24	185	37	25	<4.1	81	85	231	29	106	92310	13.5	65
28	141	59	37	6.7	61	126	289	32	97	89830	12.4	64
32	84	30	21	5.0	64	88	196	17	156	91310	6.5	65
36	67	26	17	5.1	71	61	166	13	177	90890	5.8	50
40	93	12	15	4.1	67	72	160	11	178	90400	5.3	73

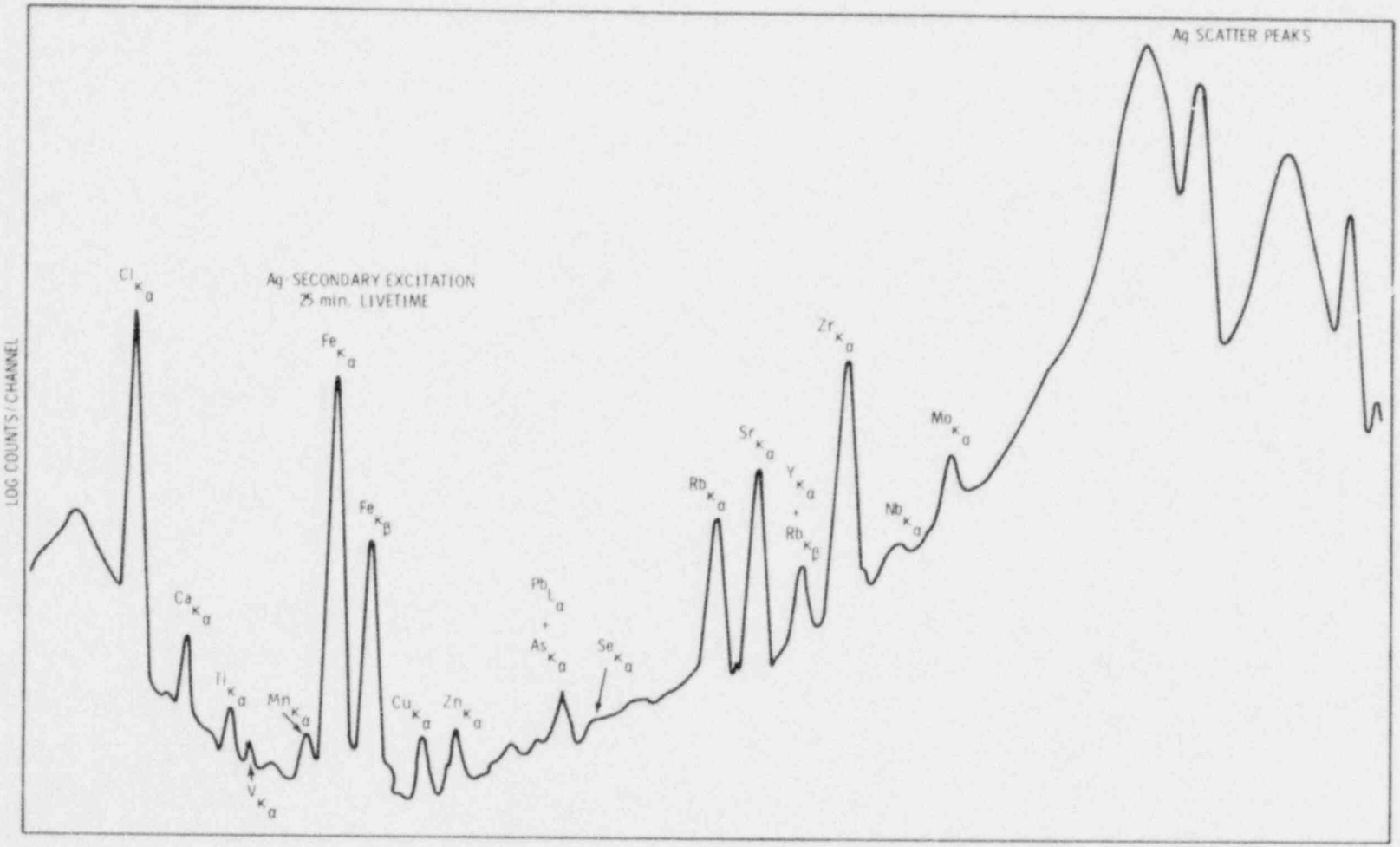

FIGURE 6. X-Ray Fluorescence Spectrum of Soil Taken Five Miles from Tailings Pile A at a Depth of One Foot

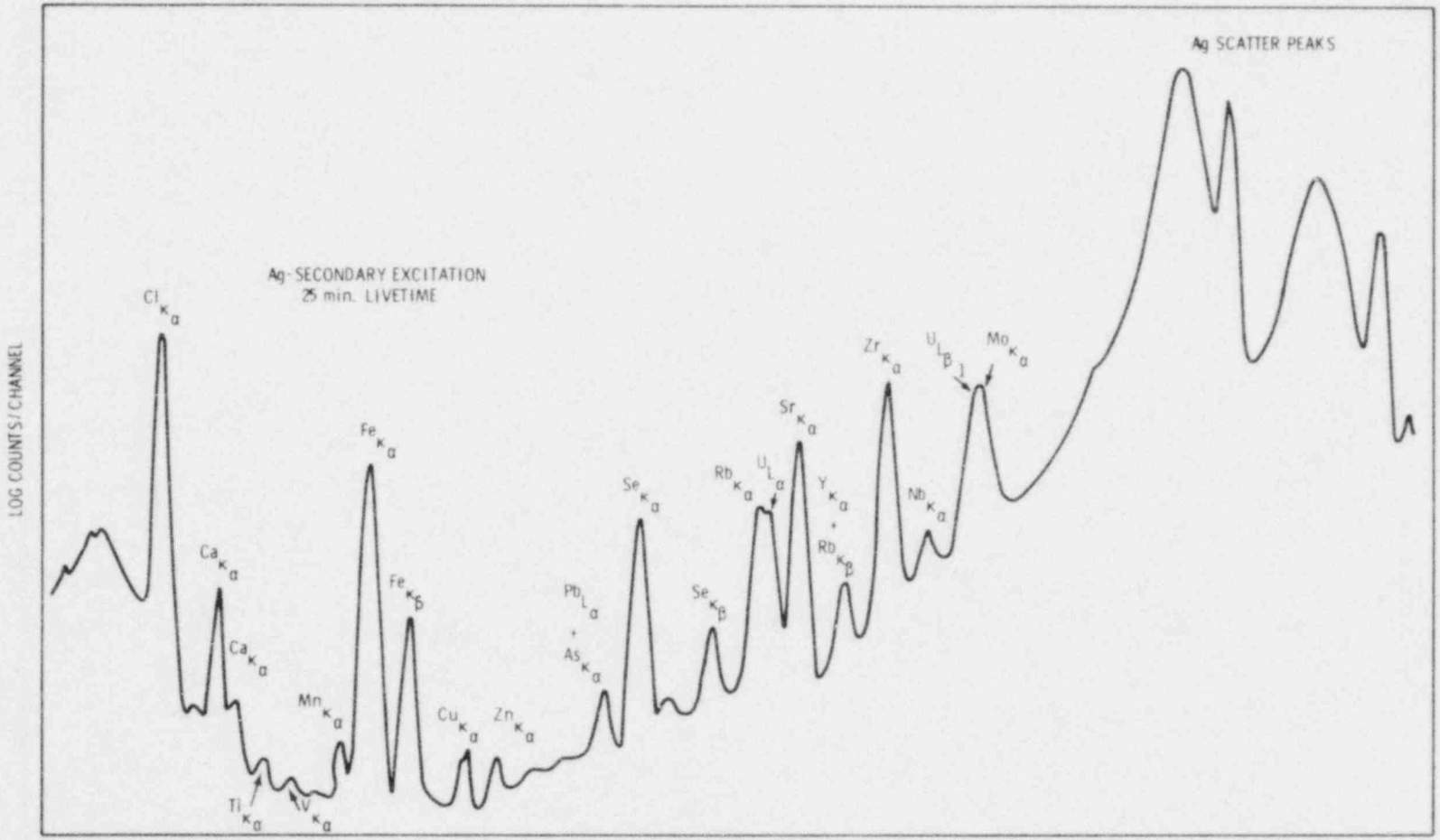

FIGURE 7. X-Ray Fluorescence Spectrum of Tailings Material from Tailings Pile A

TABLE 7. Uranium and Selenium Concentration in a Core from East Area of Tailings Pile A (Measured by X-ray Fluorescence Analysis)

Depth, cm	Se (ppm)	U (ppm)	Se/U
4	197	141.0	1.4
8	195	228.0	0.9
12	207	190.0	1.1
16	234	112.0	2.0
20	224	107.0	2.1
24	185	108.0	1.7
28	141	127.0	1.1
32	84	107.0	0.9
36	67	69.21	1.0
40	93	86.4	1.1

TABLE 8. Radionuclide Concentration in Tailings Pile B (dpm/g)

Type of Tailings	^{226}Ra	^{230}Th	^{210}Pb	^{238}U
Fines	5500	2400	6300	900
Coarse Material	600	400	700	90
From Pond Edge	700	500	800	90

Using the same methods employed as outlined earlier, we obtained a sample of tailings from the slurry being discharged to the acid leach plant tailings pile (C) and determined sizes of particles present and the associated radioactivity in the size fractions. The data relative to particle size fractions and associated activity are shown in Table 9 and the particle size data are plotted in Figure 8. The relationship between particle size and associated radionuclide radioactivity is shown in Figure 9.

There are several differences between the acid leach and alkaline leach extraction processes. In the crushing and grinding process where acid leaching is employed, coarser particles are effectively leached, but where carbonate

TABLE 9. Particle Size Versus Radionuclide Composition of Tailings from Input Slurry to Tailings Pile B

Particle Size	Weight %	dpm/g and (%) activity							
		^{210}Pb	(%)	^{238}U	(%)	^{230}Th	(%)	^{226}Ra	(%)
>250	48.4	416	23.9	35	28.2	205	23.3	306	18.3
125-250	22.4	600	16.0	41	15.3	290	15.3	676	15.9
53-125	8.7	1010	10.4	60	8.8	472	9.7	1100	10.0
44-53	2.8	3176	10.6	186	8.8	1445	9.5	4015	11.8
20-44	9.2	1124	12.3	66	10.3	511	11.1	1424	13.8
7-20	7.3	2860	24.8	155	19.1	1335	22.9	3890	29.8
1.4-7	0.9	1919	2.1	426	6.4	3555	7.5	303	0.3
<1.4	0.3	195	0.1	614	3.0	908	0.6	201	0.1

leaching is employed, the ore is ground to a finer particle size.[(a)] There is a significant difference in the solubility of the inert material and uranium chain daughters in the ore with the alkaline carbonate versus the acid sulfate process. There are also procedural differences between particular mills in discharging spent chemicals used in the ore extraction process. At the alkaline leach mill A, all waste including chemicals used are ultimately discarded with the tailings material while at the acid leach mill C a large amount of H_2O and chemicals are diverted to evaporation ponds instead of the tailings pile. Because of these differences, the tailings pile characteristics vary and the resuspension of particles by wind could be quite different.

In regard to the acid and alkaline leach tailings slurry, several comparisons can be made. Apparently there is not a large difference in the physical size spectrum for particles 250 µm and smaller (as shown in Tables 2 and 4) even though ore for the alkaline leach process normally is ground to a smaller particle size. It may be that the nominal size of grains and attached uranium-bearing deposits were such that the acid leach process reduced the sizes of

(a) Plant A (alkaline carbonate leach) grind of ore is 5% +48 mesh (297 µm) and 38% -200 mesh (72 µm). Plant B (acid leach) is 30% +48 mesh (297 µm) and 16% -200 mesh (74 µm). (Silker and Heasler 1979)

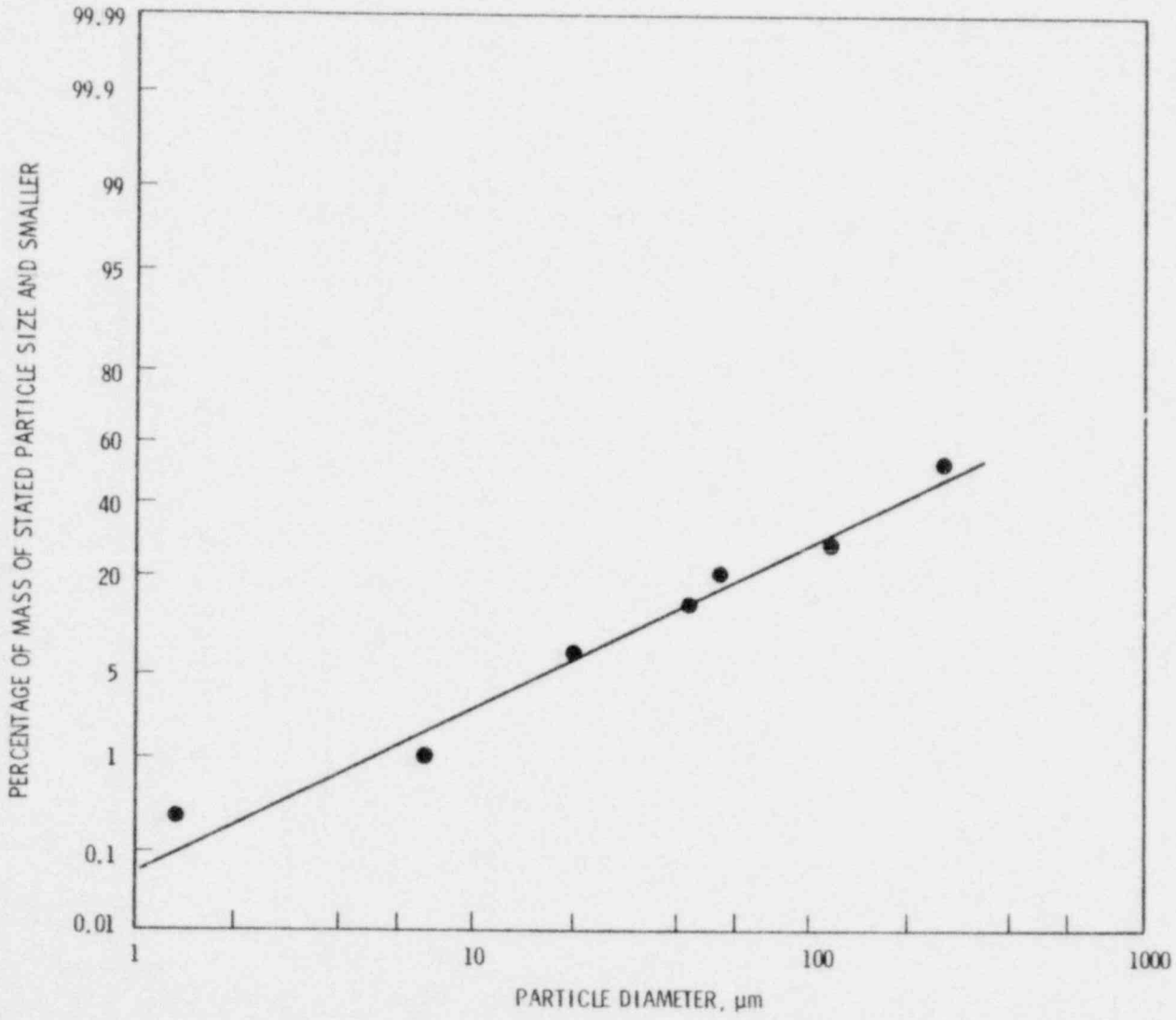

FIGURE 8. Particle Size Distribution: Particles in Slurry to Acid Leach Tailings Pile

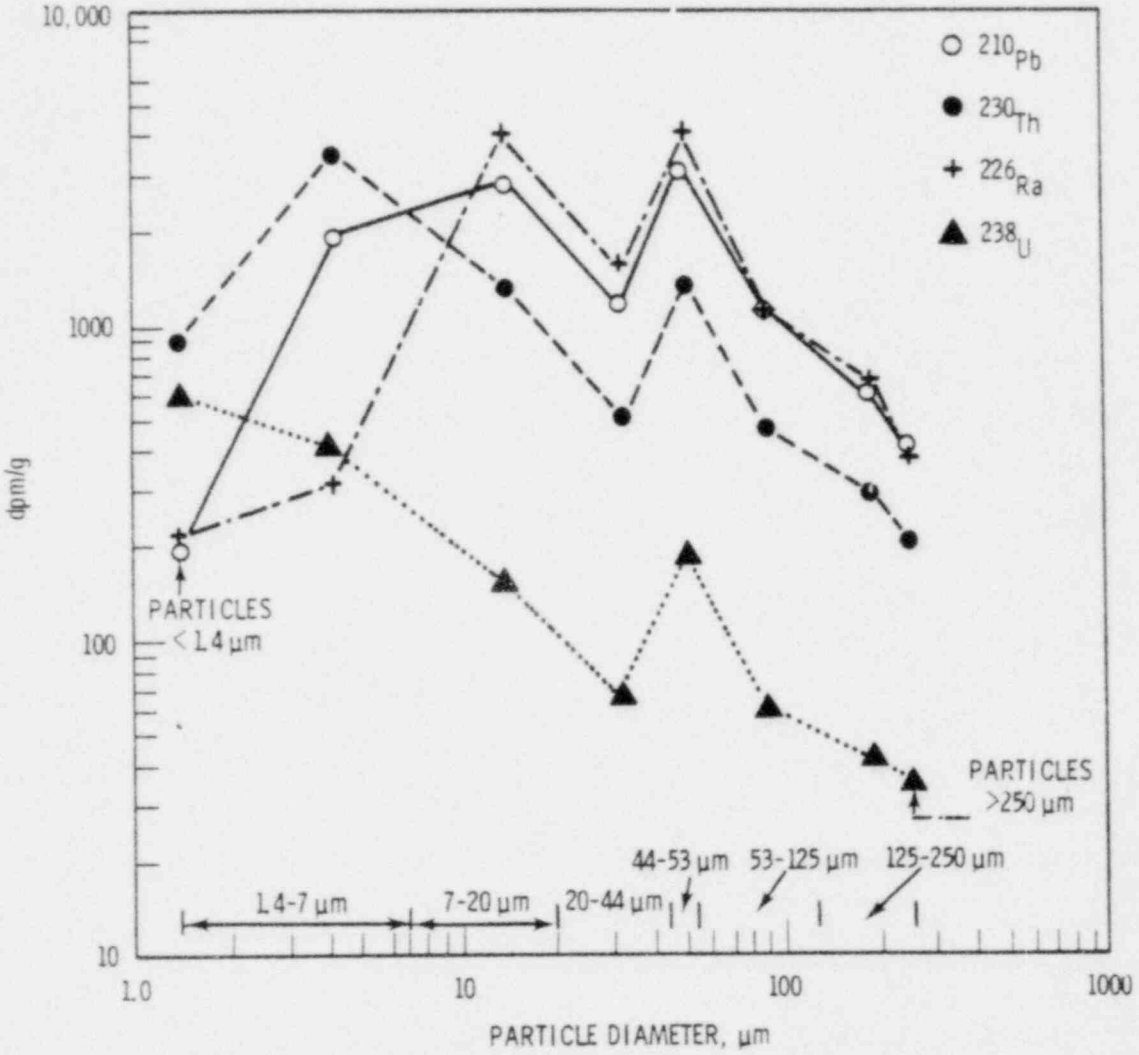

FIGURE 9. Radioactivity Associated with One Gram of Particles of Different Sizes

particles to those found. Since particles of >250 µm are separated as a group, we did not determine the largest particle sizes present. At the acid leach mill vanadium, titanium, and molybdenum are also recovered from the process, thus changing the composition of the tailings.

There were significant differences in the radiochemical composition of tailings material from the alkaline and acid leach tailings piles. In the alkaline leach tailings material, the ratios of the uranium daughter radionuclides are approximately unity, which suggests a near-equilibrium quantity

of each. In the case of the acid leach tailings, the ratio of ^{230}Th to either ^{226}Ra or ^{210}Pb is significantly less than unity. Because of the high solubility of ^{230}Th in the sulfuric acid leach solution and the fact that radium sulfate is very insoluble, there is a considerable disequilibrium of ^{230}Th relative to ^{226}Ra and ^{210}Pb in most areas of the tailings materials.

Some samples were taken from the tailings pile in the vicinity of the acid leach plant, plant C. The data are shown in Table 10. The data again show the disequilibrium between ^{230}Th, ^{226}Ra, and ^{210}Pb, particularly in the water samples taken on and near the tailings pile. The tailings material associated with soil at ∿2 km from the tailings pile contained uranium daughter concentrations that were as much as 10% of those in some areas of the tailings pile. This is discussed further in the next section.

TABLE 10. Radionuclides in Solid and Liquid Samples Taken on and Around Tailings Pile at Plant C (Acid Leach)

	dpm/g			
Sample Type	^{226}Ra	^{230}Th	^{210}Pb	^{238}U
Mill Tailings Area 1	350	300	550	70
Main Tailings Area 2	350	3300	500	175
Main Tailings Area 3	300	450	400	50
Water on Tailings	1	1100	120	75
Water Evaporation Pond	1	1050	60	15
Ore	1100	1000	1300	1100
1 Mile East of Tailings	35	50	45	

SUMMARY AND CONCLUSIONS--MILL TAILINGS CHARACTERIZATION

The extensive sampling and analysis of tailings particles from an alkaline carbonate leach tailings pile and samples taken from acid leach tailings piles lead to the following conclusions:

- The alkaline carbonate leach, tailings pile, water-dispersed particulates from the first 0.5 cm of the tailings pile are characterized by about 40% of the ^{210}Pb, ^{238}U, ^{230}Th, and ^{226}Ra being associated with particles $\sim$7 μm ($\sim$11 μm AED) and smaller in diameter. The mass of particles in this size range was about 9%. Particles collected directly from the slurry discharge point to the tailings, then size-fractionated in the liquid, were shown to have about 12% of the active material associated with the $\leq$7 μm range, but these particles accounted for only about 2.5% of the mass.
- Concentrations of ^{226}Ra, ^{230}Th, and ^{210}Pb were of the order of 400 to 900 dpm/g ($\sim$2-4 x 10^{-4} μCi/g) for the bulk surface alkaline leach tailings particles. Approximately equal concentrations of these daughter products of uranium showed them to be in secular equilibrium. Uranium-238 was $\sim$10% or less of the daughter products present. Core samples showed random variation in activity per gram with depth but practically all results were within a factor of two of the average. One anomalously active 4-cm-thick zone was found in one sample.
- Surface samples of alkaline leaching tailings, selected to represent the very fine material, were found to be about 10 times more radioactive per gram than the coarse material sampled.
- Selenium was found in the tailings at a level of about 200 ppm, about 100 times that in ambient soil. Molybdenum and uranium were also found in concentrations higher than in background soil.

TASK B. WINDBLOWN PARTICLES FROM THE TAILINGS PILE DEPOSITED ON THE SOIL IN THE VICINITY OF THE SITE

Principal Investigator: C. W. Thomas

The objective of Task B was to determine the quantity and nature of particulate material originating at the tailings site during the years of mill operation and deposited on soil in the vicinity of the mill. Models of deposition as a function of atmospheric processes and characteristics of the source might be tested by these measurements. The data would also give insight into the secondary sources of radon and resuspended particles.

EXPERIMENTAL

A polar grid system was established with radial lines $\sim 22\text{-}1/2^{o}$ apart extending out from tailings pile A. Circular arcs at 1/2, 1, 2, 3, 4, and 5 miles (0.8, 1.6, 3.2, 4.8, 6.4 and 8 km) intersected the radial lines, and at these intersections soil samples were taken.

The sampling locations and types of samples taken are shown in Figure 10. The primary sample collected consisted of a 5-cm-deep core that was subsequently sectioned into 0.5-, 1.0-, and 3.0-cm-deep layers for analysis. As indicated in Figure 10, 24-cm-deep cores were taken in some areas to determine the downward migration of deposited material. A few 1-m^2 by 1-cm deep surface samples were also taken to provide sufficient material for determining radioactivity as a function of particle size. Radionuclide measurements included the analysis of surface samples for uranium and its daughters, the analysis of core samples to determine the depth distribution of radioactivity, and the analysis of particle size to obtain some estimate of the material that had been transported. Soil samples were separated into size fractions with a Bahco particle-size classifier and with wet sieving followed by sedimentation. The Bahco classifier uses centrifugal forces and air elutriation to separate selected size fractions.

To estimate the amount of tailings material that had been carried by the prevailing winds to mill C tailings pile environs, soil samples taken over the sample network shown in Figure 11 were analyzed. Samples were collected

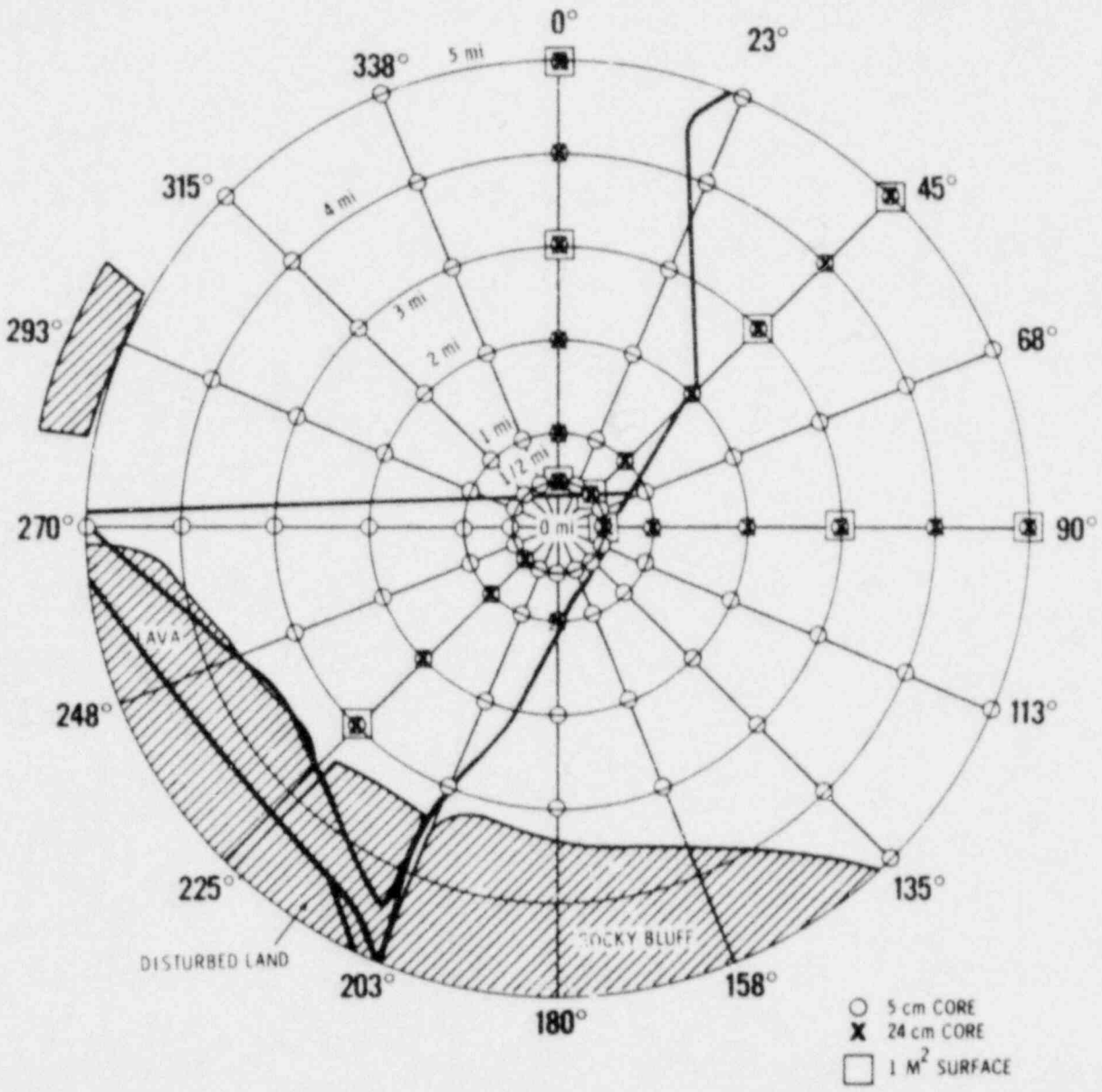

FIGURE 10. Soil Sampling Locations Around Tailings Pile A

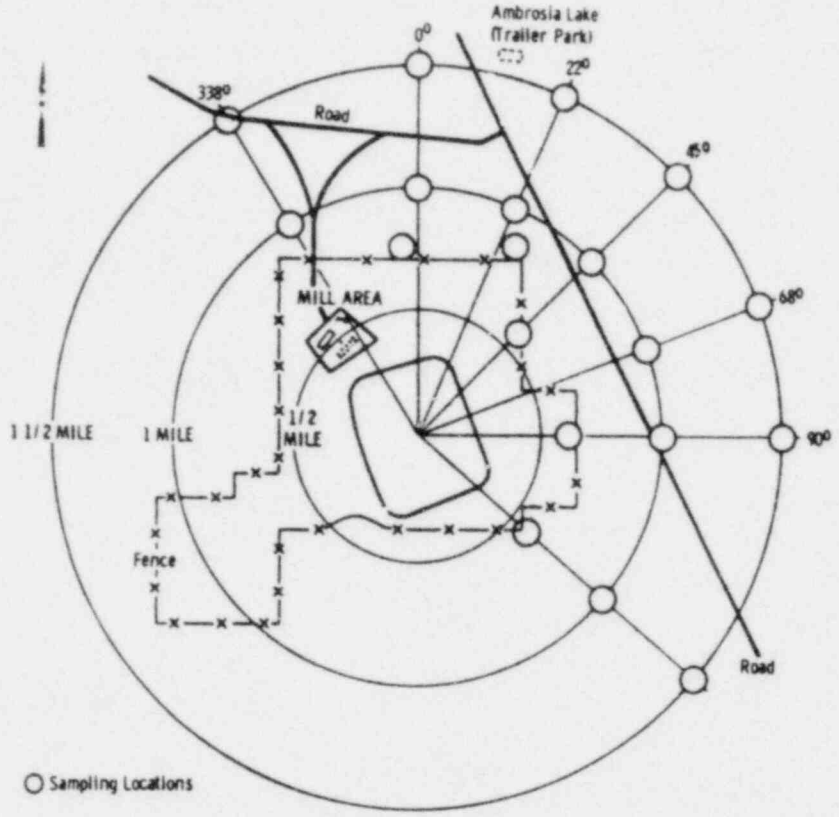

FIGURE 11. Soil Sampling Locations Around Tailings Pile C

out to distances of 1-1/2 miles (2.4 km) along selected compass points in the northeasterly direction. Collected samples consisted of a 3-cm-deep core sectioned into 1-cm sections plus an underlying sample at 30-cm depth. Radionuclide measurements included the analysis of surface samples for uranium and its daughter products and the analysis of core samples to determine the depth distribution.

RESULTS AND DISCUSSION--TAILINGS ON SOIL IN THE VICINITY OF URANIUM MILLS

Alkaline Leach Mill A

Figure 12 shows isopleths of ^{226}Ra concentrations over the sampling network surrounding tailings pile A. The concentration of ^{226}Ra ranged from over 300 dpm (136 pCi)/g at distances of about 0.25 miles (0.4 km) to 5 dpm (2.3 pCi)/g at distances ranging from one mile (1.6 km) to the south to about

5 miles (8 km) to the north-northeast. The ground deposition pattern corresponds reasonably well to the pattern of wind frequency and direction. Also seen in Figure 12 is the influence of tailings blown from mill tailings pile B about 5 miles (8 km) to the west of site A.

The total ^{226}Ra in the vicinity represented by the deposition from the mill A tailings pile was estimated by integrating areas between isopleths and assigning the average concentraton between isopleths to the area.

These calculations required a knowledge of the depth distribution of radium at various locations within these isopleths. An example of these depth

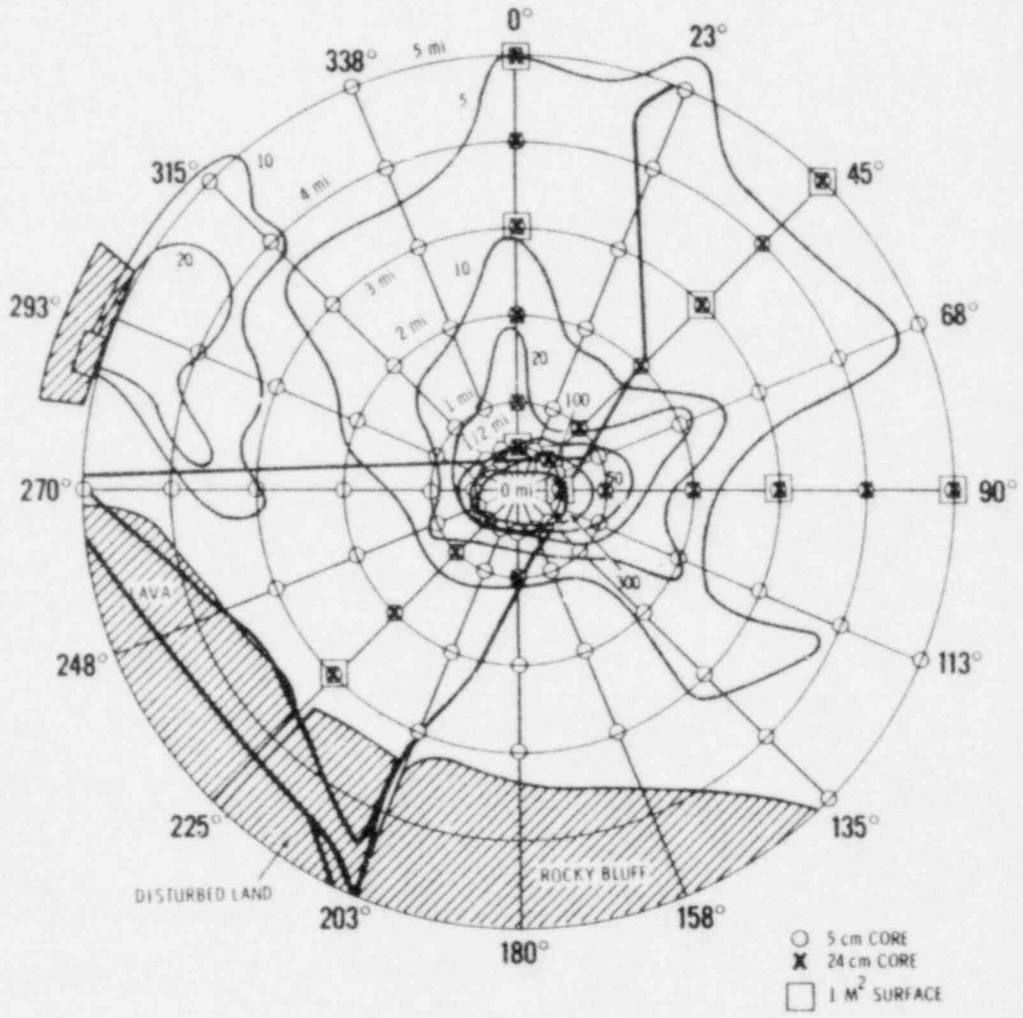

FIGURE 12. Isopleths of ^{226}Ra Soil Concentrations in Environs of Tailings Pile A (dpm/g)

distributions for ^{210}Pb is shown in Figure 13. Based on the concentrations between the isopleths and the depth distribution of ^{226}Ra, the ^{222}Rn emissions from the areas between the isopleths have been estimated and are shown in Table 11. For these calculations, only the radium content of the top 5 cm of soil was used. Values found were corrected for the natural radium content in the soil. The emission rates are based on the assumption that one-half of the radon generated in this soil from the added tailings material will be released to the atmosphere. This assumption is admittedly an approximation and accounts primarily for the availability for release of radon in the particles.

Table 11 indicates an emission rate of 1.6 Ci/day from this secondary source. This rate can be compared with an emission rate of about 8 Ci/day from the tailings pile (Silker and Heasler 1979). Thus, the secondary source of radon emission currently amounts to ~20% of that from the tailings pile itself.

Isopleths of ^{210}Pb soil concentrations in the vicinity of Plant A are shown in Figure 14. The pattern is similar to that for ^{226}Ra.

The mixing and weathering of surface-deposited tailings to soil depths up to 20 cm is clearly shown as a function of distance in Figure 13. Up to 2 miles from the tailings pile, soil concentration with depth decreases approximately exponentially with a half thickness of about 1.6 cm for the first 5 cm. At points deeper in the soil there is a slower decrease of activity with depth. At a 20-cm depth (about 8 in.) near background levels are reached for all distances from the tailings pile.

The radioactivity associated with various particle size fractions of the soil was determined on a series of samples taken on a line due north (000 transect) from the tailings pile. Samples were taken at 1/4, 1/2, 1, 1-1/2, 3, 4, and 5 miles (0.4, 0.8, 1.6, 2.4, 4.8, 6.4, and 8 km) from the outer edge of the pile. These samples were wet-sieved down to 44 μm and the remaining fractions separated by a sedimentation method. Each fraction was dried, weighed, and a radiometric determination made for ^{210}Pb, ^{238}U, ^{230}Th, and ^{226}Ra. Results of these measurements are shown in Table 12.

Samples taken at 1/4, 1/2, 1, 3, 4, and 5 miles (0.4, 0.8, 1.6, 2.4, 4.8, 6.4, and 8 km) showed a particle size distribution with a large fraction of

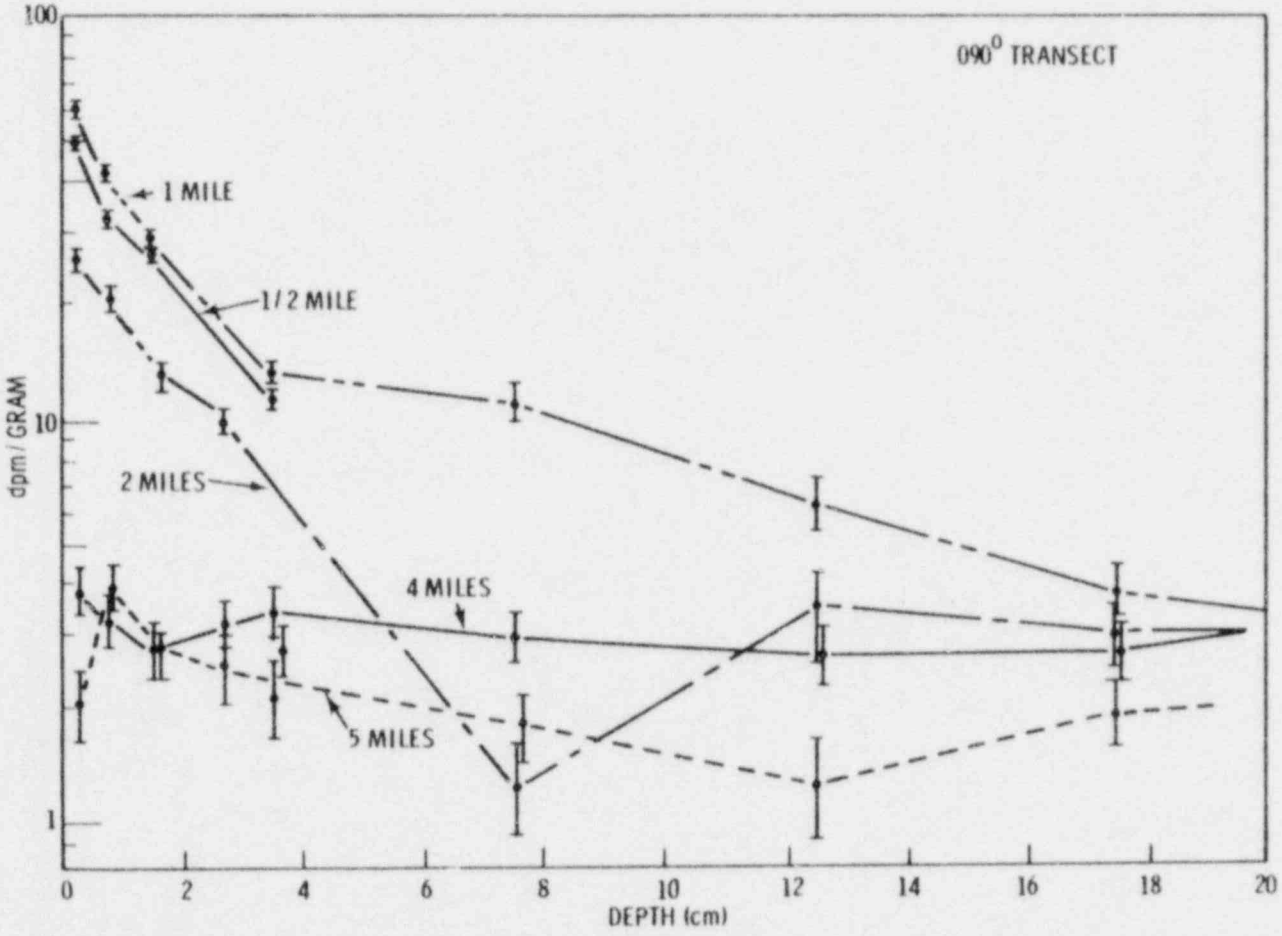

FIGURE 13. Depth Distribution of ^{210}Pb in the Environs of Tailings Pile A

TABLE 11. Radon Emission Rate from Tailings, Secondary Sources, and Background Areas

Area	Approximate Area (km^2)	$Ci/km^2/day$	Ci/Area
A	0.2	0.75[a]	0.15
B	0.35	0.37[a]	0.13
C	0.85	0.14[a]	0.12
D	1.6	0.063[a]	0.10
E	12.2	0.028[a]	0.34
F	55.1	0.014[a]	0.77
Background Area		0.007[b]	
Tailings Pile		8.[c]	
		TOTAL	1.61

(a) From top 5 cm of soil
(b) From surface soil beyond 8 km
(c) Total soil column (Silker and Heasler 1979)

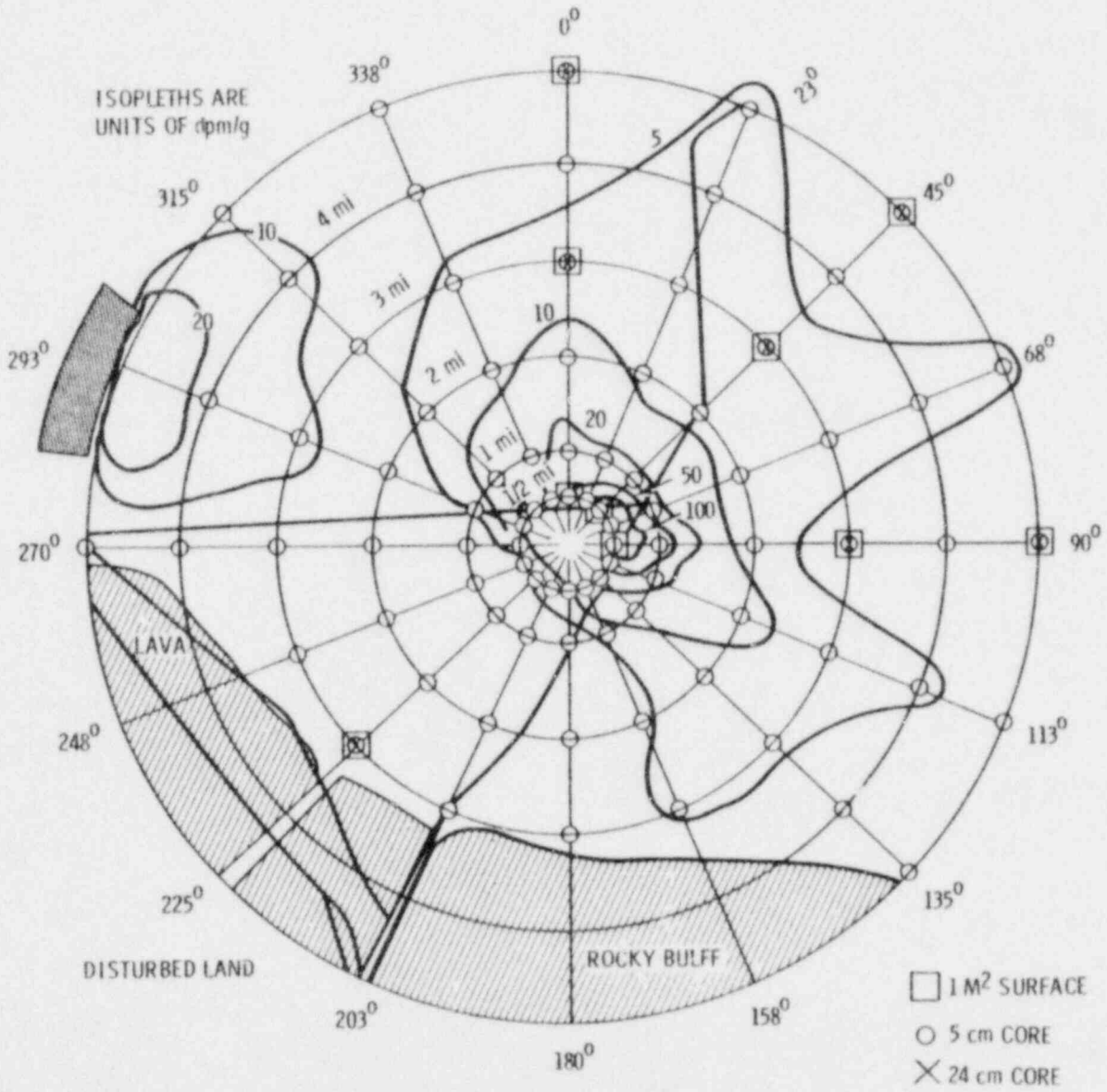

FIGURE 14. Isopleths of ^{210}Pb Concentration in Emissions of Tailings Pile A

TABLE 12. Radionuclide Composition vs. Particle Size in Soil in the Vicinity of Tailings Pile A (Activity in dpm/gram of soil)

Size Fraction	Wt. Grams	Wt %	^{210}Pb dpm/g	^{210}Pb %	^{238}U dpm/g	^{238}U %	^{230}Th dpm/g	^{230}Th %	^{226}Ra dpm/g	^{226}Ra %
					¼ mi (0.4 km)					
>250	226.8	23.9	48.2	5.1	6.2	7.4	38.3	4.3	68.0	6.0
125-250	360.3	37.9	97.4	16.3	10.3	19.2	59.6	10.5	91.3	12.9
53-150	174.7	18.4	257	20.9	21.3	19.2	23.1	19.8	263	18.0
44-53	35.0	3.7	477	7.8	30.1	5.4	379	6.5	520	7.1
20-44	52.0	5.5	612	14.9	50.3	13.8	630	16.2	828	16.9
7-20	53.6	5.6	700	17.3	63.7	17.7	842	22.0	959	19.9
1.4-7	23.5	2.5	776	8.6	66.8	8.4	842	9.8	908	8.4
<1.4	24.6	2.6	786	9.0	69.9	8.9	885	10.7	1111	10.7
Soluble salts	0.5	<.10	0.18	0.0	0.07	0.0	<.05	0.0	0.39	0.0
					½ mi (0.8 km)					
>250	425.9	42.7	7.4	8.2	1.0	15.7	<2.7	3.3	0.60	0.7
125-250	318.5	32.7	16.0	13.3	2.0	13.7	13.4	12.0	20.6	16.2
53-125	57.4	5.9	72.8	11.0	9.6	11.8	53.2	8.5	57.6	8.2
44-53	10.5	1.1	203	5.6	16.2	3.9	182	5.5	213	5.6
20-44	30.5	3.1	237	18.7	31.2	19.6	208	17.5	261	19.6
7-20	46.1	4.7	119	14.4	24.6	23.5	129	16.7	170	19.3
1.4-7	58.2	6.0	114	17.4	19.2	23.5	134	21.9	138	20.0
<1.4	26.3	2.7	164	11.3	21.2	11.8	199	14.8	158	10.4
Soluble salts	1.4	0.14	0.03	0.0	0.02	0.0	<.03	0.0	0.2	0.0
					1 mi (1.6 km)					
>250	204.9	20.9	2.4	3.5	1.7	8.9	<2.2	4.6	5.4	6.1
125-250	289.0	29.5	6.7	14.1	2.3	15.6	<3.5	9.3	7.7	12.8
53-125	68.0	6.9	17.6	8.5	2.3	4.4	17.3	11.1	22.2	8.4
44-53	9.2	0.9	47.2	2.8	11.3	2.2	29.2	2.8	36.7	1.7
20-44	143.3	14.6	31.6	32.4	9.0	28.9	22.6	30.6	35.2	28.5
7-20	116.6	11.9	21.4	17.6	7.7	20.0	14.4	15.7	28.4	19.0
1.4-7	113.0	11.5	19.8	16.2	6.9	17.8	18.3	19.4	27.6	17.9
<1.4	34.8	3.5	21.3	4.9	0.9	2.2	20.1	6.5	29.7	5.6
Soluble salts	2.0	0.2	0.01	0.0	0.01	0.0	0.03	0.0	0.05	0.0
					1-½ mi (2.4 km)					
>250	16.0	1.7	3.9	0.8	6.4	0.9	<4.8	1.0	4.6	0.6
125-250	71.3	7.4	6.3	4.1	3.7	2.8	<3.6	3.0	7.4	3.1
53-125	76.4	8.0	13.4	9.0	7.2	5.5	<6.9	6.0	10.3	4.9
44-53	11.7	1.2	20.4	1.6	7.9	0.9	15.6	2.0	21.0	1.8
20-44	229.4	23.9	14.7	28.7	11.8	25.7	12.3	29.0	20.7	30.1
7-20	338.7	35.3	12.3	35.2	11.2	36.7	9.6	34.0	16.7	36.2
1.4-7	200.4	20.9	10.9	18.9	13.4	25.7	10.8	23.0	17.0	22.1
<1.4	11.0	1.1	14.9	1.6	20.7	1.8	16.3	2.0	14.3	1.2
Soluble salts	3.4	0.4	0.01	0.0	0.15	0.0	<0.03	0.0	0.2	0.0

TABLE 12. (continued)

Size Fraction	Wt. Grams	Wt %	^{210}Pb dpm/g	^{210}Pb %	^{238}U dpm/g	^{238}U %	^{230}Th dpm/g	^{230}Th %	^{226}Ra dpm/g	^{226}Ra %
				2 mi (3.2 km)						
>250	10.9	1.1	3.0	0.3	2.2	0.3	<4.0	<0.7	5.7	0.5
125-250	61.7	6.5	3.9	2.3	2.9	2.2	<3.9	<3.8	4.3	2.0
53-125	53.5	5.6	8.8	4.5	3.2	2.1	<3.8	<3.2	10.2	4.1
44-53	15.4	1.6	12.8	1.9	5.2	1.0	15.8	3.8	14.8	1.7
20-44	180.9	19.1	13.1	22.7	9.6	21.6	4.3	12.2	13.5	18.4
7-20	273.6	28.8	13.7	35.8	10.6	36.0	9.7	41.6	13.7	28.2
1.4-7	346.4	36.5	9.6	31.8	8.3	35.7	6.2	33.7	17.1	44.6
<1.4	4.4	0.5	14.6	0.7	19.2	1.1	13.9	1.0	14.8	0.5
Soluble salts	2.2	0.2	0.01	0.0	0.09	0.0	<0.03	0.0	0.18	0.0
				3 mi (4.8 km)						
> 250	293.5	30.0	0.8	4.5	1.2	12.6	<1.9	<16.7	2.6	12.0
125-250	300.2	30.7	1.2	7.0	1.3	14.0	<1.8	<16.1	3.3	15.6
53-125	63.3	6.5	4.6	5.6	3.6	8.0	<3.3	<6.5	5.3	5.4
44-53	12.7	1.3	9.9	2.4	5.4	2.4	6.1	2.3	11.7	2.3
20-44	107.8	11.0	13.0	26.9	5.8	22.4	8.6	27.9	15.0	25.5
7-20	146.2	14.9	14.7	41.2	5.9	30.8	4.7	20.5	12.2	28.1
1.4-7	40.6	4.	12.0	9.2	5.4	7.7	7.0	8.5	13.1	8.3
<1.4	12.0	1.2	14.5	3.2	5.3	2.1	4.5	1.5	14.8	2.8
Soluble salts	2.2	0.2	<0.01	0.0	0.01	0.0	0.04	0.0	0.03	0.0
				4 mi (6.4 km)						
>250	254.7	26.0	1.2	5.9	1.3	12.1	<1.7	<12.3	3.5	16.7
125-250	380.1	38.9	1.4	10.5	2.1	47.0	<3.0	<32.6	3.4	24.2
53-125	113.5	11.6	3.5	7.8	2.7	11.0	<2.2	<7.2	4.1	8.8
44-53	13.2	1.3	8.4	2.1	4.5	2.1	4.0	1.4	8.3	2.0
20-44	85.4	8.7	15.0	25.0	5.8	18.1	9.4	22.8	11.4	18.2
7-20	52.3	5.3	20.0	20.3	6.6	12.5	7.9	11.7	12.9	12.5
1.4-7	54.8	5.6	20.3	21.8	5.3	10.7	5.7	8.9	12.3	12.7
<1.4	21.7	2.2	16.3	6.5	5.5	4.3	4.8	3.1	12.4	5.0
Soluble salts	2.1	0.2	0.02	0.0	<0.01	0.0	<0.04	0.0	<0.02	0.0
				5 mi (8 km)						
>250	489.9	49.7	1.4	14.5	1.2	31.1	<2.1	<31.5	2.3	25.4
125-250	305.6	31.2	1.4	9.1	1.4	22.8	<3.2	<30.3	4.2	29.2
53-125	68.5	7.0	4.2	6.0	2.5	9.3	<2.4	<5.2	4.0	6.3
44-53	10.8	1.1	8.3	1.9	4.8	2.6	<4.6	<1.5	7.1	1.8
20-44	36.5	3.7	17.8	13.7	6.2	11.9	6.9	7.9	12.0	9.8
7-20	32.2	3.3	34.9	23.9	5.8	9.8	13.1	13.0	16.7	12.3
1.4-7	27.2	2.8	39.9	23.2	6.0	8.8	9.9	8.5	17.2	10.7
<1.4	11.1	1.1	33.9	7.7	6.3	<3.6	<6.1	<2.1	17.8	4.5
Soluble salts	1.2	0.1	0.2	0.0	<0.01	0.0	<0.06	0.0	<0.02	0.0

particles in the larger size fractions (50% to 80% 125 μm and larger). Samples taken at 1-1/2 miles (2.4 km) and 2 miles (3.2 km) showed a much smaller size distribution with less than 10% larger than 125 μm. These locations corresponded to a run-off river plain which accounted for the large fraction of silty fine particles present. The soil particle size distribution data are shown plotted in Figure 15 on log-probability scales.

The activity density was greatest in the smaller size fractions, but when this activity was weighted by the actual mass of sample in each size fraction, the radionuclide concentration showed a bimodal characteristic peak concentration occurring in the 53- to 125-μm range and in the 7- to 20-μm range as shown in Figures 16 and 17, in which are plotted the distribution of ^{210}Pb on particles of soil.

The activity density of ^{210}Pb as a function of particle size at distances to 5 miles (8 km) is plotted in Figures 18 and 19. There is a significant difference in the distribution and concentration of ^{210}Pb as compared to ^{226}Ra at the 5-mile sample (Table 12). This might be due to the contribution of ^{210}Pb via the decay of airborne radon giving rise to relatively more ^{210}Pb associated with smaller particle sizes than those of ^{226}Ra. The percent of tailings in the various size fractions was calculated using the spectrum obtained from characterizing the tailings slurry, and those fractions are shown in Figures 20 and 21. These results show that the amount of tailings material in the greater than 250-μm, 125- to 250-μm, 53- to 125-μm, 44- to 53-μm-diameter particles decrease rapidly with distances out from the tailings pile while those particles in the 20- to 44-μm, 7- to 20-μm, 1.4- to 7-μm and less than 1.4-μm-diameter particles decrease out to 2 miles but increase at further distances. The minimum noticed at 2 miles for the smaller size fractions is believed to be due to the river flood plain. The large fraction of particles in the small size range appears to effectively dilute the radioactive particles at this distance.

Several random samples of tailings, soil, ore, and seepage water were taken around mill A and analyzed for radionuclides. These data are shown in Table 13. A perspective can be gained from data in this table of the relative importance of uranium and its daughter products present at various locations around the mill.

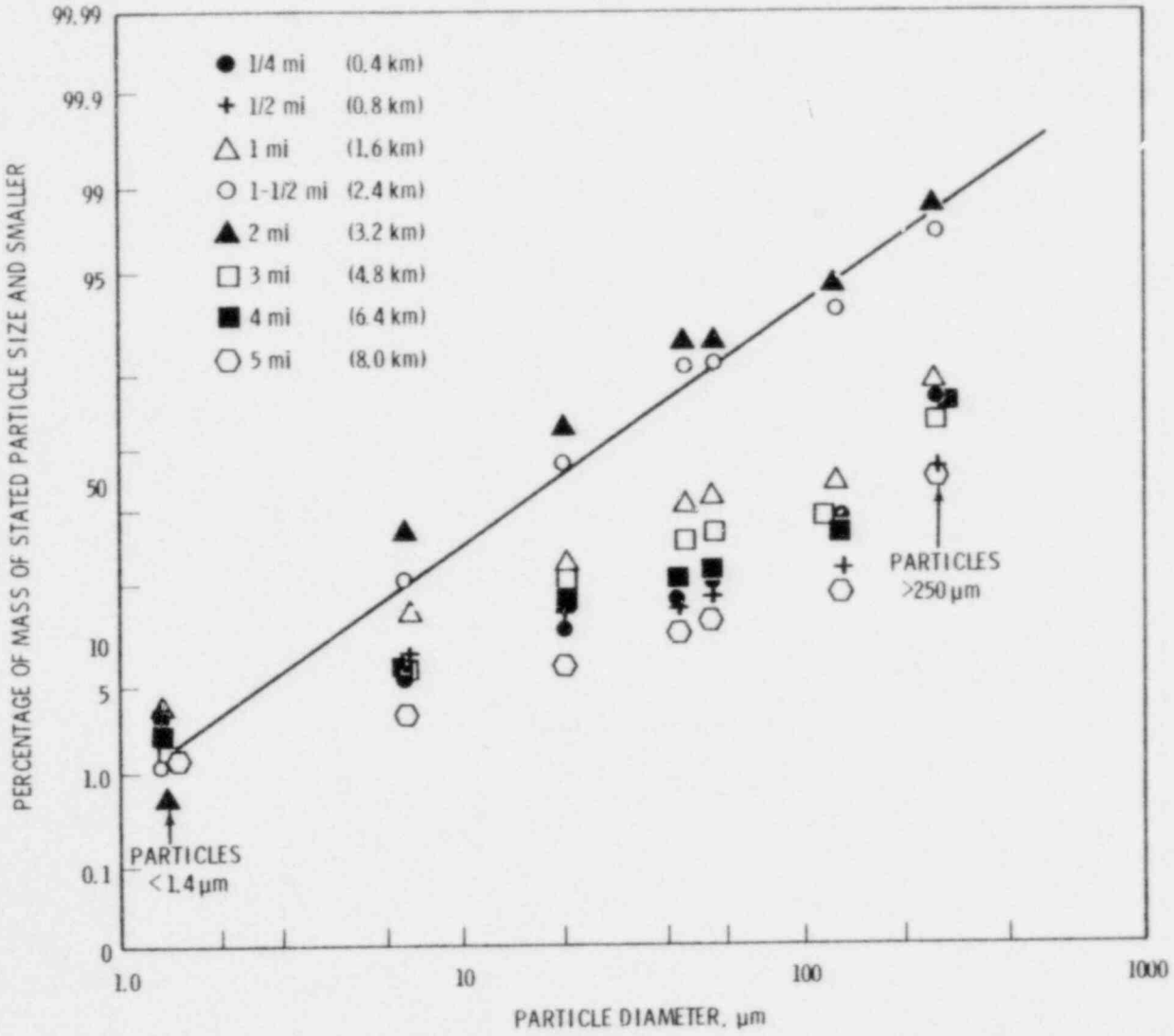

FIGURE 15. Soil Particle Size Distributions--Samples Taken Along a Line Running Due North of Tailings Pile A

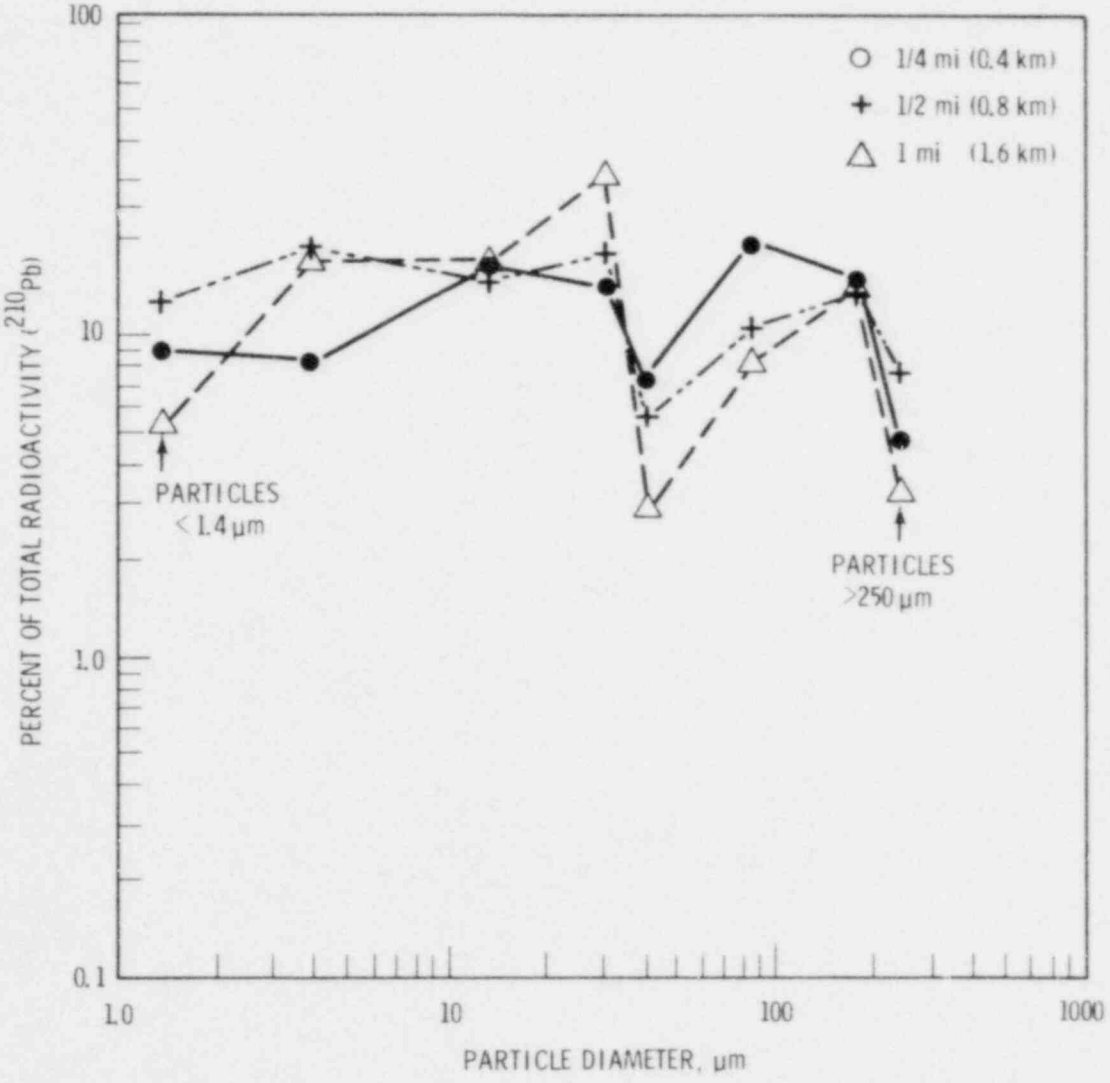

FIGURE 16. Percent of Total ^{210}Pb Radioactivity Associated with Particle Size Fractions. Soil samples taken from 1/4, 1/2, 1 mile (0.4, 0.8, 1.6 km) north of tailings Pile A

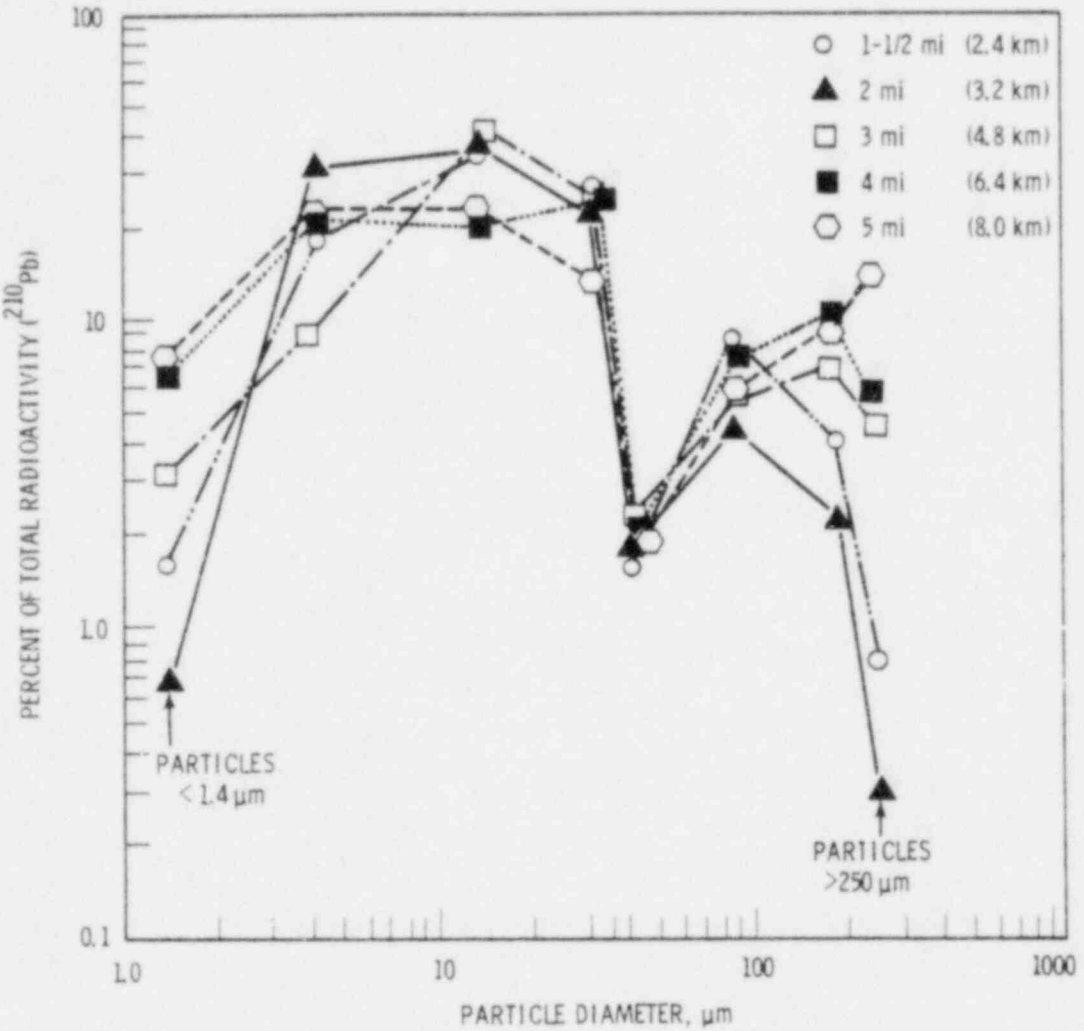

FIGURE 17. Percent of Total ^{210}Pb Radioctivity Associated with Particle Size Fractions. Soil samples taken from 1-1/2, 2, 3, 4, 5 miles (2.4, 3.2, 4.8, 6.4, 8 km) north of tailings pile A.

Acid Leach Plant C

A much less extensive sampling program was undertaken in the vicinity of the acid leach plant C. Surface samples were taken at points shown earlier in Figure 11. Sampling points were generally downwind from the tailings pile. These samples were analyzed for ^{226}Ra, ^{210}Pb, ^{230}Th, ^{238}U, and some limited particle size and activity-with-depth determinations were carried out.

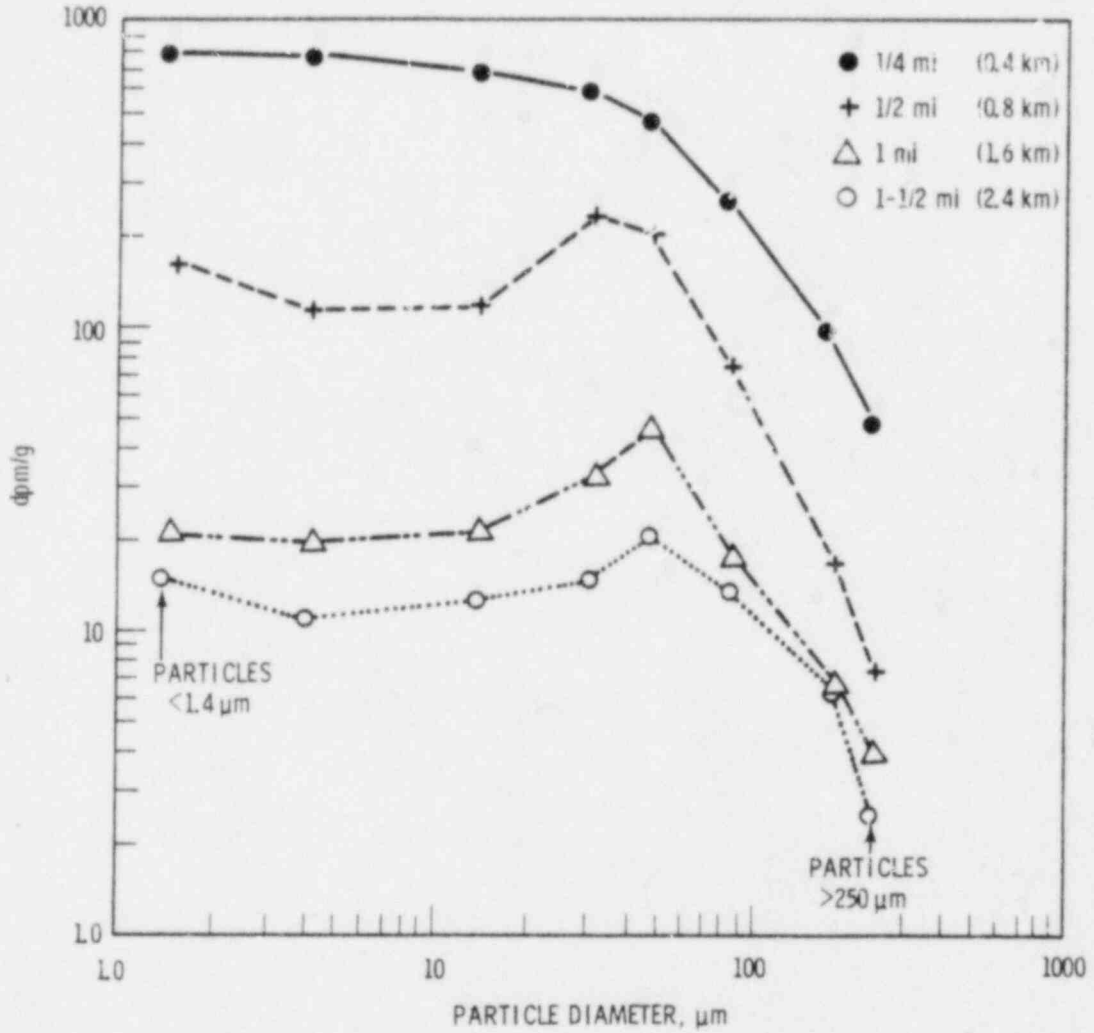

FIGURE 18. Activity Density dpm/g ^{210}Pb as a Function of Soil Particle Size at Distances of 1/4, 1/2, 1, and 1-1/2 Miles (0.4, 0.8, 1.6, and 2.4 km)

A sample was taken from the top 1 cm of surface soil at a distance of 1/2 mile (0.8 km) on a northeast compass heading. This crusted material was dried, pulverized in a somewhat arbitrary manner, and subjected to a size distribution analysis using a Bahco size classifier. The results of these measurements and the ^{210}Pb associated with the particle sizes are shown in Table 14.

These data would suggest that most of the radioactivity in this soil is associated with particles greater than about 10 µm in diameter. Whether there

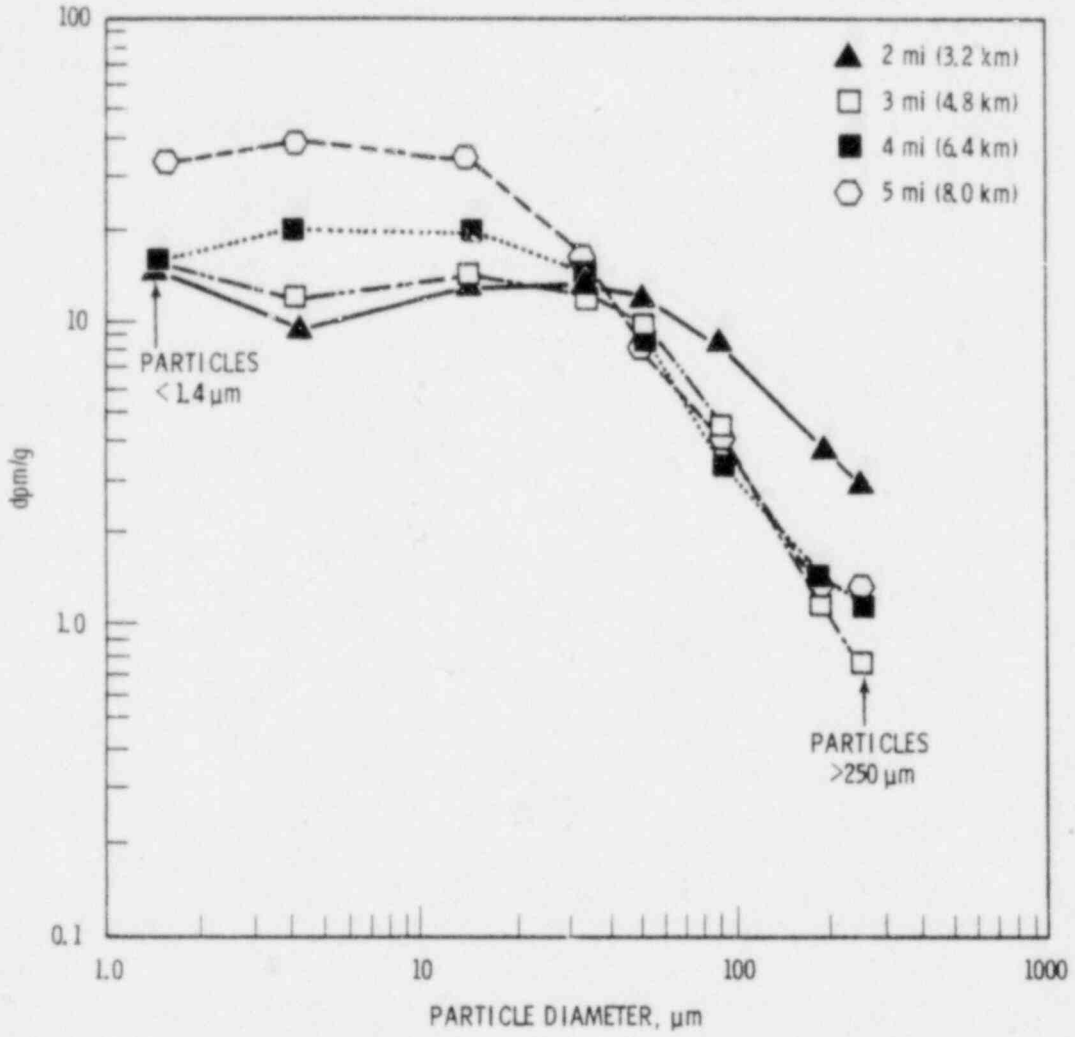

FIGURE 19. Activity Density dpm/g ^{210}Pb as a Function of Soil Particle Size at Distances of 2, 3, 4, and 5 Miles (3.2, 4.8, 6.4 and 8 km)

has been substantial modification of the tailings materials due to weathering or other effects is not known. The degree to which this sizing technique used separated very small particles from large particles was not determined, but data on particle sizing by wet sieving and sedimentation clearly showed a larger fraction than shown in Table 14 of the radioactive constituents associated with the smaller soil particles. The aerodynamic availability and mobility of particles for wind pickup may possibly as well be represented by the pulverized sample and air elutriation-gravity method for separation of

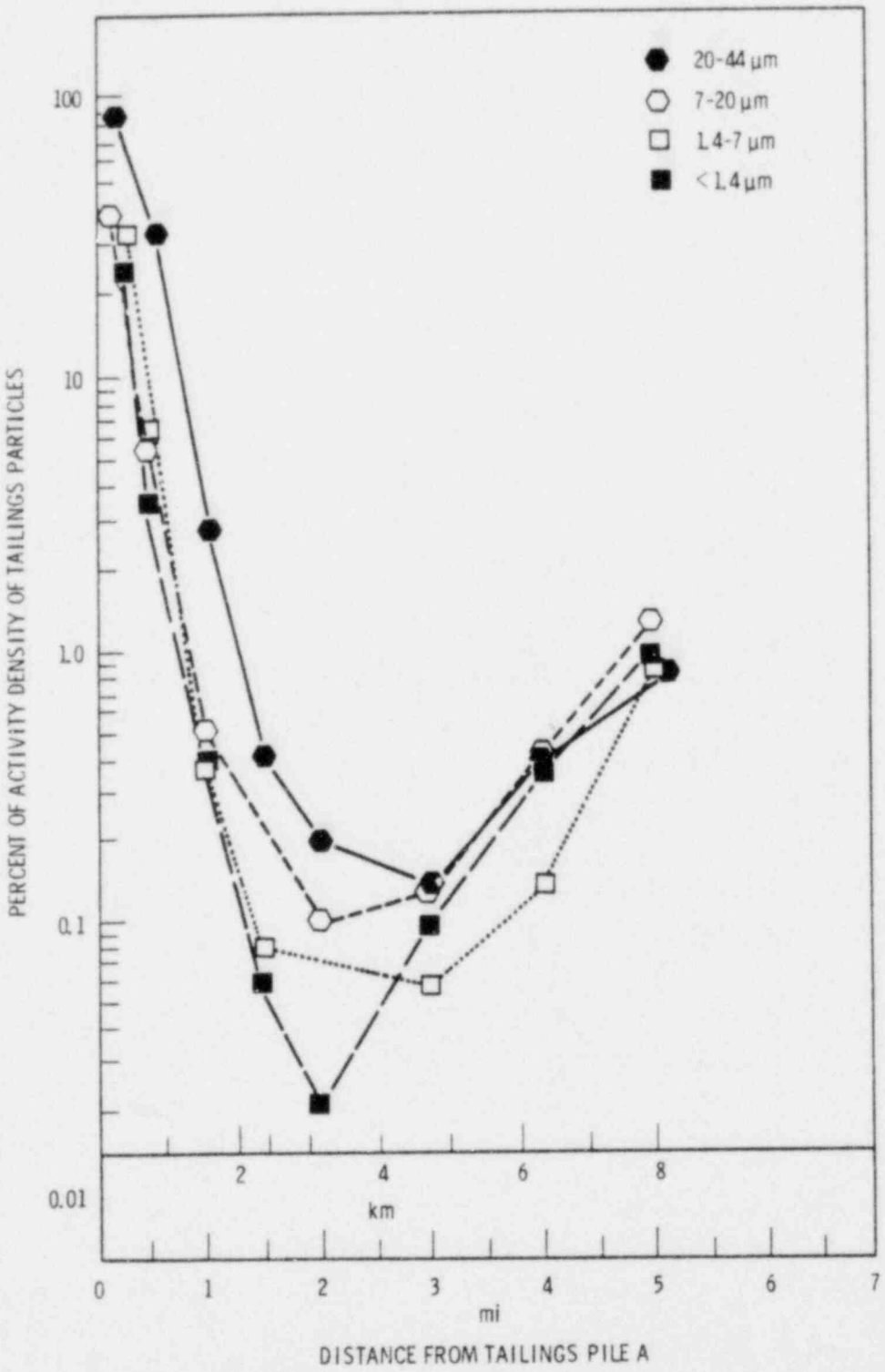

FIGURE 20. Percent of Activity Density of Tailings A Particles Found on Surface Soil Samples Taken at Distances North of the Site. Relationship with particle size fraction and distance: ≤1.4-44 µm particles.

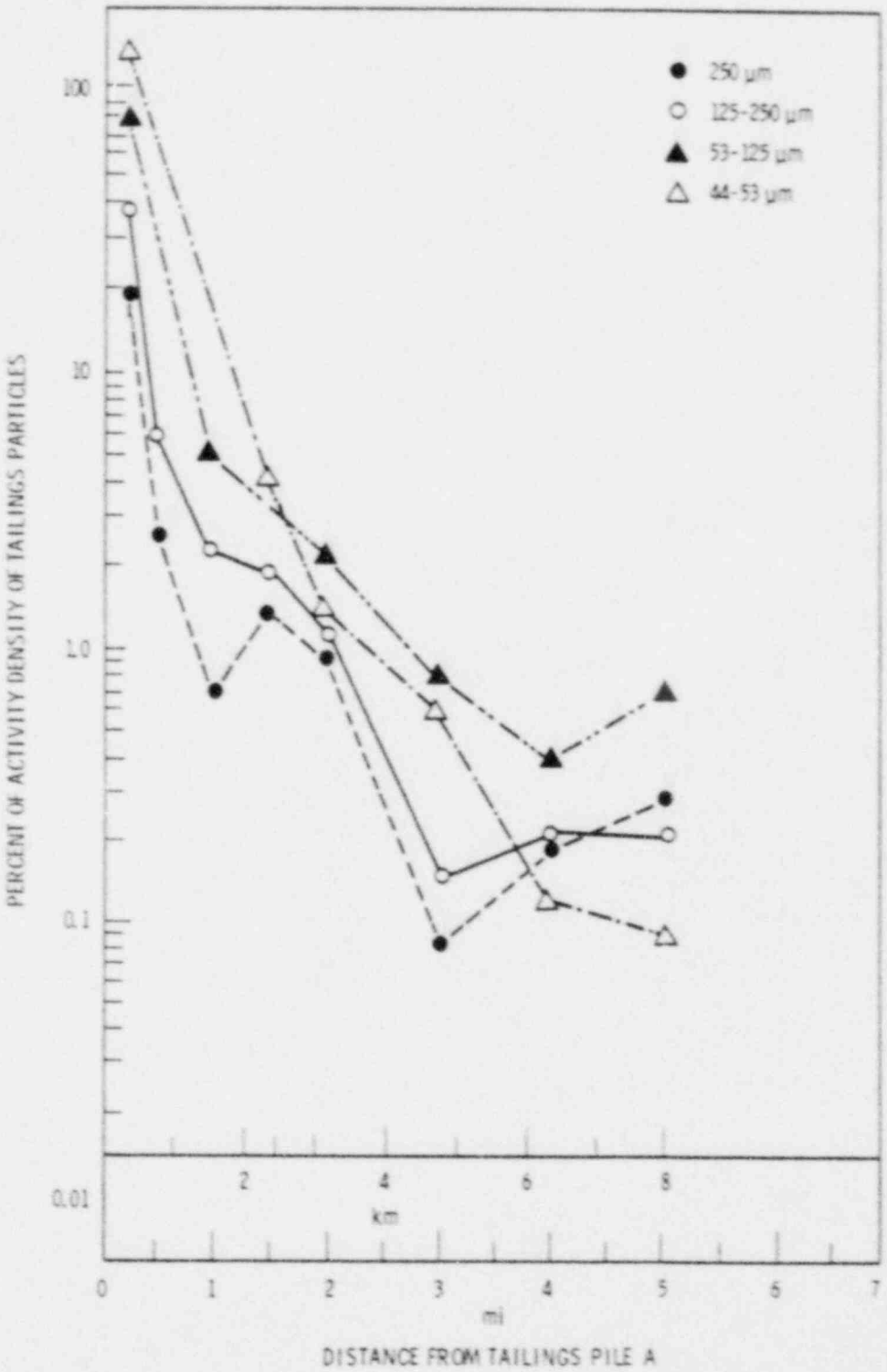

FIGURE 21. Percent of Activity Density of Tailings A Particles Found on Surface Soil Samples Taken at Distances North of the Site. Relationship with particle size fraction and distance: 44-≥250 µm particles.

TABLE 13. Radionuclide Concentration in and Around Uranium Tailings From Mill A in Ambrosia Lake, New Mexico (dpm/g or for water dpm/mℓ)

	^{226}Ra	^{210}Pb	^{230}Th	^{238}U
Mill A - Loading Area	412 ± 4	502 ± 11	398 ± 31	459 ± 7
Mill A - Salts Seepage Pond	<13	24.1 ± 8.9	<58	1330 ± 8
Mill A - Fine Tailings	335 ± 2.2	449 ± 6	313 ± 17	148 ± 2.4
Mill A - Fine Tailings	339 ± 2.2	529 ± 6	269 ± 17	31.2 ± 2.0
Mill A - ½ mi NW of Tailings	3.26 ± 0.36	12.3 ± 2.2	<8.1	4.11 ± 0.89
Mill A - ½ mi N of Tailings	586 ± 9	731 ± 22	500 ± 71	54.7 ± 8
Mill A - ½ mi NE of Tailings	92.4 ± 1.2	103 ± 3	77 ± 9	22 ± 1
Mill A - ½ mi E of tailings	265 ± 7	263 ± 16	271 ± 54	97 ± 7
Mill A - ½ mi N of tailings	403 ± 4	685 ± 24	462 ± 37	71 ± 7
Mill A - Dust Near Grinder	884 ± 2.8	889 ± 11	784 ± 28	922 ± 6
Mill A - Ore Composite	743 ± 4.7	847 ± 17	662 ± 42	651 ± 9
Mill A - Seepage H_2O North	<1.7	<2.57	<10.6	40.6 ± 1

TABLE 14. Particle Size Distributions and ^{210}Pb Concentrations[a] in Surface Soil in the Vicinity of Tailings Pile C

Size Fraction	Surface Soil[a] wt%	^{210}Pb dpm/g	Total dpm/g in Fraction	dpm/g in Soil / dpm/g in Tailings
>100	78	38	30	0.05
10-100	21	180	38	0.20
3-10	0.37	440	1.6	0.26
1-3	0.18	490	0.9	0.24
<1	0.05	460	0.2	0.30

(a) One-half mile northeast of tailings pile.

sizes. Current understanding of the relationships between resuspension and the detailed nature of soil, discrete particle properties and atmospheric processes does not allow a reliable prediction of airborne particle sizes and amounts raised from a complex surface such as the soils in question.

Samples of soil collected in the vicinity of tailings pile C at distances out to 1-1/2 miles (2.4 km) were analyzed for uranium and uranium daughter products. Figure 22 shows surface soil concentrations of ^{210}Pb, ^{226}Ra, and ^{238}U over the sampling network surrounding tailings pile C. The concentrations of ^{226}Ra, ^{210}Pb, and ^{230}Th in the top centimeter of soil at distances out to 1-1/2 miles are similar to those measured at mill A; however, the concentration of ^{238}U is much higher and in many instances approaches that of the daughter products. We conclude that some of the material is associated with ore dust from the large amount of mining industries near the mill or with natural outcroppings containing significant uranium. For example, at 1-1/2 miles along the north intersect, the concentration of ^{226}Ra, ^{210}Pb, ^{230}Th, and ^{238}U were 23, 26, 16, and 19 dpm/g, respectively.

The distribution of ^{210}Pb with depth in the soil is shown in Figure 23. Activity per gram decreases with depth roughly exponentially. A possible indication of a subsurface source exists at the sample point 0.5 miles from the tailings pile, since the concentration is greater at 2 and 4 cm than at 1 cm.

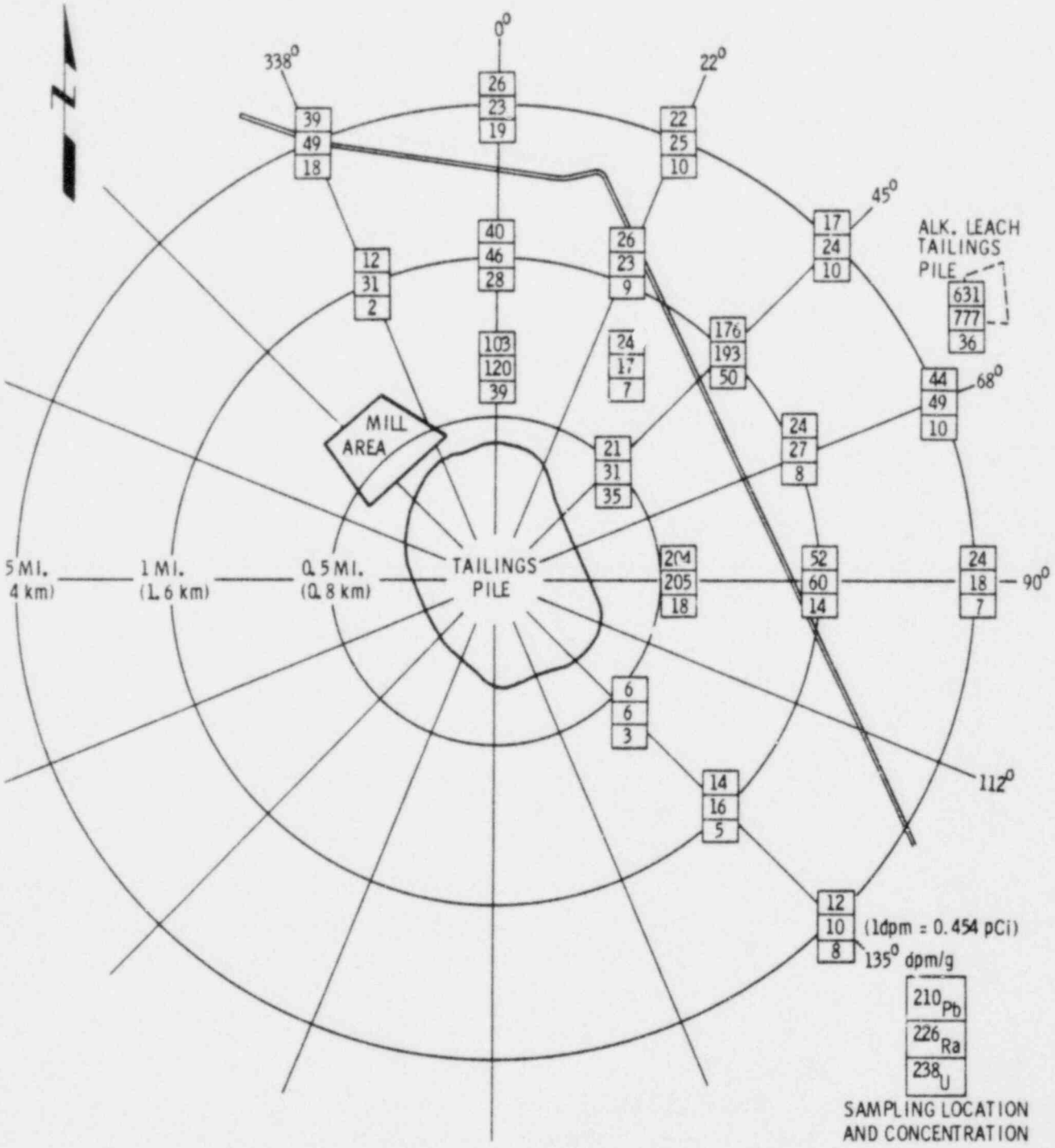

FIGURE 22. Surface Soil Concentrations of ^{210}Pb, ^{226}Ra, and ^{238}U in the Vicinity of Site C

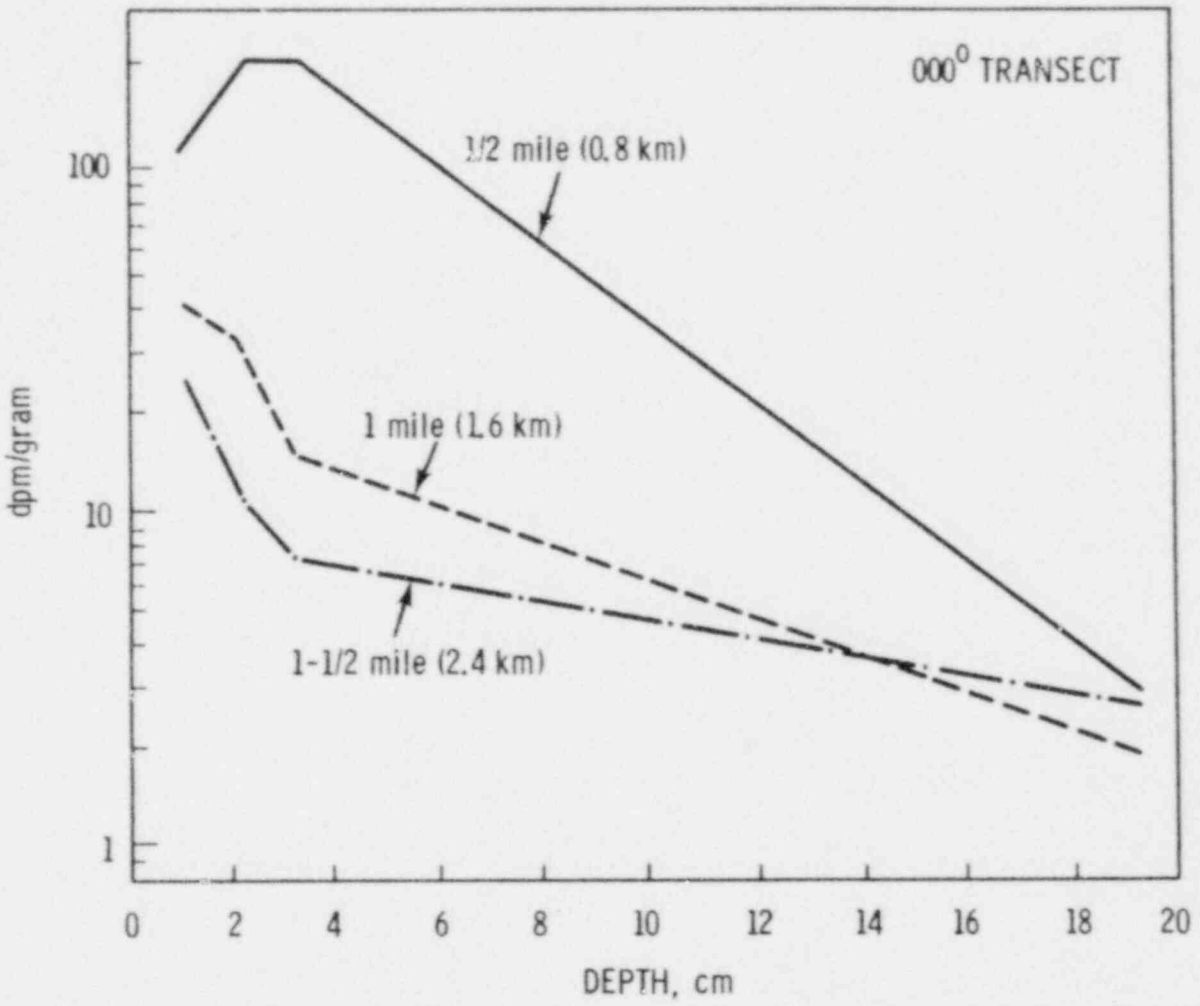

FIGURE 23. ^{210}Pb Concentrations in Soil as a Function of Depth and Distance from Site C.

Mixing or covering with lower concentration material in constructing ponds or other disturbances may have caused this. The half thickness is about 2 cm for the initial part of the distribution based on profiles at 1 mile (1.6 km) and 1-1/2 miles (2.4 km). At depths greater than about 4 cm, the concentration decreases at a slower rate.

Some random samples of water, ore near the mill, and soil about 1 mile (1.6 km) to the east were taken in and around the tailings pile C. These samples were analyzed for uranium and daughter products. Results are shown in Table 15.

TABLE 15. Radionuclides in and Around Tailings Pile C (dpm/g) or (dpm/ml)

Sample Type	^{226}Ra	^{230}Th	^{210}Pb	^{238}U
Main Tailings Area	350	300	550	70
Main Tailings Area	350	3300	500	175
Main Tailings Area	300	450	400	50
Water on Tailings	1	1100	120	75
Water Evaporation Pond	1	1050	60	15
Ore	1100	1000	1300	1100
1 Mile (1.6 km) East of Tailings	35	50	45	--

There is considerable disequilibrium between ^{230}Th, ^{226}Ra, and ^{210}Pb, both in tailings material and in water from the evaporation ponds on this tailings material. This major fractionation in radionuclide concentration which exists within tailings areas will be reflected in the suspension of tailings material along with fugitive ore dust down wind from these areas. The tailings material associated with soil at 1 mile (1.6 km) from the tailings pile contained uranium daughter concentrations that were up to 10% of those in some areas of the tailings pile.

SUMMARY AND CONCLUSIONS: TASK B

Particles containing uranium and daughter product radionuclides are readily detected on soil samples within several kilometers from both alkaline leach and acid leach tailings piles. At the alkaline leach plant A, the ^{226}Ra in soil will emit about 20% of the radon currently emitted from the tailings pile itself.

Surface layers of soil (1 to 2 cm) contain much higher concentrations than deeper layers of soil. At distances beyond about 4 miles (6.4 km) the decrease with depth is much less, but at these distances background concentrations are being approached. Soil particles classified by a wet sieving and sedimentation method showed the radioactive material present to be associated with all particle size fractions with a large fraction associated with soil particles less

than 125 μm in diameter. A clearly bi-modal distribution of fractions of ^{210}Pb associated with particle size increments was shown with one mode centering on about 7 to 20 μm and the other mode centering on about 100 to 150 μm.

Soil modification by river flood action was manifest in flood-plain regions. These regions showed unusually large fractions of particles in the 7- to 20-μm range.

The results of Task B show clearly the long-term deposition of tailings particles in the vicinity of the uranium mills. In principal, these concentrations in soil could be reconciled with transport and deposition models. At this writing, the overall study has not accounted for the concentrations of radionuclides found in the environment through the use of deposition and transport models.

TASK C. NATURE AND QUANTITY OF WINDBLOWN PARTICLES FROM AN ACTIVE TAILINGS PILE

Principal Investigator: G. A. Sehmel

INTRODUCTION

The interim report on this study described a series of field experiments carried out at tailings pile A to determine the flux and nature of particles moving from the tailings pile as a function of wind speed (Schwendiman et al. 1979). Emphasis in the first field studies of this task was placed on determining particle flux on the tailings pile itself and in the downwind vicinity of the tailings pile. The field experiments did include some more distant downwind measurements of airborne particles concentrations. The experiments were designed to establish the mass leaving the tailings pile per unit time in various particle size ranges and to determine the associated radionuclides on the particles. The dilution with distance was also measured. The reader is directed to the interim report for the detailed field experiment design and data developed. A great many samples were taken and the particle flux determined under various wind conditions. The results did not disclose a clear-cut relationship between wind speed and particle flux. In fact, we were able to show that from one side of the tailings pile to the other the flux during the same period would be highly variable. These and other observations brought out the very complex nature of the suspension process and the practical difficulties in measuring close-in fluxes and the quality of particles suspended.

The second field program of Task C, discussed in this report, was designed to measure particles airborne from the same tailings pile, but with more emphasis on particle fluxes at distances further downwind from the tailings pile. More consistent, directly applicable results were anticipated by focusing on the particles being transported at a distance of about 200-m downwind from the tailings pile.

The end objective was to determine the quantity and nature of particles transported per unit time as a function of wind speed at downwind distances. The scope of the task also emphasized identification of radionuclides and

stable elements associated with the airborne particles. The data were to be used in testing dispersion and deposition models (see Task D).

EXPERIMENTAL

Sampling Array

A new sampling array was designed and installed near the tailings pile A and in the terrain generally north (downwind) of the tailings pile. The location and description of the elements of the sampling array are shown in Figures 24, 25, and 26. To orient the reader, the original array of sampling towers and stations used to obtain the data presented in the interim report is shown in Figure 24. The former array included a windvane-anemometer station at an 8-m elevation and upwind of the tailings pile (at site A). This was also the background sampling station. Three sampling towers were located on the west half of the tailings pile (inactive) and were designated sites B-1, B-2, and C. Nine sampling stations were located along the north property-line fence. Other sampling stations were located on the land across the east-west road north of the plant.

For the study to be reported here, several changes were made in the locations of the sampling stations. The new locations are shown in Figures 25 and 26. Site A still remained as the background station. The windvane-anemometer station from which "start" and "stop" signals were sent to the sampling stations was relocated to site E about 150-m north of the tailings pile perimeter. Sampling towers were erected at D-1, D-2, and E, on which were mounted high-volume isokinetic samplers at elevations of 0.3 m, 1.5 m, 3 m at D-1 and D-2, and at 0.3 m, 1.5 m, 3 m, 12 m, and 15 m at E. Three samplers were mounted at each elevation. One at each elevation was activated when the wind was 3 to 5 m/sec; the second was activated when the wind was 5 to 7 m/sec; and the third was activated when the wind speed was 7 to 11 m/sec. The activating signals were initiated by the anemometer. All wind-speed signals (u) were transmitted only when the wind direction was in a preselected sector (θ). The signals controlled 110-volt samplers at sites A, D-1, D-2, E, and the nine on the north fence line. Self-contained remote stations designated R-1, R-2, R-3,

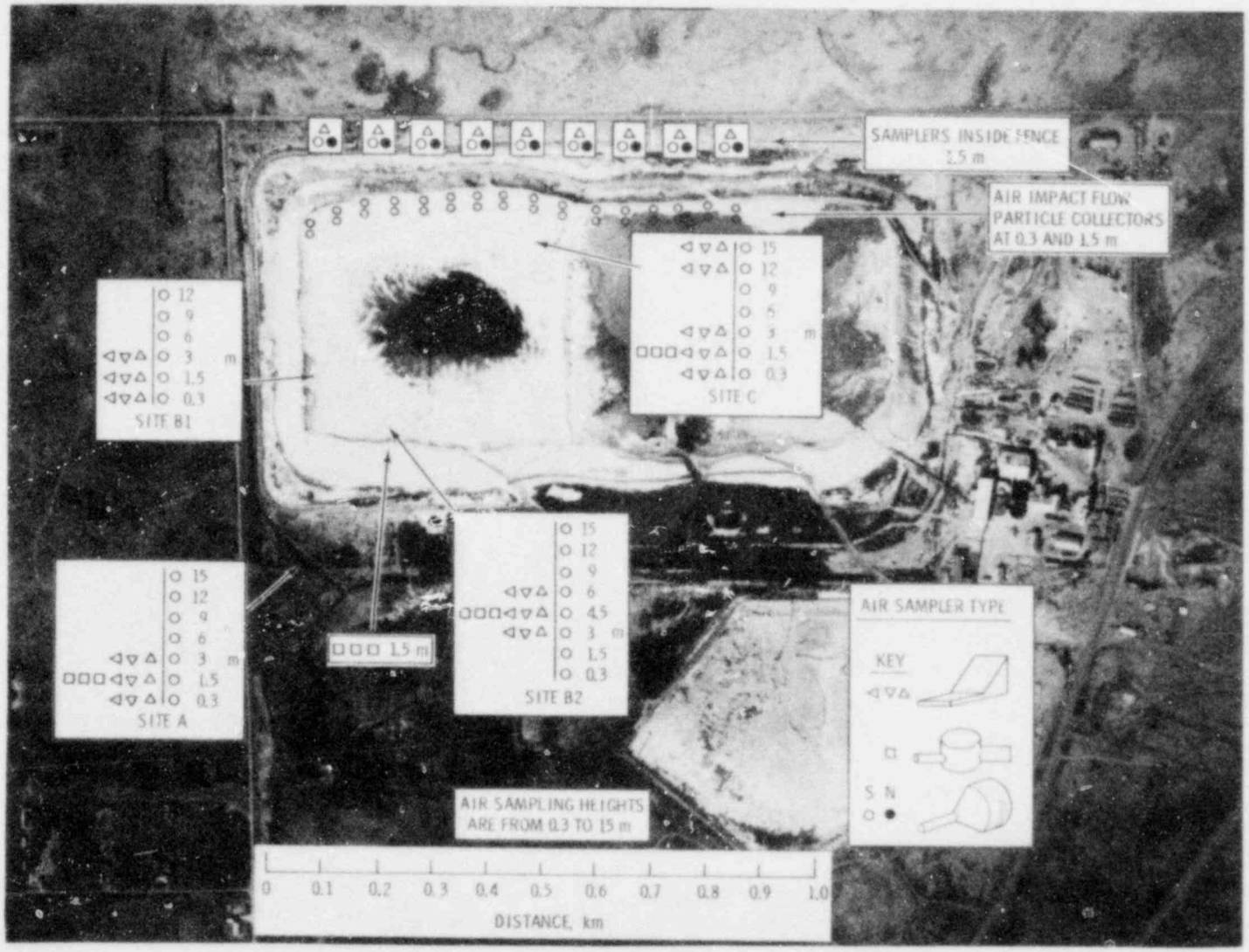

FIGURE 24. Air Sampling Arrays (7808002-1)

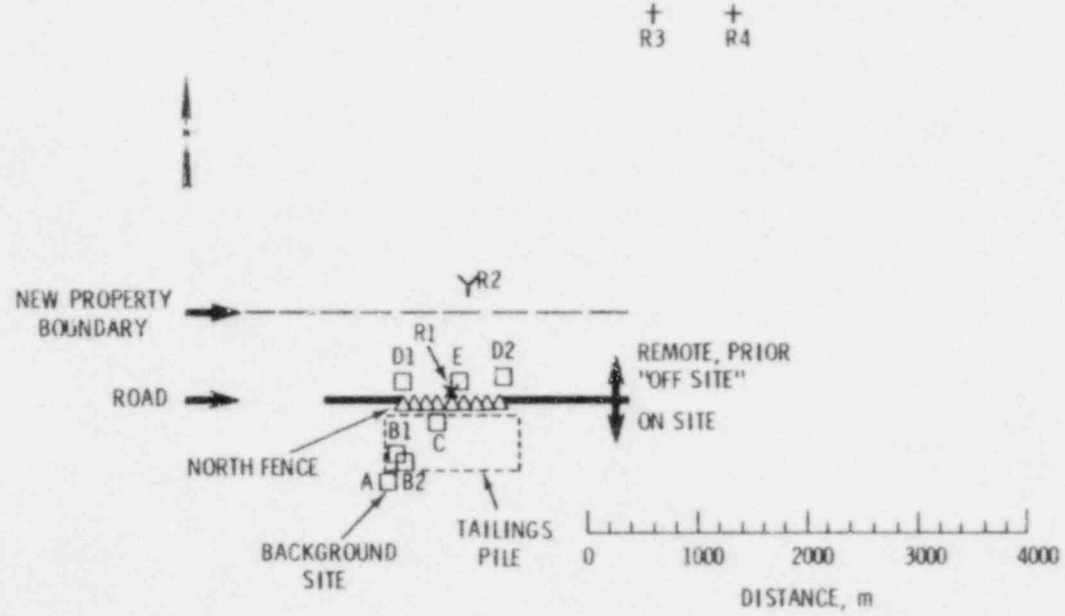

Δu, Δθ AIR SAMPLERS

□ f(Δu, Δθ)

△ f(MAX Δu, Δθ)

ALL u AIR SAMPLERS

× f(ALL u, $\Delta 90^0$) R1

Y f(ALL u, $\Delta 60^0$) R2

\+ f(ALL u, $\Delta 15^0$) R3, R4

FIGURE 25. Nomenclature and Locations of Electrically Powered Airborne-Particulate Samplers (80B731-2)

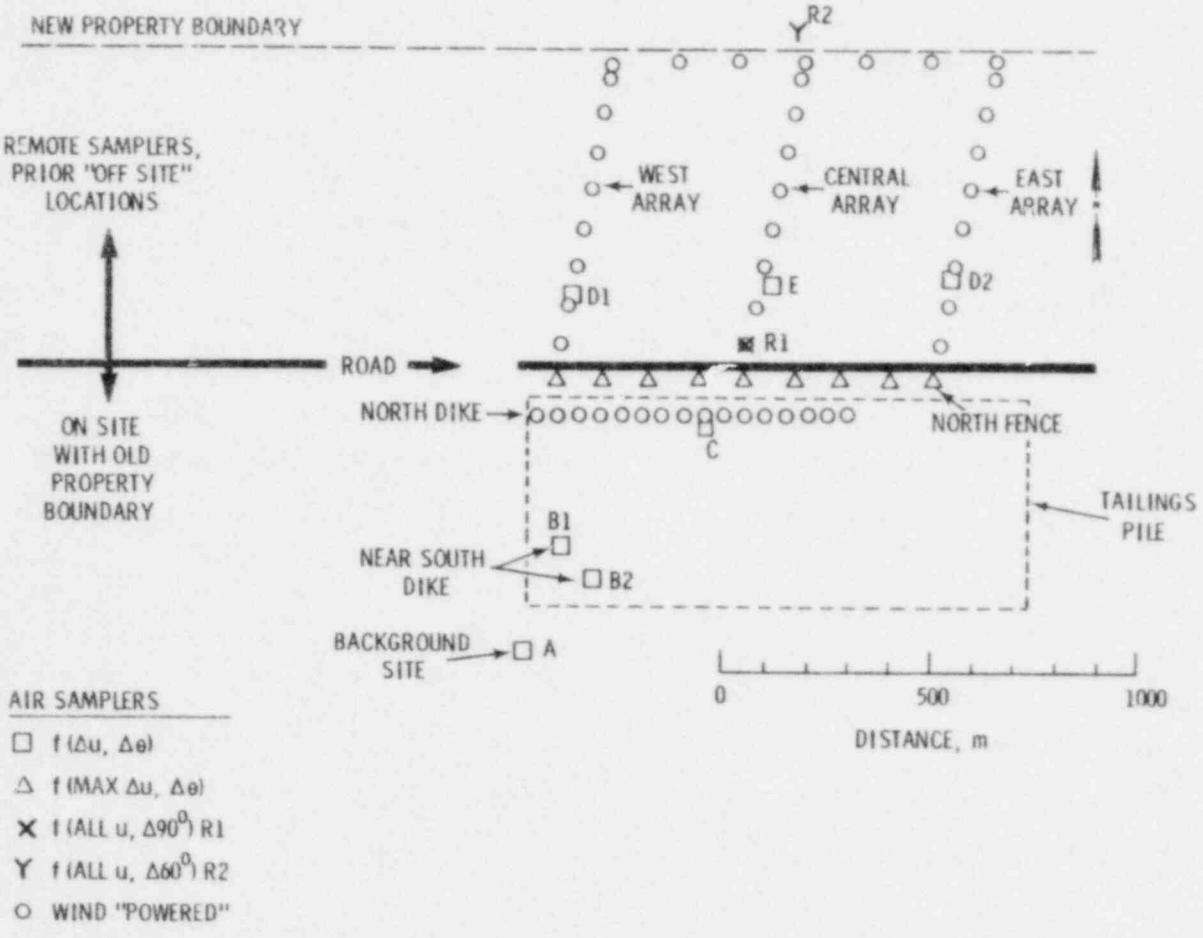

FIGURE 26. Nomenclature and Locations of Airborne-Particulate Samplers (80B731-1)

and R-4 operated for all wind speeds but only when the local wind direction was in the selected sector from the tailings pile, i.e., 90^{o}, 60^{o}, 15^{o}, and 15^{o}, respectively.

The high-volume samplers and other samplers employed are described more fully in the following section.

Particle Sampling Equipment

Airborne particulates were collected using electrically powered (see Figure 27) and inertial or wind-powered samplers (see Figure 28). The electrically powered samplers were the prime sampling instrumentation, whereas inertial samplers were used primarily as an index of relative horizontal flux changes in the cross- and downwind directions. The electrically powered samplers were either large-volume isokinetic air samplers or particle cascade impactors with a cyclone preseparator. The airflow rate through the isokinetic samplers was 1.3 m^3/min, and the airflow rate through the particle cascade impactors was 1.1 m^3/min. The airflow accuracy was $\sim\pm$10%.

Both the isokinetic samplers and the cyclone-cascade, particle-impactor, electrically powered systems were automatically activated with electrical control signals that opened an inlet on each of the samplers. When the control signal was off, inlets were automatically closed.

Airborne particulates were classified into two or more size fractions with both sets of electrically powered samplers. For the isokinetic samplers, particles either settled in the sampler inlet or were collected on a backup 20- x 25-cm filter. The relative collection efficiency on the inlet versus filter as a function of particle diameter was not determined. Aerodynamic considerations indicate that essentially all respirable particles would be collected on the filter. The relative collection site for nonrespirable particles within the sampler is a function of particle diameter as well as the isokinetic sampler used. Some differences in fractional collection on isokinetic sampler inlet transition and filter for these larger particles are expected since the internal geometries of the isokinetic samplers were different for the three wind-speed increments. Geometry differences might allow gravity settling to be relatively more important in the inlet. Geometry

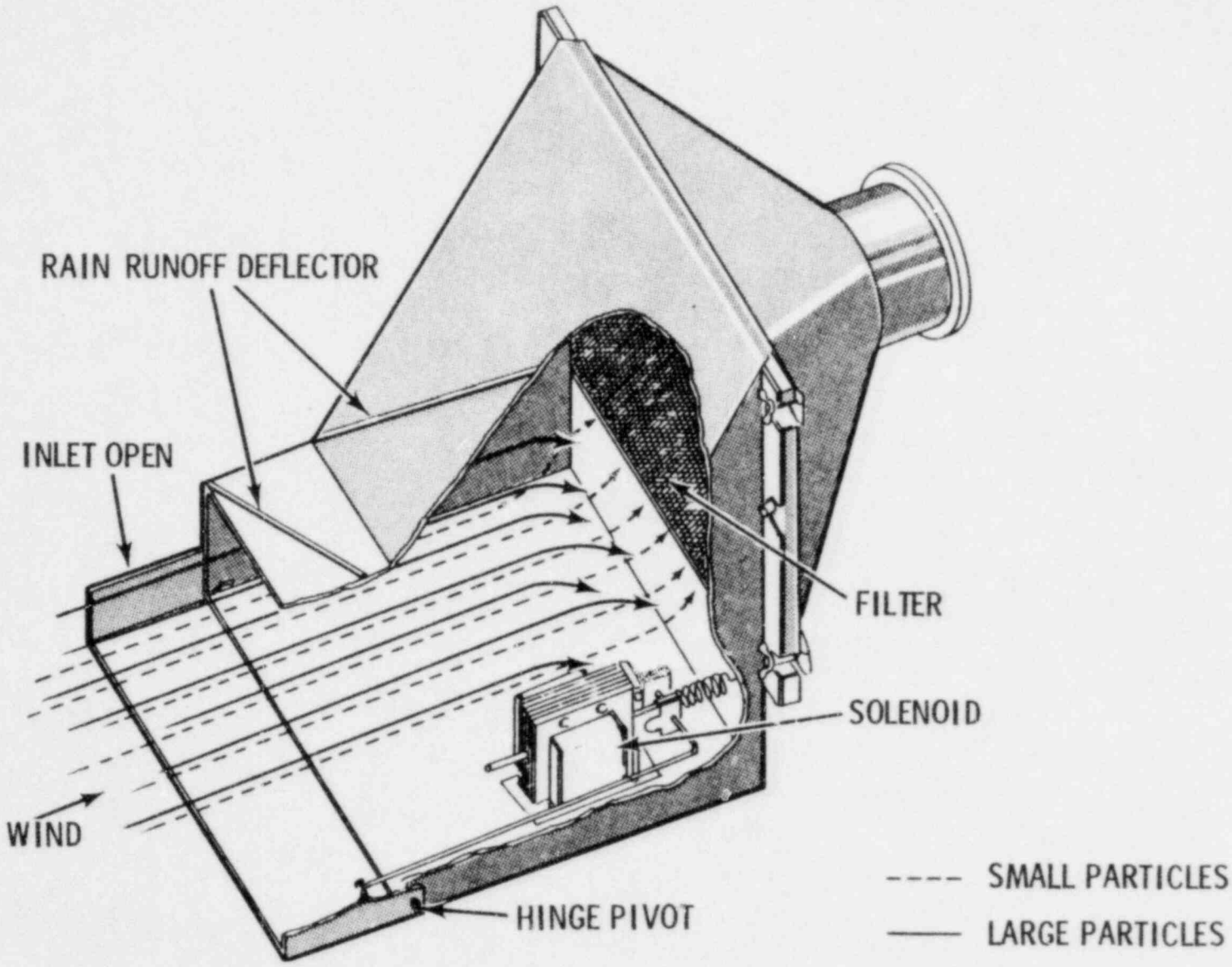

FIGURE 27. Isokinetic Sampler - Inlet Open (7711495-9)

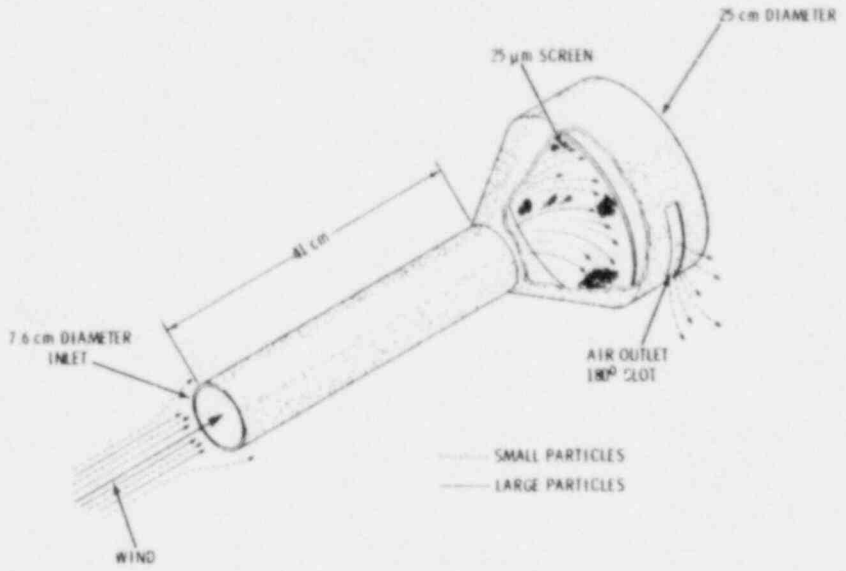

FIGURE 28. Inertial and Impact Pressure Sampler (7807917-3)

differences reflected the three wind speeds sampled, which were 3 to 5, 5 to 7, and 7 to 11 m/sec. For all three wind-speed increments, the isokinetic sampler width was held constant; only the inlet depth was changed in order to obtain isokinetic sampling at the average increment wind speed.

More complete size distribution data were obtained with particle cascade impactors. The cascade impactor was Model 235 manufactured by the Sierra Instrument Company.(a) A cyclone preseparator (Model 230CP) preceded the particle cascade impactor; the effective cutoff diameter was 6 µm. Thus, all nonrespirable particles should have been collected within the cyclone preseparator. For the particle cascade impactors the 50% cutoff diameters for each collection stage were, respectively, 7.2, 3, 1.5, 0.95, and 0.49 µm AED. Particles 0.49 µm diameter were collected on the impactor backup filter.

The nonelectrically powered air samplers used inertia of the particles driven by the wind and are described in detail in the interim report (Schwendiman et al. 1979). These samplers consisted of an open 3-in. tube

(a) Sierra Instrument Company, P.O. Box 909, Carmel Valley, CA 93924

pointing towards the selected direction with a funnel-shaped exit 10 in. in diameter. Airborne particles wind driven into the tube inlet were collected in the tube or upon a 25-μm screen. Relative airborne horizontal solid fluxes for "large" particles were determined with these samplers.

The Sampling Run

Following the deployment of samplers and checking of equipment, a field experiment was initiated by activating the sampling array. Performance of the sampling array was checked several times a day and observations made concerning operation. The array was turned off automatically when rain fell and was reactivated when the sensing element was dry. Running time meters at each sampling site were read to determine operating hours for like samplers. The duration of the run was determined through judging sampler mass load and equipment reliability. Sampling runs and results to be discussed are listed in Table 16 for airborne solids and stable elements and in Table 17 for airborne radionuclides.

At the end of the run all samplers were carefully removed from the towers and the collected samples recovered. Particles in the inlet sections of the isokinetic samplers and inertial samplers were transfered to containers and their weight determined. Filters were removed and reweighed.

Prior to the start of a second run all samplers were cleaned, and new filters or other collectors were mounted. The assemblies were then mounted at the appropriate location.

Radionuclide Measurement

Samples were submitted for gamma spectroscopic analyses which were conducted in PNL laboratories in Richland, Washington. The equipment and methods employed were the same used in Task B and are described in Appendix A.

Airborne Stable Element Concentrations

Airborne stable element concentrations were investigated at the on-pile location site C and at remote sites R-2 and R-4. Analysis was by x-ray fluorescence. Samples were collected at site C with a virtual cascade impactor

TABLE 16. Sampling Times and Results to be Presented

Sampling Period	Airborne Solids							Stable Elements
	Mass Loading, g/m^3		Mass Flux, $g/(m^2\ day)$			Erosion Threshold Speed	Particle Size Distr.	Airborne Concent. ng/m^3
	Filter Collect.	Filter + Inlet	Isokinetic Inlet	Particle Diameter	Inertial Collector			
Aug. 10 Oct. 12 1977								X
Mar. 30 Apr. 17 1978					X		X	
May 26 June 16 1978							X	
June 28 Aug. 8 1978					X			
Feb. 24 Apr. 24 1979	X		X		X			
Mar. 8 Apr. 18 1979	X	X						
Apr. 27 May 7 1979	X	X	X			X		
Apr. 27 July 9 1979					X			
May 15 July 9 1979	X		X					X

TABLE 17. Radionuclide Results to be Presented (^{235}U, ^{238}U, ^{230}Th, ^{226}Ra, ^{214}Pb and ^{210}Pb)

Sampling Period	Activity Density dpm/g	Activity Ratios	Airborne Concen. $\mu Ci/cm^3$
Mar 30 Apr 17 1978	X	X	
Mar 8 Apr 18 1979	X	X	X
Apr 27 May 7 1979	X	X	X
Apr 27 July 9 1979	X	X	X
May 15 July 9 1979	X	X	X

(Model 243 Virtual Impactor, Sierra Instrument Company), and particles collected on the <3.5-μm-diameter stage were analyzed. At remote sites R-2 and R-4, airborne particles were collected in cyclone preseparators and particle cascade impactors.

RESULTS

Results are reported for airborne solids, airborne stable elements and airborne radionuclides. The time periods for which airborne solids, radionuclides and stable elements were investigated are shown in Table 16. For airborne solids, airborne mass loadings, g/m^3, airborne mass fluxes, $g/(m^2\ day)$, and particle size distributions were determined. Mass loadings were calculated from isokinetic sampler filter mass collections and also filter plus inlet mass collection. Mass fluxes were calculated from mass collection within isokinetic sampler inlets and from inertial particle collectors. Particles from these collectors are identified as "nonrespirable." Particle size distributions were

determined with particle cascade impactors. In addition to the indicated data, relative mass collection on the filter (mainly respirable) versus filter-plus-inlet collection was also calculated. Results are presented as the percent of airborne solids collected on the filters.

Also shown in Table 16 are time periods for which stable element concentrations were determined. Airborne stable element concentrations were determined during the first time period using the virtual cascade impactor. For the last time period, stable element concentrations were determined using five-stage particle cascade impactors with cyclone preseparators.

The time periods for which airborne radionuclides were investigated are shown in Table 17. Airborne radionuclide concentrations were determined for ^{235}U, ^{238}U, ^{230}Th, ^{226}Ra, ^{214}Pb and ^{210}Pb. Airborne radionculide concentrations, $\mu Ci/cm^3$, were determined (except for ^{214}Pb due to subsequent in-growth) for particles collected on filters in the isokinetic samplers and also within five-stage particle cascade impactors. Radionuclide concentration on airborne solids, dpm/g, were determined for particles collected on filters in the isokinetic samplers, particles collected within the cascade particle impactors, and particles collected within the inertial particle collectors.

In addition to radionuclide concentrations, radionuclide activity ratios were determined to investigate relationships between radionuclide daughter products. Radionuclide activity concentrations of ^{238}U, ^{230}Th, ^{226}Ra, and ^{214}Pb were normalized to the ^{210}Pb radionuclide activity. In addition, the $^{214}Pb/^{210}Pb$ activity ratios were calculated. Activity ratios significantly less than unity for $^{214}Pb/^{210}Pb$ are an indication that reported ^{210}Pb concentrations are for ^{210}Pb collected during field sampling rather than from radon daughter product decay during the period between sampling and analyses.

Data for each time period will be discussed separately. These data include calculated results for airborne solids, airborne stable elements, and airborne radionuclides. The three most complete data sets are for sampling times from March 8 to July 9, 1979. Of these the data set from April 27 to May 7, 1979 is most extensive and, hence, will be discussed in detail first. Based upon this discussion, data sets for other periods will be discussed in less detail. The remaining two data sets will be discussed in chronological

order. Subsequently, the remaining data sets will be discussed. These subsequent discussions include radionuclide data obtained along the north bank with inertial particle collectors in 1978.

April 27 to May 7, 1979

Mass Loading

Airborne mass loadings (mg/m^3) are shown for this most extensive data set sampling period in Figure 29. During this sampling period, wind direction ($211^o \pm 35$) and wind-speed increments (3 to 5 m/sec, 5 to 7 m/sec, and 7 to 11 m/sec) were used for controlling sampling times for airborne particulate samplers.

There are six individual subfigures within Figure 29 corresponding to sites A, north fence, D-1, E, D-2, and remote. Each subfigure will be discussed separately from left to right, i.e., as the wind and airborne pollutants are transported from upwind background concentrations at site A, across the pile, and finally as particle concentrations decrease in the "remote" regions downwind. This order of data presentation from upwind background to downwind remote gives a visual "snapshot" of the airborne impact of suspended uranium mill tailings from the pile.

At site A airborne mass loadings for both filter collection and filter-plus-isokinetic-inlet collection are shown as a function of sampling height and the three different wind-speed increments. Mass loadings range from 3×10^{-5} to 1×10^{-4} g/m^3, i.e., 30 to 100 $\mu g/m^3$, a reasonable range for background air. Mass loadings are nearly uniform as a function of height and show an undefined variation as a function of wind speed.

Airborne mass loadings increase across the tailings pile. As shown in the second subfigure, airborne mass loadings increase as indicated by airborne mass loadings along the north fence. These data were obtained for the entire wind-speed increment from 3 to 11 m/sec as compared to the three wind-speed increments shown in the first subfigure. Along the north fence, airborne mass loadings increase by up to one order of magnitude above background mass loadings at site A.

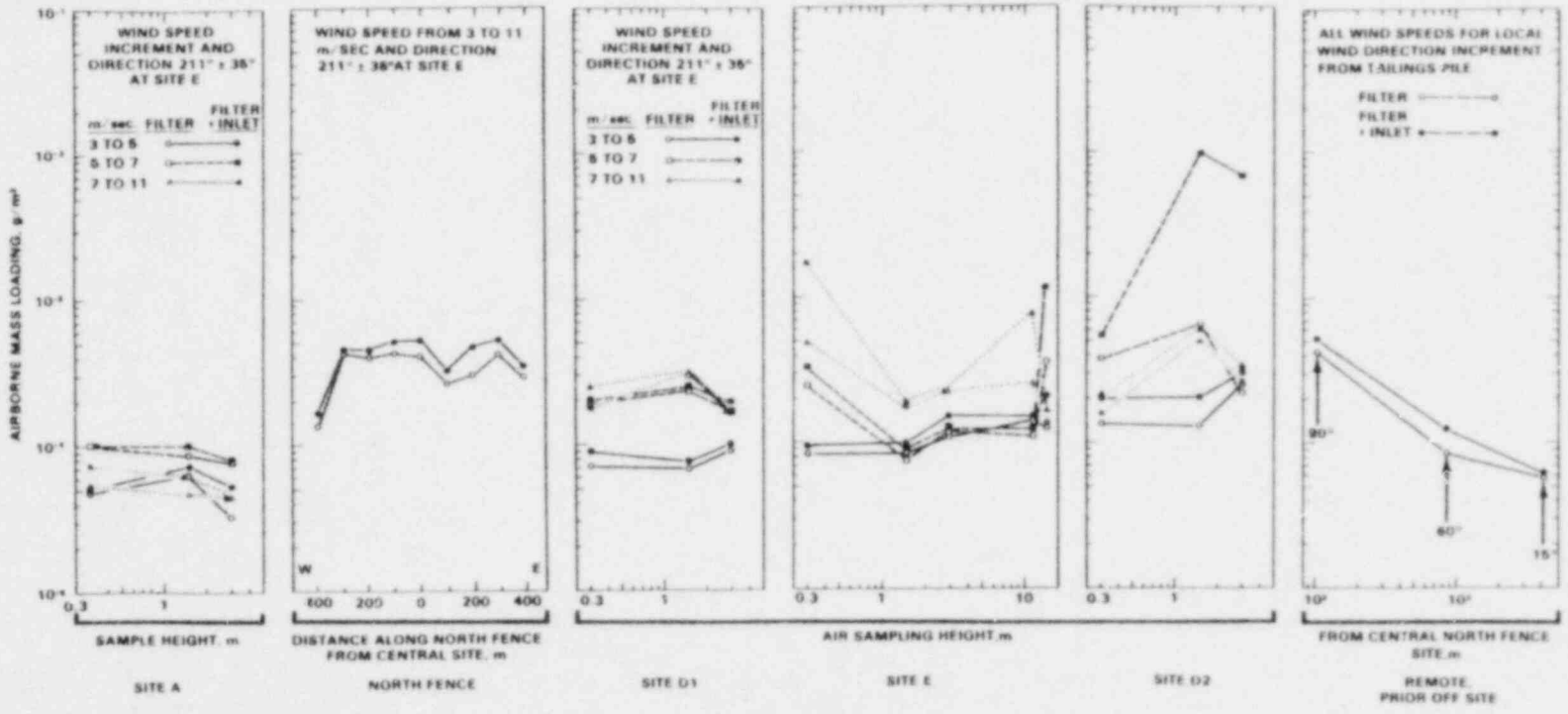

FIGURE 29. Airborne Solid Concentrations at Each Site During April 27 to May 7, 1979 (80B236-2)

In the next three subfigures, data for sites D-1, E, and D-2 show airborne mass loadings variations as a function of height, wind-speed increment, and crosswind distance. Similar to results reported in the interim report, airborne mass loadings are a complex function of wind speed. Indeed, for results in Figure 29, maximum mass loadings at site D-2 were for the intermediate, 5 to 7 m/sec wind-speed increment. These maximum airborne mass loadings resulted from "large" particles collected in the isokinetic sampler inlets at 1.5- and 3-m heights. From these data, we conclude that the maximum airborne plume concentrations were passing above uppermost sampler heights.

Data for the remote sites are shown as a function of distance from the central north fence sampling site in the sixth subfigure. Sampling times at these sites were for all wind speeds for the indicated wind direction sector, approximately encompassing the wind direction coming from the pile towards each sampling site. Data for sampling site R-1 are shown as the 90^{o} wind-direction sector, R-2 as 60^{o}, and R-3 and R-4 as 15^{o}. Airborne mass loadings decrease with increasing distance from the north fence and tend to approximate background mass loadings at site A for distances greater than about 1 km.

Airborne Fluxes and Loadings

In Figure 30, "inlet" airborne mass fluxes, $g/(m^2 \cdot day)$, for material collected within the isokinetic air sampler inlet are shown along with "filter" airborne mass loadings from Figure 29. These mass fluxes were calculated from the cross-sectional area of the isokinetic-sampler inlet and wind speed.

Although these "inlet" airborne mass fluxes are a simple recalculation of data shown in Figure 29, mass fluxes are shown for several reasons:

- to make cross-comparisons with mass fluxes shown later for particles collected in inertial particle collectors;
- to be able to estimate the total suspension source strength from either mass fluxes or from airborne mass loadings multiplied by average wind speed (either value must then be multiplied by the available cross-sectional area--pile width multiplied by plume height);

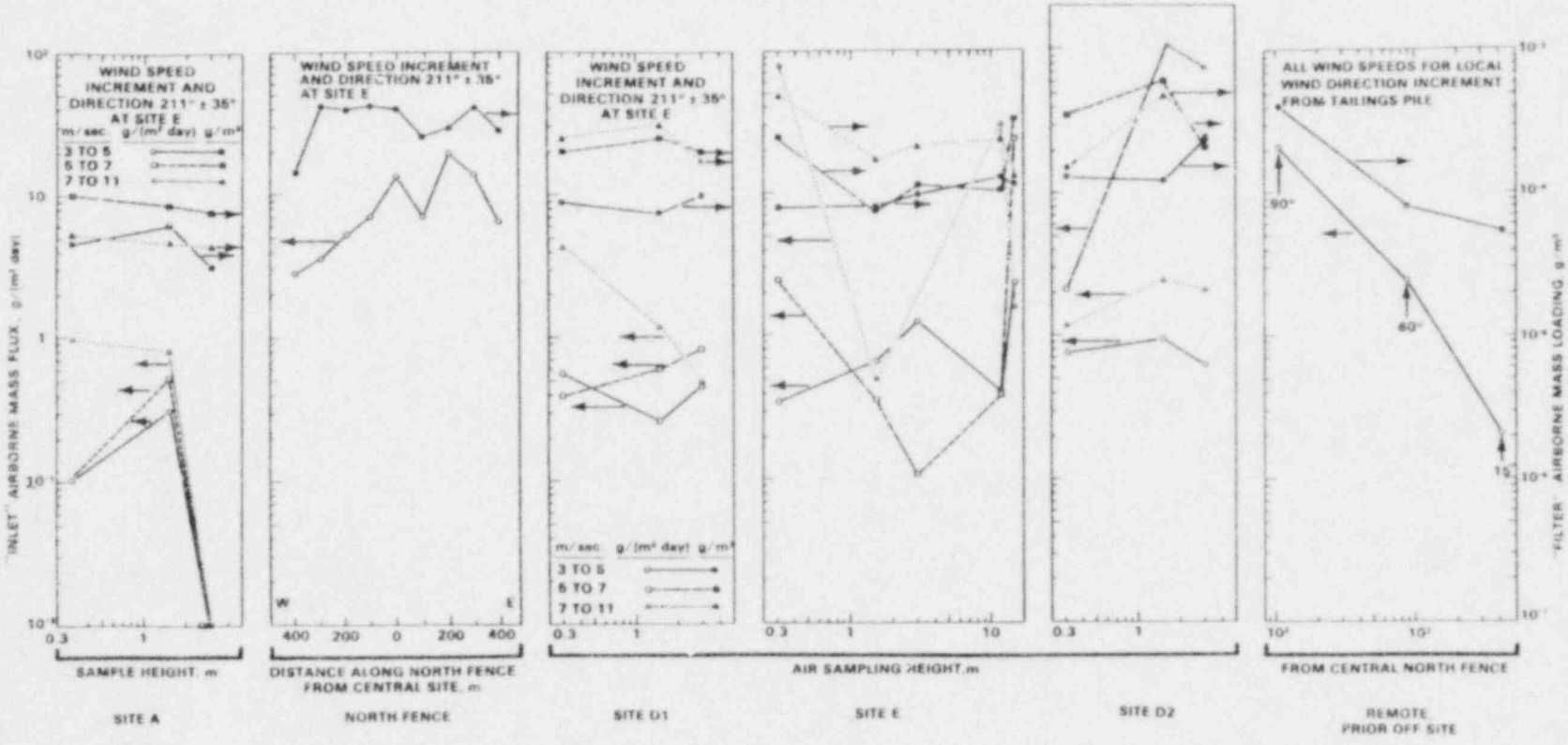

FIGURE 30. Average Airborne Fluxes and Concentrations During April 27 to May 7, 1979 (80B236-55)

- to improve predictive accuracy since calculation accuracy is often minimal if mass fluxes are directly estimated from numerical differences between solid and open data symbols from Figure 29.

The "inlet" airborne mass flux data in Figure 30 will be discussed in detail. At sampling site A, mass fluxes increased with increasing wind speed. Although mass fluxes increased, the data are too limited to determine with confidence the wind-speed dependency. Along the north fence, airborne mass fluxes increased 1 to 2 orders of magnitude above background at site A. At sites D-1, E and D-2, the mass flux wind-speed dependency becomes more complex. Mass fluxes at sites D-1 and E are usually greatest for the 7 to 11 m/sec wind-speed increment. However, at site D-2 mass fluxes are greatest for the intermediate wind-speed increment of 5 to 7 m/sec. For the remote sites, mass fluxes decrease rapidly with distance. The decrease is a function of particle diameter as exhibited by "large" particles being collected in the isokinetic sampler inlet and "small" particles being collected on the filter. The inlet particle mass flux decrease with distance, X, is a power function, $X^{-0.6}$. In comparison, the "filter" airborne mass loading decrease with distance is proportional to $X^{-1.3}$. The larger exponent, -1.3 compared to -0.6 for the "large" inlet particles, may be caused in part by the higher deposition velocities for "large" inlet particles as compared to smaller deposition velocities for "small" filter-collected particles.

Relative Collection Site

The relative collection sites of "small"-diameter, filter-collected particles versus total airborne particle collection within isokinetic samplers are shown in Figure 31. Airborne solids collected on the filter are shown as a percentage of total solids collected on the filter plus isokinetic sampler inlet. In most cases, over 70% of the solids are collected on the filter. The principal exceptions are the data for the highest wind-speed increment, 7 to 11 m/sec, at site D-2.

Threshold Speed

An expanded sampling effort was made at site E to determine the airborne mass loading wind-speed dependency and consequently, wind erosion dependency

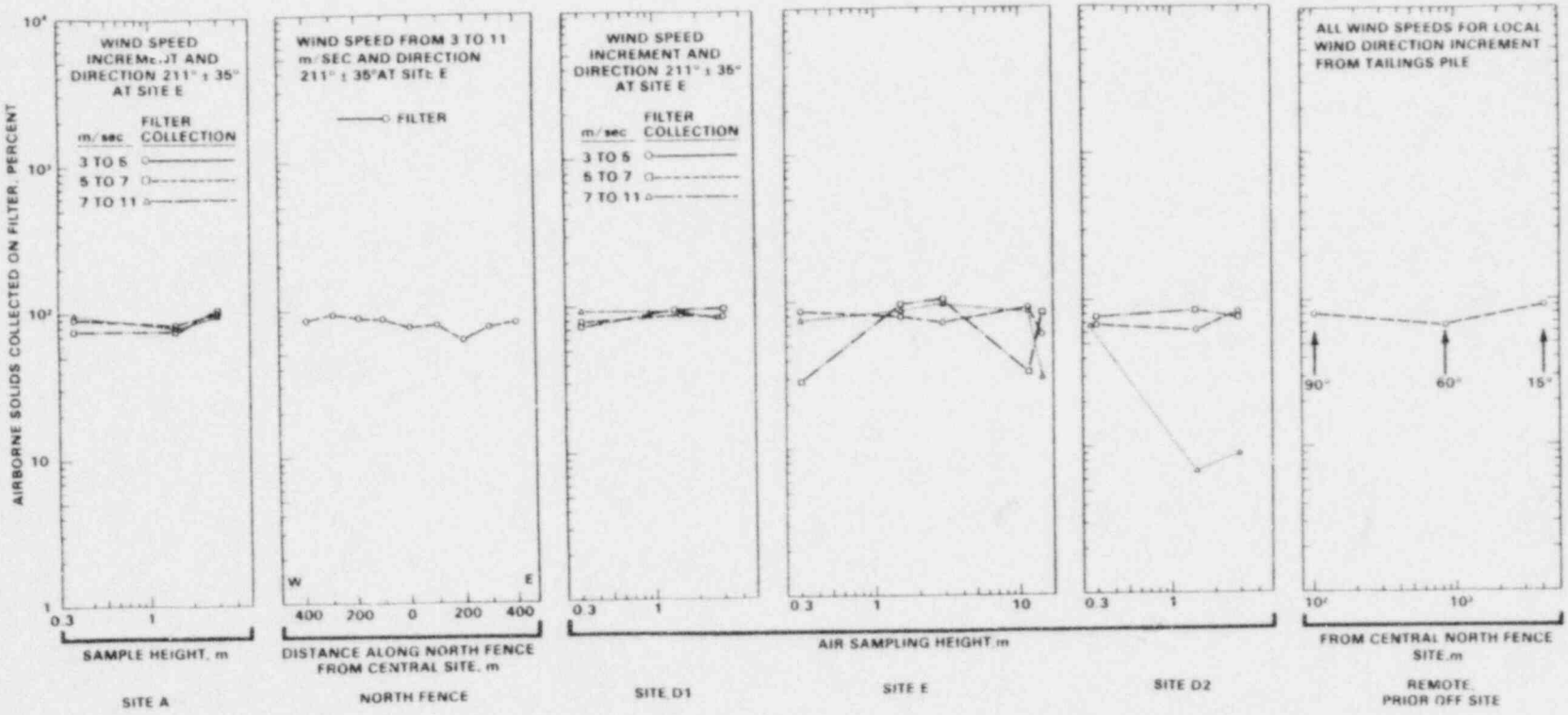

FIGURE 31. Percent Airborne Solids Collected on the Filter at Each Site During April 27 to May 7, 1979 (80B236-24)

on wind speed. Airborne particulates were collected during six rather than three wind-speed increments. Both lower and higher wind speeds were investigated. The additional wind-speed increments were 0.5 to 3 m/sec, 11 to 13 m/sec, and 13 to 15 m/sec. In addition to investigating the wind-speed dependency, airborne mass loading was also investigated as a function of particle-diameter increments. For particle sizing, cyclone preseparators and particle cascade impactor systems were used; each system sampled one of the six wind-speed increments. In order to improve the particle sizing accuracy, the first collection stage of each particle cascade impactor was coated with silicon oil to minimize particle bounce-through to succeeding collection stages and backup filter. Airborne mass fluxes will be reported for the 1) entire particle cascade-impactor collection, minus the first stage, 2) for the cyclone preseparator collection, and 3) for the total cyclone preseparator plus particle cascade-impactor collection minus the first stage.

Airborne mass loadings, g/m^3, are shown in Figure 32 as a function of six wind-speed increments and as a function of the solids collection site within the cyclone preseparator-particle cascade impactor systems. The wind-speed increments for each data point are shown only for the circle symbols showing the impactor, minus first stage, solids collection. Airborne mass loadings were minimum for the 5 to 7 m/sec wind-speed increment. This 5 to 7 m/sec wind speed may be an index of a "threshold" wind speed above which wind erosion occurs rapidly from the mill tailings pile. Of course, this apparent "threshold" wind speed has caveats; particle dry deposition and diffusion occur between the mill tailings pile and the samplers, and the wind speed at site E may not be the same wind speed occurring on the mill tailings pile. The apparent "threshold" wind speed of 5 to 7 m/sec is supported by agricultural wind erosion data. For agricultural erosion, the threshold velocity is often reported in the range of 10 to 12 miles/hr, i.e., 4.5 to 5.4 m/sec. The differences between 4.5 to 5.4 m/sec and 5 to 7 m/sec are considered negligible compared to spatial variations of wind speed.

Airborne mass loadings for wind speeds less than the "threshold" wind speed continue to increase as wind speed decreases. Obviously, there must be some wind speed below which airborne mass loadings must be constant or

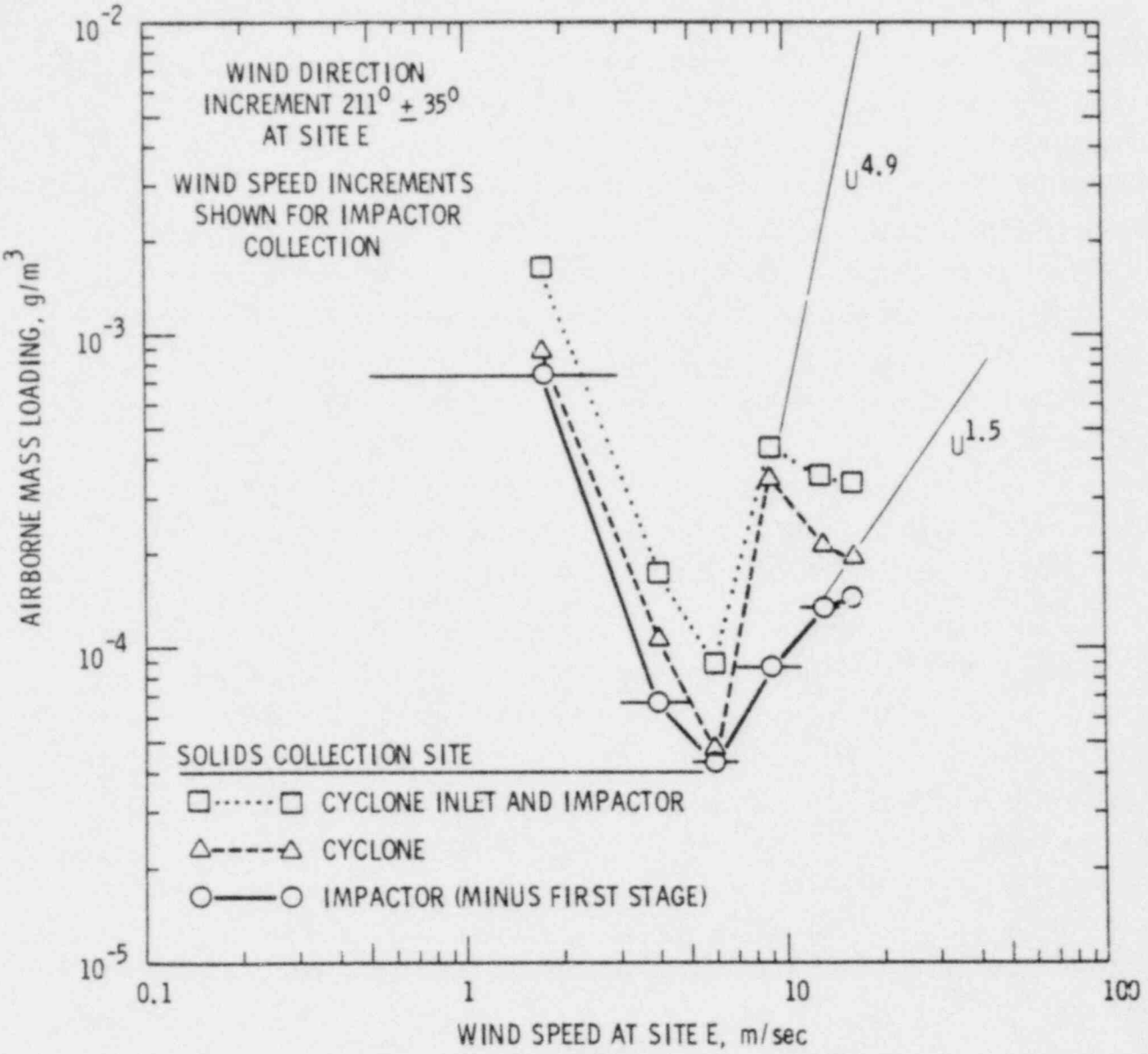

FIGURE 32. Airborne Solid Concentrations at Site E as a Function of Wind Speed During April 27 to May 7, 1979 (80B378-79)

decrease. For the lowest wind-speed increment investigated, an average mass loading of 10^{-3} g/m^3, or 100 µg/m^3, is indicated. Compared to many unpolluted areas, this is a high airborne mass loading and may reflect the presence of airborne solids arising from the mill tailings pile. For wind speeds above the "threshold" wind speed, there are two airborne mass loading wind-speed

dependencies as a function of particle size. For respirable particles collected in the particle cascade impactor, airborne mass loadings increase approximately as a power of wind speed, $U^{1.5}$. A line corresponding to a $U^{1.5}$ slope is drawn on the graph. Similarly, for nonrespirable particles collected in the cyclone preseparator, a line is drawn as a power of wind speed, $U^{4.9}$. However, for nonrespirable particles the airborne mass loadings do not continually increase with increasing wind speed. Above an 11 m/sec wind speed, airborne mass loadings of nonrespirable particles tend to be constant or decrease with increasing wind speed.

Radionuclide Activity Density on Airborne Solids

Selected airborne particulate samples were analyzed for ^{235}U, ^{238}U, ^{230}Th, ^{226}Ra, ^{214}Pb, and ^{210}Pb radionuclide content. Sample selection for radionuclide analysis was based on a decision, after sample weighing, that sufficient airborne solids were collected for radiochemical results to be above radiochemical detection limits. Not all samples were analyzed. Sufficient solids were required to suggest the activity on collected solids was above the blank glass-fiber filter activity. These did not include samples from background site A since insufficient solids were collected. Measured radionculide activities (disintegrations per minute, dpm) were normalized by the amount of solids collected on each sample. Activity densities, dpm/g, were calculated. Activity densities will be shown with confidence limits corresponding to the 1σ limit for radiochemical analysis. In some cases, confidence limits are not shown since the limits would be within the data symbols as plotted. In other cases, the radionuclide activity was less than radiochemical detection limits. Activity densities calculated from these less-than numbers are shown plotted as a datum symbol with an arrow pointing down towards smaller numerical values. Calculated results from the radionuclide data will be presented first for ^{235}U and then for the ^{238}U decay series.

Uranium-235, dpm/g. Activity densities for ^{235}U are shown in Figure 33. Most of these results were calculated from "less-than" radiochemical detection limit data as indicated by the arrows. Nevertheless, the data are sufficient to show ^{235}U was wind-eroded from the tailings pile. The largest activity densities were measured at site D-2 and occurred during the lowest wind-speed increment. Surprisingly, the next highest activity density was measured nearly 4000 m

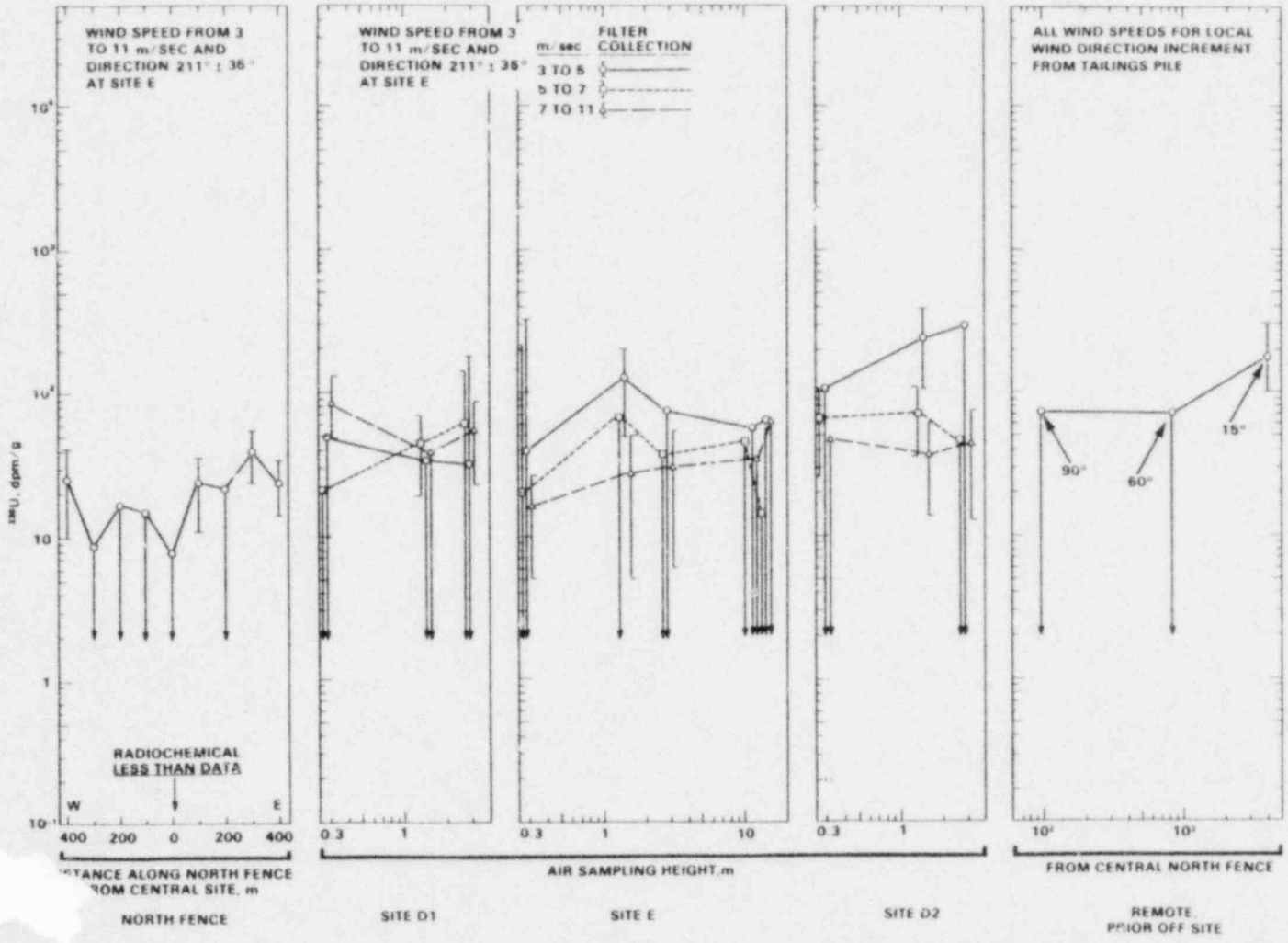

FIGURE 33. ^{235}U Concentrations on Airborne Solids at Each Site During April 27 to May 7, 1979 (data symbols for 5 to 7 and 7 to 11 m/sec offset from sampling heights to show the 1σ counting limits) (80B236-1)

from the central north fence site. This is the datum indicated by the 15° wind-direction sector in the last subfigure.

Uranium-238, dpm/g. Activity densities for ^{238}U are shown in Figure 34. For solids collected on isokinetic sampler filters, activity densities are approximately uniform as a function of site from the north fence to remote sites. Any activity density wind-speed dependency is unclear from data in this figure. A decreased activity density is indicated for smaller particles collected on particle cascade impactor backup filters at the 60° and 15° remote sites. For these small particles, the activity density decreased about 1 order of magnitude below that for the isokinetic sampler total filter collection. Reasons for this decrease are not entirely clear. The decrease is unexpected since it was reported in the interim report that the activity density was generally greater for the smaller particles. (For immediate reference, these data are shown in Figures 35 through 38 for ^{238}U, ^{235}U, ^{226}Ra, and ^{210}Pb, respectively.) The largest activity densities were for respirable-sized particles. Possibly, the decreased activity density for particles collected on the backup filter is caused by collecting both particles eroded from the mill tailings pile as well as a significant proportion of particles whose origin was other than the mill tailings pile. If significantly large proportions of collected solids were nonradionculide-containing particles, a diluting effect would occur. Activity densities would decrease as suggested by the finest particle size fraction shown in the last subfigure in Figure 34 (cascade backup filter).

Of particular concern in estimating the source strength of wind erosion is the source strength crosswind variability. The wind erosion source is nonuniform in the crosswind direction as indicated by results from the north-fence samplers shown in the first subfigure. There is almost 1 order of magnitude variation in activity densities between solids collected at the western and eastern north fence sampling sites.

An additional datum point is shown for site E in Figure 34. This datum point represents large particles collected at a height of 15 m within the isokinetic sampler inlet for the 5 to 7 m/sec wind speed. This activity density level, $\sim 10^3$ dpm/g, was the largest activity density measured for this time period. This activity density is considered associated with eroded mill

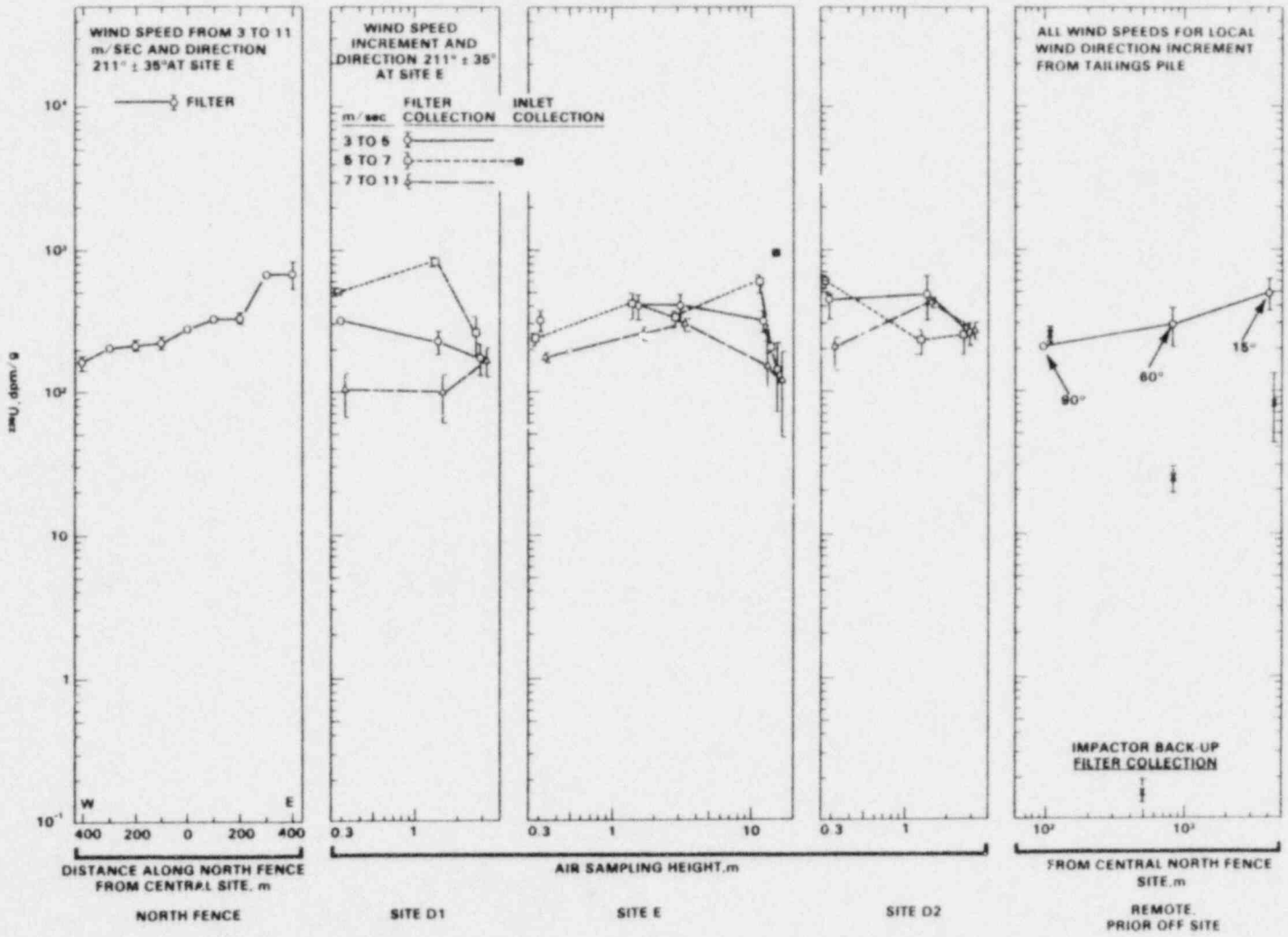

FIGURE 34. ^{235}U Concentrations on Airborne Solids at Each Site During April 27 to May 7, 1979 (data symbols for 5 to 7 and 7 to 11 m/sec offset from sampling heights to show the 1σ counting limits) (808236-38)

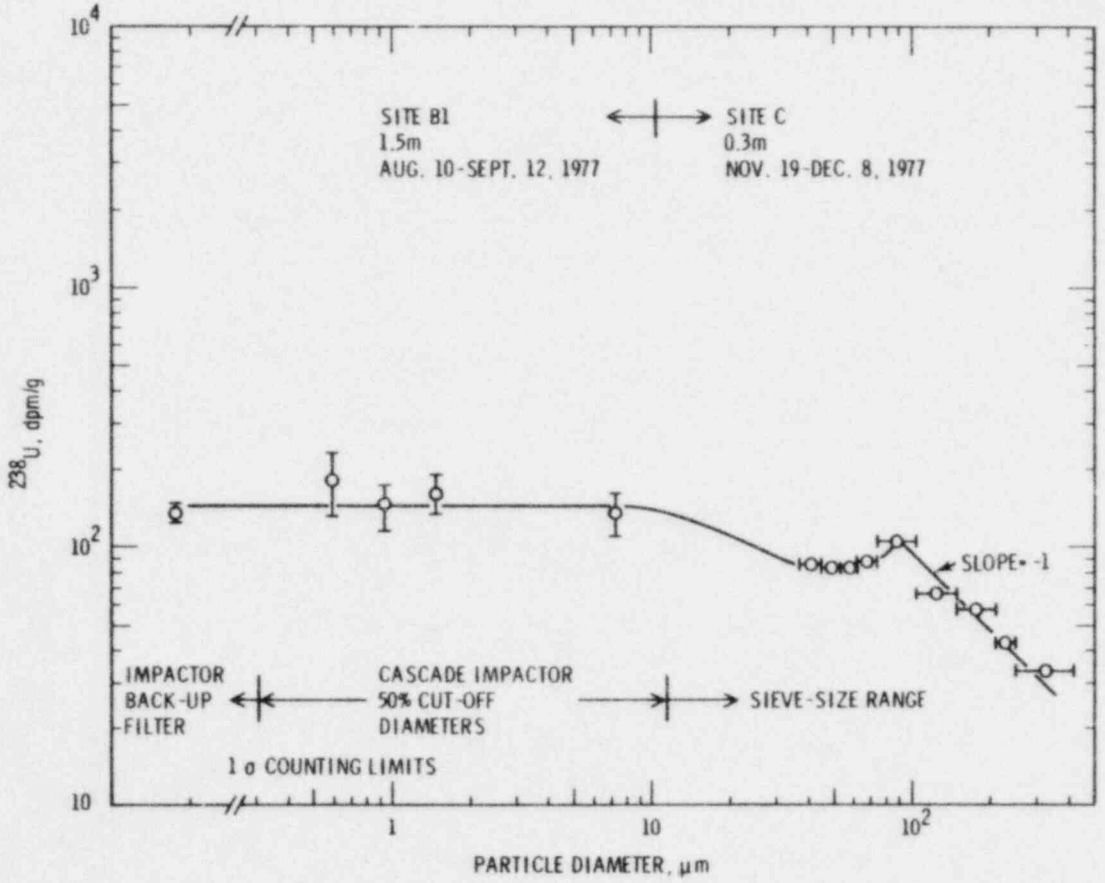

FIGURE 35. 238U Concentration on Airborne Solids as a Function of Particle Diameter (7807917-6)

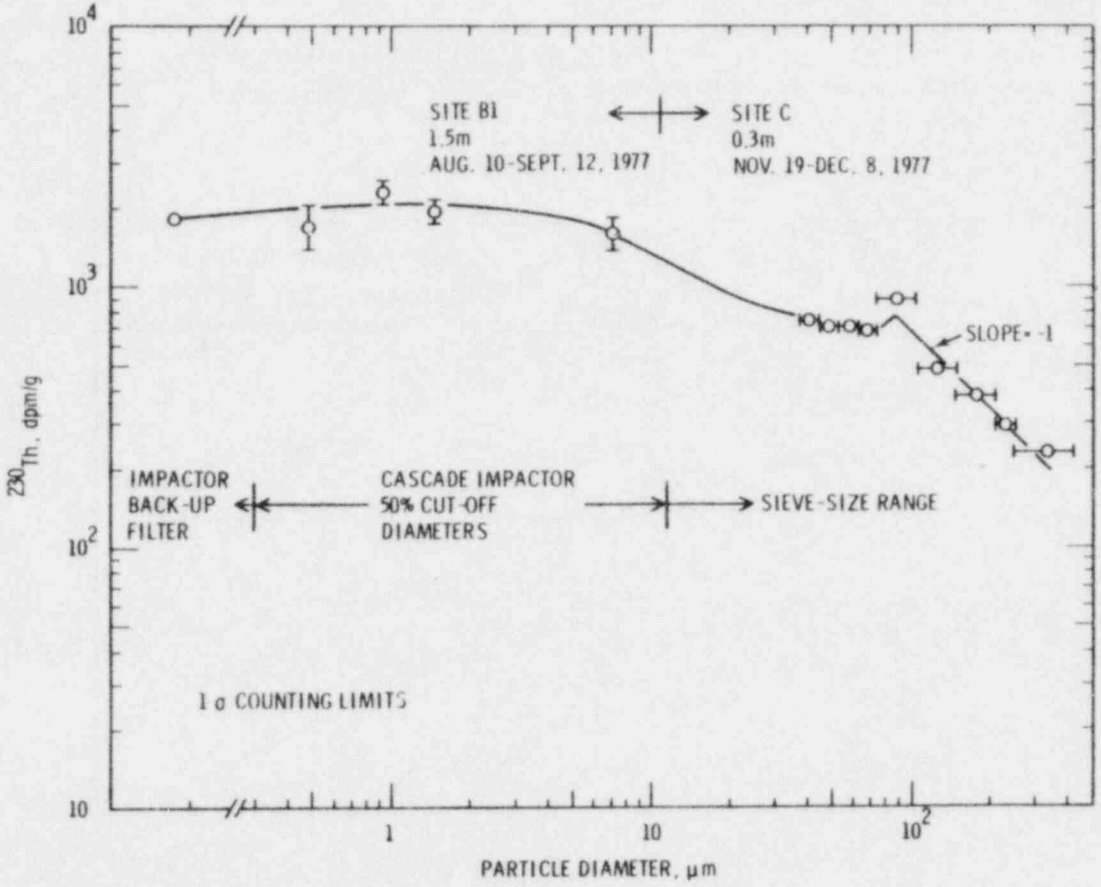

FIGURE 36. ^{230}Th Concentration on Airborne Solids as a Function of Particle Diameter (7807917-5)

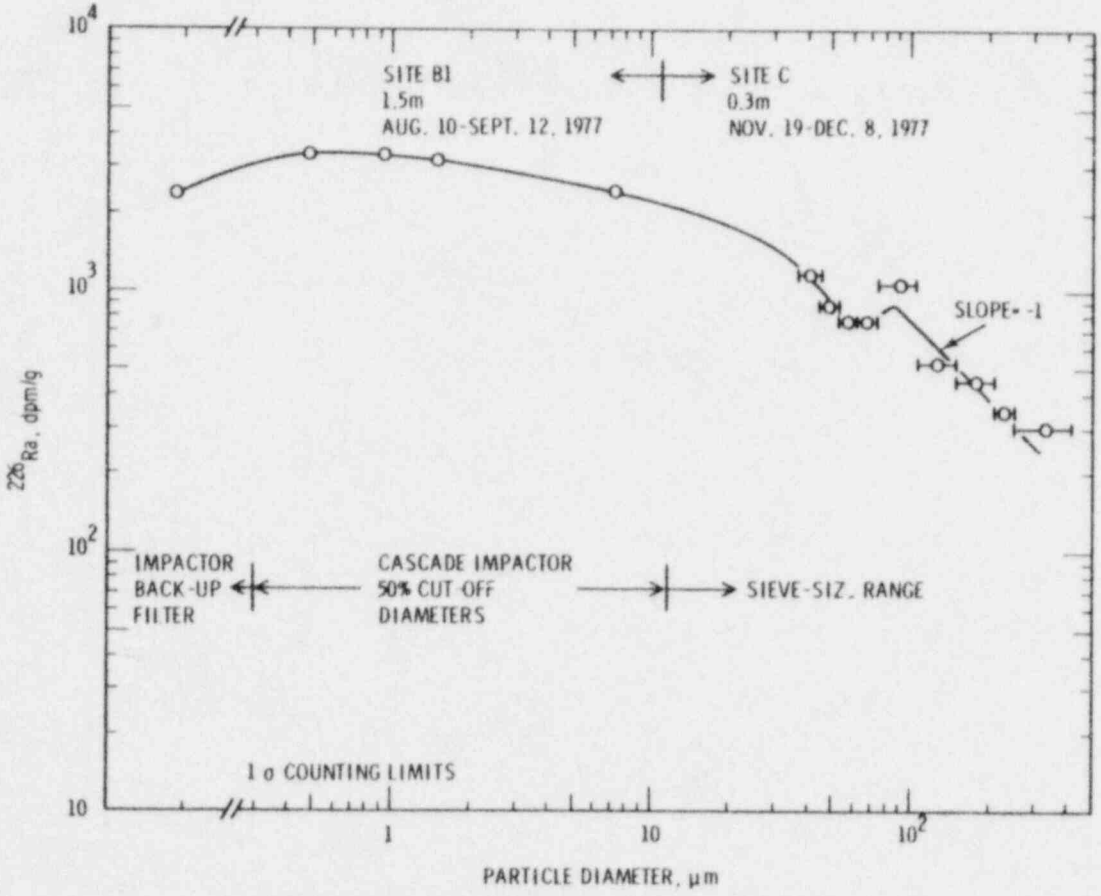

FIGURE 37. ^{226}Ra Concentration on Airborne Solids as a Function of Particle Diameter (7807917-2)

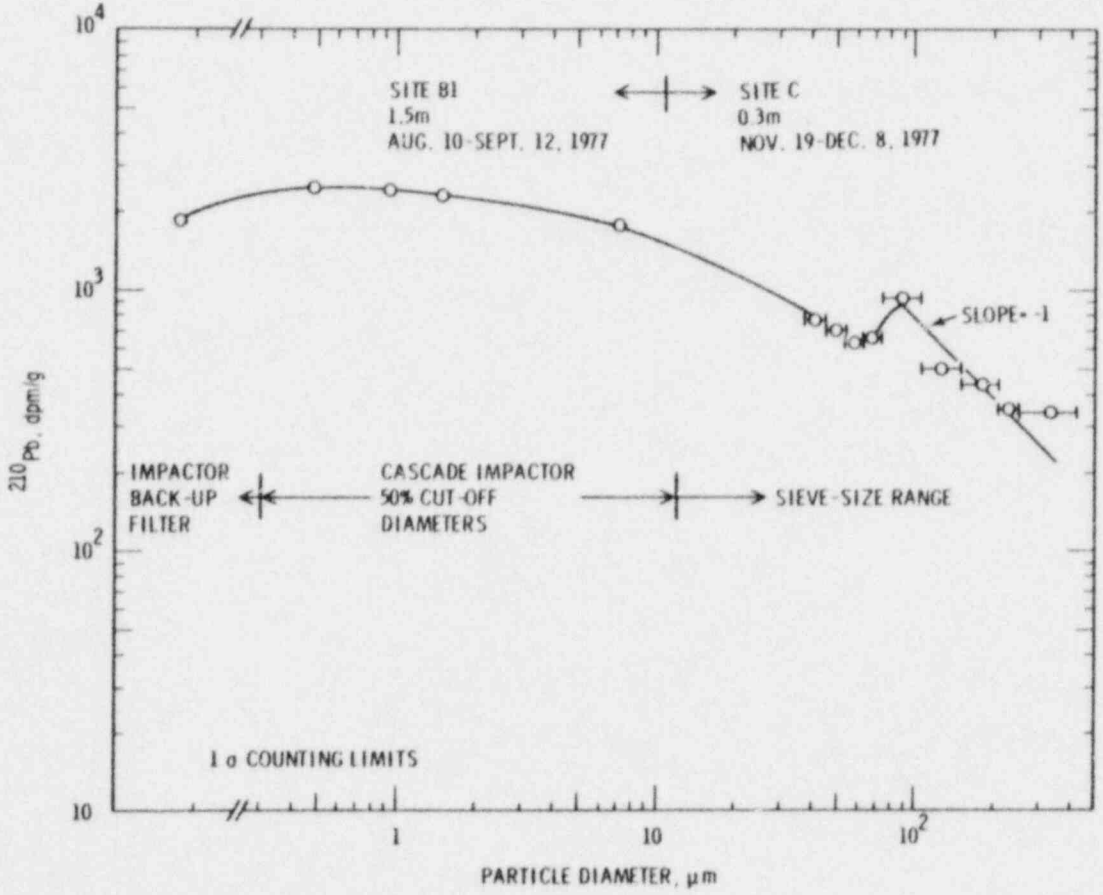

FIGURE 38. ^{210}Pb Concentration on Airborne Solids as a Function of Particle Diameter (7807917-4)

tailings collected at the sampling height, rather than having been contaminated with solids after sample collection. The lack of contamination is suggested since even along the north fence activity densities are approximately 1 order of magnitude less than 10^3 dpm/g. These north fence data will be discussed later (see discussion of Figure 92).

Thorium-230, dpm/g. Activity densities for ^{230}Th are shown in Figure 39. Again, there is no obvious wind-speed dependency. In all subfigures, activity densities were nearly uniform for all sampling locations including the 15-m uppermost height at site E and the impactor backup filter at the 90^o remote site. In comparing ^{230}Th to ^{238}U activity densities, the ^{230}Th erosion source appears more nearly uniform in the crosswind direction as indicated from results for the north-fence samplers.

Radium-226, dpm/g. Activity densities for ^{226}Ra are shown in Figure 40. For ^{226}Ra the crosswind source strength is nearly uniform, any wind-speed dependency is unclear, and activity densities are nearly uniform at all sites. However, there are significant differences as a function of particle size at the 60^o and 15^o remote sampling locations. Caution is indicated in interpreting these data at the 15^o location. The filter collection datum is a less-than radiochemical detection limit number rather than a datum point with confidence limits around it. At the 60^o location, activity densities for particles collected on the cascade impactor backup filter are over 1 order of magnitude less than activity densities collected on a total filter sample. In contrast, at the 15^o sampling location, the activity density measured from the cascade impactor backup filter collection is 1 order of magnitude greater than the activity density determined from the total filter sample.

Lead-214, dpm/g. Activity densities for ^{214}Pb are shown in Figure 41. These data are presented mainly for interest at this time, but are a reference in comparisons with ^{210}Pb concentrations. Lead-214 is a short-lived ^{222}Rn daughter product. Consequently, ^{214}Pb activity densities reflect in-growth and decay after field sampling. Lead-214 activity densities should be a function of ^{226}Ra activity densities, but the functional relationship is unclear since some radon gas undoubtedly escaped from the samples. There was no attempt to prevent radon release.

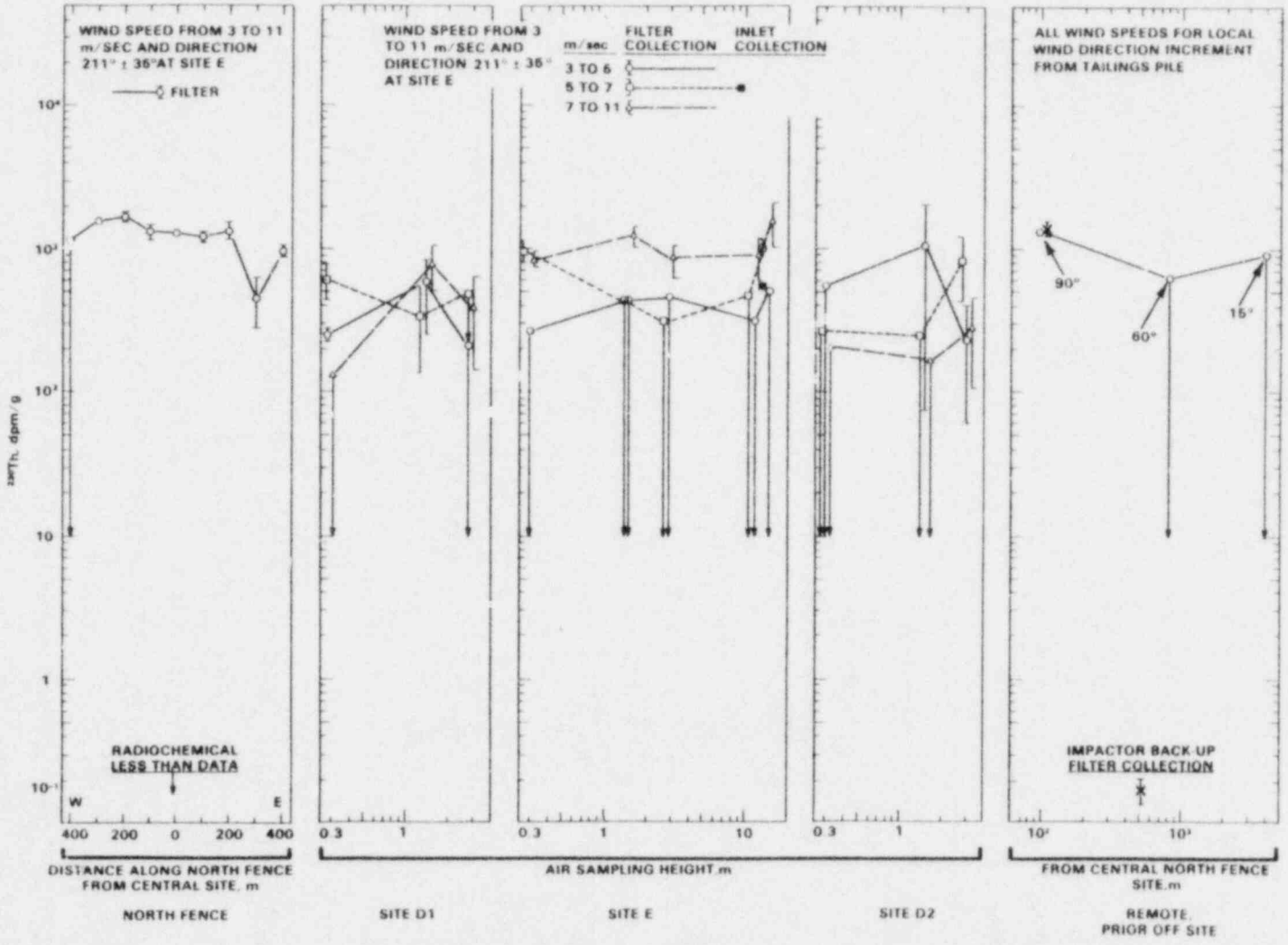

FIGURE 39. ^{230}Th Concentrations on Airborne Solids During April 27 to May 7, 1979 (data symbols for 5 to 7 and 7 to 11 m/sec offset from sampling heights to show the 1σ counting limits) (80B236-32)

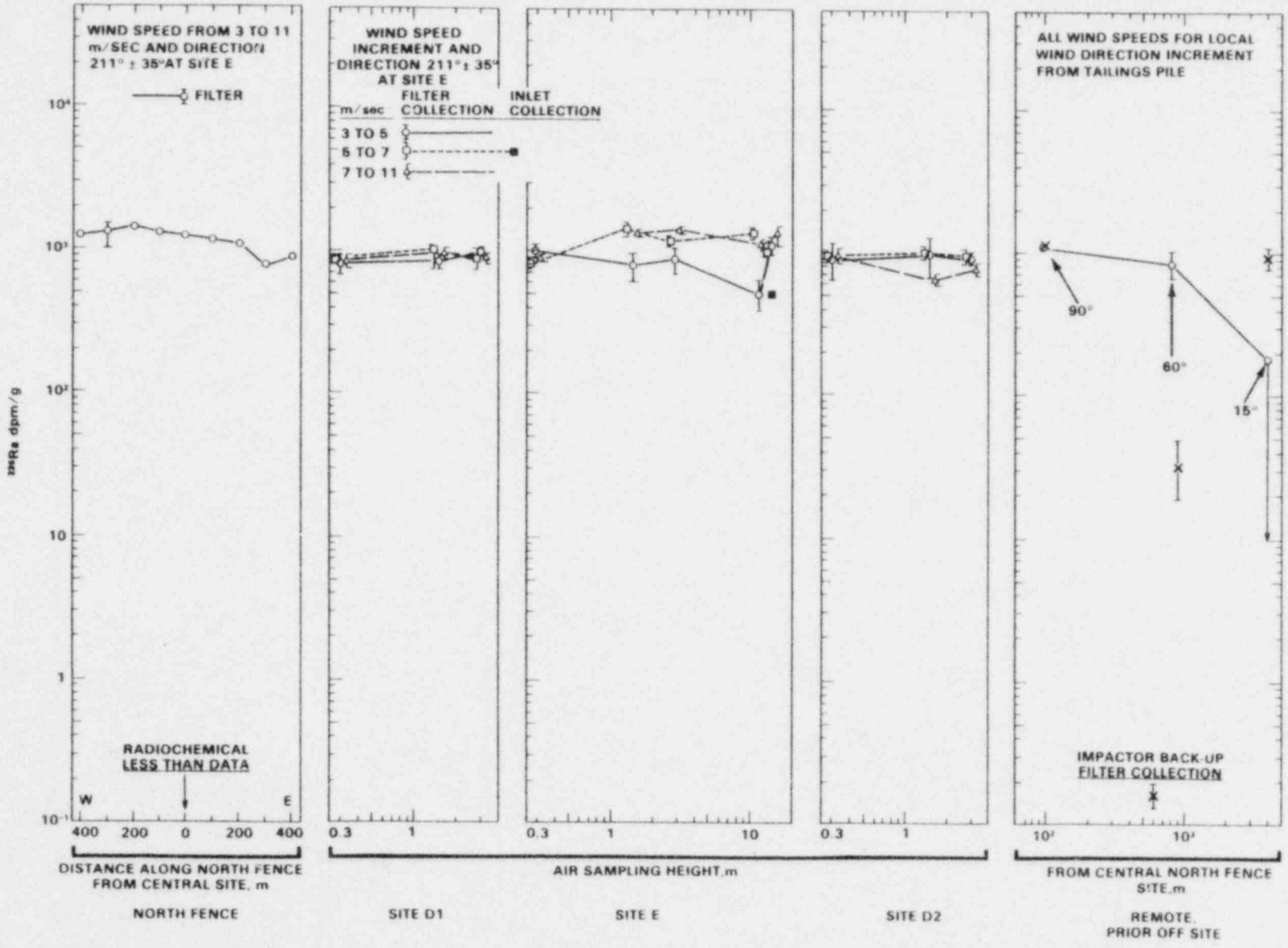

FIGURE 40. ^{226}Ra Concentrations on Airborne Solids During April 27 to May 7, 1979 (data symbols for 5 to 7 and 7 to 11 m/sec offset from sampling heights to show the 1σ counting limits) (80B236-27)

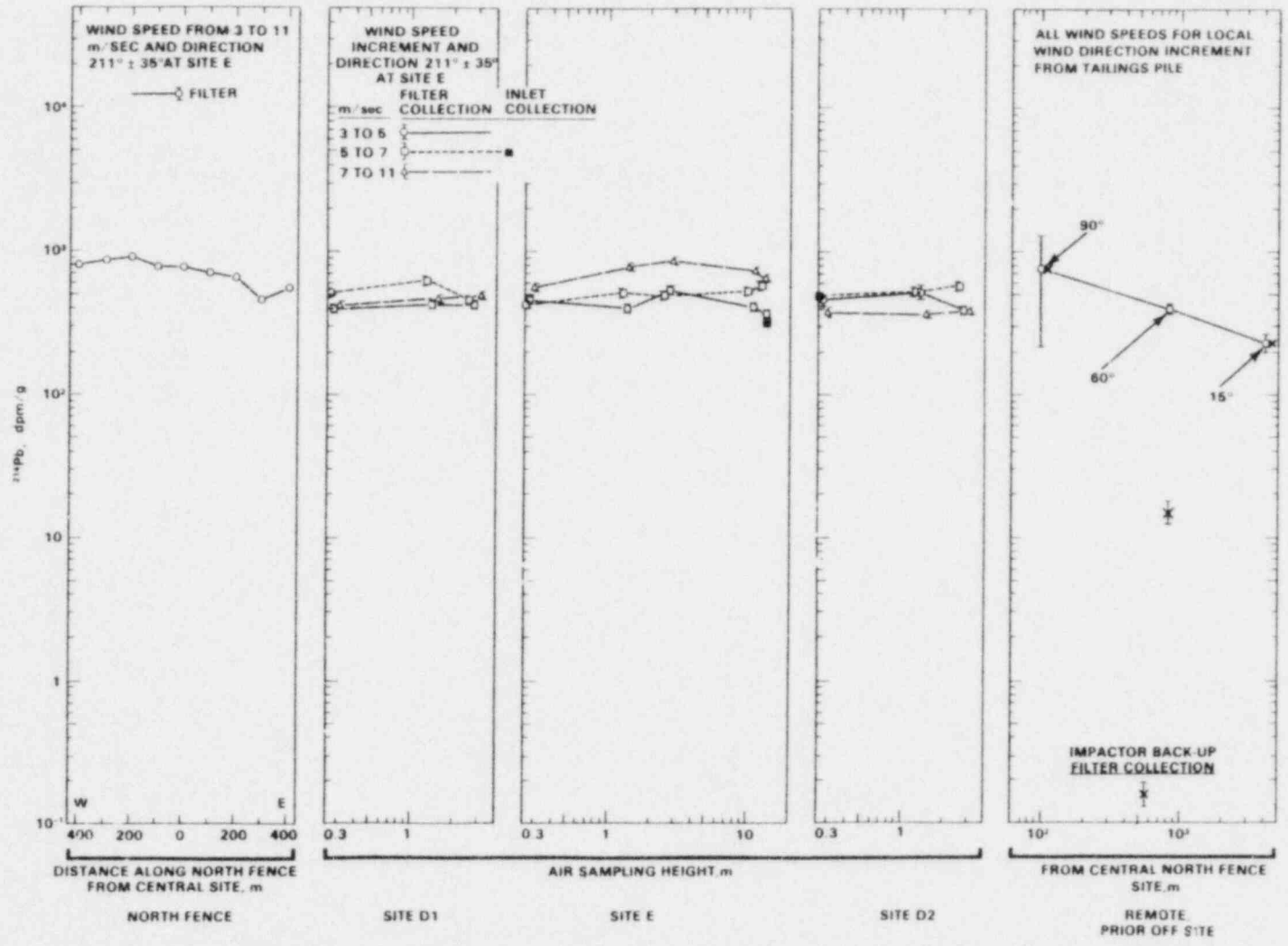

FIGURE 41. ^{214}Pb Concentrations on Airborne Solids at Each Site During April 27 to May 7, 1979 (data symbols for 5 to 7 and 7 to 11 m/sec offset from sampling heights to show 1σ counting limits) (80B236-42)

Lead-210, dpm/g. Activity densities for ^{210}Pb are shown in Figure 42. Activity densities are $\sim 10^3$ dpm/g for all sampling locations. The source strength crosswind variations are small and the wind-speed dependency is unclear. Surprisingly, the activity density at the 15^o remote site is comparable to all other activity densities. This similarity between activity densities could be caused in part by ^{210}Pb resuspension from secondary ground surface sources previously deposited from prior mill tailings pile wind erosion. The ground surface area extent of this secondary source is greater than the pile surface area. Another possibility to explain the magnitude of ^{210}Pb activity densities is that most of the measured ^{210}Pb may have resulted from decay of ^{226}Ra to ^{222}Rn and daughter products while in the laboratory. This second possibility will be discussed later in connection with Figure 51.

Airborne Radionuclide Concentrations

Airborne radionuclide concentrations, $\mu Ci/cm^3$, were calculated for ^{235}U, ^{238}U, ^{230}Th, ^{226}Ra, ^{214}Pb and ^{210}Pb. In figures in which these data are presented, airborne radionuclide concentrations are compared to Appendix B Table I and II guidance levels from 10 CFR 20 (1979). Table I guidance levels are for licensee worker occupational exposure while Table II guidance levels are permissible radionuclide concentrations in effluents to unrestricted areas. In most cases guidance levels for airborne soluble particles are given. However, in some cases, guidance levels for insoluble particles are given if the guidance level for insoluble particles is less than the guidance level for soluble particles. For both Table I and II values shown, minimum guidance levels from 10 CFR 20 (1979) are listed for each radionuclide on their respective figure. In most figures guidance levels are also indicated by horizontal dotted lines extending across all subfigures. These dotted lines are included when the guidance level is within the range of the ordinate scale.

Uranium-235, $\mu Ci/cm^3$. Airborne ^{235}U concentrations are shown in Figure 43. Airborne concentrations range from approximately 10^{-15} to $10^{-14}\mu Ci/cm^3$ with the maximum concentrations measured at site D-2. Maximum airborne concentrations were 2 orders of magnitude less than Table II guidance levels.

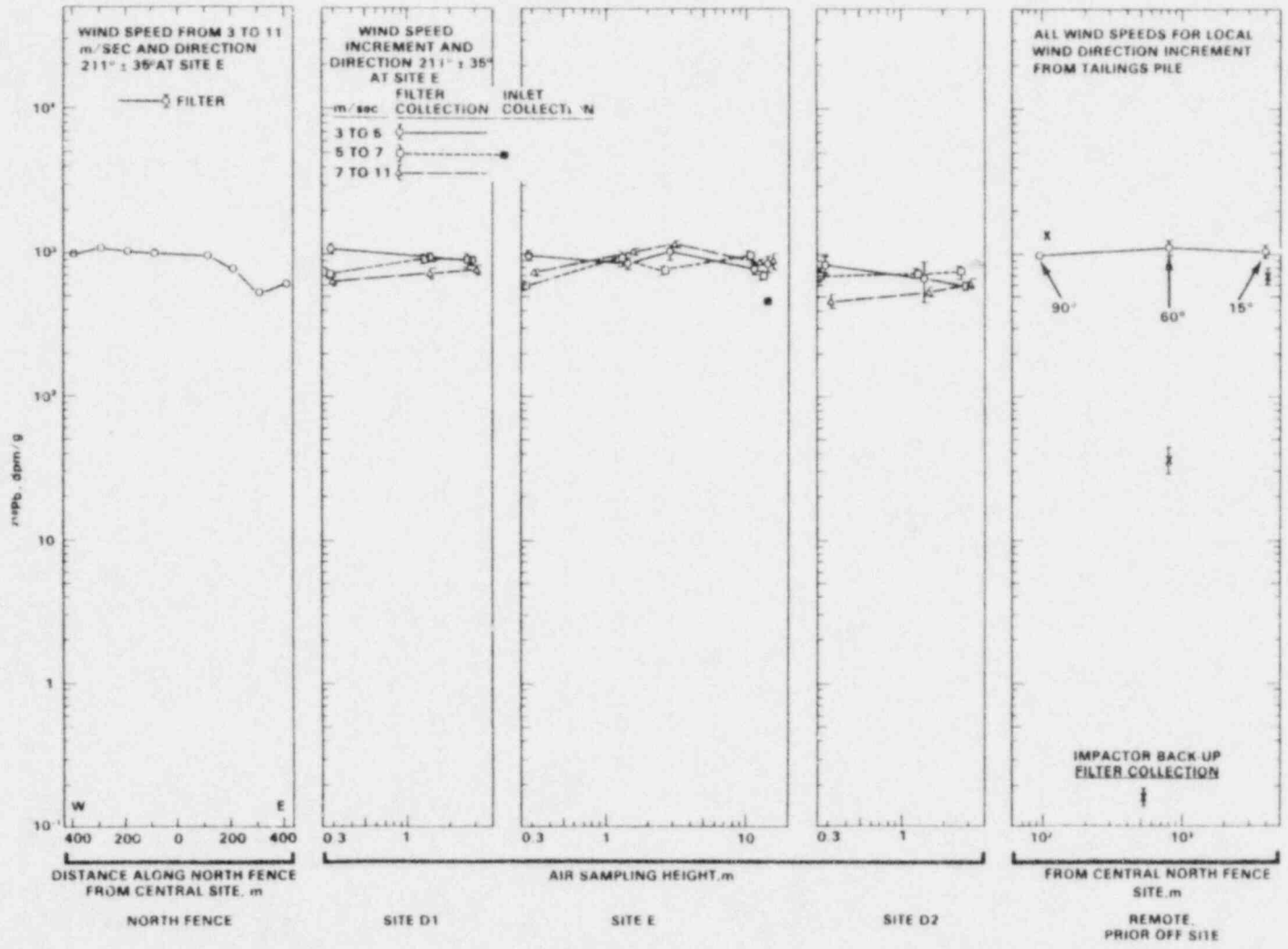

FIGURE 42. ^{210}Pb Concentrations on Airborne Solids at Each Site During April 27 to May 7, 1979 (data symbols for 5 to 7 and 7 to 11 m/sec offset from sampling heights to show the 1σ counting limits) (80B236-45)

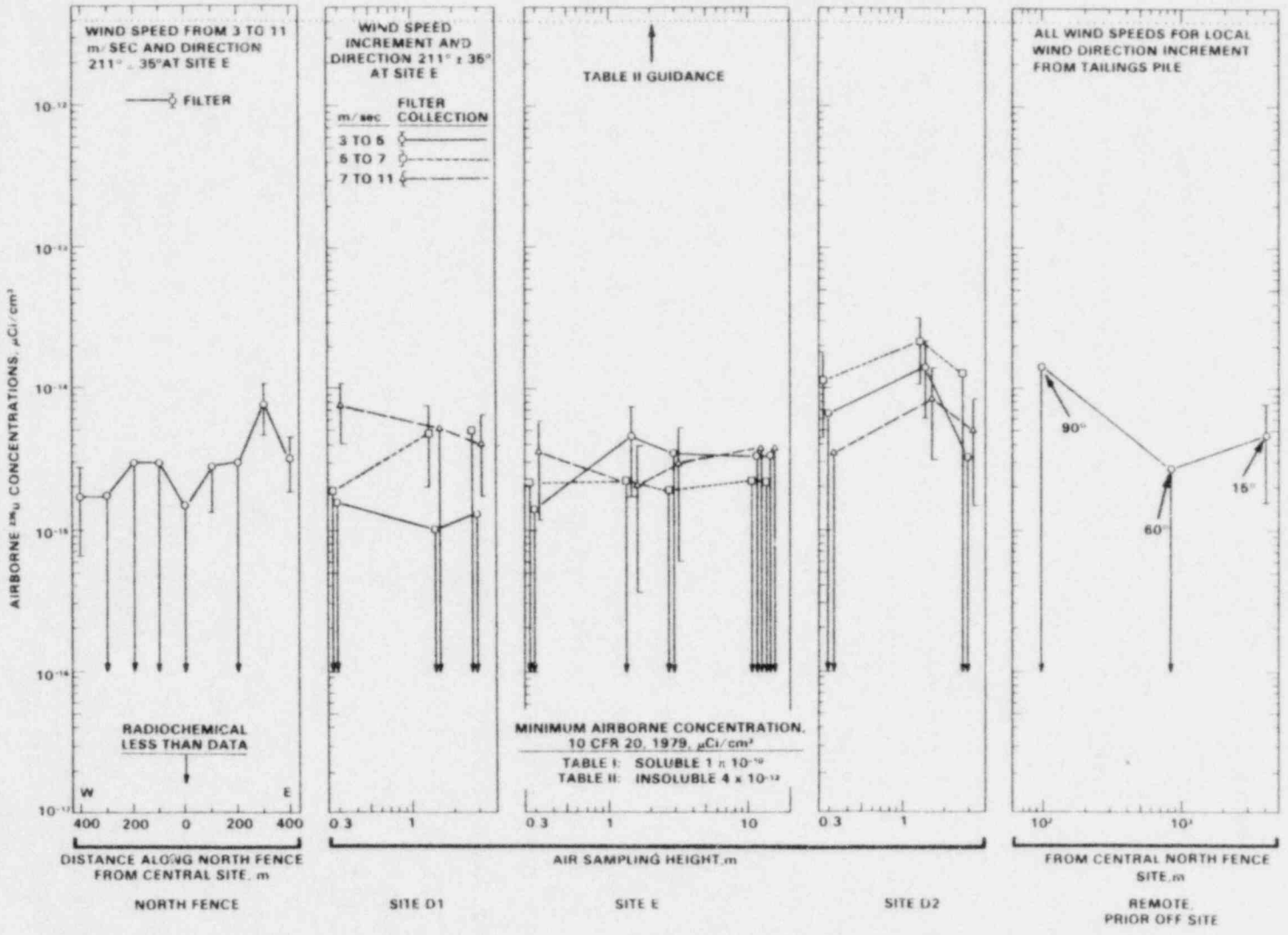

FIGURE 43. Airborne ^{235}U Concentrations at Each Site During April 27 to May 7, 1979 (data symbols for 5 to 7 and 7 to 11 m/sec offset from sampling height to show the 1σ counting limits) (80B452-40)

Uranium-238, $\mu Ci/cm^3$. Airborne ^{238}U concentrations are shown in Figure 44. Airborne concentrations range from approximately 10^{-14} to $10^{-13} \mu Ci/cm^3$. Maximum airborne concentrations were 2 orders of magnitude less than Table II guidance levels.

Airborne ^{238}U concentrations range within 1 order of magnitude along the north fence. The minimum airborne concentration was at the west end of the fence; the maximum airborne concentrations were near the east end of the fence. Although large concentration variations occur, airborne concentrations were essentially constant for the central six sampling sites. This near uniformity for 60% of the data is encouraging when estimating the wind erosion source strength for ^{238}U. If airborne radionculide concentrations were uniform along the crosswind distance, a reasonable approach for estimating wind erosion source strengths is to multiply an average airborne concentration by an average wind speed. Unfortunately, as will be shown, this airborne concentration uniformity is the exception rather than the rule.

Downwind at sites D-1, E, and D-2, a nonuniformity in airborne ^{238}U concentrations is shown. Airborne concentrations are maximum at the outer two sampling sites, i.e., sites D-1 and D-2 rather than at the central site E. These maximum airborne ^{238}U concentrations occurred during the intermediate, 5 to 7 m/sec, wind-speed increment.

The maximum airborne ^{238}U concentration, $4 \times 10^{-13} \mu Ci/m^3$, was measured for large inlet-collected particles collected at the 15-m uppermost height of site E. As mentioned previously, the airborne large particle plume appears to have been contained from ground level to elevations above the highest point sampled.

Attention is now directed to the last subfigure showing airborne ^{238}U concentrations for the three 90^o, 60^o, and 15^o sites. At each site, concentrations are shown for both total sample collection on an "isokinetic" sampler filter and also for sample collection on a particle cascade impactor backup filter. At the 90^o sampling sector site, airborne concentrations measured by both sampling devices are approximately the same. Measured concentrations increasingly diverge with increasing distance. Airborne concentrations of the

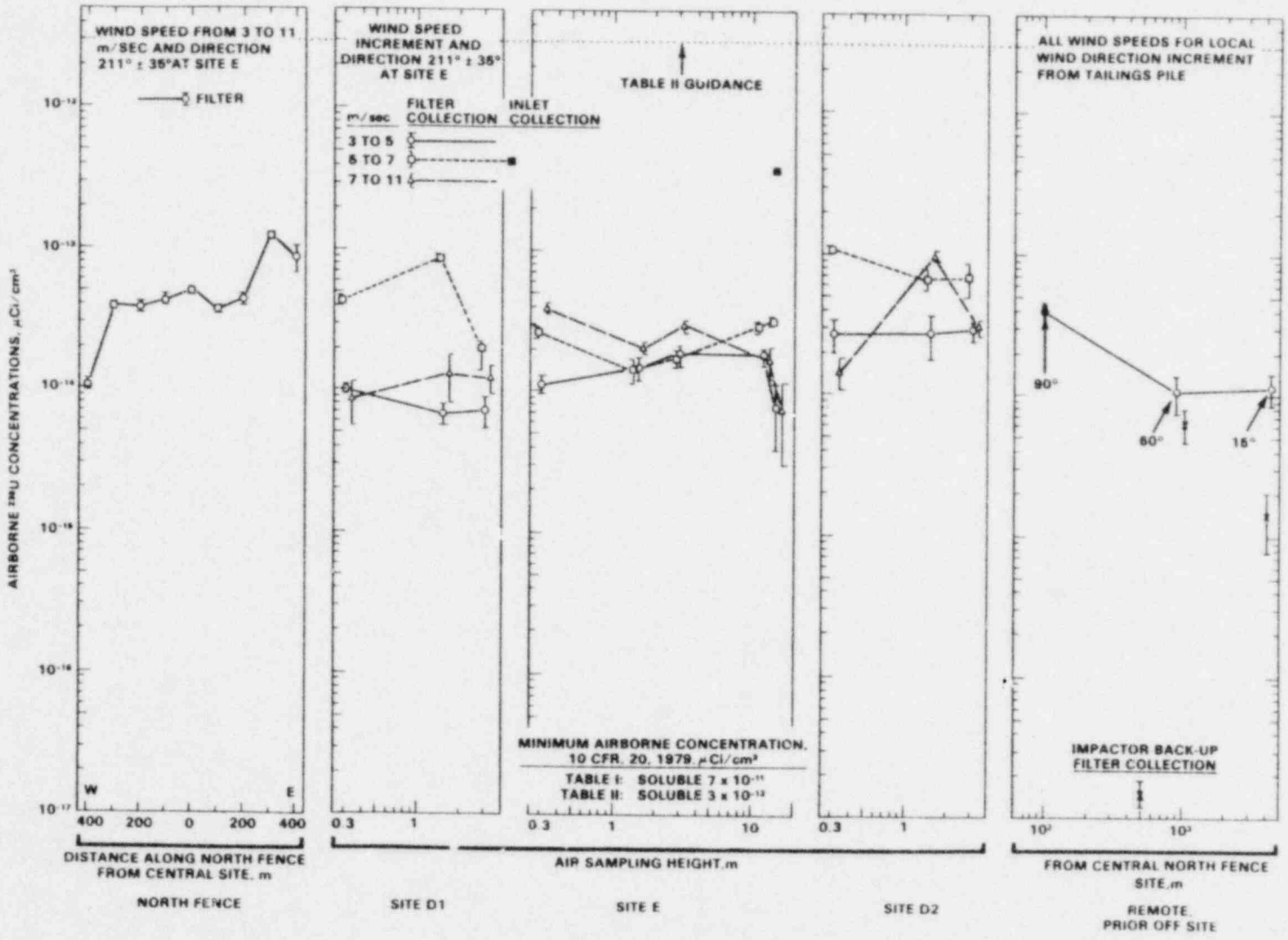

FIGURE 44. Airborne ^{238}U Concentrations at Each Site During April 27 to May 7, 1979 (data symbols for 5 to 7 and 7 to 11 m/sec offset from sampling height to show the 1σ counting limits) (80B236-41)

submicron particles calculated from the impactor backup filter collection become increasingly less than airborne concentrations calculated from total filter sample collection. This decrease may be a function of 1) dry deposition removal of submicron particles near ground level and 2) the airborne plume relative height above ground and plume transport distance of "large" particles.

Consider a possible plume trajectory scenario for "large" particles. If this airborne plume passed over the 90^{o} site and subsequently subsided with increasing distance, particle concentrations increase near ground level with increasing distance. If this scenario were the mechanism for causing the divergence between data points, the airborne plume of large particles started to impact the ground surface near the 60^{o} sampling site. For greater distances the plume impact was even greater.

Thorium-230, $\mu Ci/cm^3$. Airborne ^{230}Th concentrations are shown in Figure 45. Thorium-230 may be the most important radionuclide when considering the environmental impact of airborne particulates from a mill tailings pile. As shown in the figure, airborne ^{230}Th concentrations often exceed Table II guidance levels and were only 1 order of magnitude less than Table I guidance levels.

In the case of ^{230}Th, airborne concentrations could have been compared to the 10 CFR 20 guidance level for insoluble rather than soluble particles. As mentioned previously, only the minimum guidance level for either soluble or insoluble particles is shown in the figures. For ^{230}Th, the Table II guidance level for insoluble particles is 3×10^{-13} $\mu Ci/cm^3$, a numerical value essentially corresponding to the maximum ^{230}Th concentrations shown in Figure 45.

Airborne ^{230}Th concentrations along the north fence, except for the western-most sample, tended to decrease from the west to east. This concentration decrease from west to east is the opposite trend previously shown for ^{238}U in Figure 44. For ^{238}U, maximum airborne concentrations were for the two most eastern sampling stations along the north fence.

Relative y and z dimensions of the airborne plume, with airborne ^{230}Th concentrations above Table II guidance, can be estimated from data shown for sites D-1, E, and D-2. Airborne concentrations were less at sites D-2 and D-1.

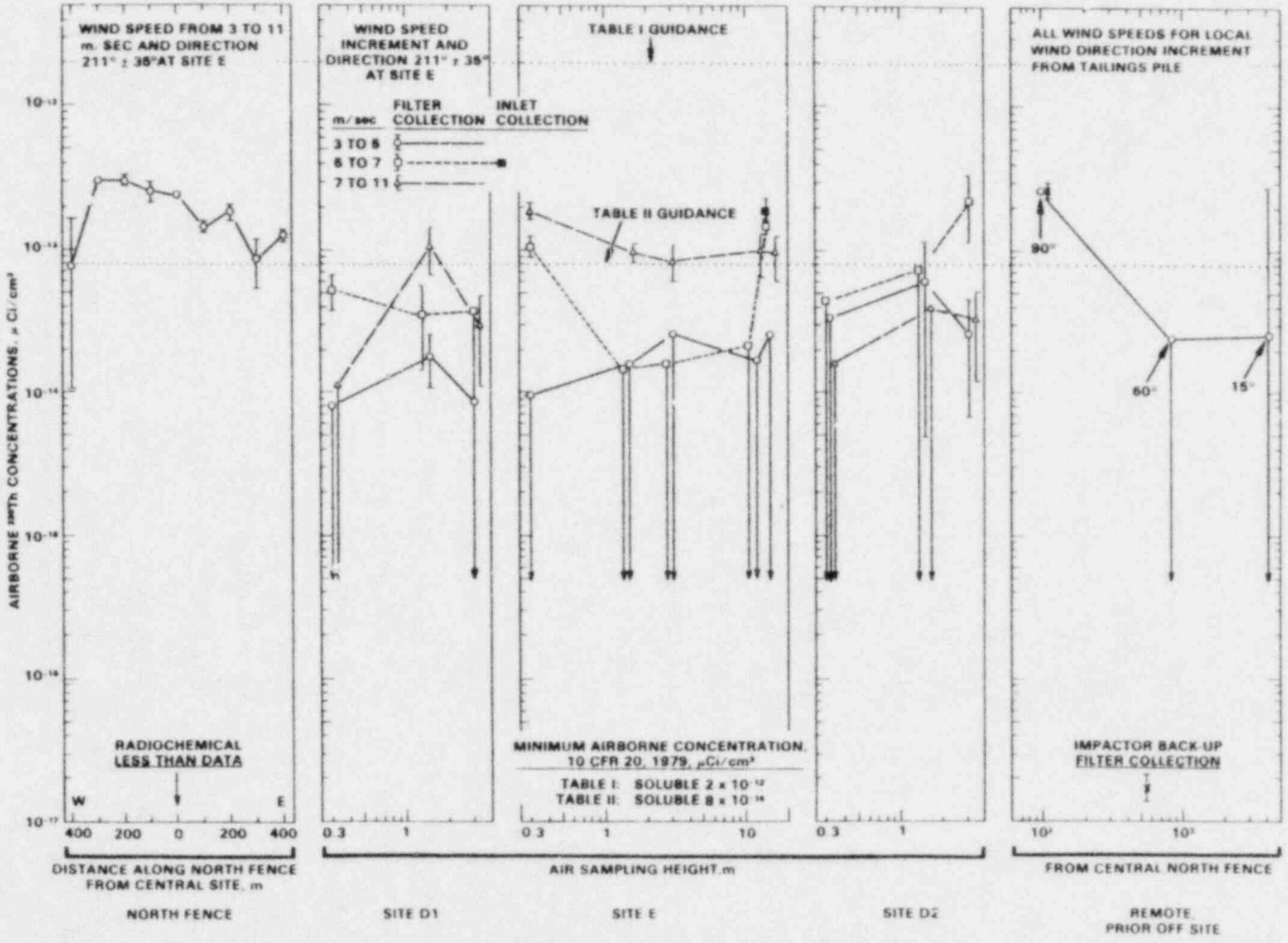

FIGURE 45. Airborne ^{230}Th Concentrations at Each Site During April 27 to May 7, 1979 (data symbols for 5 to 7 and 7 to 11 m/sec offset from sampling heights to show the 1σ counting limits) (80B236-11)

The plume height extends above the 15-m uppermost sampling location at site E. Airborne ^{230}Th concentrations at site E were above the guidance level for all sampling heights during the 3 to 5 m/sec wind-speed increment, the intermediate wind speed investigated.

That the airborne plume is contained in a height from the ground to above the central site E uppermost sampler is also suggested by the one data point for particles collected on the isokinetic inlet for the 5 to 7 m/sec sampler located at the 15-m sampling height. This datum point represents the one sample which had sufficient solids collection for recovery from the isokinetic sampler inlet. These were "nonrespirable" particles. The airborne ^{230}Th concentration calculated for these nonrespirable particles was also above Table II guidance. Table II is for respirable particles, not for nonrespirable particles. The possibility exists that all airborne concentrations above Table II guidance might be attributed to nonrespirable rather than respirable particles. However, many particles may be respirable; this interpretation is from the 90^{o}remote sampling site data. Airborne concentrations were comparable for both a total particle size distribution collected on the isokinetic sampler filter, and the less than 0.49-μm particle diameter size fraction collected on the particle cascade impactor backup filter.

Radium-226, $\mu Ci/cm^3$. Airborne ^{226}Ra concentrations are shown in Figure 46. At all sampler locations, airborne ^{226}Ra concentrations are about 1 order of magnitude less than the Table II guidance level. These data sets tend to exhibit more fully airborne concentration dependencies which were originally expected, i.e., 1) the possibility of measuring end effects for the outer-most samplers along the north fence, concentrations being less than for the central samplers, 2) airborne concentrations being a function of wind-speed increments at sampling sites D-1, E, and D-2, and 3) airborne concentrations decreasing with increasing distance as shown along the remote sites.

Airborne concentrations at site E, except for one datum point, increased with increasing wind speed. In contrast, it should again be pointed out that airborne ^{235}U, ^{238}U, and ^{230}Th concentrations showed more complex, but unclear

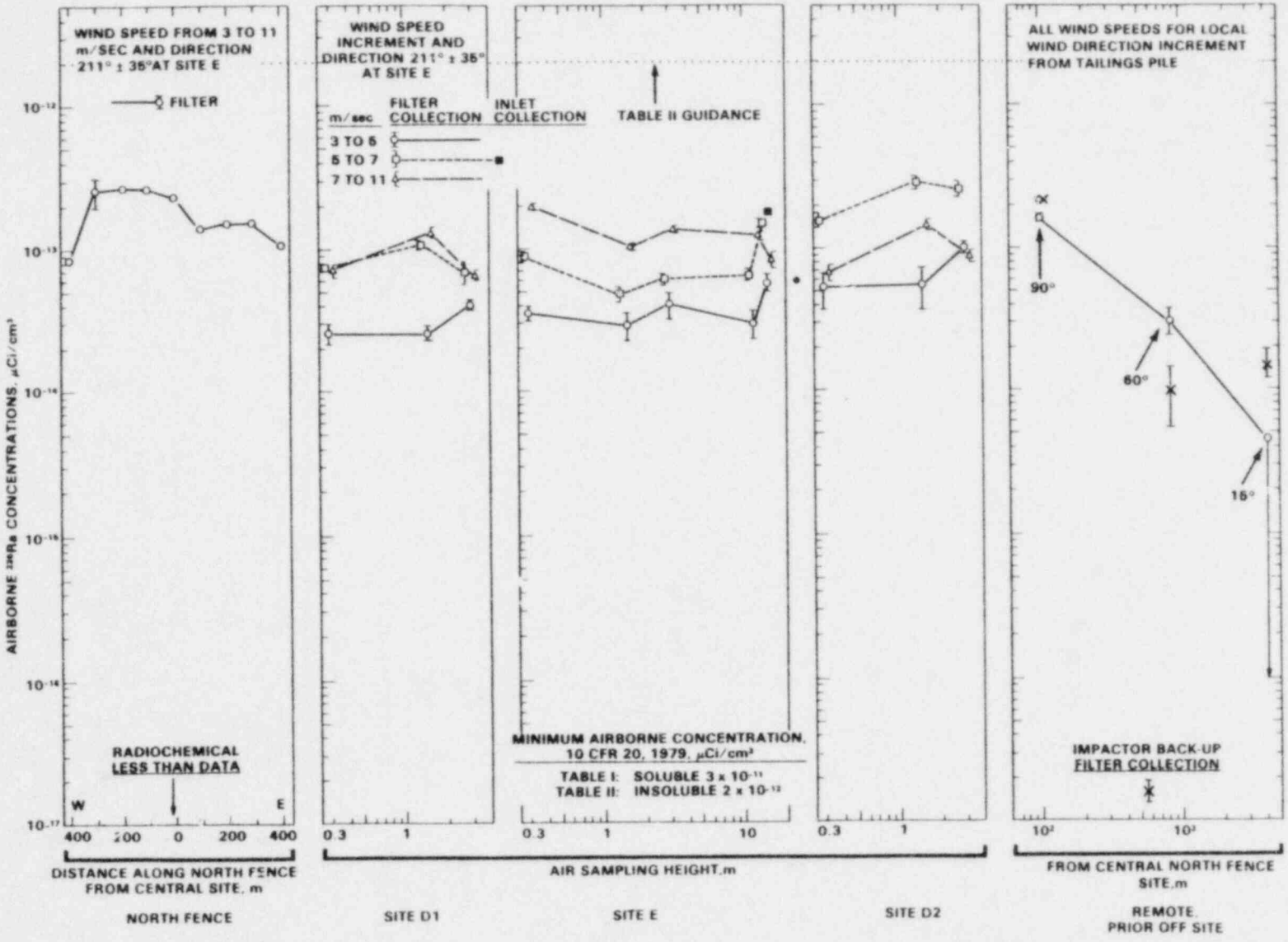

FIGURE 46. Airborne ^{226}Ra Concentrations at Each Site During April 27 to May 7, 1979 (data symbols for 5 to 7 and 7 to 11 m/sec offset from sampling heights to show the 1σ counting limits) (80B236-20)

wind-speed dependencies. The dependency is also unclear for airborne ^{226}Ra concentrations for sites D-1 and D-2. At the lowest wind-speed increment of 3 to 5 m/sec airborne concentrations were least for all three sites. However, at site D-1 airborne concentrations for the 5 to 7 m/sec and 7 to 11 m/sec wind-speed increments were comparable. At site D-2 airborne concentrations for the 7 to 11 m/sec wind-speed increment were intermediate between airborne concentrations for the two lower wind-speed increments.

Airborne ^{226}Ra concentrations decreased with increasing distance along the remote sites. The decrease was a function of particle size. At the 90^{o} site, airborne concentrations were comparable for particulates collected on both the total isokinetic filter sampler (all particle diameters were collected) as well as the particle cascade impactor backup filter (particles <0.49 µm diameter). At the 60^{o} site, airborne concentrations calculated from the backup filter were less than for the isokinetic filter. This concentration decrease is similar to decreases reported for other radionuclides. However, at the 15^{o} sampling location, airborne ^{226}Ra concentrations calculated from the cascade backup filter were greater than airborne ^{226}Ra concentrations calculated from the total isokinetic filter sampler. This apparent concentration may possibly result from airbor[illegible]al concentration variations between samplers.

Lead-210, $\mu Ci/cm^3$. Airborne ^{210}Pb concentrations are shown in Figure 47. All airborne concentrations were over 1 order of magnitude less than Table II guidance. Airborne concentrations showed the same general trends as airborne ^{230}Th concentrations. Along the north fence airborne ^{210}Pb concentrations were minimum at the extreme east and west sampling locations. At site E airborne ^{210}Pb concentrations increased with increasing wind speed, although the increase is not as clear as was shown for ^{230}Th. At sites D-1, E, and D-2, airborne ^{210}Pb concentrations were least in numerical value for the lowest wind-speed increment, 3 to 5 m/sec. At site D-1 airborne concentrations increased for the two higher wind speeds, but airborne concentrations were approximately equal for both wind speeds. At site D-2, airborne concentrations were greatest for the intermediate 5 to 7 m/sec wind-speed increment. At remote sites airborne concentrations decreased with increasing distance. The decrease

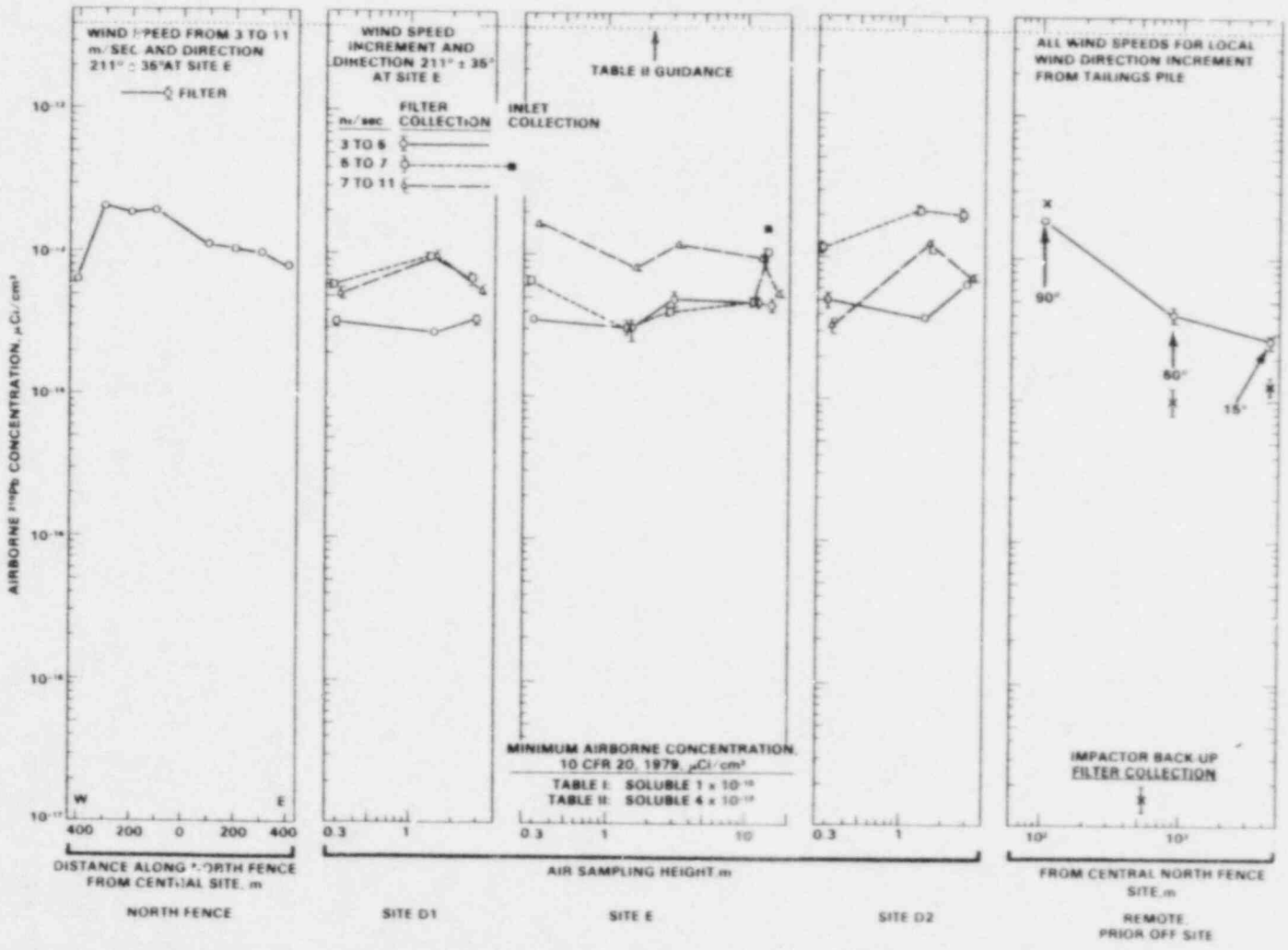

FIGURE 47. Airborne ^{210}Pb Concentrations at Each Site During April 27 to May 7, 1979 (data symbols for 5 to 7 and 7 to 11 m/sec offset from sampling heights to show the 1σ counting limits) (80B452-15)

was consistent as a function of particle size. Airborne concentrations at both the 60^{o} and 15^{o} sampling locations were smaller for airborne concentrations calculated from the cascade impactor backup filter than from the total filter sample collected in the isokinetic sampler.

Normalized Activity Densities

Activity densities are used to estimate the apparent nonequilibrium between radioactive decay products on airborne solids. To estimate this non-equilibrium, activity densities for ^{238}U, ^{230}Th and ^{226}Ra were normalized by corresponding activity densities for ^{210}Pb. Activity density ratios other than unity indicate a non-one-to-one correspondence between airborne transport for different radionuclide members of the ^{238}U decay series.

Normalized to ^{210}Pb. Activity ratios for $^{238}U/^{210}Pb$, $^{230}Th/^{210}Pb$ and $^{226}Ra/^{210}Pb$ are shown in Figures 48, 49 and 50, respectively.

In cross comparing activity ratio data from the last three figures, it is seen that airborne concentrations of ^{230}Th, ^{226}Ra and ^{210}Pb are greater than airborne concentrations of ^{238}U. This observation is in accord with the fact that over 90% of the uranium was removed in the uranium mill.

Lead-214 Normalized Activity. Activity ratios for $^{214}Pb/^{210}Pb$ and $^{214}Pb/^{226}Ra$ were investigated as indices for the concentration accuracy of ^{222}Rn daughters and of radon release after sample collection. Activity ratios for $^{214}Pb/^{210}Pb$ are shown in Figure 51.

Insight into the amount of radon released from samples after field collection is shown by $^{214}Pb/^{226}Ra$ activity ratios given in Figure 52.

March 8 to April 18, 1979

Mass Loadings

Airborne mass loadings are shown for the March 8 to April 18, 1979 sampling period in Figure 53. During this sampling period only wind direction (211 ± 30^{o}) was used for controlling sampling times for airborne particulate samplers. Airborne mass loadings for filter collection plus isokinetic inlet

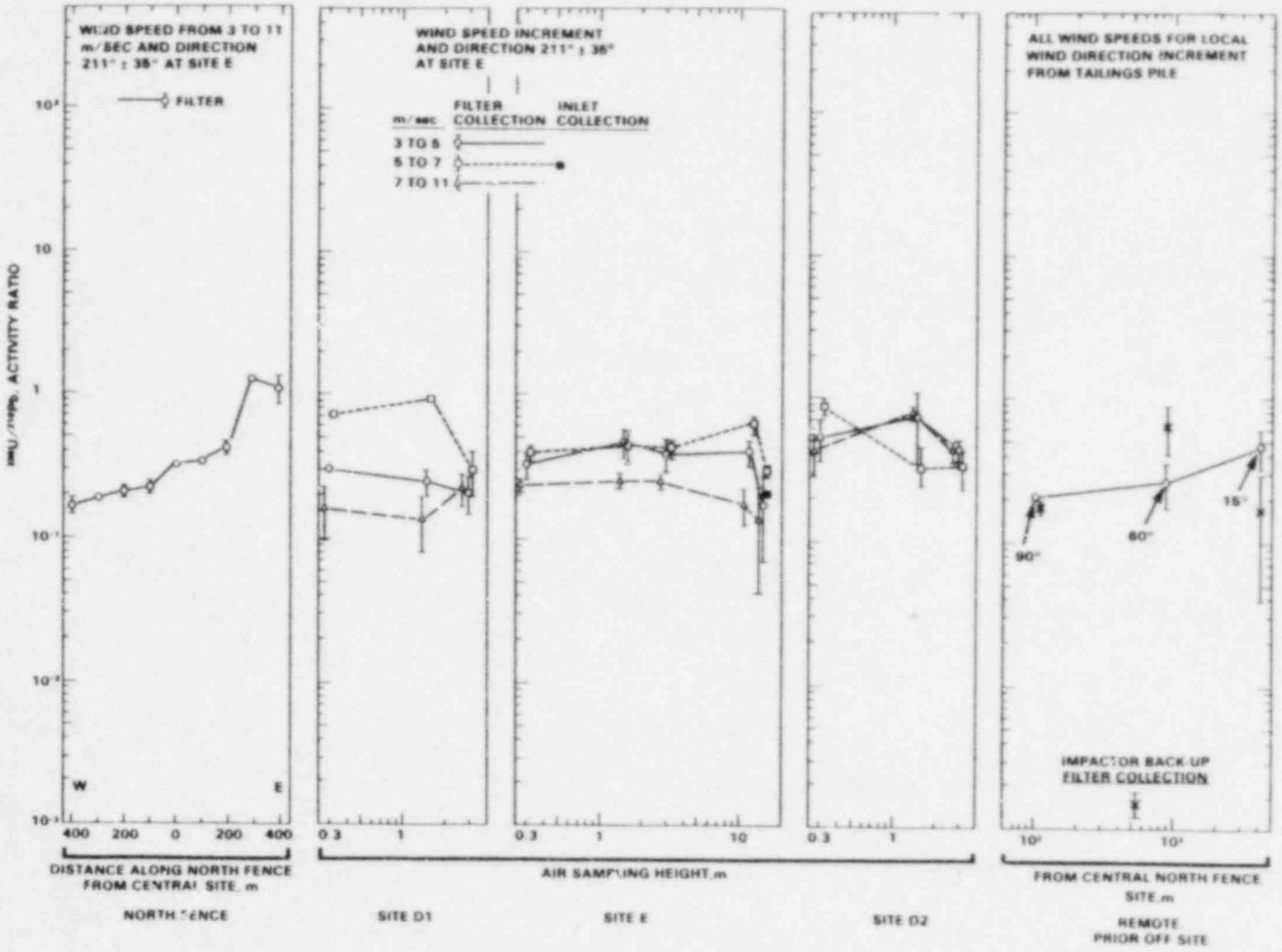

FIGURE 48. Airborne ^{238}U Activity Normalized to ^{210}Pb Activity on Airborne Solids at Each Site During April 27 to May 7, 1979 (data symbols for 5 to 7 and 7 to 11 m/sec offset from sampling heights to show the 1σ counting limits) (80B318-76)

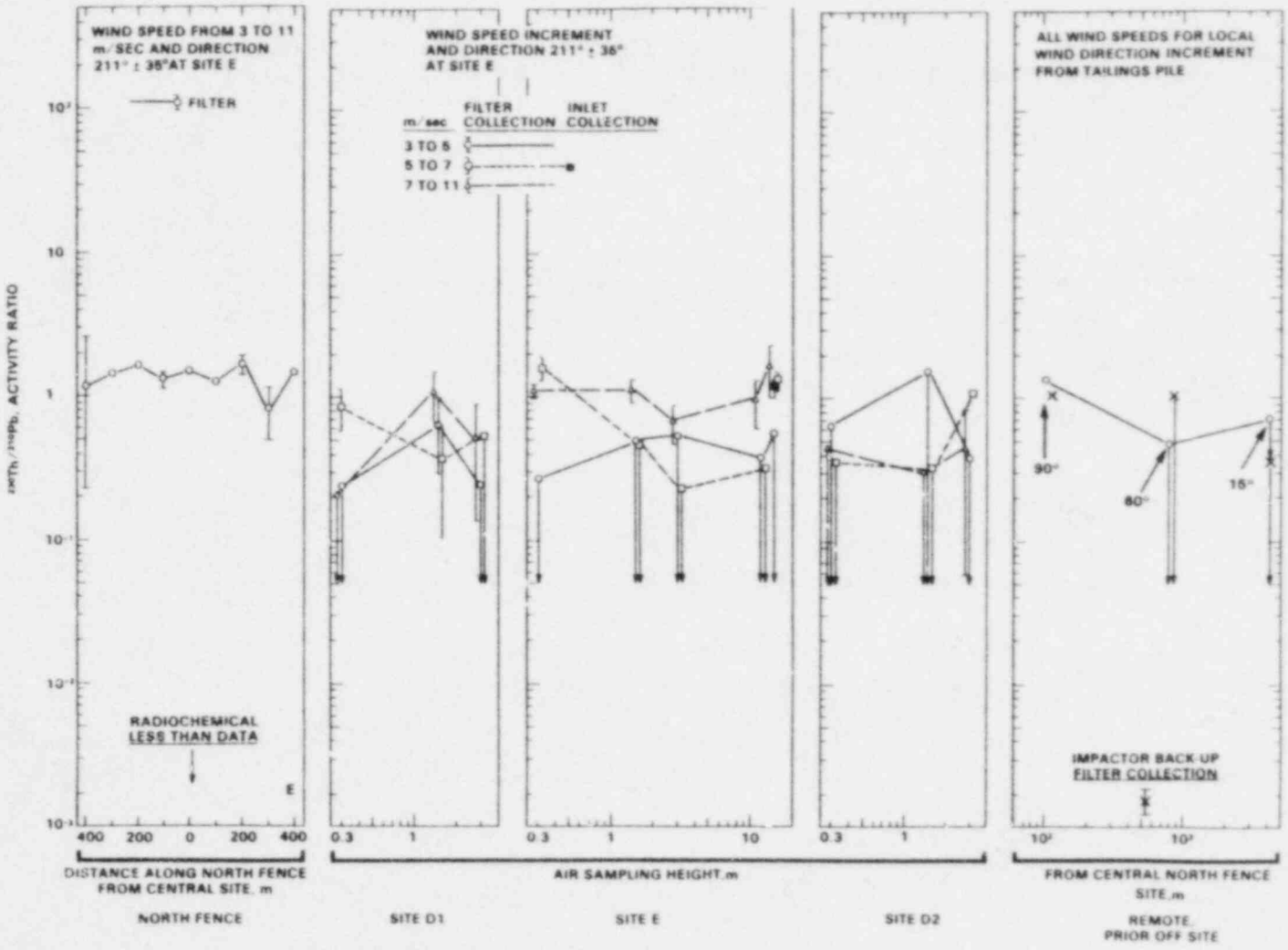

FIGURE 49. Airborne ^{230}Th Activity Normalized to ^{210}Pb Activity on Airborne Solids at Each Site During April 27 to May 7, 1979 (data symbols for 5 to 7 and 7 to 11 m/sec offset from sampling heights to show the 1σ counting limits) (808318-73)

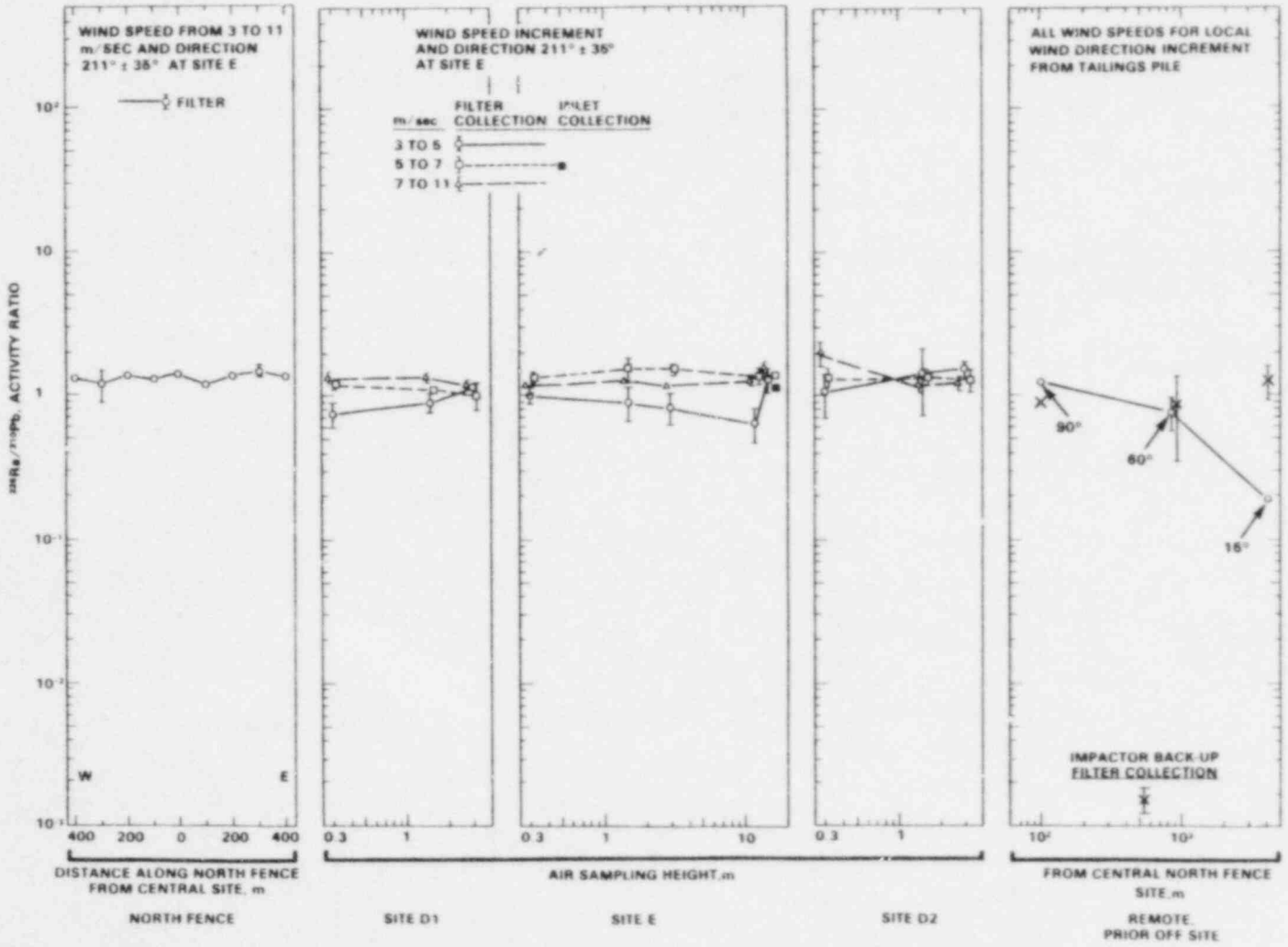

FIGURE 50. Airborne ^{226}Ra Activity Normalized to ^{210}Pb Activity on Airborne Solids at Each Site During April 27 to May 7, 1979 (data symbols for 5 to 7 and 7 to 11 m/sec offset from sampling heights to show the 1σ counting limits) (80B318-74)

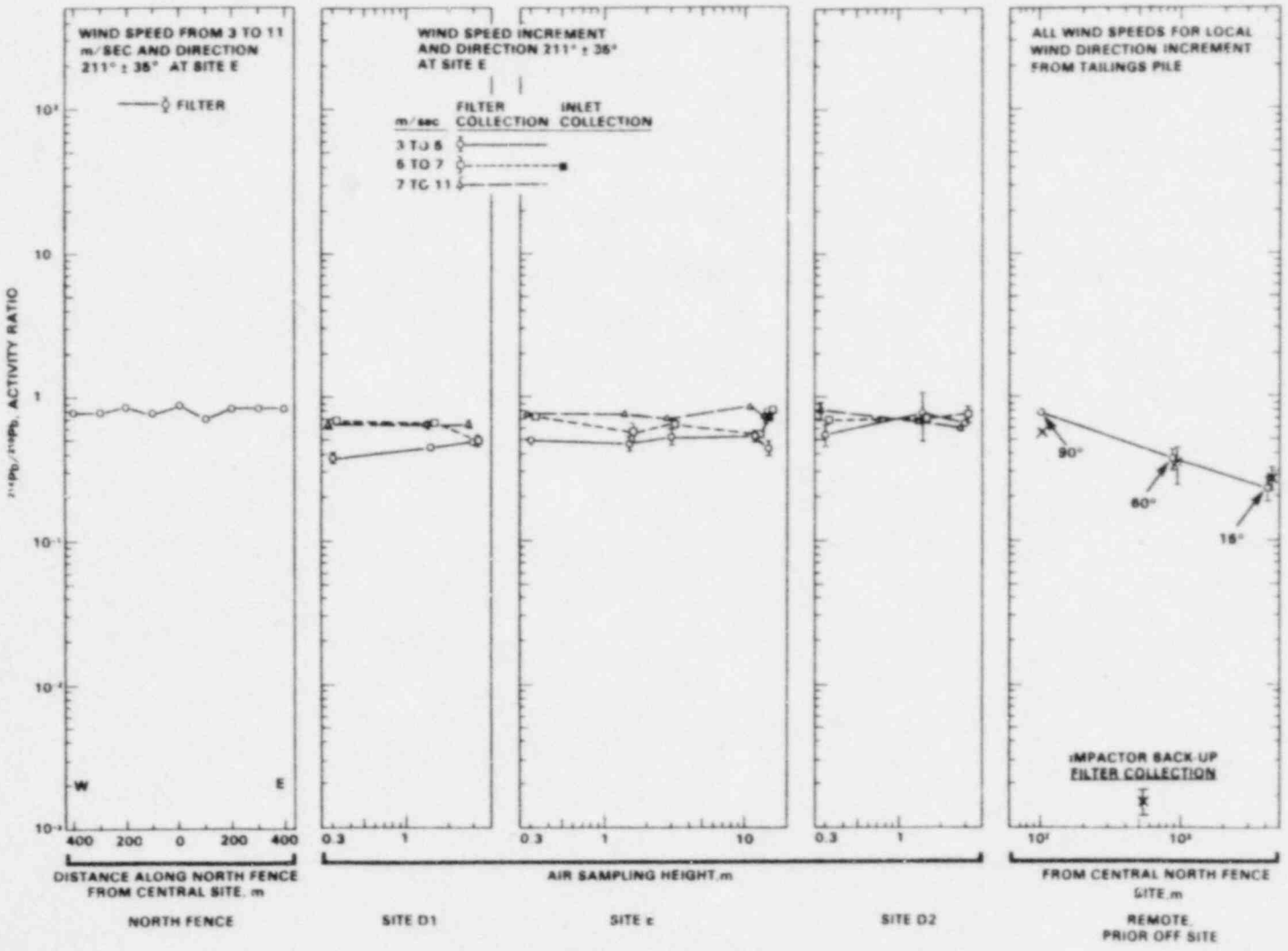

FIGURE 51. Airborne ^{214}Pb Activity Normalized to ^{210}Pb Activity on Airborne Solids at Each Site During April 27 to May 7, 1979 (data symbols for 5 to 7 and 7 to 11 m/sec offset from sampling heights to show the 1σ counting limits) (808318-75)

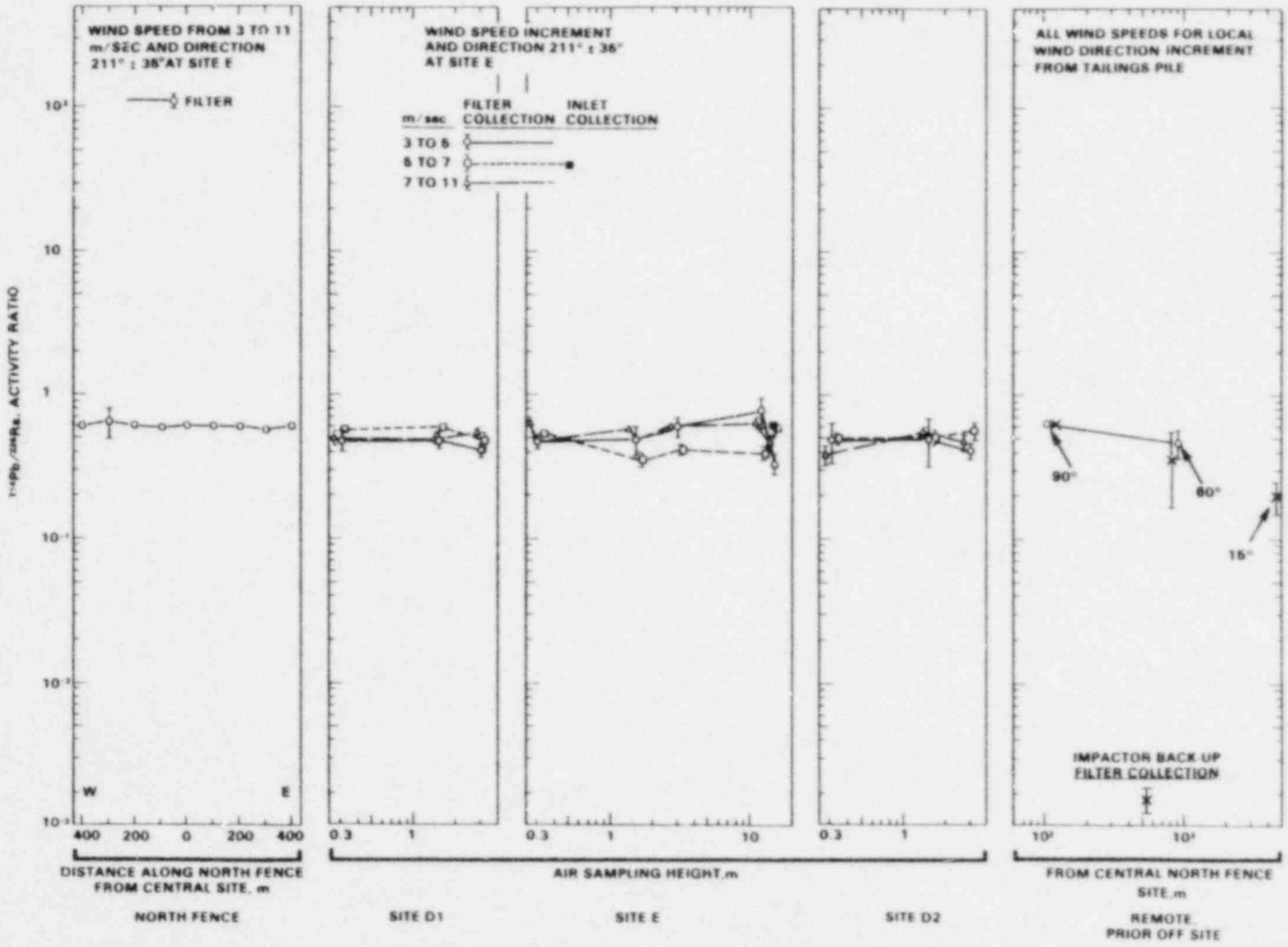

FIGURE 52. Airborne ^{214}Pb Activity Normalized to ^{210}Pb Activity on Airborne Solids at Each Site During April 27 to May 7, 1979 (data symbols for 5 to 7 and 7 to 11 m/sec offset from sampling heights to show the 1σ counting limits) (80B318-77)

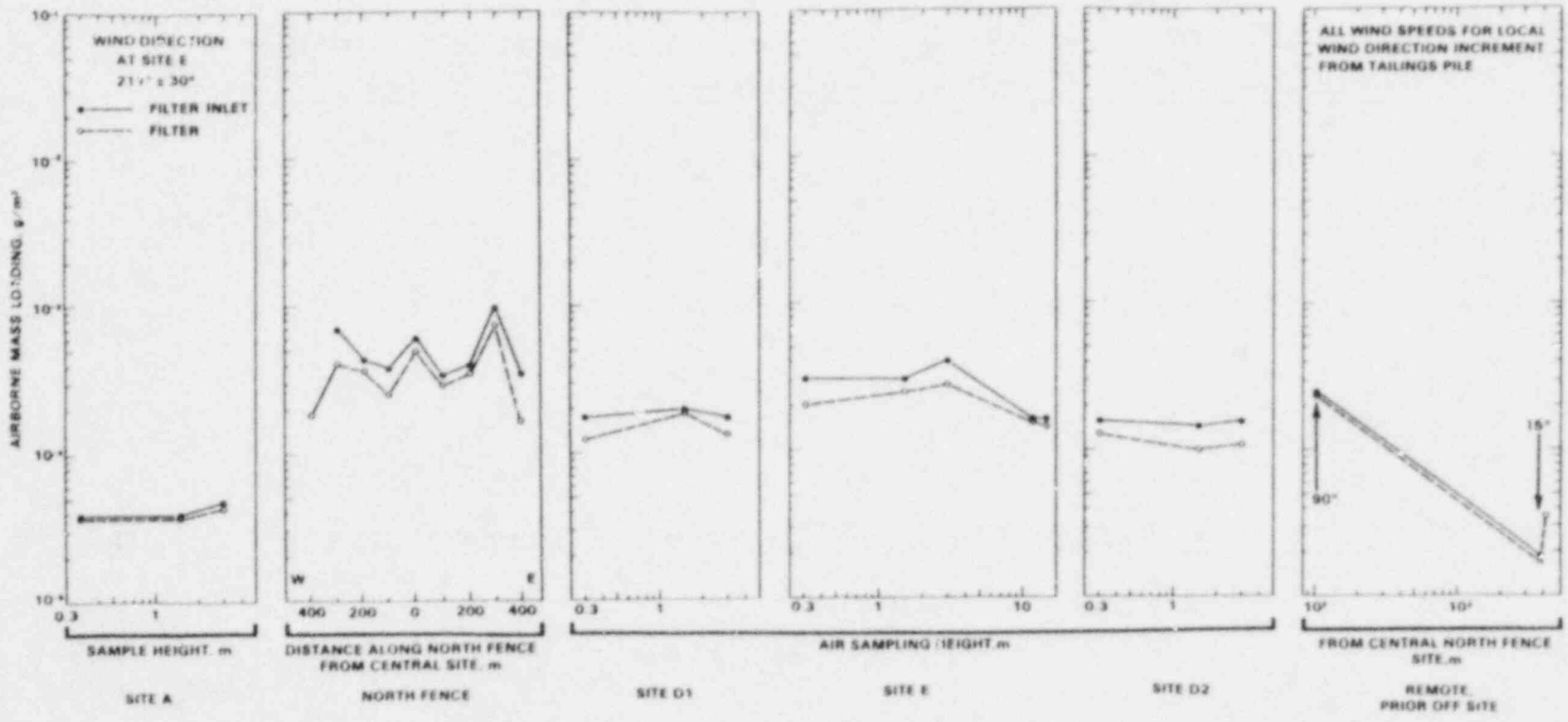

FIGURE 53. Airborne Solid Concentrations at Each Site During March 8 to April 18, 1979 (80B236-7)

collections are shown as a function of sampling height at site A. Mass loadings are nearly constant, 4×10^{-5} g/m^3, i.e., 40 µg/m^3.

Airborne mass loadings increased across the tailings pile. As shown in the second subfigure, airborne mass loadings were greater along the north fence. Airborne mass loadings increased up to 1 order of magnitude above background mass loadings. In the next three subfigures (for sites D-1, E, and D-2), airborne mass loadings variations are a function of height and crosswind distance. The maximum mass loadings were near the central site E. Airborne mass loadings decreased on either side as indicated by data for sites D-1 and D-2. At all three sites airborne mass loadings were nearly uniform as a function of height. From this uniformity we conclude that a fraction of the airborne plume was passing above the uppermost sampler.

Data for remote sites are shown in the sixth subfigure as a function of distance from the central north fence sampling site. Sampling times at these sites were during all wind speeds for the indicated wind direction sector, approximately encompassing the wind direction coming from the pile towards each sampler site. Data for sampling site R-1 are shown as a 90^{o} wind-direction sector and sites R-3 and R-4 by the 15^{o} wind direction sectors. Airborne mass loadings decrease with increasing distance from the north fence and tend to approximate background mass loadings at site A for distances greater than about 800 m.

Relative Collection Site

The percent of filter-collected particles of the total airborne particle collection within isokinetic samplers is shown in Figure 54. In all cases, over 90% of the solids are collected on the filter.

Radionuclide Activity Density on Airborne Solids

Selected airborne particulates samples were analyzed for ^{235}U, ^{238}U, ^{230}Th, ^{226}Ra, ^{214}Pb, and ^{210}Pb radionuclide content.

Uranium-235, dpm/g. Activity densities for ^{235}U are shown in Figure 55. Approximately one-half of these results were calculated from less-than

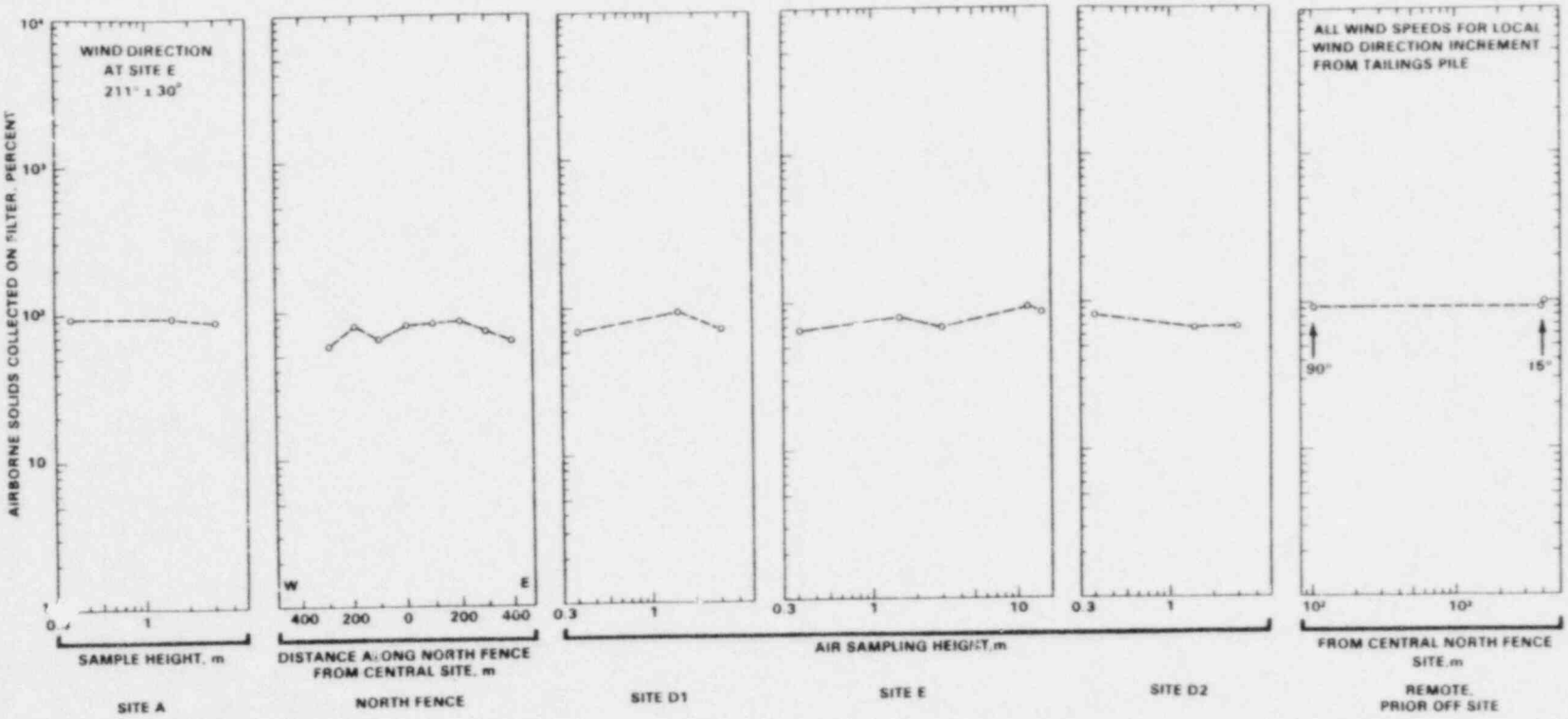

FIGURE 54. Percent Airborne Solids Collected on the Filter at Each Site During March 8 to April 18, 1979 (80B236-21)

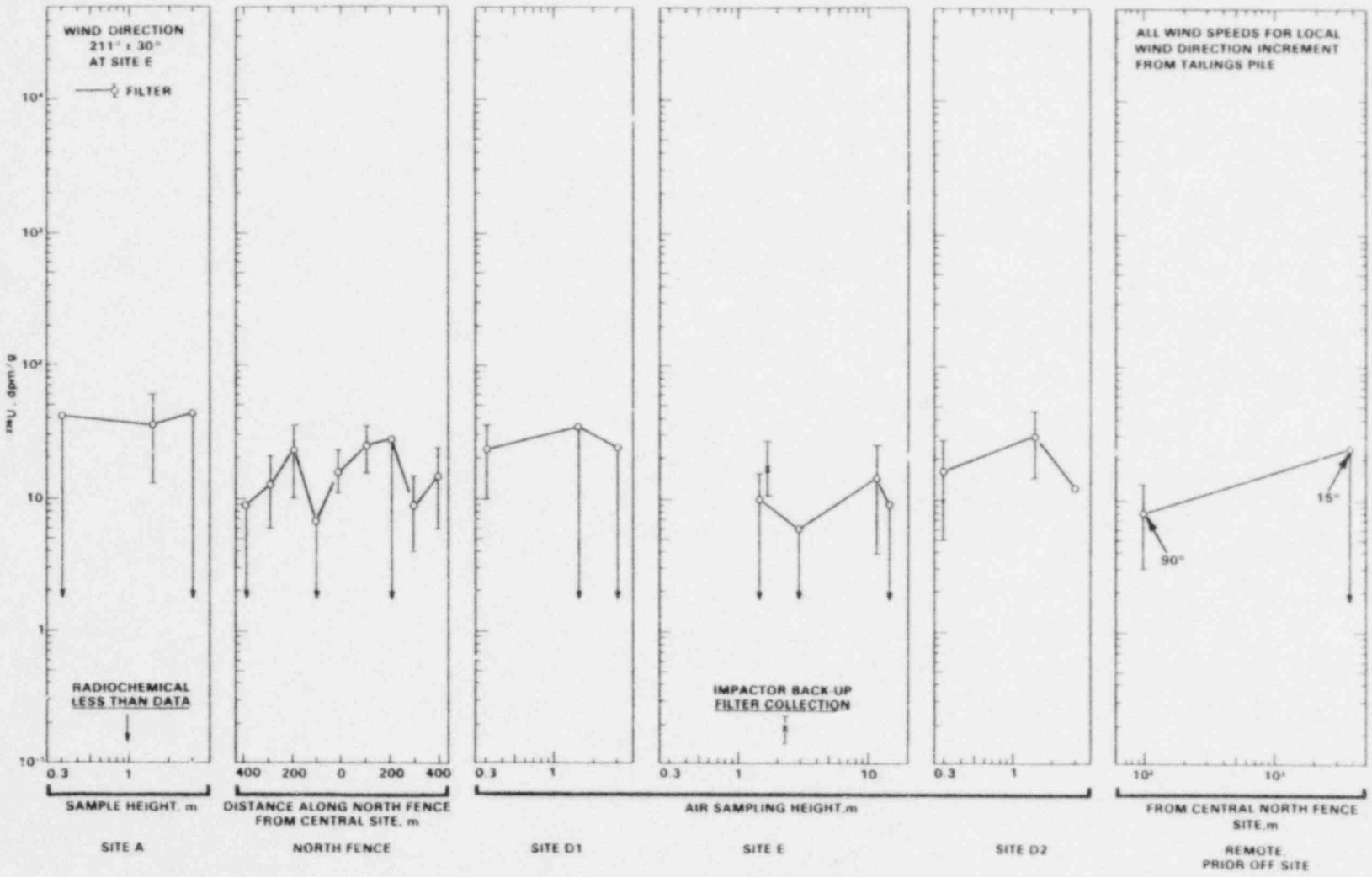

FIGURE 55. ^{235}U Concentrations at Each Site During March 8 to April 18, 1979 (80B236-39)

radiochemical detection limit data as indicated by the arrows. The greatest activity density was measured at the background site A, rather than at one of the down-wind sampling sites. For all other sampling sites activity densities are uniform within the data scatter.

Uranium-238, dpm/g. Activity densities for ^{238}U are shown in Figure 56. Activity densities are uniform for all sampling sites including background site A. This uniformity in activity densities for all sampling sites may reflect a secondary source of ^{238}U wind erosion upwind of the mill tailings pile and rapid deposition downwind of site A.

Thorium-230, dpm/g. Activity densities for ^{230}Th are shown in Figure 57. Thorium-230 was definitely wind eroded from the mill tailings pile. Background activity densities might be approximated by the 15^{o} remote site data shown in the extreme righthand subfigure. At this site the activity density is in the range indicated by the less-than numbers at site A. Activity densities along the north fence and remote sites D-1, E, and D-2 were approximately 1 order of magnitude greater than background.

Radium-226, dpm/g. Activity densities for ^{226}Ra are shown in Figure 58. This data set definitely shows increased activity densities above background. Background activity densities are shown for site A and are approximately uniform as a function of height. Downwind along the north fence and sites D-1, E, and D-2, activity densities increased almost 1 order of magnitude. At the 15^{o} remote site, the activity density determined with the filter sample is comparable to background activity densities at site A. At the second 15^{o} remote site, the activity density determined from the cascade particle impactor backup filter collection is closer to activity densities determined along the north fence, and sites D-1, E, and D-2. Thus, these 15^{o} remote site data are inconsistent. In some cases, activity densities are greater than background for distances greater than 4000 m.

Lead-214, dpm/g. Activity densities for ^{214}Pb are shown in Figure 59. These data are presented merely for interest at this time, but are a reference in comparison with ^{210}Pb concentrations. Lead-214 is a short-lived ^{226}Ra daughter product. There appears to be some particle size dependency shown by

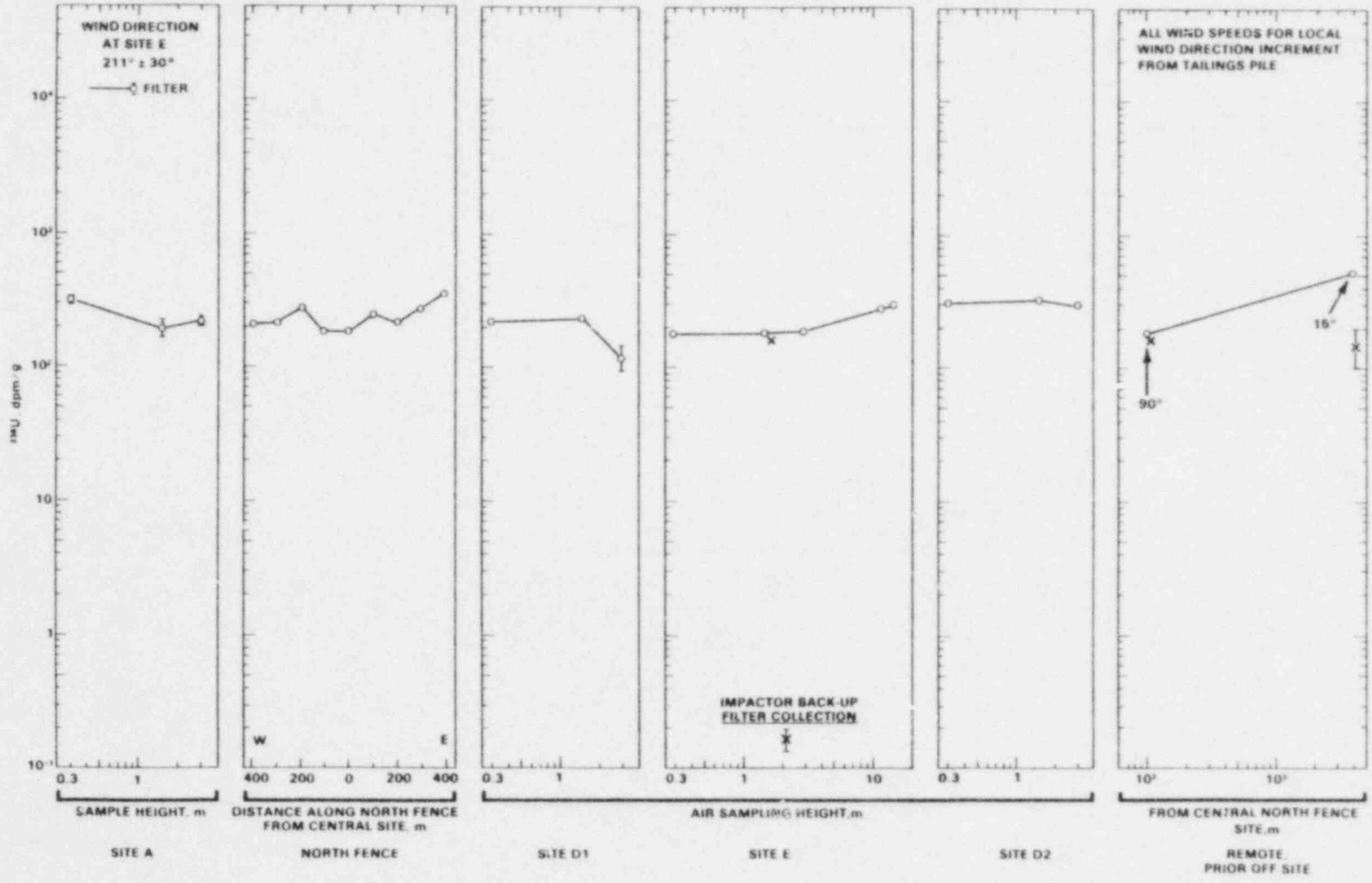

FIGURE 56. ^{238}U Concentrations on Airborne Solids at Each Site During March 8 to April 18, 1979 (80B236-43)

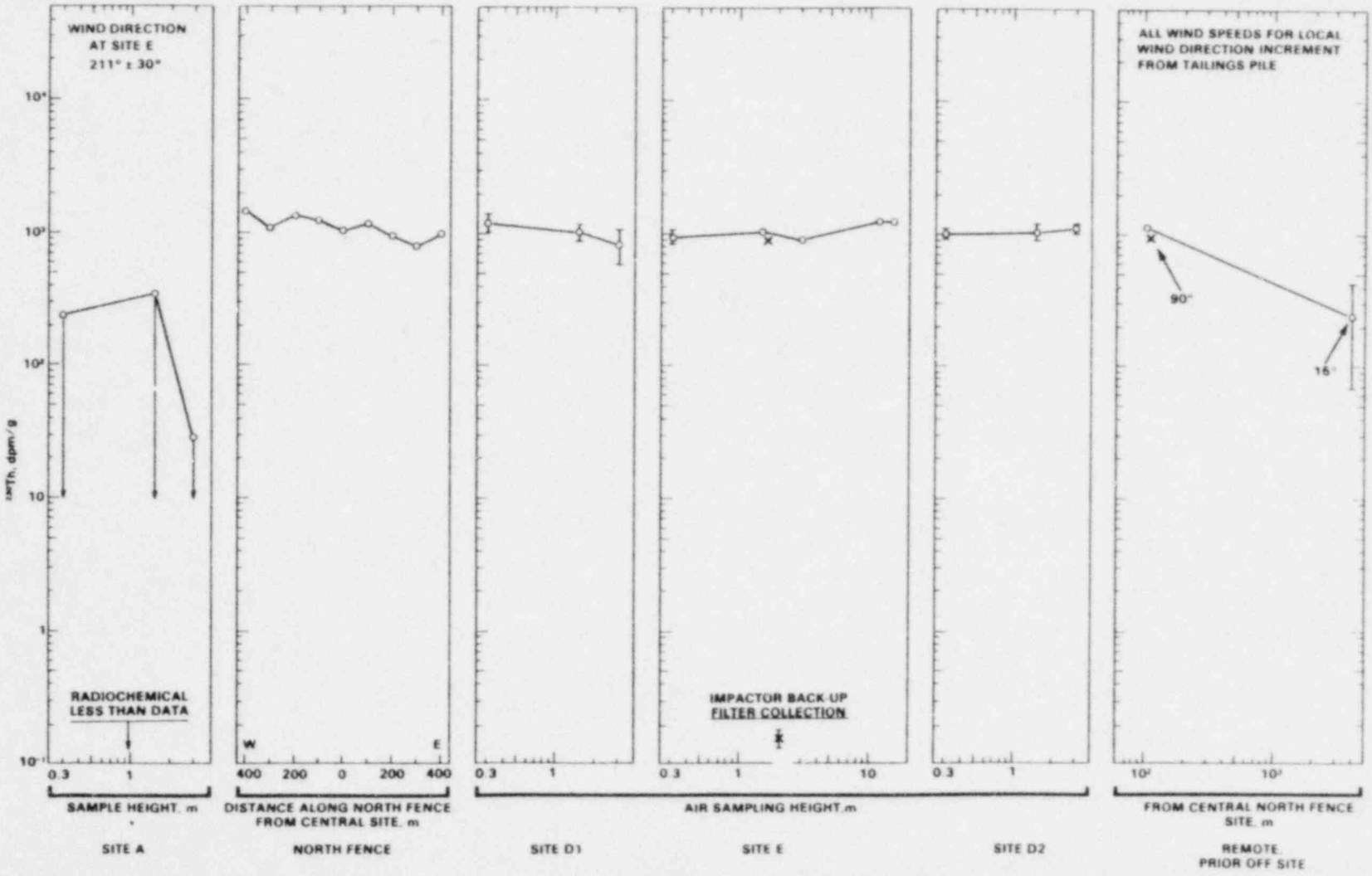

FIGURE 57. ^{230}Th Concentrations on Airborne Solids at Each Site During March 8 to April 18, 1979 (80B236-48)

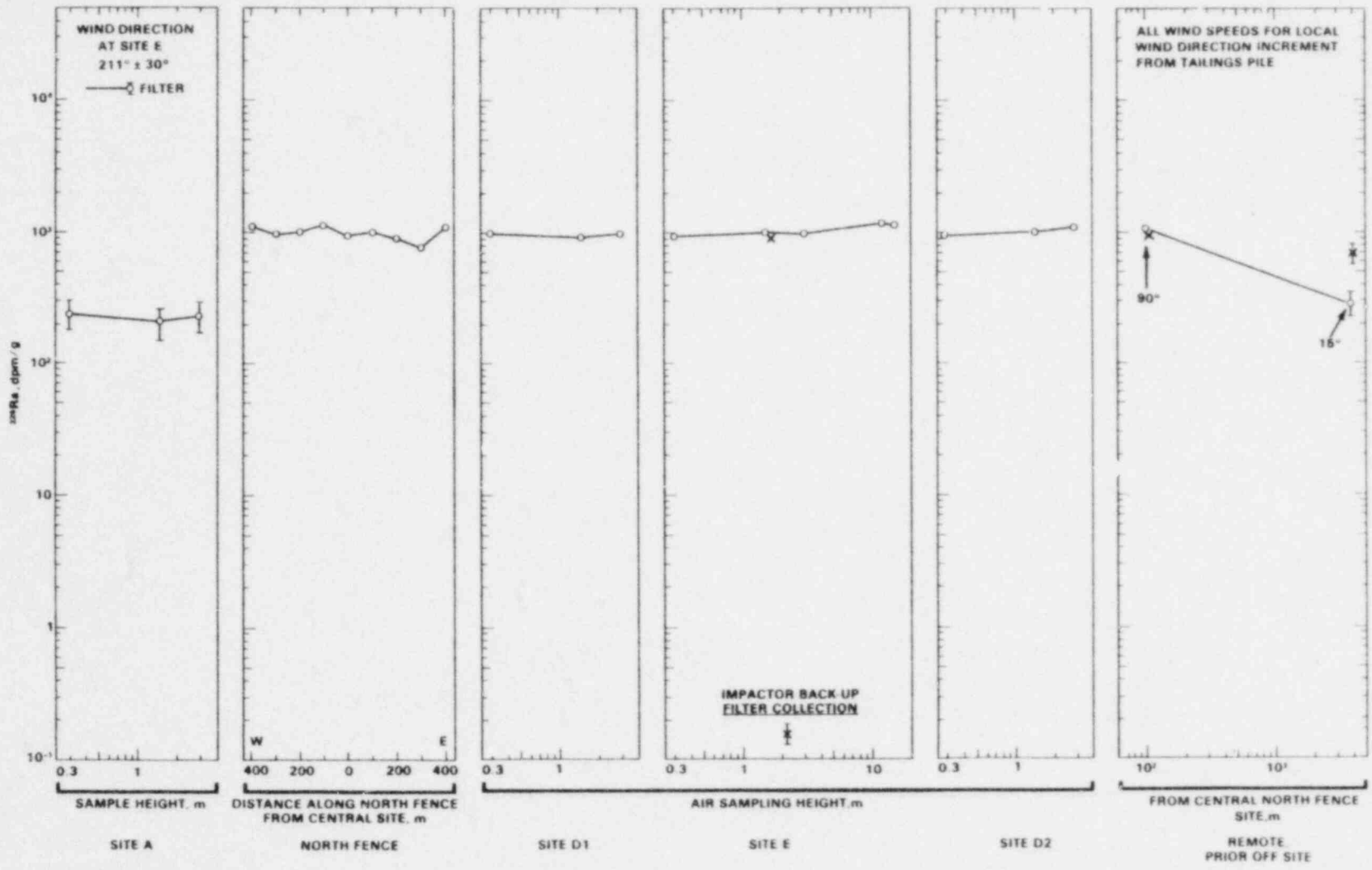

FIGURE 58. ^{226}Ra Concentrations at Each Site on Airborne Solids at Each Site During March 8 to April 18, 1979 (80B236-46)

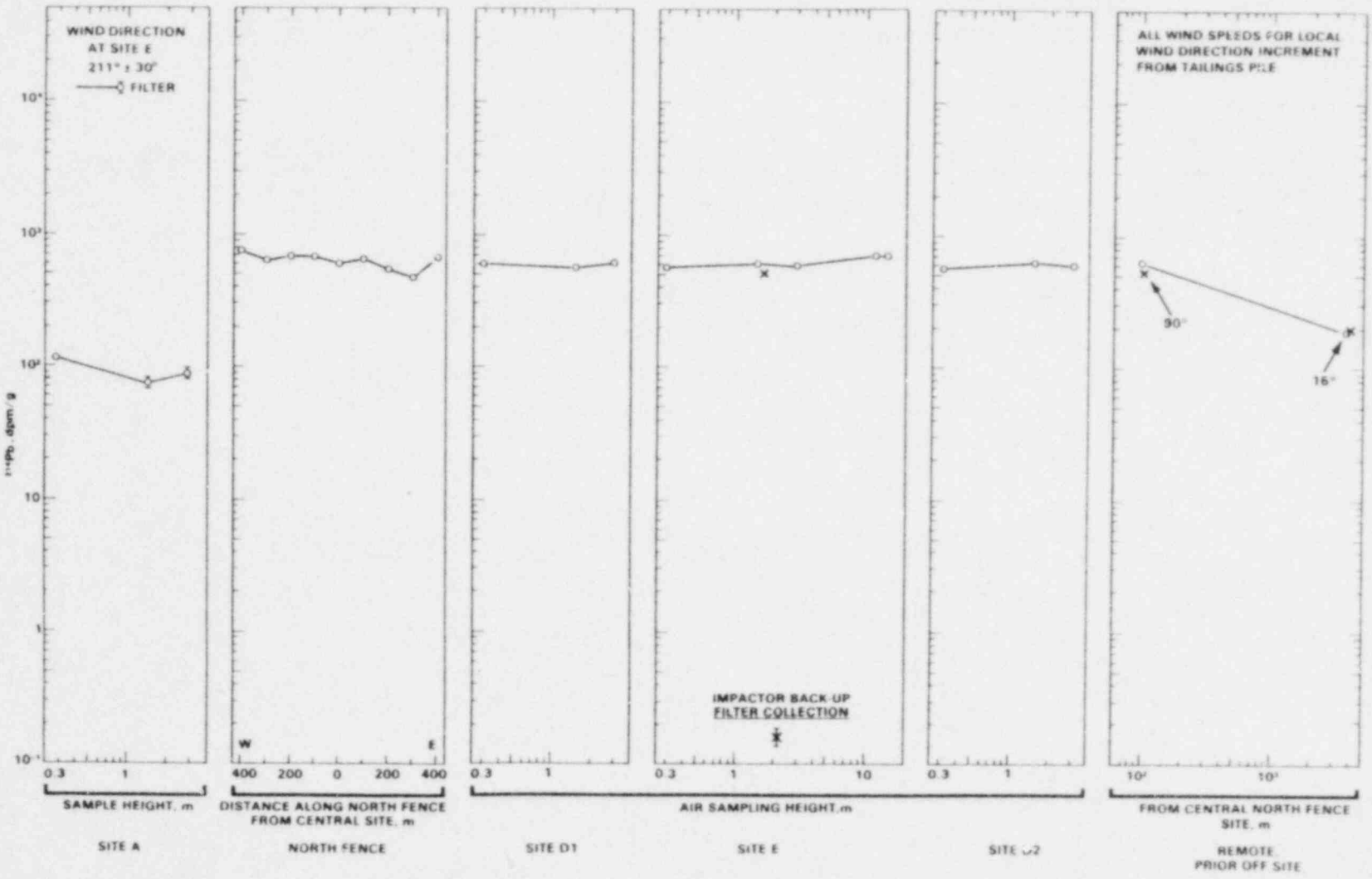

FIGURE 59. ^{214}Pb Concentrations on Airborne Solids at Each Site During March 8 to April 18, 1979 (80B236-47)

these ^{214}Pb activity densities. At the background site A, activity densities were approximately 1 order of magnitude lower than activity densities determined for the north fence sites and at remote sites D-1, E, and D-2. Decreased activity densities at site A may reflect more rapid radon diffusion from particles collected at site A.

Lead-210, dpm/g. Activity densities for ^{210}Pb are shown in Figure 60. Activity densities are approximately 10^2 dpm/g for the background sampling site A while activity densities are appoximately 10^3 dpm/g for all other sites. Surprisingly, activity densities at the two 15^o remote sites are the greatest activity densities determined during this time period. These large activity densities at the 15^o sites are probably caused in part by ^{210}Pb resuspension from secondary ground sources previously deposited from mill tailings erosion. The ground surface area of the secondary source is greater than the pile surface area.

Airborne Radionuclide Concentrations

Airborne radionuclide concentrations, $\mu Ci/cm^3$, were calculated for ^{235}U, ^{238}U, ^{230}Th, ^{226}Ra, and ^{210}Pb. Airborne radionuclide concentrations are compared to Table I and II guidance levels from 10 CFR 20 (1979).

Uranium-235, $\mu Ci/cm^3$. Airborne ^{235}U concentrations are shown in Figure 61. Airborne concentrations range from approximately 10^{-16} to 10^{-14} $\mu Ci/cm^3$. Maximum airborne concentrations were three orders of magnitude less than Table II guidance levels.

Background airborne ^{235}U concentrations for site A are shown in the first subfigure. Only the datum for the 1.5-m sampling height was above radiochemical detection limits. Airborne concentrations increased during air transport across the mill tailings pile. Airborne ^{235}U concentrations vary within 1 order of magnitude along the north fence and are approximately five times airborne concentrations measured at site A. At sites D-1, E, and D-2, airborne concentrations do not show large decreases from concentrations measured along the north fence. Since airborne concentrations are approximately uniform as a function of height, we again conclude the airborne plume from the mill tailings pile was probably passing over the uppermost sampling heights at sites D-1, E, and

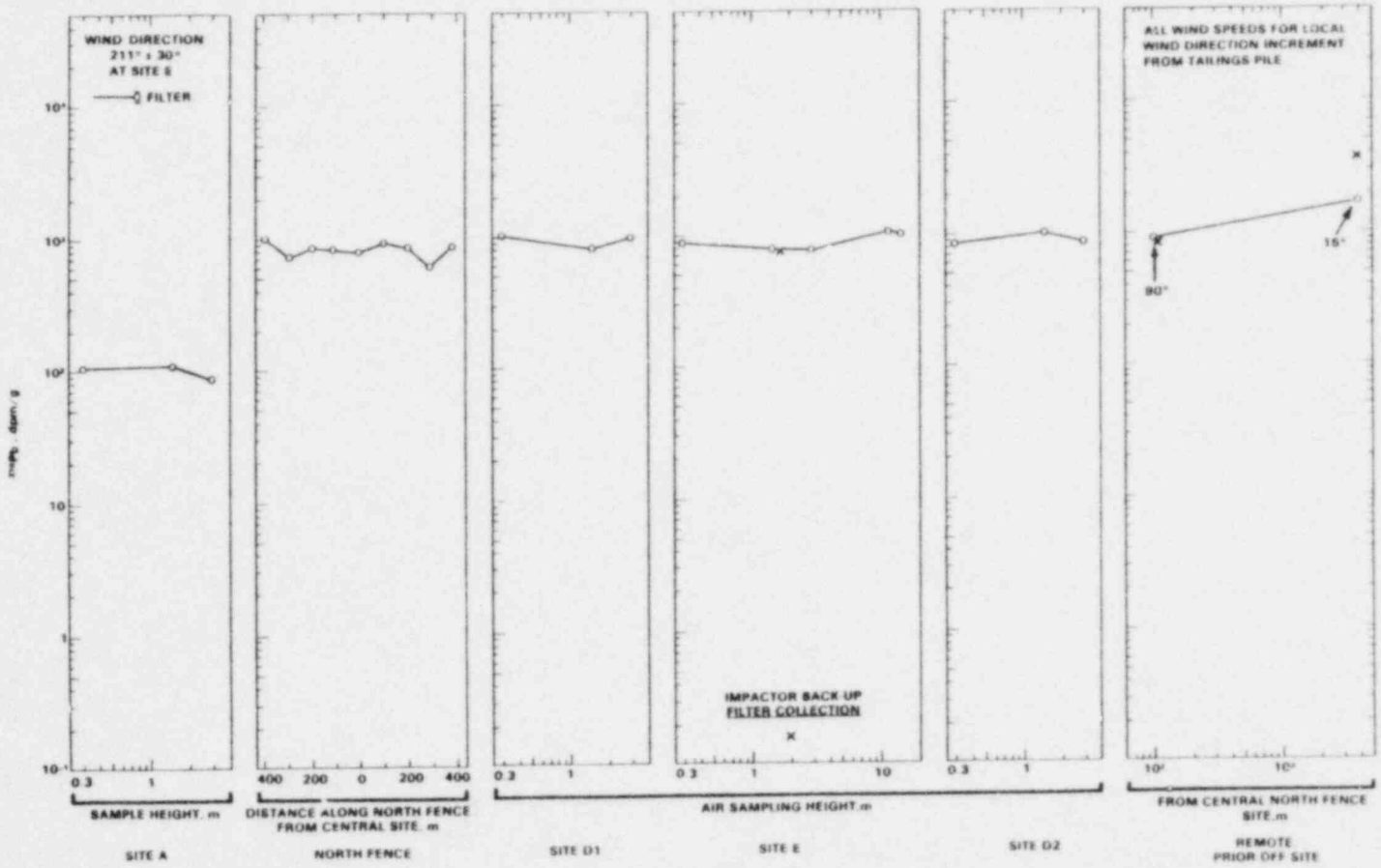

FIGURE 60. ^{210}Pb Concentrations on Airborne Solids at Each Site During March 8 to April 18, 1979 (80B731-3)

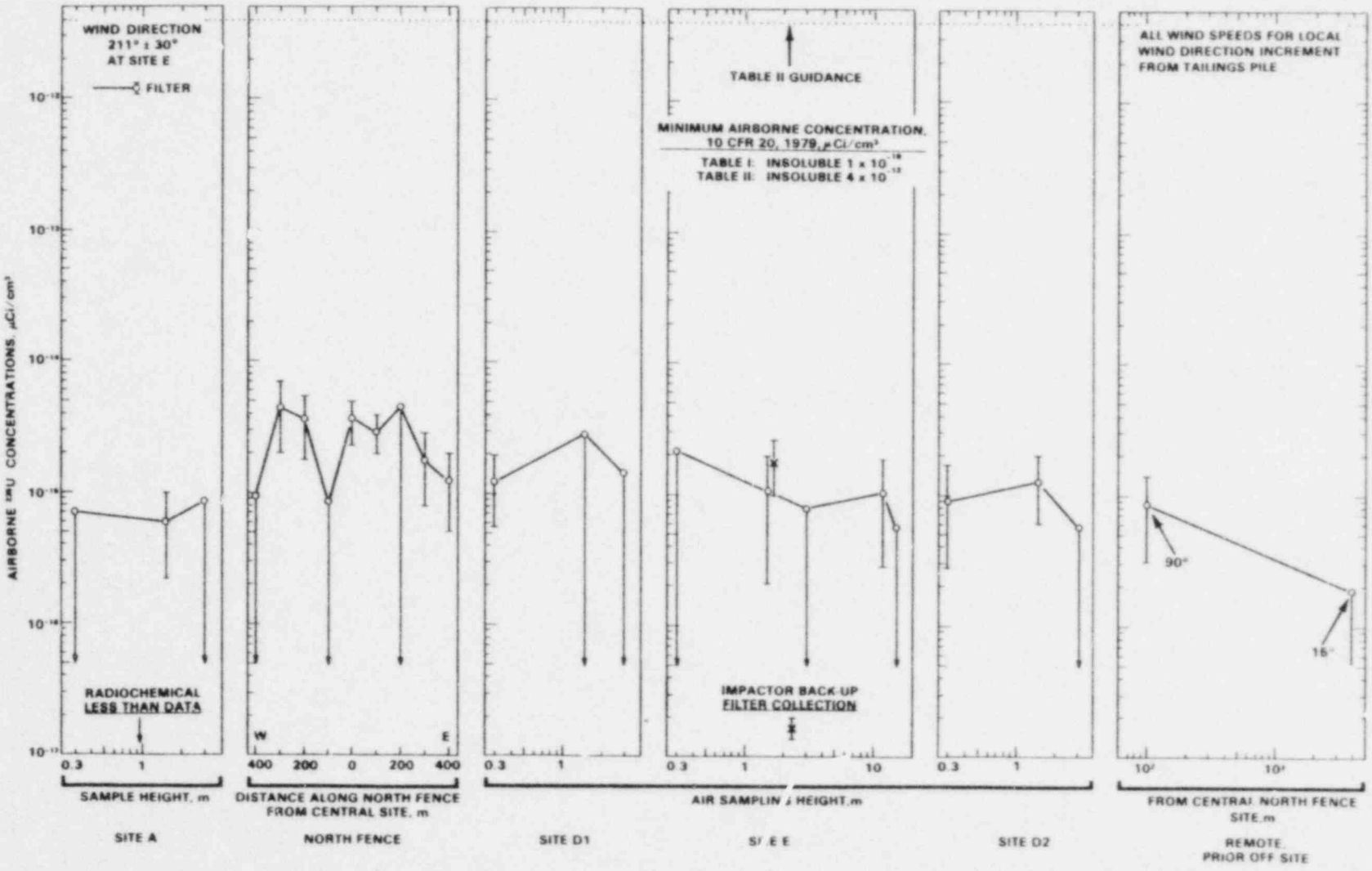

FIGURE 61. ^{235}U Concentrations on Airborne Solids at Each Site During March 8 to April 18, 1979 (80B236-36)

D-2. At the 15° remote site the calculated airborne concentration was a less-than number. Nevertheless, this 15° remote site datum point is significantly less than site A background measured at 1.5-m height. A comparison of the 15° datum and site A datum suggests secondary sources of wind-eroded ^{235}U are present upwind of site A. Secondary sources could be mill tailings materials previously wind eroded and deposited around the mill tailings area.

Uranium-238, $\mu Ci/cm^3$. Airborne ^{238}U concentrations are shown in Figure 62. Airborne concentrations range from approximately 10^{-15} to 10^{-13} $\mu Ci/cm^3$. Maximum airborne concentrations were over 1 order of magnitude less than Table II guidance levels.

Calculated airborne ^{238}U concentrations are well-defined by narrow radiochemical analysis confidence limits at all sampling locations. Concentrations determined from the particle cascade impactor backup filter collection were less than concentrations determined from a total isokinetic filter sample. At background site A airborne ^{238}U concentrations were approximately 4×10^{-15} $\mu Ci/cm^3$. Background concentrations were again observed approximately 4,000-m downwind from the mill-tailings area.

Downwind of site A, airborne ^{238}U concentrations increased about 1 order of magnitude along the north fence. Subsequently, concentrations decreased with increasing distance. Concentrations at sites D-1, E, and D-2 were less than concentrations measured along the north fence. Since concentrations were nearly uniform as a function of sampling height at sites E and D-2, we conclude that the airborne ^{238}U plume was passing over the uppermost samplers at these sites. In contrast at site D-1, airborne concentrations showed a significant decrease at the 3-m height. Thus, at site D-1, the airborne plume appeared to be transported closer to ground level than at sites E and D-2. Airborne concentrations at remote sites decreased with increasing distance.

Thorium-230, $\mu Ci/cm^3$. Airborne ^{230}Th concentrations are shown in Figure 63. In comparison, Table I and II guidance levels are also shown. Airborne concentrations were greater than Table II guidance at sites along the north fence, D-1, E, D-2, and the 90° remote site.

Airborne ^{230}Th concentrations were above site A background concentrations at all sites except the 15° remote site. All results from site A were

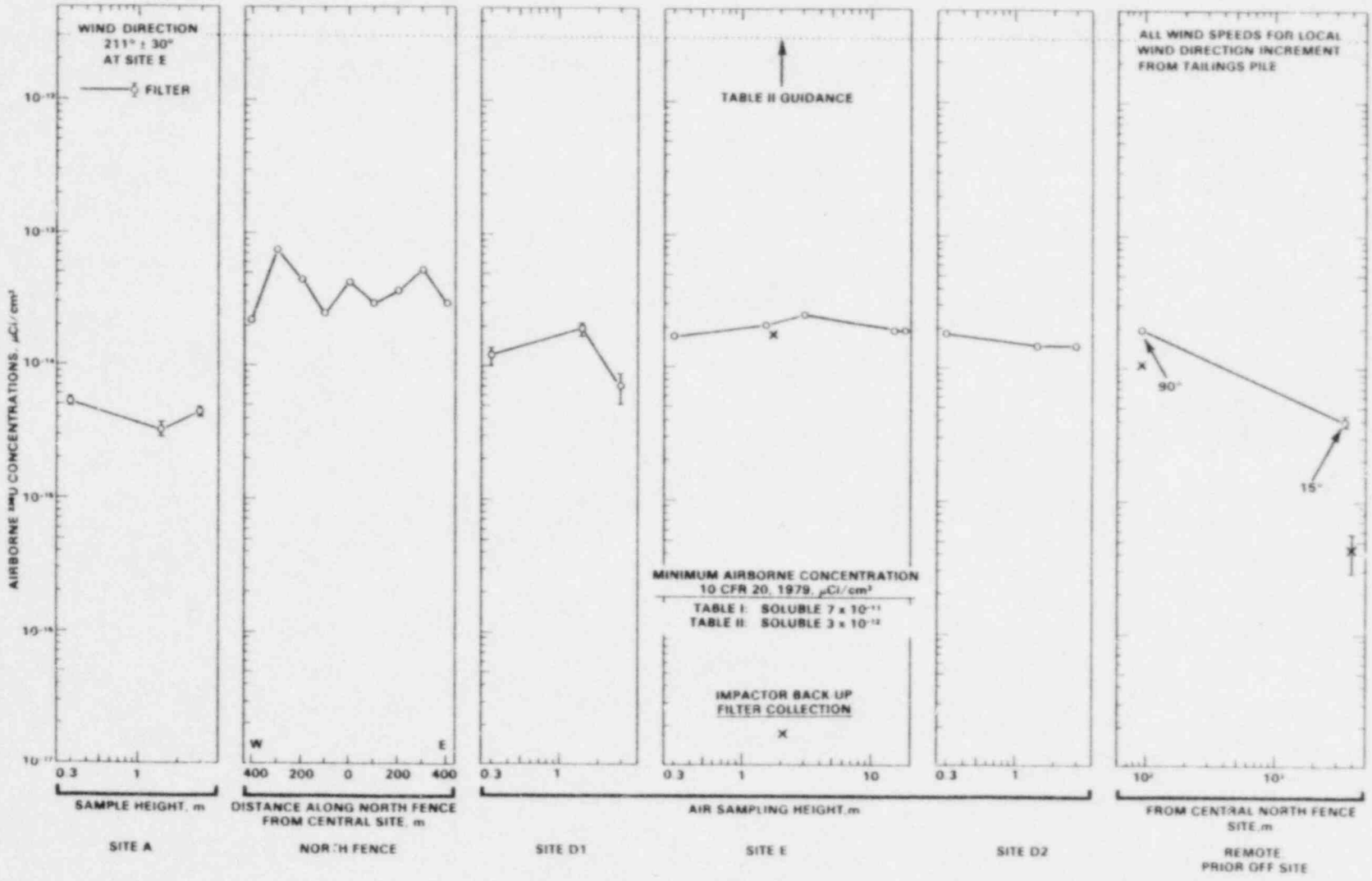

FIGURE 62. ^{238}U Concentrations on Airborne Solids at Each Site During March 8 to April 18, 1979 (80B236-35)

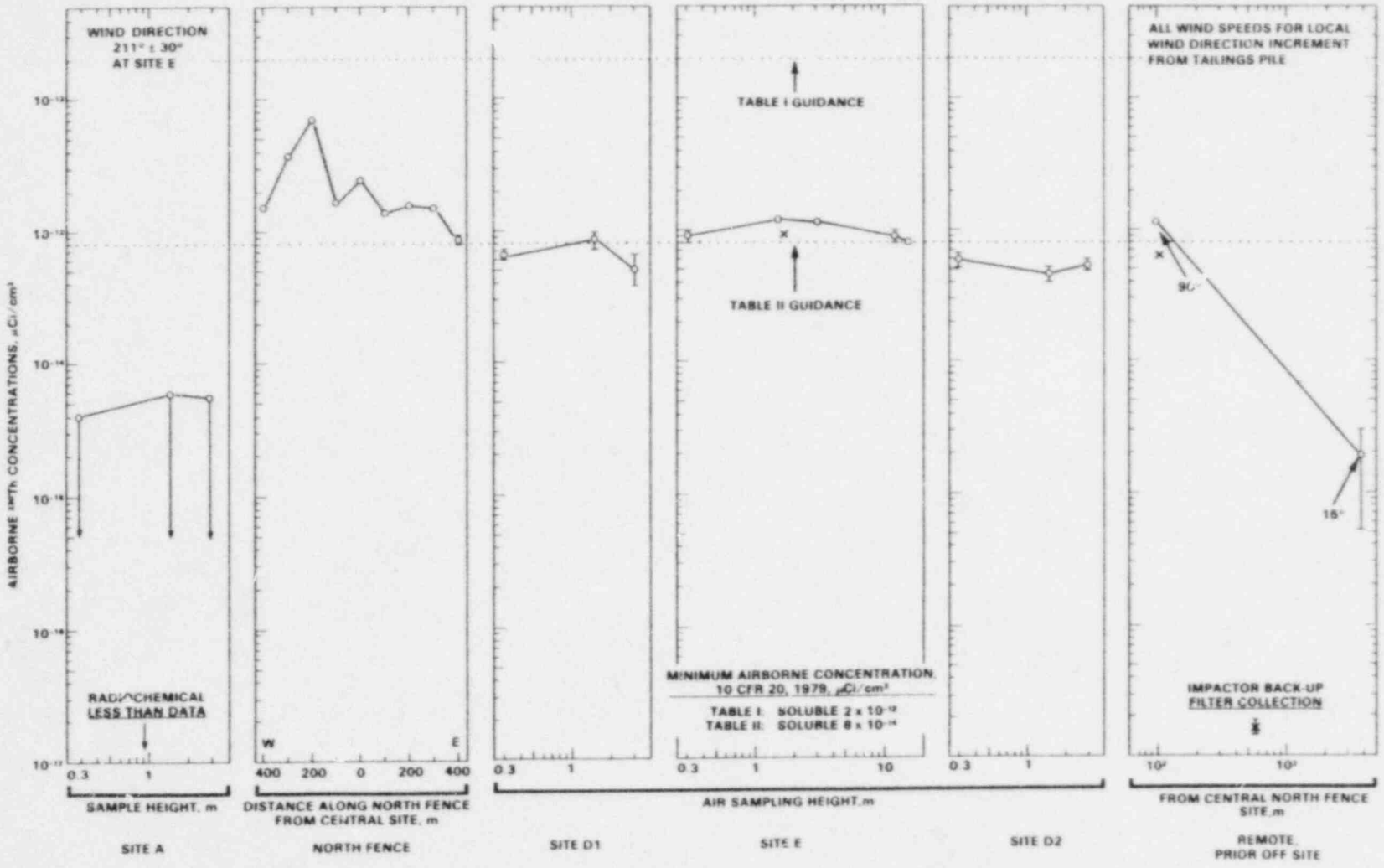

FIGURE 63. Airborne ^{230}Th Concentrations at Each Site During March 8 to April 18, 1979 (data symbols for 5 to 7 and 7 to 11 m/sec offset from sampling heights to show the 1σ counting limits) (80B236-30)

calculated from less-than radiochemical detection limits. Background is estimated to be about 2×10^{-15} $\mu Ci/cm^3$ from the 15° sampling site datum and cross-comparisons with background data shown for site A.

Airborne ^{230}Th concentrations were maximum along the north fence. Except for the two most western samples, airborne ^{230}Th concentrations tended to decrease from west to east. This concentration decrease from west to east is similar to the concentration decrease previously shown for ^{230}Th in Figure 45.

Similar to the discussion of Figure 45, the relative y and z dimensions of the airborne plume with ^{230}Th concentrations above Table II guidance can be estimated from concentrations shown for D-1, E, and D-2. In Figure 45 the plume width was relatively narrow, and the width did not extend to either site D-1 or D-2. In the present case for Figure 63, plume width is wider. Plume width extends at least 450 m, the distance between site D-1 and E. Probably plume width also extends to site D-2. Plume height extended above the 15-m uppermost sampler at site E.

The airborne plume at site E may be composed principally of respirable size particles. This is inferred from the one datum for the impactor backup filter collection. The concentration for this datum point is only slightly less than concentrations for filter-collected total-samples collected at site E.

Radium-226, $\mu Ci/cm^3$. Airborne ^{226}Ra concentrations are shown in Figure 64. Airborne ^{226}Ra concentrations are about 1 order of magnitude less than Table II guidance level at sites along the north fence, D-1, E, and D-2. The majority of ^{226}Ra transport was on respirable size particles, which is inferred from data points for impactor backup filter collections and filter-collected total samples at site E and the two remote sites.

Background concentrations at site A may be influenced by secondary resuspension sources. Airborne concentrations at site A were approximately twice concentrations at the 15° remote site.

Lead-210, $\mu Ci/cm^3$. Airborne ^{210}Pb concentrations are shown in Figure 65. All airborne concentrations were 1 order of magnitude less than Table II

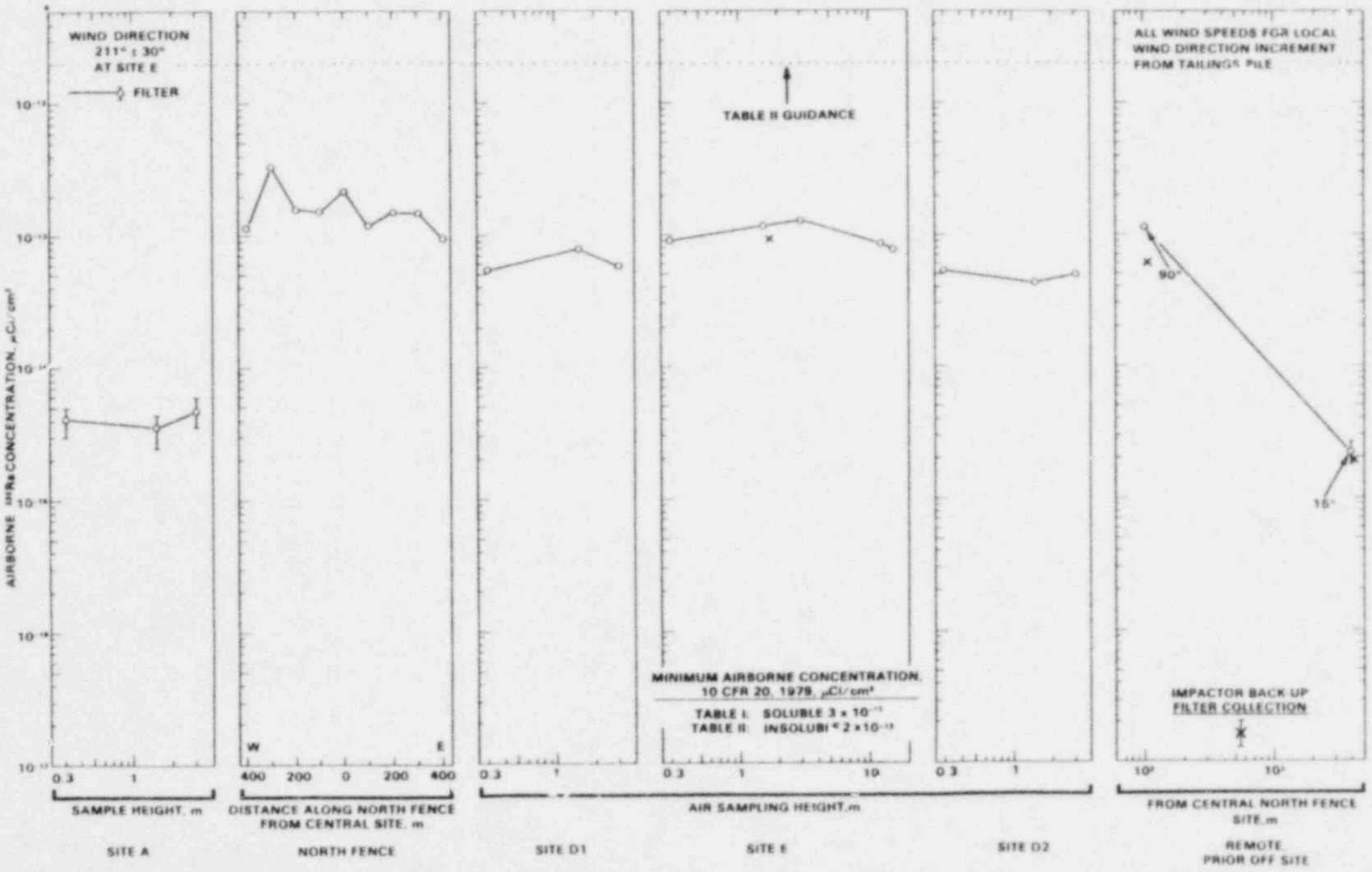

FIGURE 64. ^{226}Ra Concentrations at Each Site During March 8 to April 18, 1979 (80B236-34)

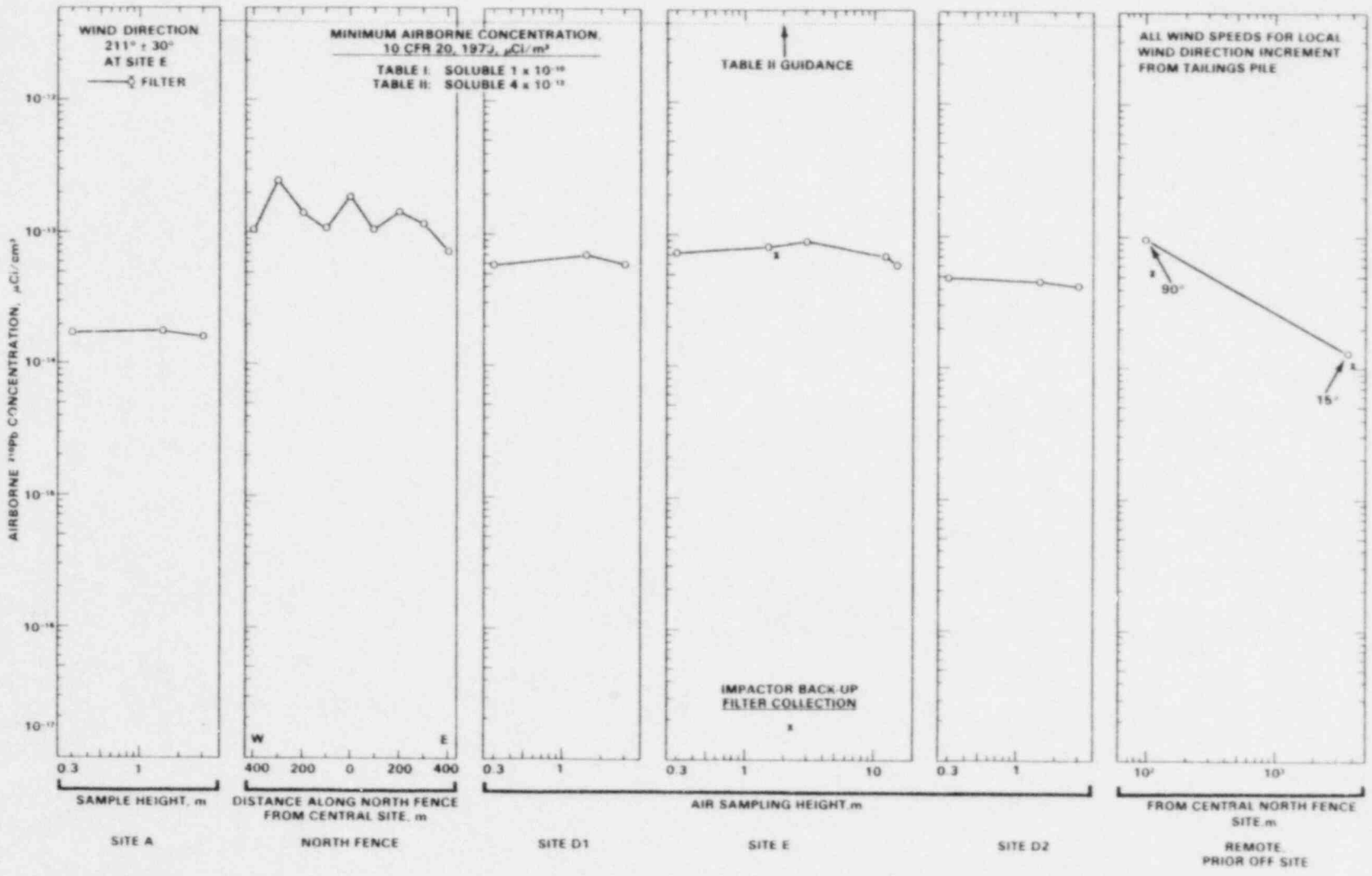

FIGURE 65. Airborne ^{210}Pb Concentrations at Each Site During March 8 to April 18, 1979 (80B236-37)

guidance levels. Airborne concentrations showed the same general trends along the north fence as previously reported in Figure 47. Airborne ^{210}Pb concentrations, except for the westernmost sampling location, tended to decrease from west to east. The airborne ^{210}Pb plume height and width extended beyond and above sampling sites D-1, E, and D-2. Airborne concentrations at the 15^{o} remote sites were approximately background.

Normalized Activity Densities

Activity densities are used to estimate the apparent nonequilibrium between radioactive decay products on airborne solids. To estimate this nonequilibrium, activity densities for ^{238}U, ^{230}Th and ^{226}Ra were normalized by corresponding activity densities for ^{210}Pb. Activity density ratios other than unity indicate a non-one-to-one correspondence between airborne transport for different radionuclide members of the ^{238}U decay series.

Normalized to ^{210}Pb. Activity ratios for $^{238}U/^{210}Pb$ are shown in Figure 66. Activity ratios were nearly uniform at all sites, ranging from 0.1 to 0.5, except for the impactor backup filter collection at the 15^{o} remote site. Activity ratios at the 15^{o} remote site show a particle-size dependency not observed for backup filter collections at site E or the 90^{o} remote site.

Activity ratios for $^{230}Th/^{210}Pb$ are shown in Figure 67. In contrast to the prior figure, activity ratios for $^{230}Th/^{210}Pb$ were a function of sampling location. At both the background site A and 15^{o} remote site, the activity ratio was approximately 0.1. At all other sites, activity ratios were approximately unity.

Activity ratios for $^{226}Ra/^{210}Pb$ shown in Figure 68 show similar results. At both sites A and 15^{o}, activity ratios were approximately 0.2. At all other sites, activity ratios were approximately unity.

In cross comparing activity ratio data from the last three figures, it is seen that airborne radionuclides are transported with an apparent nonequilibrium between radioactive decay products on airborne solids. That is, airborne concentrations of ^{230}Th, ^{226}Ra and ^{210}Pb are greater than airborne concentrations of ^{238}U. This observation is in accord with the fact that over 90% of the uranium was removed in the uranium mill.

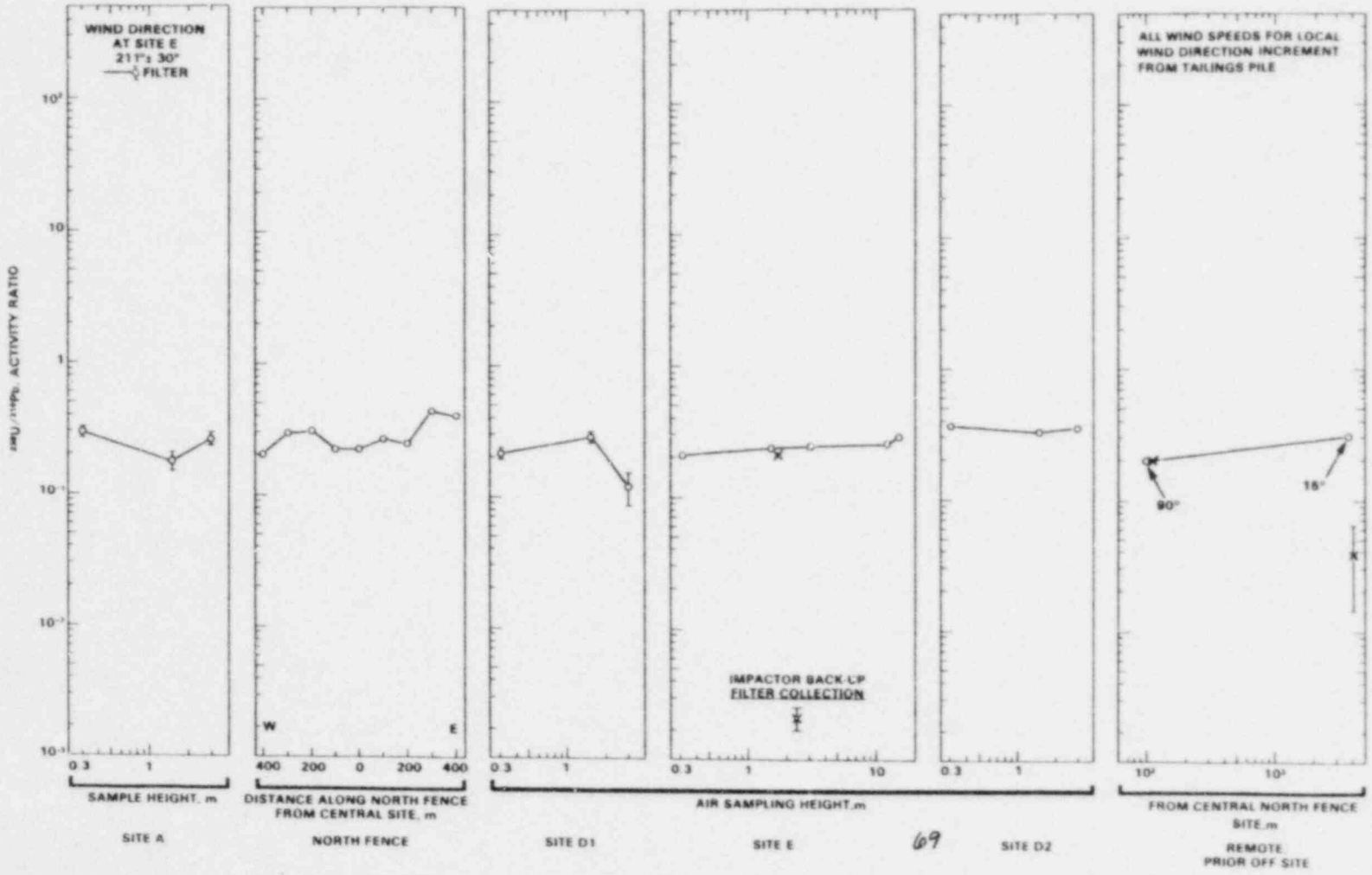

FIGURE 66. Airborne ^{238}U Activity Normalized to ^{210}Pb Activity on Airborne Solids at Each Site During March 8 to April 18, 1979 (80B318-69)

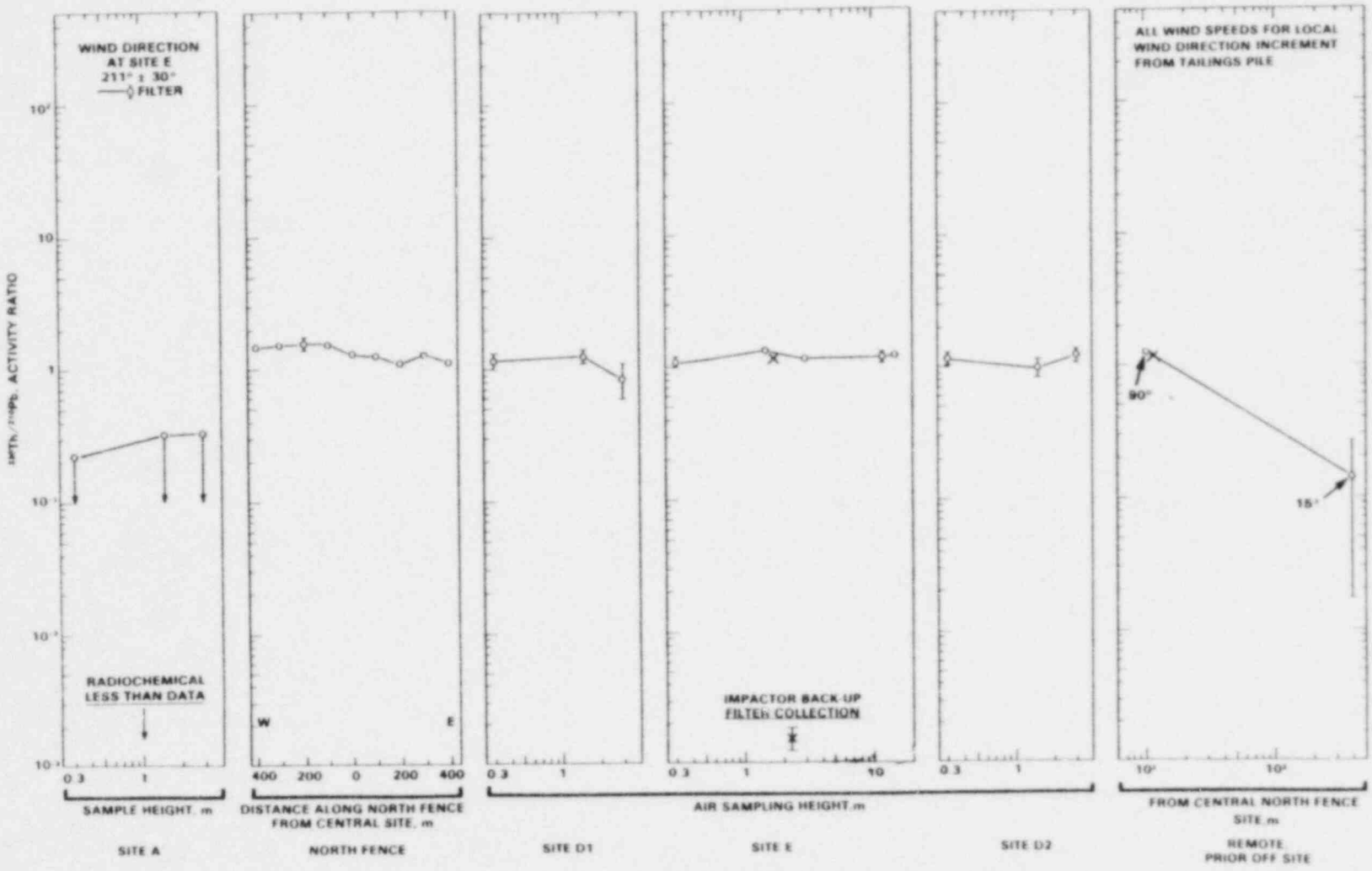

FIGURE 67. Airborne ^{230}Th Activity Normalized to ^{210}Pb Activity on Airborne Solids at Each Site During March 8 to April 18, 1979 (80B318-68)

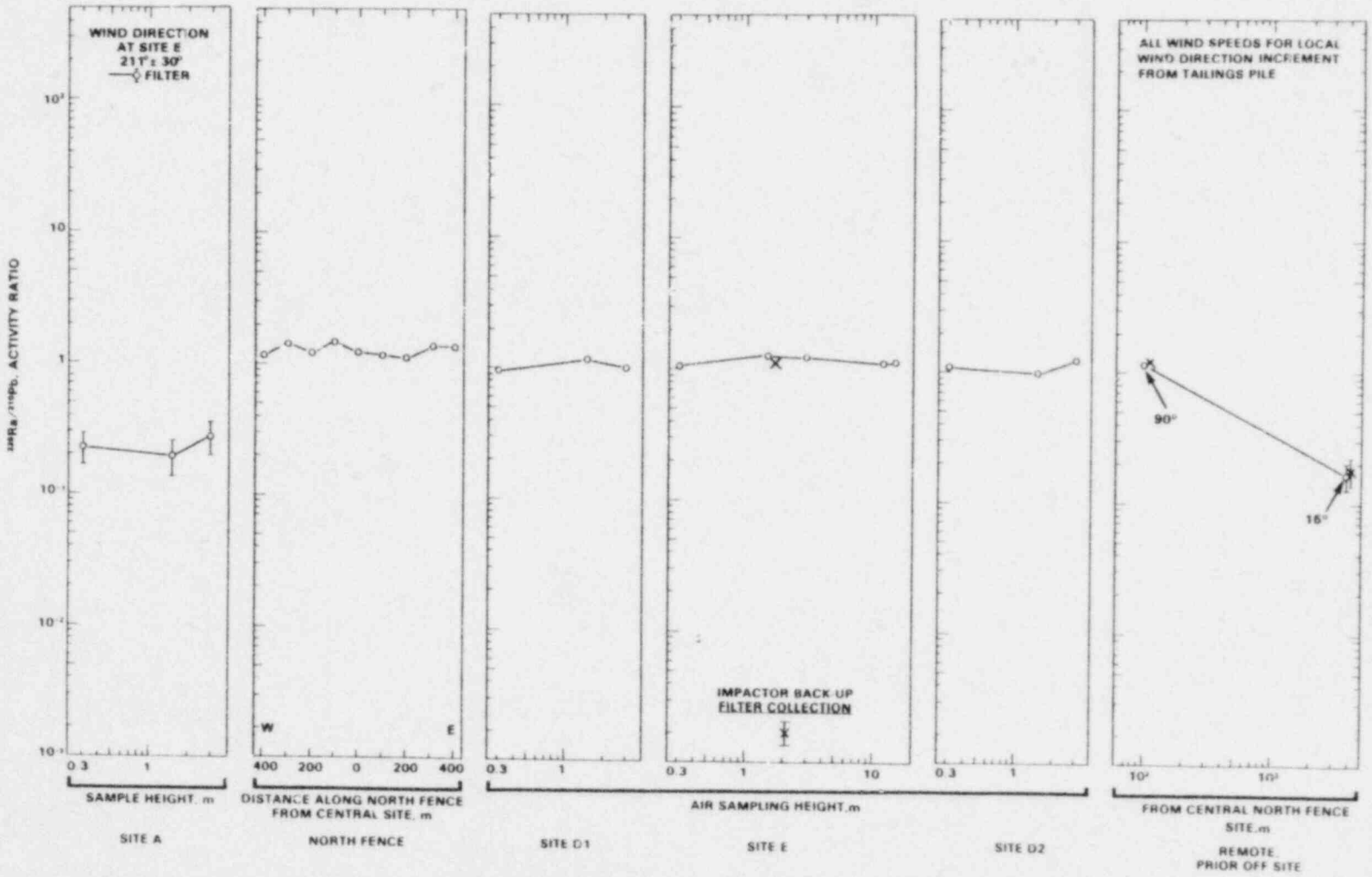

FIGURE 68. Airborne ^{226}Ra Activity Normalized to ^{210}Pb Activity on Airborne Solids at Each Site During March 8 to April 18, 1979 (808318-70)

Lead-214 Normalized Activity. Activity ratios for $^{214}Pb/^{210}Pb$ and $^{214}Pb/^{226}Ra$ were measured as indices for the presence of all radionuclides in secular equilibrium, and thus indicators for radon release after sample collection. Activity ratios for $^{214}Pb/^{210}Pb$ are shown in Figure 69. Two activity ratio ranges were observed. At both sampling site A and the 15° remote site, $^{214}Pb/^{210}Pb$ activity ratios were approximately 0.1 indicating loss of radon. At the other sites, in contrast, activity ratios were greater, approximately 0.7. Apparently at both site A and the 15° remote site, radon more readily escaped from these samples, or relatively greater ambient airborne ^{210}Pb concentrations were at site A and the 15° remote site.

The $^{214}Pb/^{210}Pb$ activity ratios of approximately 0.7 are significant to adequate data interpretations of reported airborne ^{210}Pb concentrations, $\mu Ci/cm^3$, or activity densities, dpm/g. Reported ^{210}Pb activity may be partly due to radon decay in the air as well as carried on tailings particles.

Insight into the amount of radon released from samples after field collection is shown by $^{214}Pb/^{226}Ra$ activity ratios given in Figure 70. The $^{214}Pb/^{226}Ra$ activity ratio at site A is low, only about 0.4. This low ratio suggests approximately 60% of the radon escaped after sample field collection at site A. Less radon escaped than from particles collected at the other sampling sites. At all other sites, the $^{214}Pb/^{226}Ra$ activity ratio was about 0.6. Thus, radon escape was only 40%, rather than 60%. This decreased release may be a function of the larger average particle diameter collected at those other sites, and the greater relative resistance to radon gas diffusion.

May 15 to July 9, 1979

Airborne particulates were sampled during a wind direction of $211° \pm 35°$ and wind-speed increments of 3 to 5 m/sec, 5 to 7 m/sec, and 7 to 11 m/sec measured at site E. Samples were collected at site A, north fence, D-1, E, D-2, and remote sites. Calculated results are shown for mass loadings, activity densities, airborne concentrations, and activity ratios.

Mass Loadings, g/m^3

Airborne mass loadings are shown in Figure 71. Wind-speed effects are unclear. Background mass loadings at site A ranged from 2×10^{-5} to $7 \times$

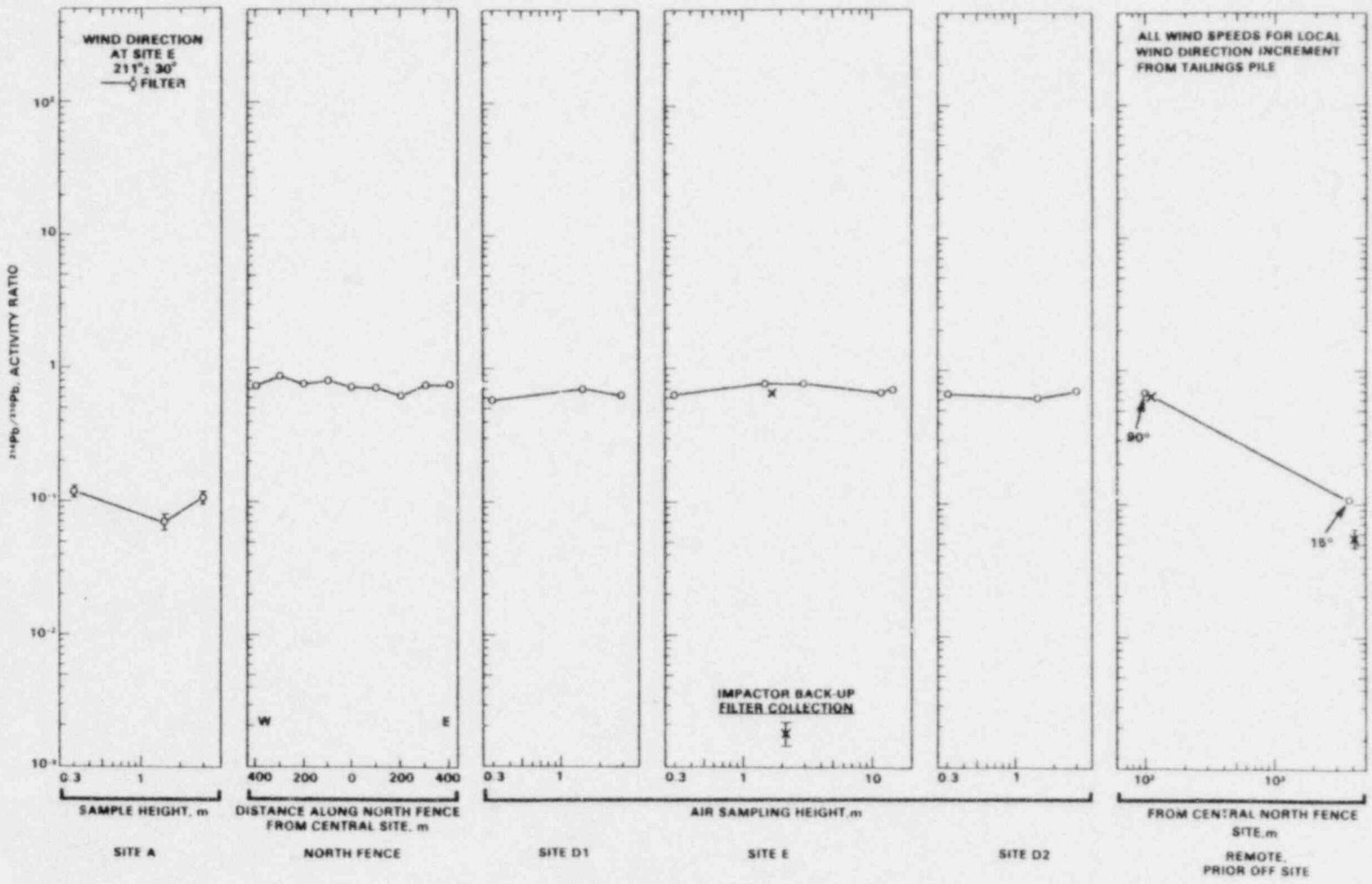

FIGURE G9. Airborne ^{214}Pb Activity Normalized to ^{210}Pb Activity on Airborne Solids at Each Site During March 8 to April 18, 1979 (80B318-71)

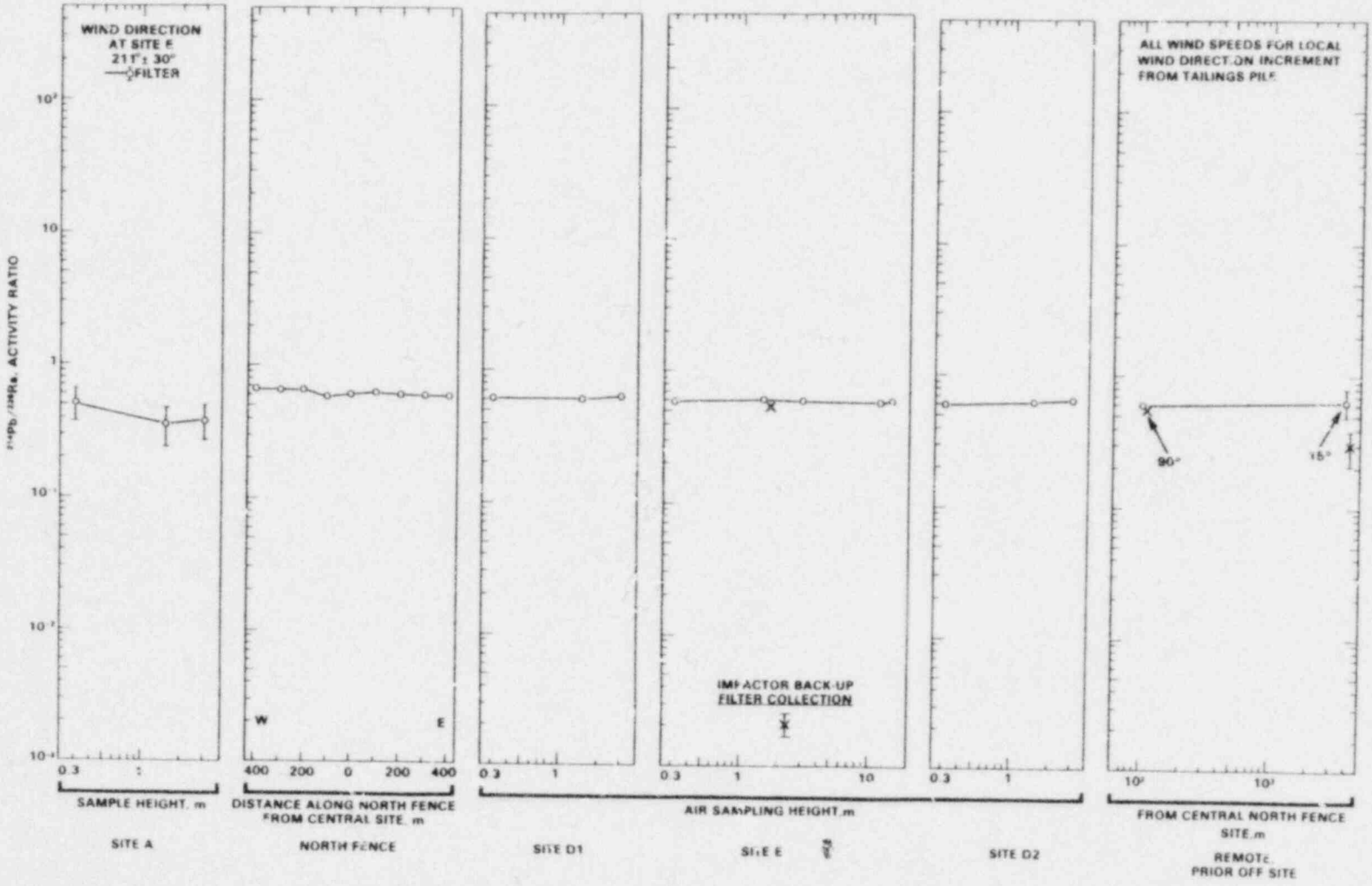

FIGURE 70. Airborne ^{214}Pb Activity Normalized to ^{226}Ra Activity on Airborne Solids at Each Site During March 8 to April 18, 1979 (80B318-72)

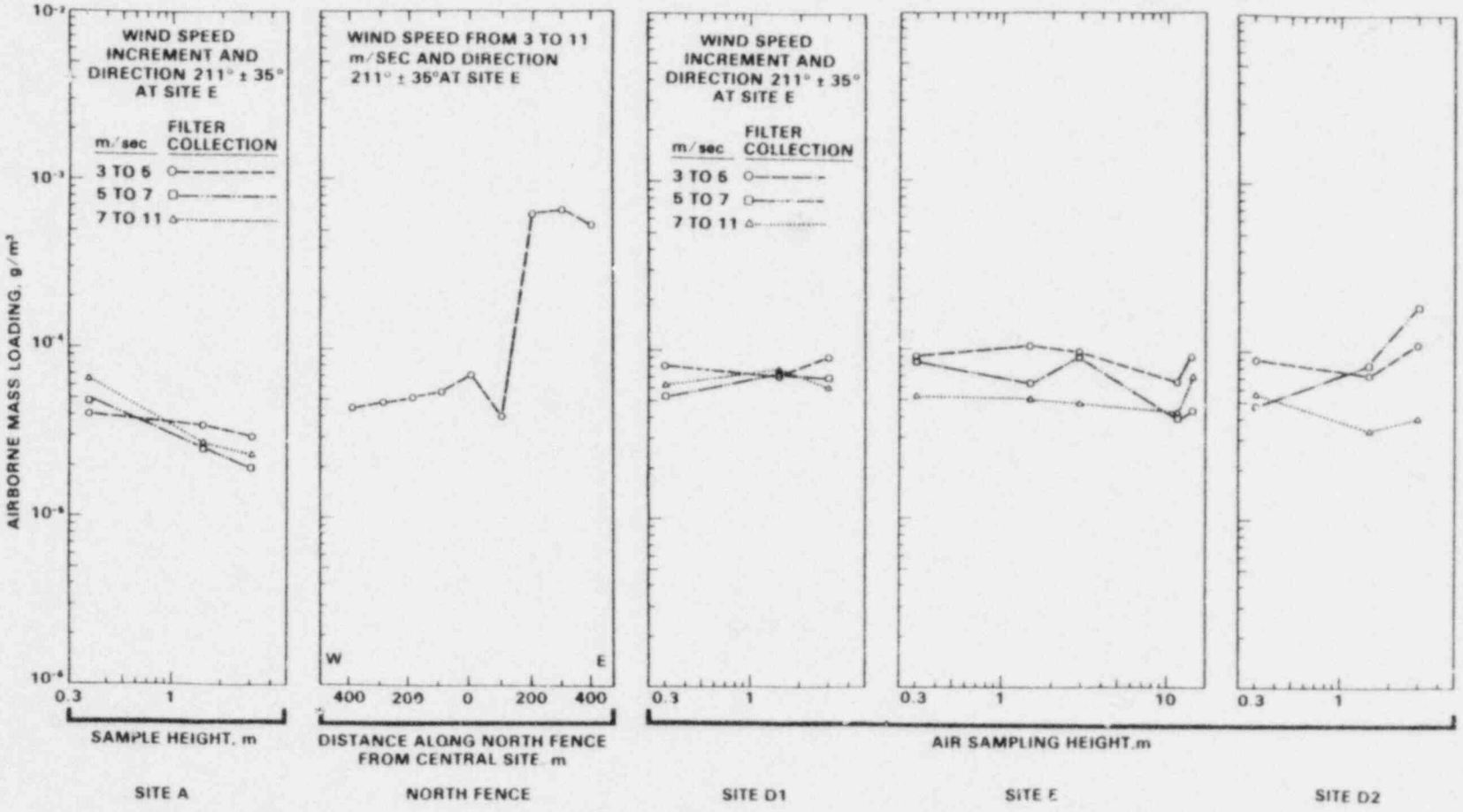

FIGURE 71. Airborne Solid Concentration at Each Site During May 15 to July 9, 1979 (80B236-8)

10^{-5} g/m^3, i.e., 20 to 70 µg/m^3. At site A mass loadings decreased with increasing sampling height. This decrease with height is indicative of local resuspension occurring immediately upwind from site A. Along the north fence airborne mass loadings increased approximately 1 order of magnitude for the three most eastern sampling locations. Increased airborne mass loadings were not, however, reflected in airborne mass loadings measured at site D-2 compared to those at site D-1.

Along the north fence increased mass loading in the east reflects operational usage of the mill tailings pile. As shown in Figure 24, the mill tailings pile consists of an eastern and western area separated by a dike. For the current time period the western area was partially covered with water, similar to conditions shown in Figure 24, while the eastern area was dry. Thus, increased airborne mass loadings in the east were caused by wind erosion from the dry eastern area.

Airborne Fluxes and Loading

Airborne mass fluxes and filter mass loadings were calculated from solids collections on isokinetic sampler inlets and filters. In Figure 72 the "inlet" airborne mass flux, g/(m^2 day), is shown along with "filter" mass loadings g/m^3, from Figure 71. Downwind from the pile mass loadings decreased with increasing distance. Mass loadings at the two 15^o remote sites were approximately the background mass loadings determined at site A.

"Inlet" mass fluxes show greater variation as a function of wind speed than airborne mass loading variation. Nevertheless, the mass flux variation as a function of wind speed is still unclear. Mass fluxes at site D-2 for the 5 to 7 m/sec wind-speed increment may reflect an increased source strength from erosion of the dry eastern area of the mill tailings pile. Mass fluxes decreased with distance from the 90^o to 15^o remote sampling sites. However, the 15^o locations mass fluxes were greater than mass fluxes measured at background site A.

Relative Collection Site

The relative collection sites of "small"-diameter, filter-collected particles versus total airborne particles collection within isokinetic samplers are

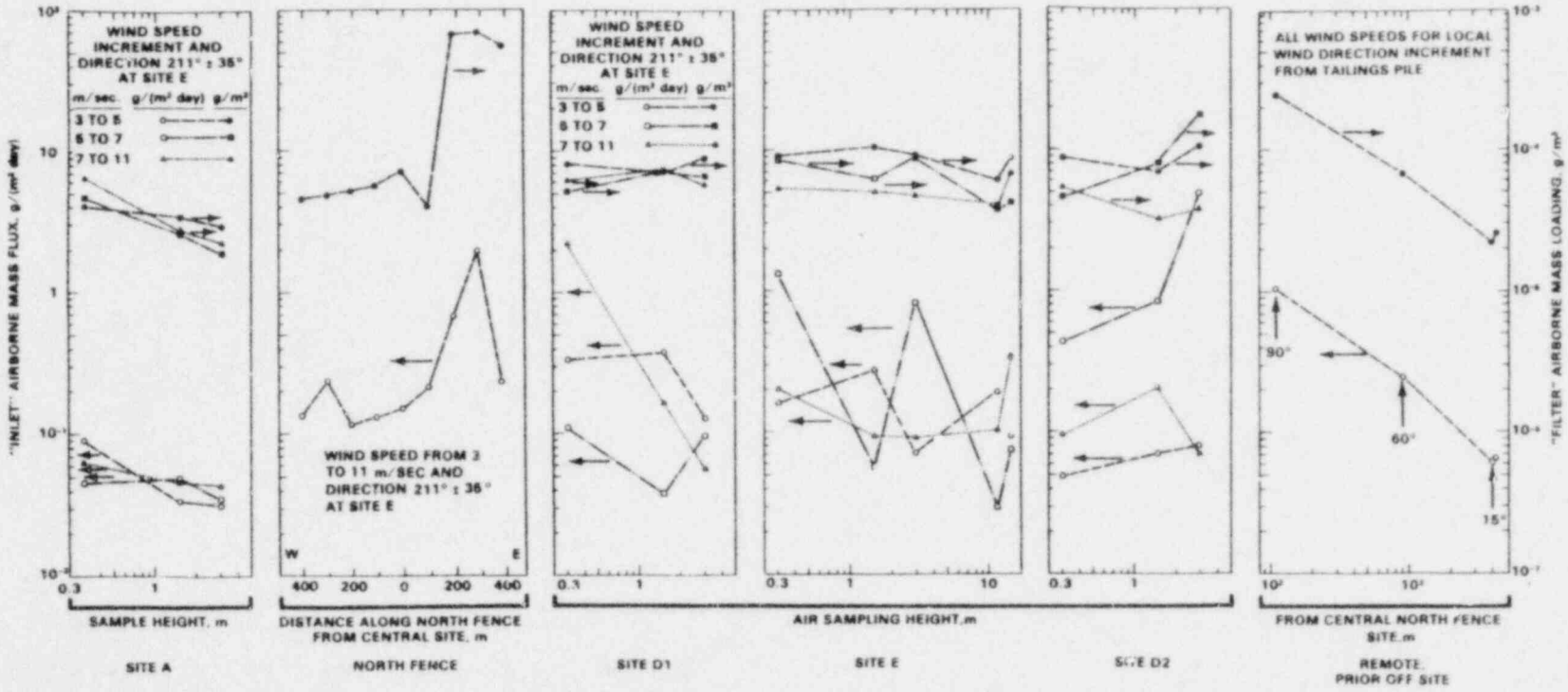

FIGURE 72. Average Airborne Fluxes and Concentrations During May 15 to July 9, 1979 (80B236-23)

shown in Figure 73. Airborne solids collected on the filter are shown as a percentage of total solids collected on the filter plus isokinetic sampler inlet. In most cases, over 80% of the solids are collected on the filter.

Radionuclide Activity Density on Airborne Solids

Selected airborne particulate samples were analyzed for ^{235}U, ^{238}U, ^{230}Th, ^{226}Ra, ^{214}Pb, and ^{210}Pb radionuclide content. Activity densities as a function of wind speed are unclear.

Uranium-235, dpm/g. Activity densities for ^{235}U are shown in Figure 74. Over 60% of these results were calculated from less-than radiochemical detection limit data as shown by the arrows.

Uranium-238, dpm/g. Activity densities for ^{238}U are shown in Figure 75. Activity densities were a function of sampling site. Activity densities at sites D-1, E, and D-2 were greater than at the background site A. At site E activity densities were uniform as a function of height. Thus, the airborne plume extended above the uppermost sampler.

Activity densities tended to increase from the western site, D-1, towards the eastern site, D-2. This west-to-east increase in activity density may reflect increased wind erosion from the eastern area of the mill tailings pile, or some sampled southwest winds being transported from west of the pile rather than passing over the pile.

Thorium-230, dpm/g. Activity densities for ^{230}Th are shown in Figure 76. Over 40% of these results were calculated from less-than radiochemical detection limit data as indicated by the arrows. Activity densities are uniform within the data scatter.

Radium-226, dpm/g. Activity densities for ^{226}Ra are shown in Figure 77. Activity densities at sites D-1, E, and D-2 were greater than at the background site A. In comparison to increased activity densities at site D-2 compared to site D-1 for ^{238}U (see Figure 25), activity densities for ^{226}Ra were nearly uniform in the crosswind distance. Any downwind effects of the dry eastern pile area were not observed for ^{226}Ra. Thus, from these data one might conclude ^{226}Ra is wind eroded from the dike areas, and not from the flat surface of the mill tailings pile.

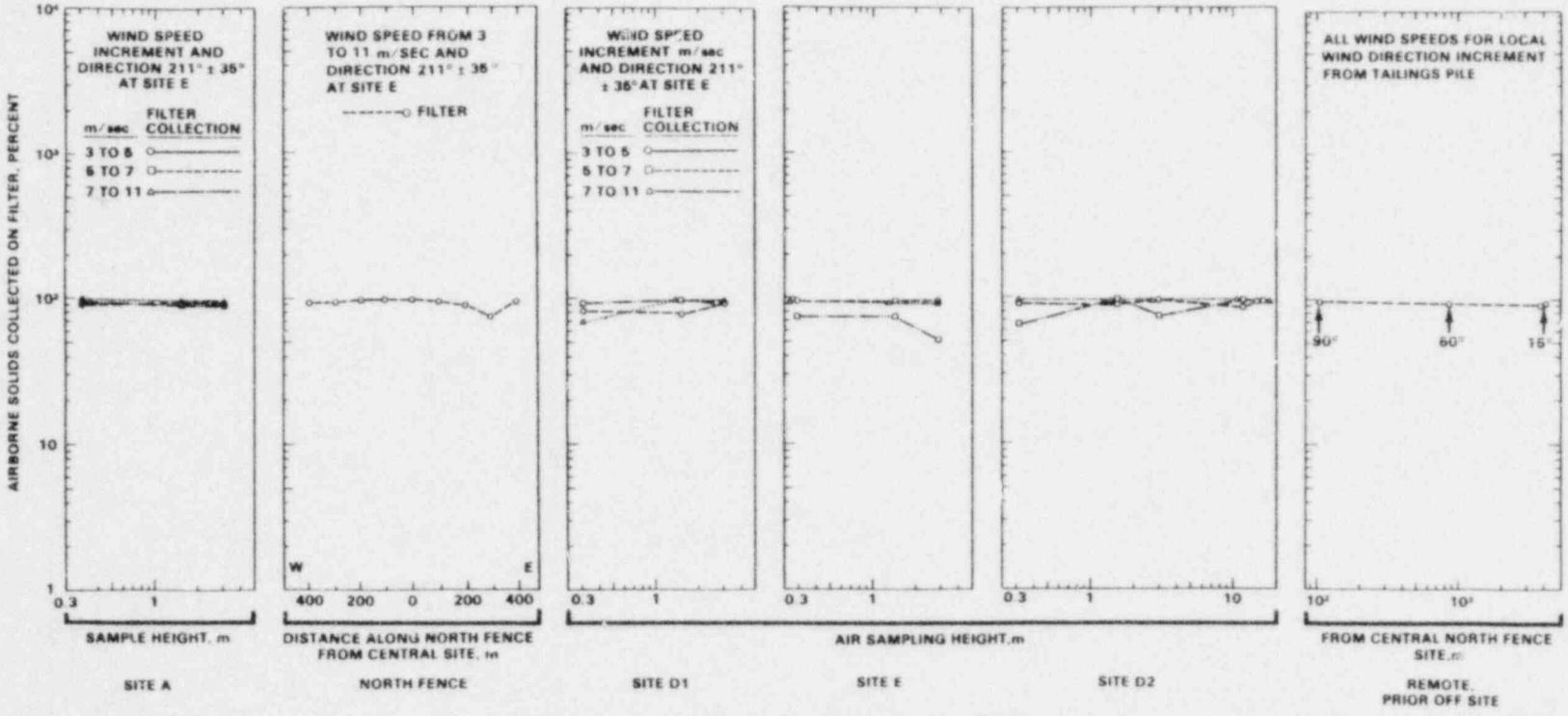

FIGURE 73. Percent Airborne Solids Collected on the Filter at Each Site During May 15 to July 9, 1979 (80B236-22)

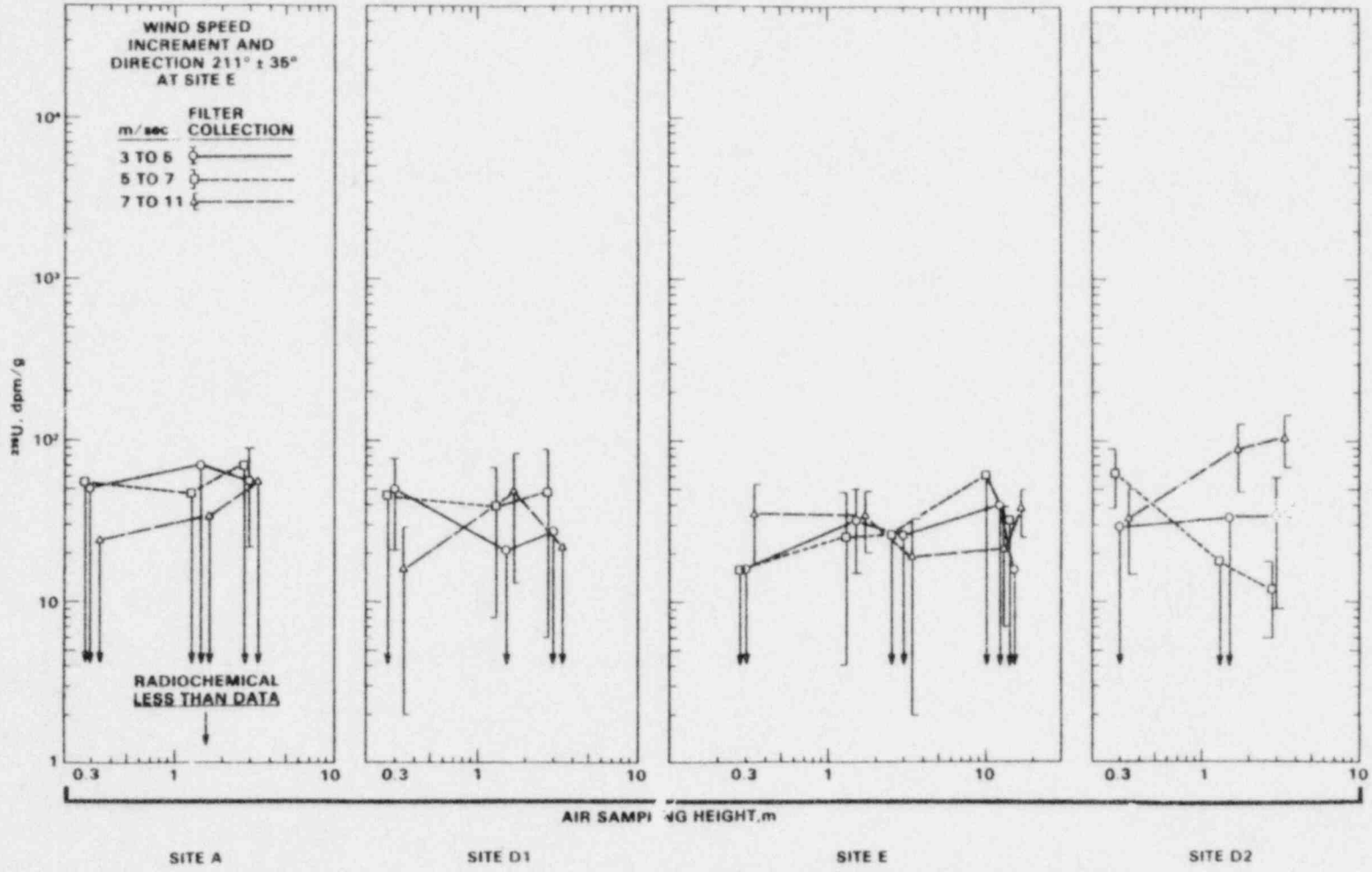

FIGURE 74. ^{235}U Concentrations on Airborne Solids at Each Site During May 15 to July 9, 1979 (data symbols for 5 to 7 and 7 to 11 m/sec offset from sampling heights to show the 1σ counting limits) (80B236-3)

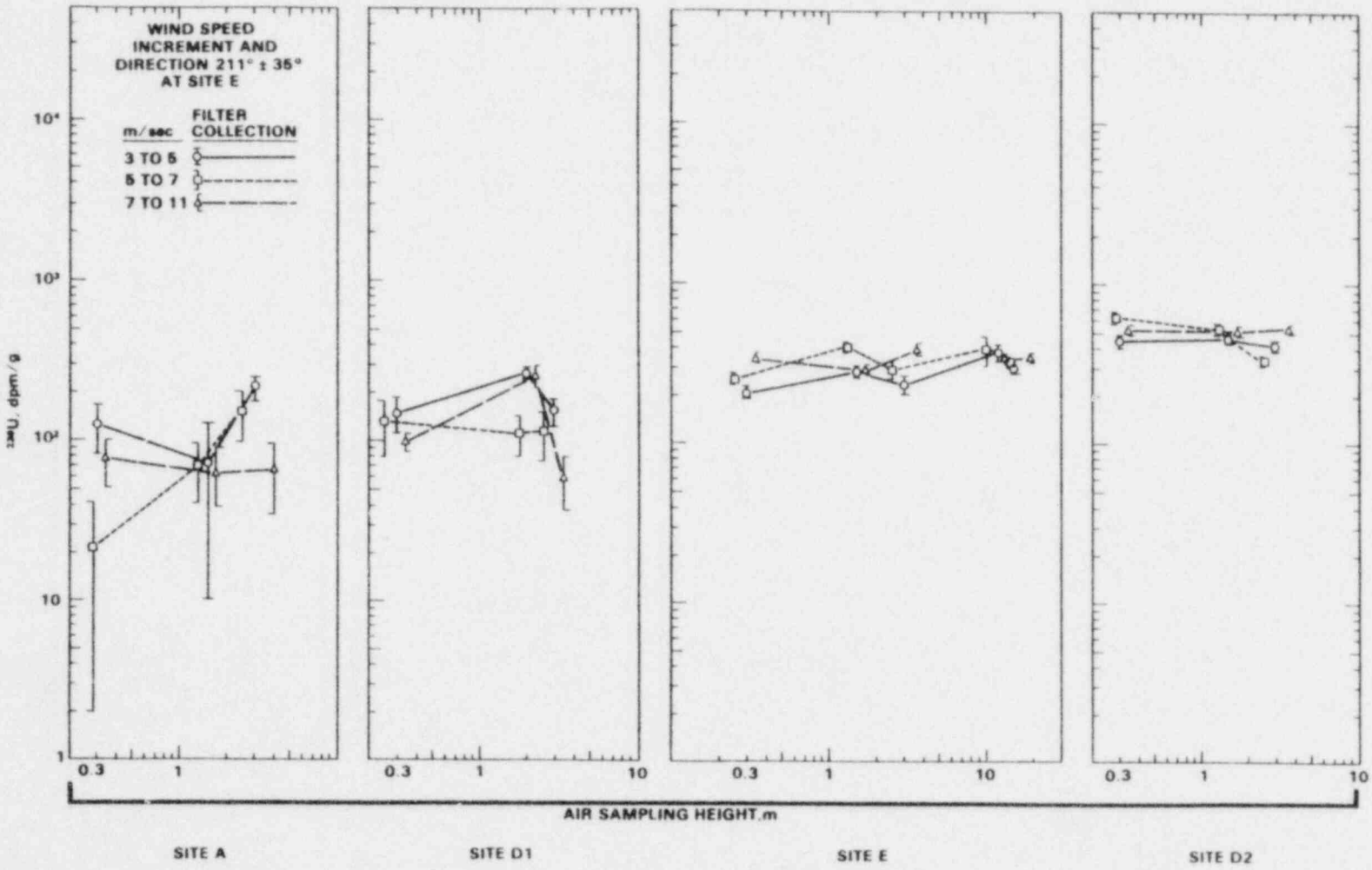

FIGURE 75. ^{238}U Concentrations on Airborne Solids During May 15 to July 9, 1979 (data symbols for 5 to 7 and 7 to 11 m/sec offset from sampling heights to show the 1σ counting limits) (80B236-25)

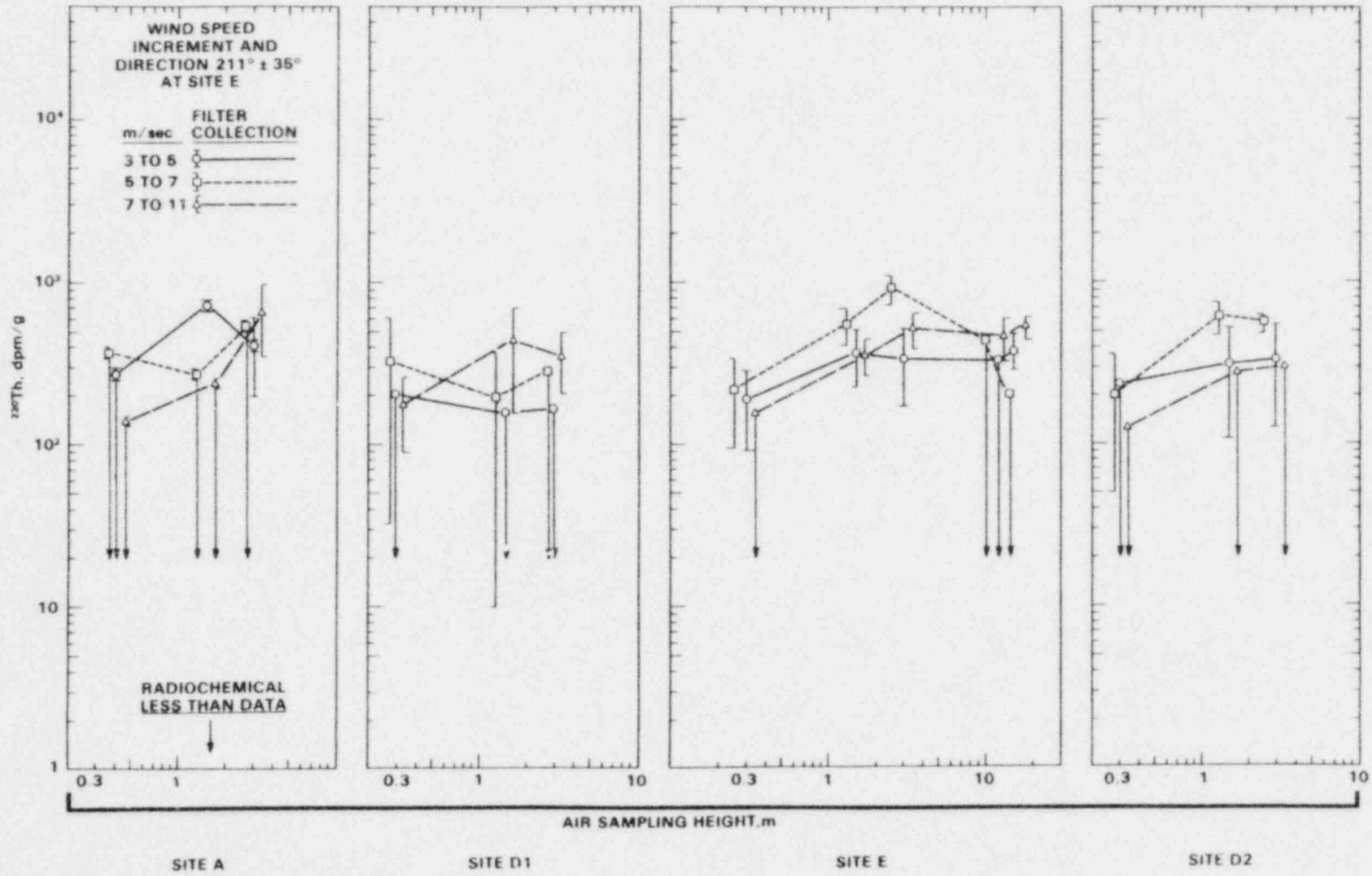

FIGURE 76. ^{230}Th Concentrations on Airborne Solids During May 15 to July 9, 1979 (data symbols for 5 to 7 and 7 to 11 m/sec offset from sampling heights to show the 1σ counting limits) (80236-26)

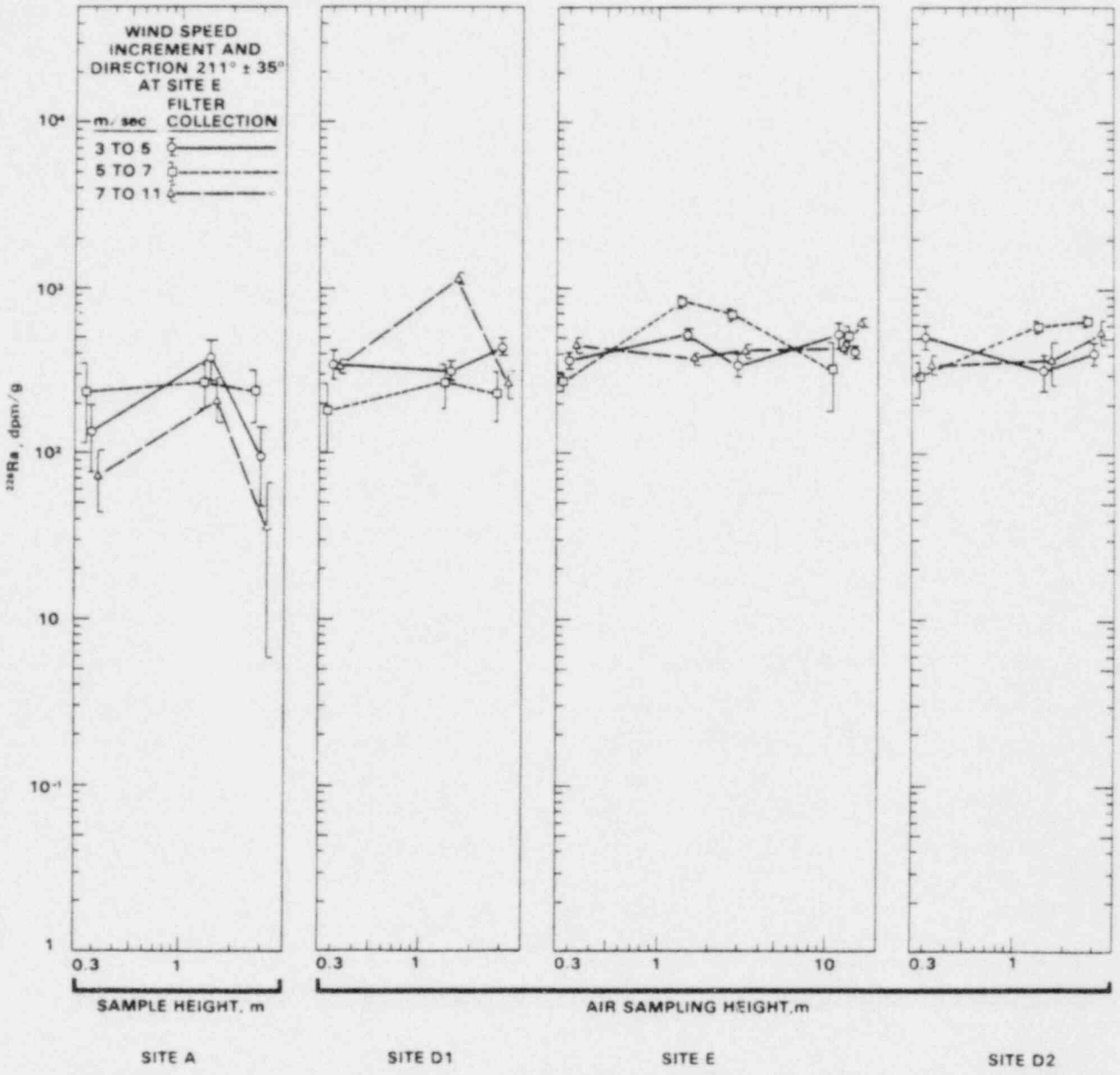

FIGURE 77. ^{226}Ra Concentrations on Airborne Solids During May 15 to July 9, 1979 (data symbols for 5 to 7 and 7 to 11 m/sec offset from sampling heights to show the 1σ counting limits) (80B236-19)

Lead-210, dpm/g. Activity densities for ^{210}Pb are shown in Figure 78. Activity densities at sites D-1, E, and D-2 were greater than at the background site A. Activity densities for ^{210}Pb were nearly uniform in the crosswind distance. Any downwind effects of the dry eastern pile area were not observed for ^{210}Pb. Activity densities for ^{210}Pb are also shown in Figure 79. Although activity densities are approximately uniform at all sites, activity densities at site A tend to be greater than activity densities for downwind sites D-1, E, and D-2. Increased activity densities at background site tend to support the concept that radionuclide wind erosion also occurs from secondary sources arising from prior deposition of wind-eroded mill tailings.

Airborne Radionuclide Concentrations

Airborne radionuclide concentrations, $\mu Ci/cm^3$ were calculated for ^{235}U, ^{238}U, ^{230}Th, ^{226}Ra, and ^{210}Pb. In addition to the isokinetic filter sample data, airborne concentrations are shown as a function of aerodynamic particle diameter as determined with particle cascade impactors. These particle cascade impactors were located at remote sites R-2 and R-4, i.e., the 60^o and 15^o wind-direction sampling sites. Airborne radionuclide concentrations are compared to Table I and II guidance levels from 10 CFR 20 (1979).

Uranium-235, $\mu Ci/cm^3$. Airborne ^{235}U concentrations are shown in Figure 80. Airborne concentrations are nearly uniform within the data scatter from radiochemical uncertainty.

Uranium-238, $\mu Ci/cm^3$. Airborne ^{238}U concentrations are shown in Figure 81. Airborne ^{238}U concentrations as a function of wind speed are unclear. However, there is a tendency for airborne concentrations at the lowest wind-speed increment to be greater than airborne concentrations at the higher two wind-speed increments. At sites D-1, E, and D-2, airborne concentrations increased about 1 order of magnitude above background concentrations at site A. At site E airborne concentrations were nearly uniform as a function of height. Thus, an unknown fraction of the ^{238}U airborne plume was passing over the uppermost sampler at site D. Airborne concentratons at site D-2, being greater than at D-1, probably reflect increased wind erosion from the dry eastern mill tailings area.

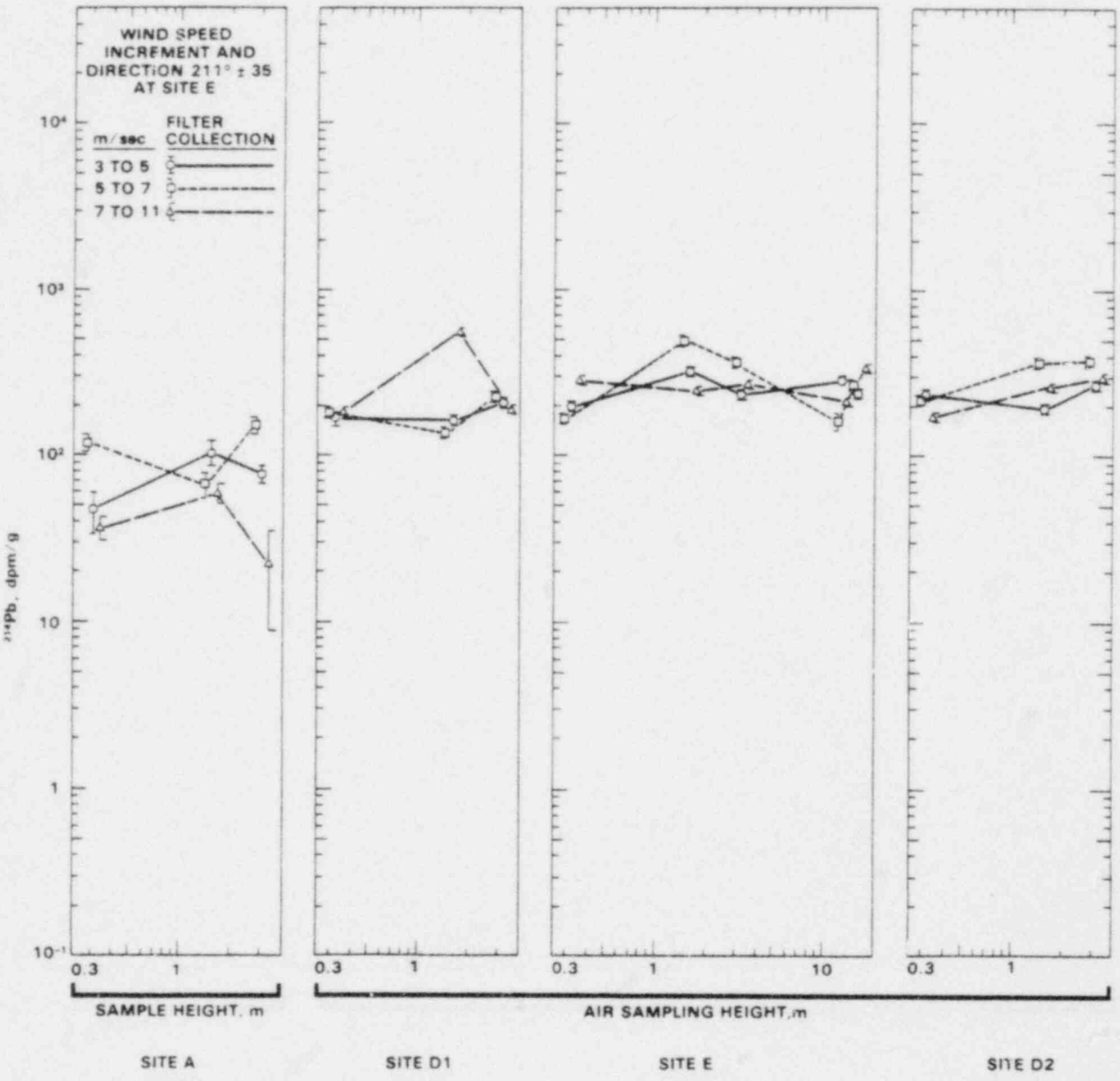

FIGURE 78. ^{214}Pb Concentrations on Airborne Solids During May 15 to July 9, 1979 (data symbols for 5 to 7 and 7 to 11 m/sec offset from sampling heights to show the 1σ counting limits) (80B236-18)

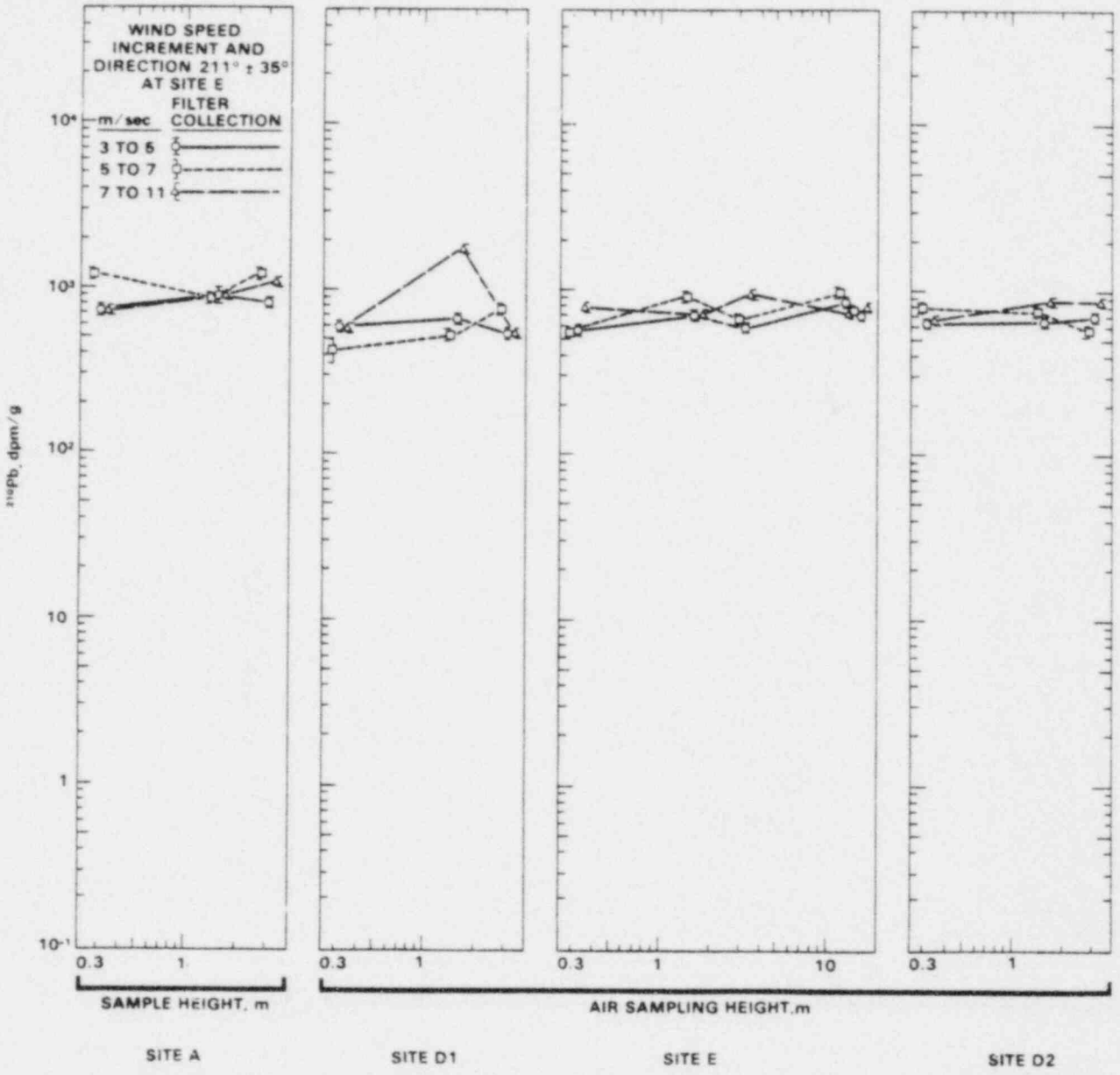

FIGURE 79. ^{210}Pb Concentrations on Airborne Solids During May 15 to July 9, 1979 (data symbols for 5 to 7 and 7 to 11 m/sec offset from sampling heights to show the 1σ counting limits) (80B236-17)

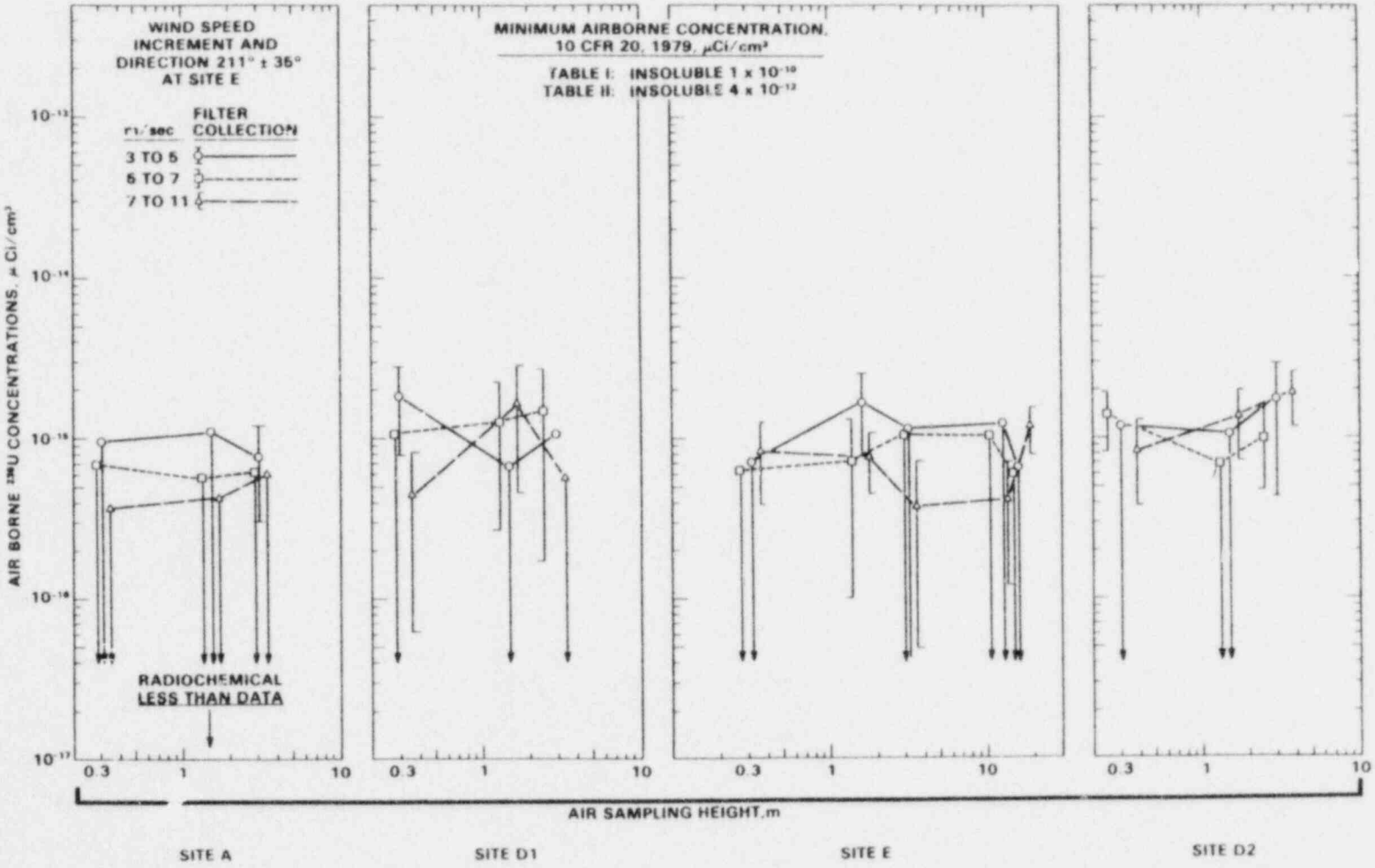

FIGURE 80. Airborne ^{235}U Concentrations at Each Site During May 15 to July 9, 1979 (data symbols for 5 to 7 and 7 to 11 m/sec offset from sampling heights to show the 1σ counting limits) (80B452-4)

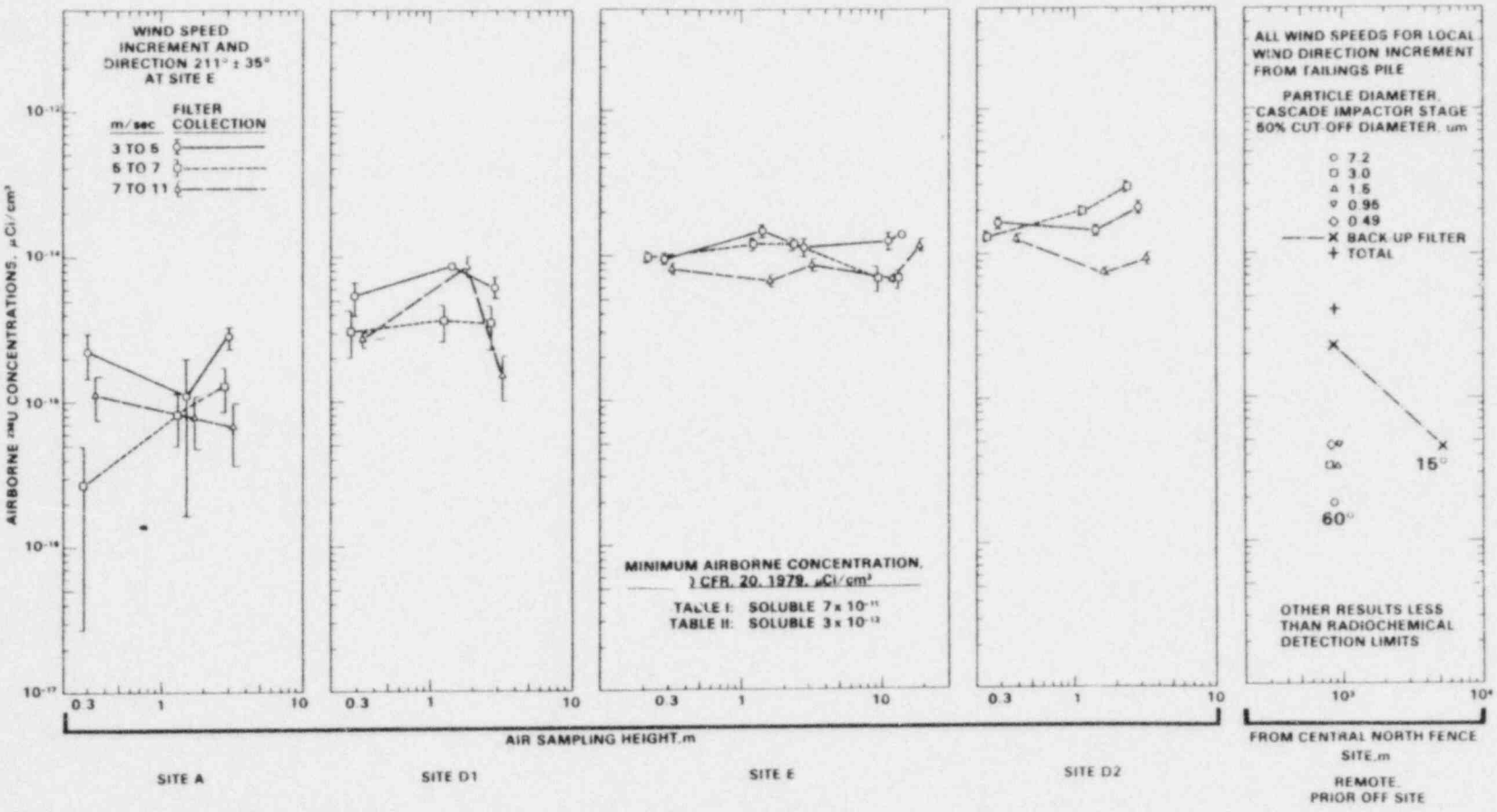

FIGURE 81. Airborne ^{238}U Concentrations at Each Site During May 15 to July 9, 1979 (data symbols for 5 to 7 m/sec offset from sampling heights to show the 1σ counting limits) (80B328-6)

Airborne ^{238}U concentrations as a function of aerodynamic particle diameter are shown for two remote sites. At the 60^{o} site, airborne concentrations are shown for each cascade particle impactor size fraction as well as total collection within the cascade particle impactor. At this site, the majority of airborne ^{238}U was transported on particles collected on the particle cascade impactor backup filter. For the 15^{o} site, the ^{238}U content was above radiochemical detection limits only for the backup filter collection. For these particles, airborne concentrations decreased nearly 1 order of magnitude between the 60^{o} and 15^{o} remote sites.

Thorium-230, $\mu Ci/cm^3$. Thorium-230 concentrations are shown in Figure 82. Except for concentrations calculated from radiochemical less-than results, all concentrations are greater than 5% of Table II guidance levels. The airborne concentration dependency on wind speed is unclear.

Radium-226, $\mu Ci/cm^3$. Airborne ^{226}Ra concentrations are shown in Figure 83. Airborne concentrations were approximately 2 orders of magnitude lower than Table II guidance levels. At sites D-1, E, and D-2, airborne concentrations increased approximately 1 order of magnitude above airborne concentrations measured at site A and were nearly uniform in the crosswind direction. At site E airborne concentrations were nearly uniform as a function of sampling height. At site D-2, however, airborne concentrations tended to increase with increasing height, reflecting both airborne radionuclide plume passage over the uppermost air sampler and plume depletion by particle deposition between the tailings pile and site D-2.

Airborne concentrations for several aerodynamic particle diameters are shown for the 60^{o} and 15^{o} remote sampling sites. Airborne concentrations decreased with increasing distance; however, the rate of decrease was a function of particle diameter. The rate of concentration decrease was greatest for particles collected on the particle cascade backup filter.

Lead-210, $\mu Ci/cm^3$

Airborne ^{210}Pb concentrations are shown in Figure 84. All airborne concentrations were 2 to 3 orders of magnitude less than Table II guidance levels. Airborne concentration wind-speed dependencies are unclear. Airborne

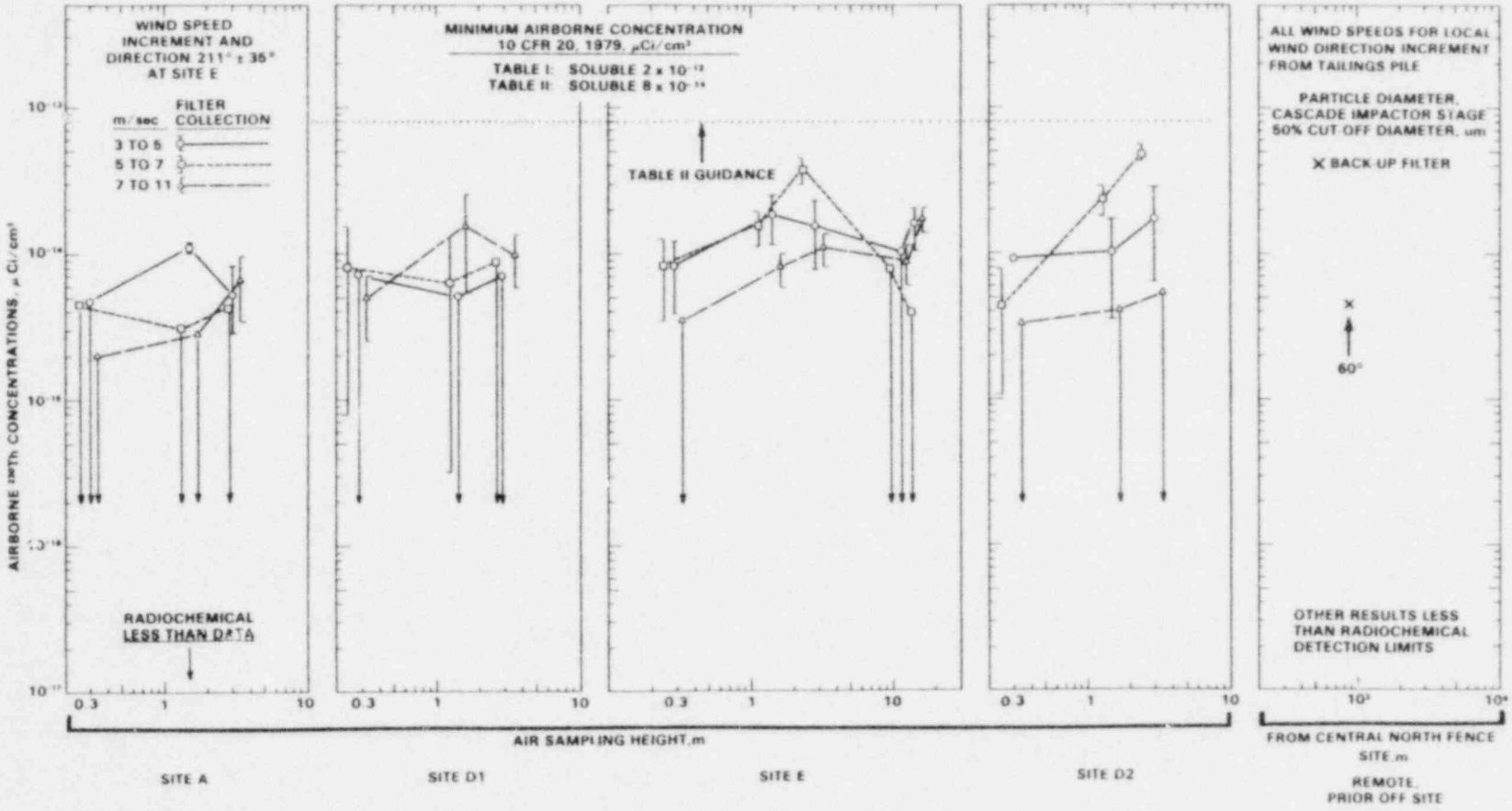

FIGURE 82. Airborne ^{230}Th Concentrations at Each Site During May 15 to July 9, 1979 (data symbols for 5 to 7 and 7 to 11 m/sec offset from sampling heights to show the 1σ counting limits) (808378-5)

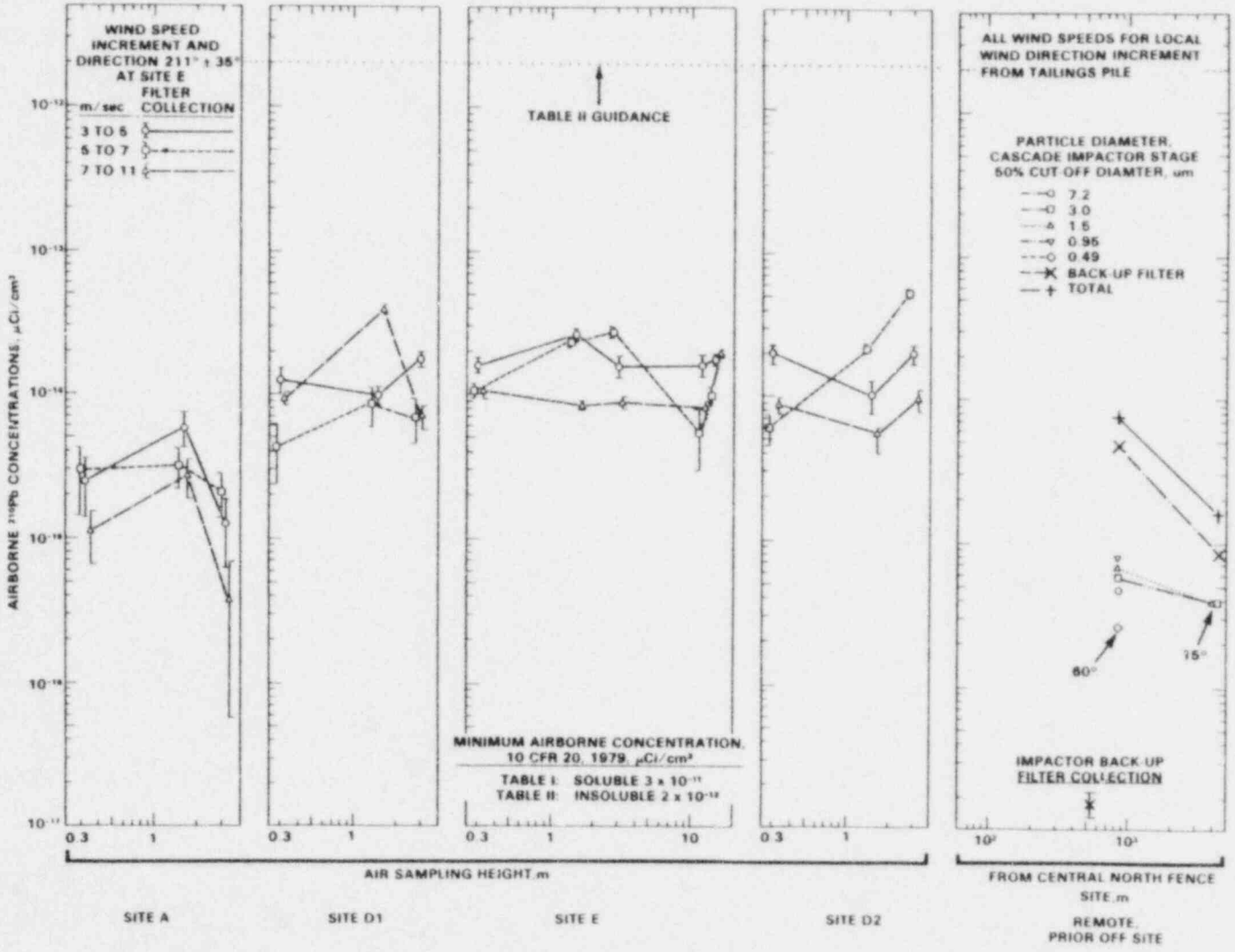

FIGURE 83. Airborne ^{226}Ra Concentrations at Each Site During May 15 to July 9, 1979 (data symbols for 5 to 7 and 7 to 11 m/sec offset from sampling heights to show the 1σ counting limits) (80B378-29)

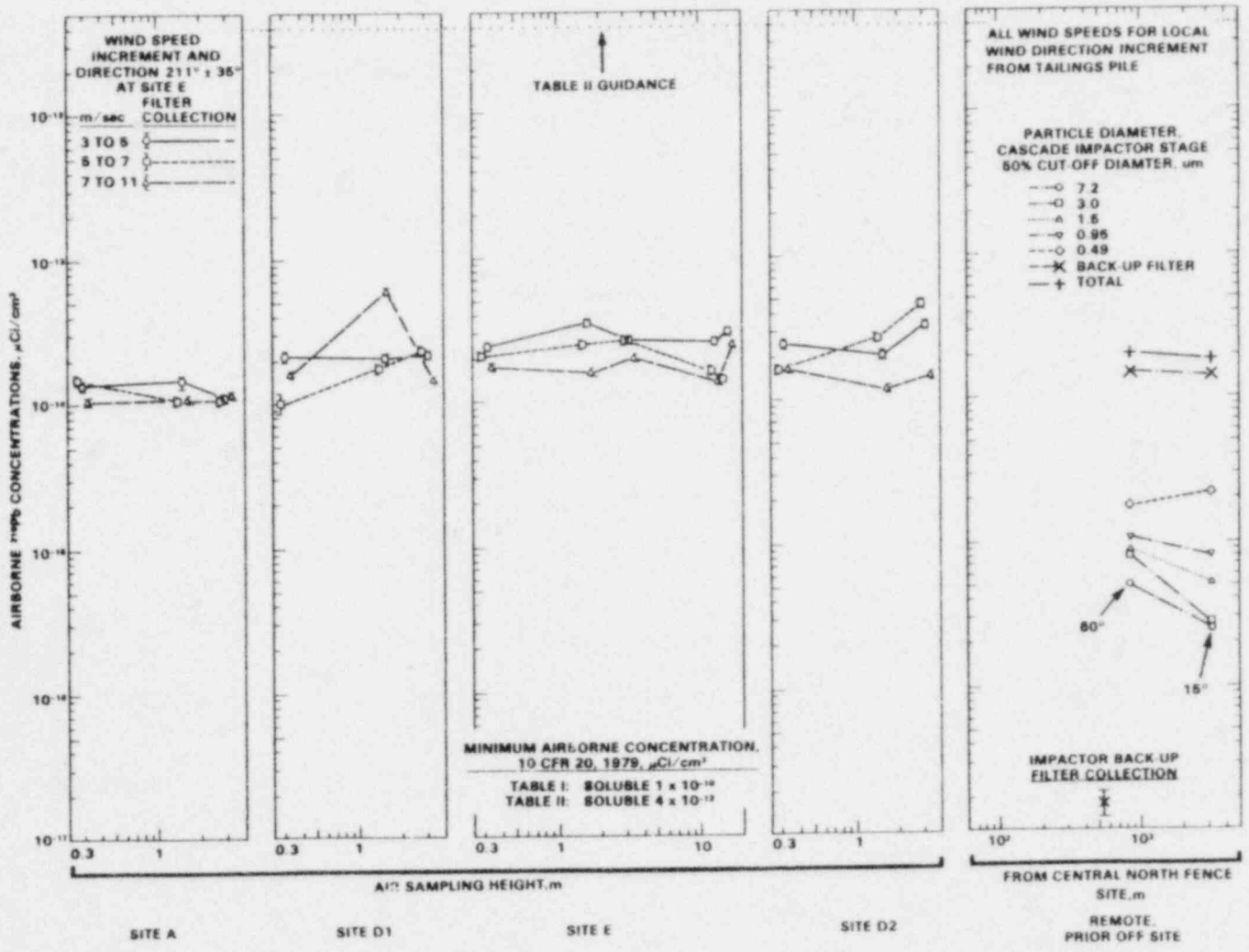

FIGURE 84. Airborne ^{210}Pb Concentrations at Each Site During May 15 to July 9, 1979 (data symbols for 5 to 7 and 7 to 11 m/sec offset from sampling heights to show the 1σ counting limits) (80B378-31)

concentrations at sites D-1, E, and D-2 were approximately two to three times greater than background measured at site A. Airborne concentrations were nearly uniform in crosswind direction at sites D-1, E, and D-2. Downwind at the 60^{o} and 15^{o} remote sites, airborne concentrations were similar as at other sites; thus, the airborne ^{210}Pb concentrations were nearly uniform at all sampling sites for this time period.

Airborne concentration as a function of aerodynamic particle diameter are shown for the 60^{o} and 15^{o} remote sites. Most ^{210}Pb was collected on the cascade impactor backup filter. This backup filter concentration was uniform with increasing distance. Nevertheless, for the first four stages of the particle cascade impactor some decrease in airborne ^{210}Pb concentration with distance is indicated.

Normalized Activity Densities

Activity densities are used to estimate the apparent equilibrium between radionuclide decay products on airborne solids. To estimate this nonequilibrium, activity densities for ^{238}U, ^{230}Th, and ^{226}Ra were normalized by corresponding activity densities for ^{210}Pb. Activity densities other than unity indicate a non-one-to-one correspondence between airborne transport for different radionuclide members of the ^{238}U decay series.

Normalized to ^{210}Pb. Activity ratios for $^{238}U/^{210}Pb$ are shown in Figure 85. Activity ratio wind dependencies are unclear. However, activity ratios are a function of sampling site. At the background site A, ratios ranged from about 0.02 to 0.3. Activity ratios were greater at sites D-1, E, and D-2 and tended to increase from sites D-1 to D-2, i.e., from west to east. This west-to-east increase may reflect, in part, wind erosion from the dry eastern mill tailings area. Nevertheless, one should not rule out the possibility that some fraction of airborne solids collected at site D-1 were ambient particles, rather than particles currently wind eroded from the mill tailings pile. This possibility is suggested since a wind direction of 211 $\pm 35^{o}$ was sampled, possibly allowing some southwesterly winds to bypass the western edge of the mill tailings pile and be sampled at site D-1.

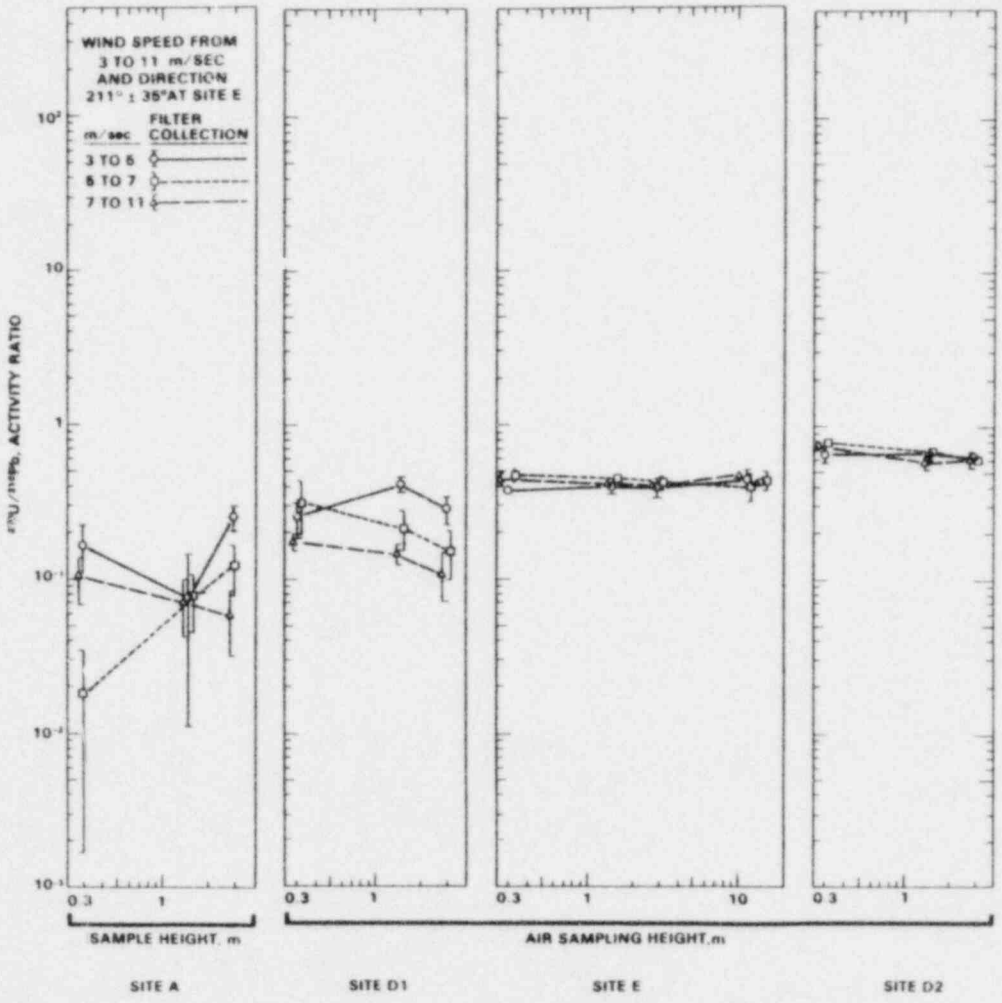

FIGURE 85. Airborne ^{238}U Activity Normalized to ^{210}Pb Activity at Each Site During May 15 to July 9, 1979 (data symbols for 5 to 7 and 7 to 11 m/sec offset from sampling height to show the 1σ counting limits) (80B318-63)

Activity ratios for $^{230}Th/^{210}Pb$ are shown in Figure 86. In contrast to the prior figure, activity ratios for $^{230}Th/^{210}Pb$ were nearly uniform at all sampling sites. The average $^{230}Th/^{210}Pb$ activity ratio was about 0.4.

Activity ratios for $^{226}Ra/^{210}Pb$ are shown in Figure 87. These results show trends which are a combination of trends from previous figures, i.e., activity ratios for $^{226}Ra/^{210}Pb$ at site A were less than at sites D-1, E, and D-2. However, at these three sites, activity ratios were nearly uniform, about 0.6.

Lead-214 Normalized Activity. Activity ratios for $^{214}Pb/^{210}Pb$ and $^{214}Pb/^{226}Ra$ were investigated as indicators of both concentration accuracy of ^{222}Rn daughters and radon release after sample collection. Activity ratios for $^{214}Pb/^{210}Pb$ are shown in Figure 88. Two activity ratio ranges were observed, similar to the results previously shown in Figure 75. Although two ranges were observed, the absolute value of each range is different. Ranges for Figure 75 will be shown in parentheses in the following discussion. In Figure 88, the $^{214}Pb/^{210}Pb$ activity ratio at background site A was approximately 0.08 (0.01). At the other sites, in contrast, the activity ratios were greater, approximately 0.04 (0.7). Apparently, at sites D-1, D-2, and E, either radon more readily escaped from these samples, or greater ambient airborne ^{210}Pb concentrations were at the background site A.

The $^{214}Pb/^{210}Pb$ activity ratios of approximately 0.4 are of less significant concern for adequate data interpretations than were inferred from the 0.7 ratio previously discussed in Figure 75. For the present figure, reported ^{210}Pb activity may be near actual airborne concentrations, rather than being an artifact of radionuclide decay. Actual airborne concentrations may have been at least 60%, i.e., (1 - 0.4) x 100 of reported concentrations.

Insights into the fraction of radon released from samples after field collection are inferred from $^{214}Pb/^{226}Ra$ activity ratios shown in Figure 89. The $^{214}Pb/^{226}Ra$ activity ratio at site A is the lowest, an average of about 0.4. This ratio suggests approximately 60% of the radon escaped after sample field collection at site A. Less radon escaped from samples collected at sampling sites D-1, E, and D-2; an average $^{214}Pb/^{226}Ra$ activity ratio was about 0.6. Thus, radon escape was about 40% rather than 60%. This decreased relative

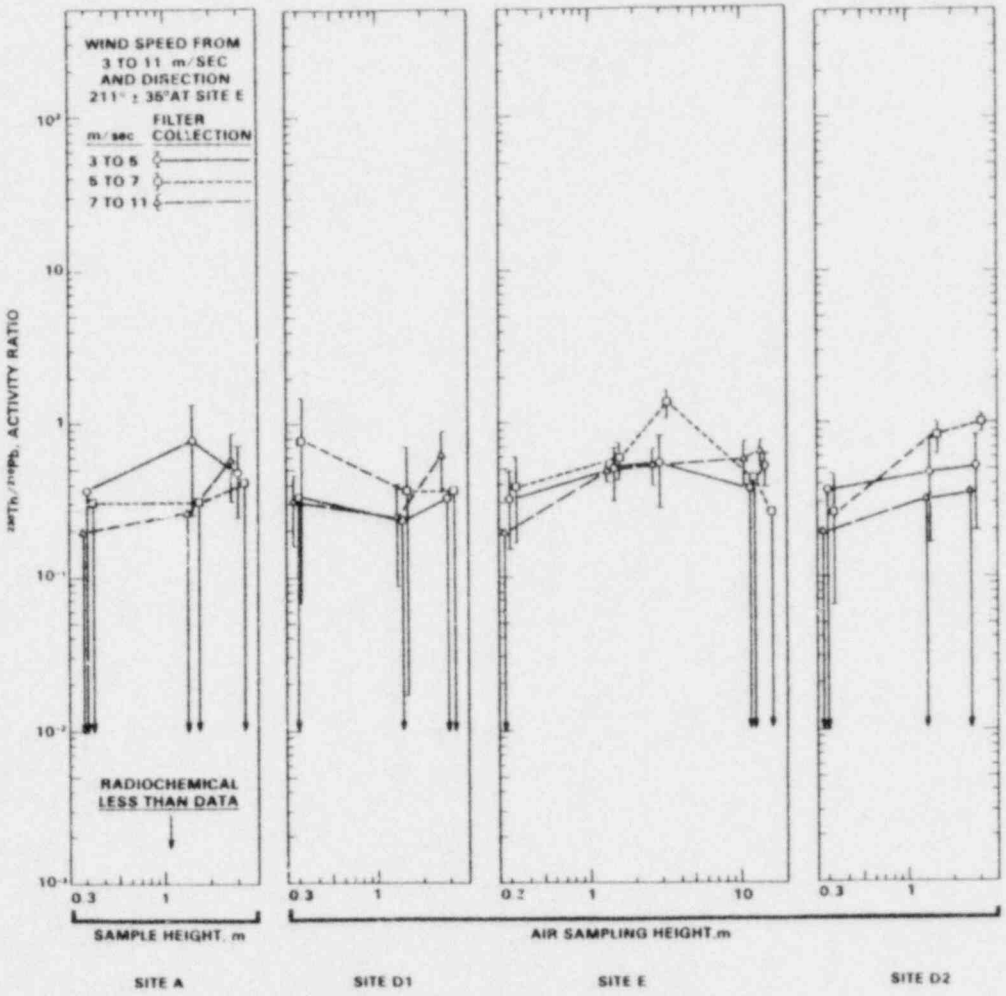

FIGURE 86. Airborne ^{230}Th Activity Normalized to ^{210}Pb Activity on Airborne Solids at Each Site During May 15 to July 9, 1979 (data symbols for 5 to 7 and 7 to 11 m/sec offset from sampling heights to show the 1σ counting limits (80B542-65)

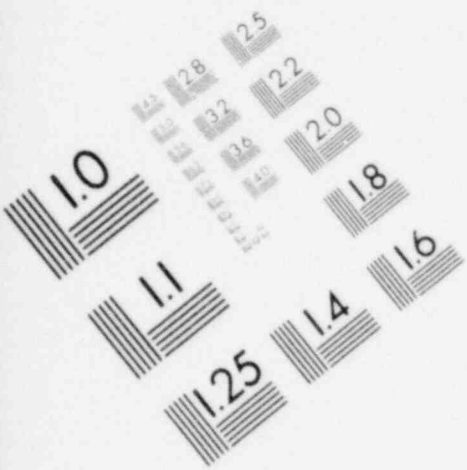

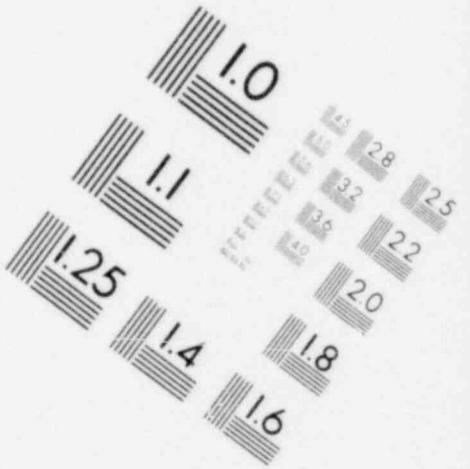

IMAGE EVALUATION TEST TARGET (MT-3)

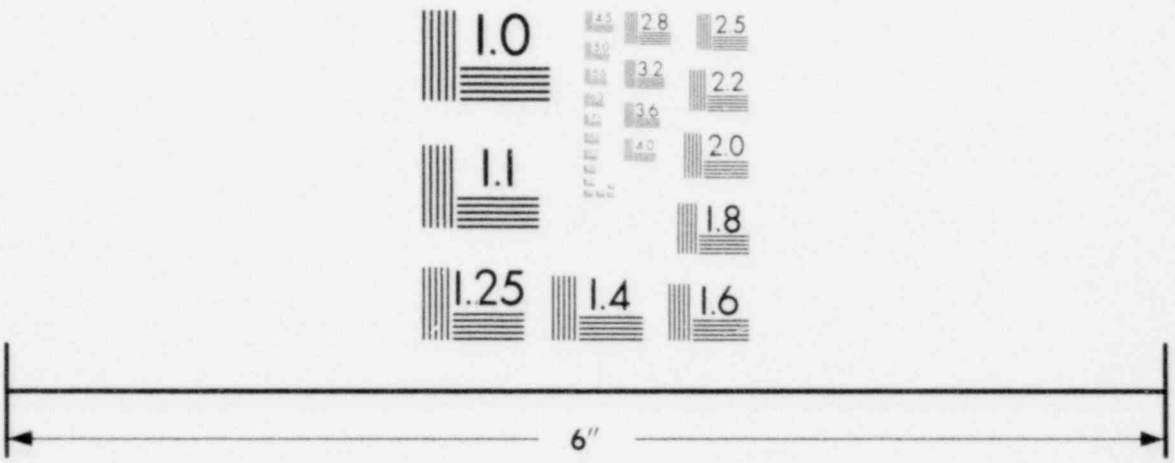

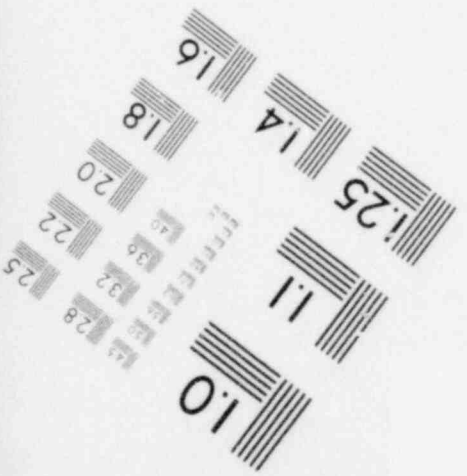

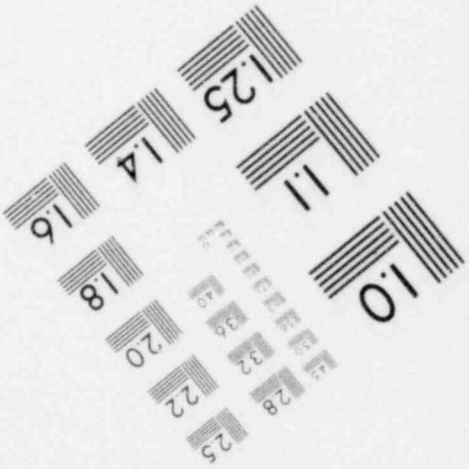

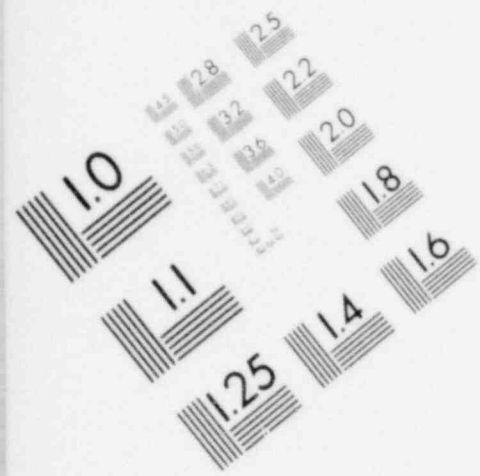

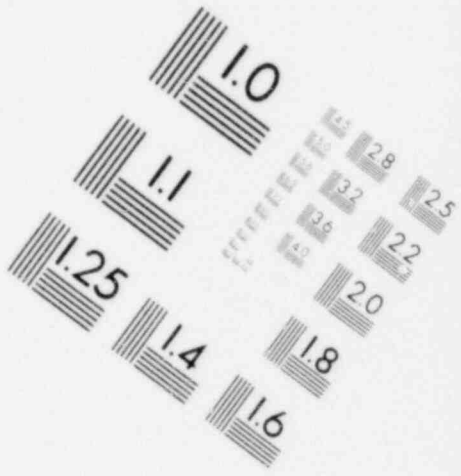

IMAGE EVALUATION TEST TARGET (MT-3)

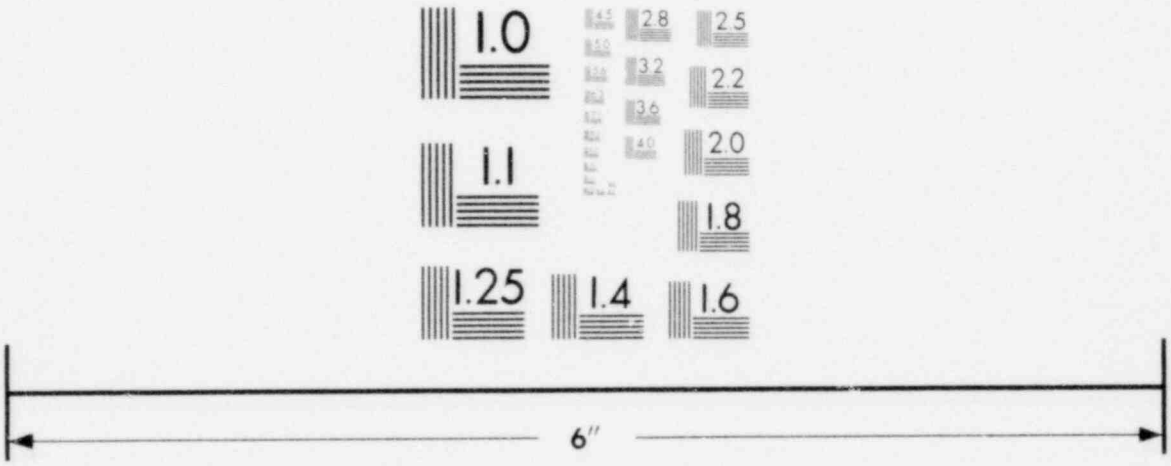

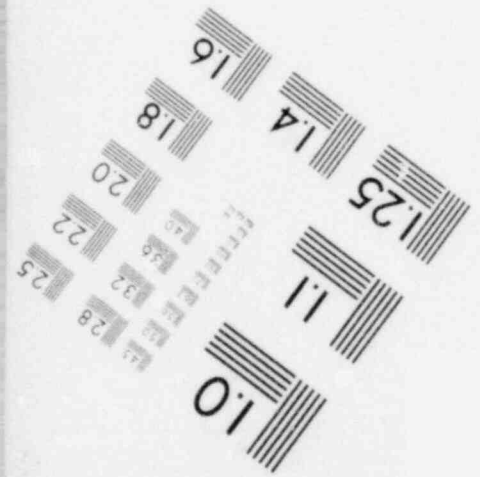

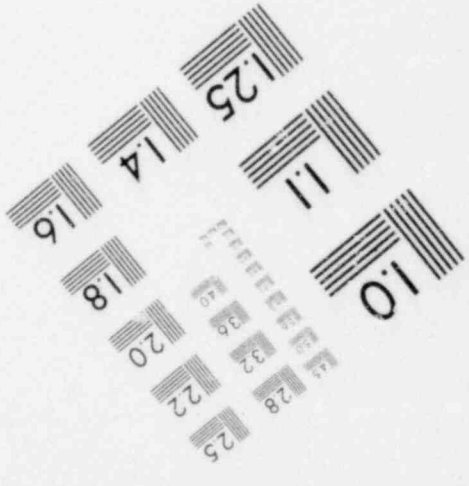

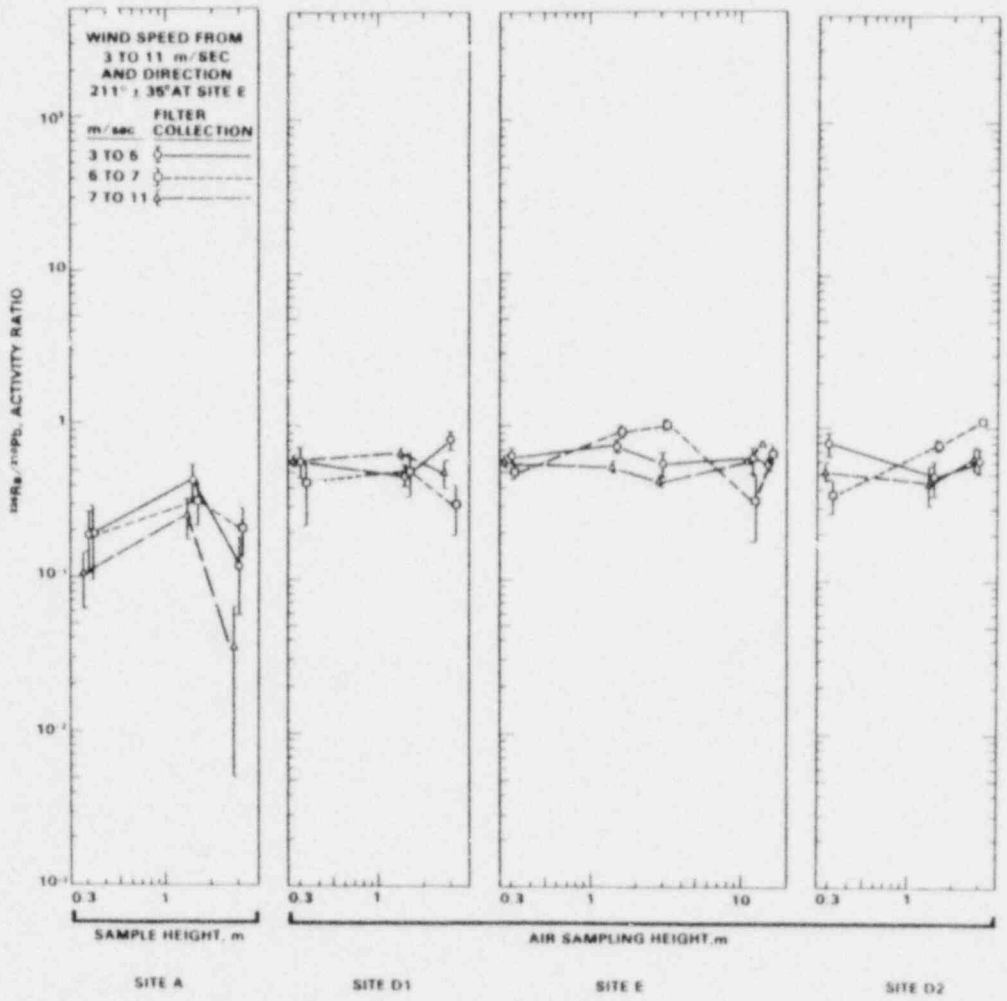

FIGURE 87. Airborne ^{226}Ra Activity Normalized to ^{210}Pb Activity at Each Site During May 15 to July 19, 1979 (data symbols for 5 to 7 and 7 to 11 m/sec offset from sampling height to show the 1σ counting limits) (808318-64)

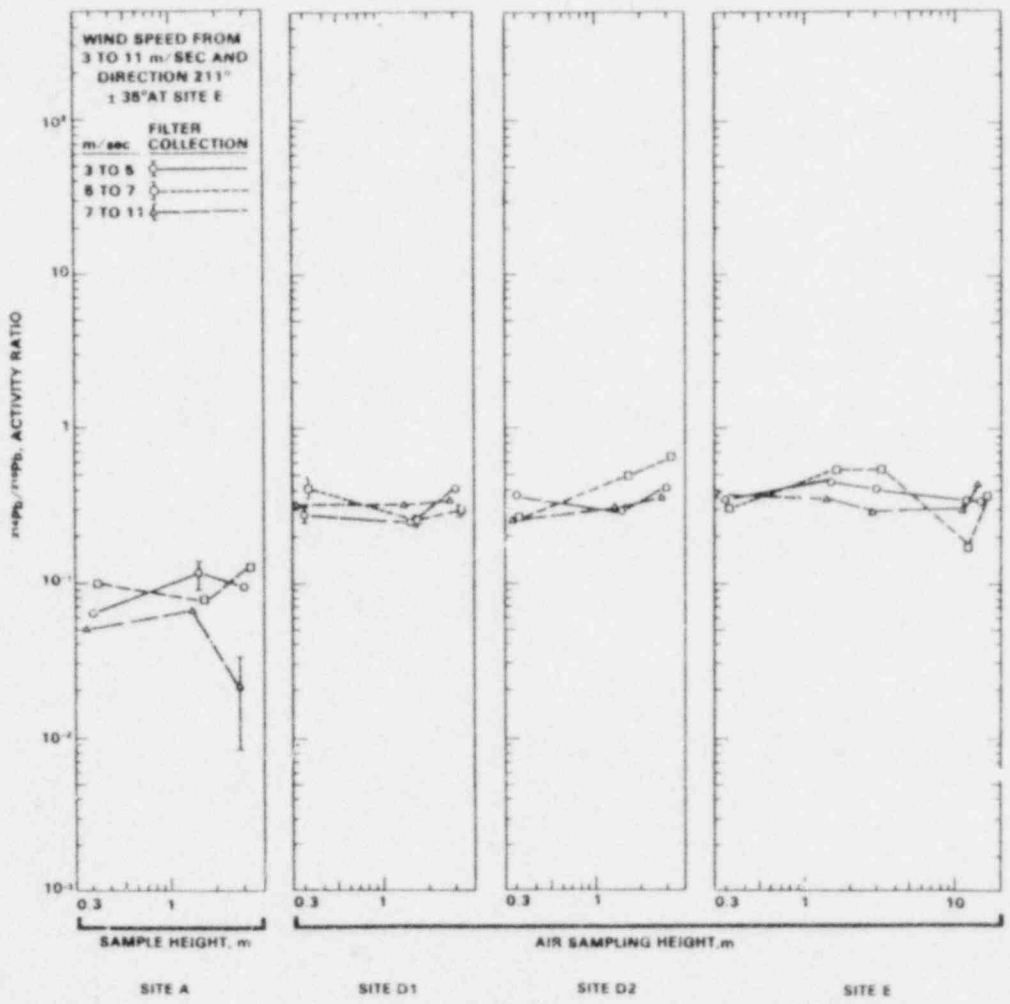

FIGURE 88. Airborne ^{214}Pb Activity Normalized to ^{210}Pb Activity at Each Site During May 15 to July 9, 1979 (data symbols for 5 to 7 and 7 to 11 m/sec offset from sampling height to show the 1σ counting limits) (80B318-66)

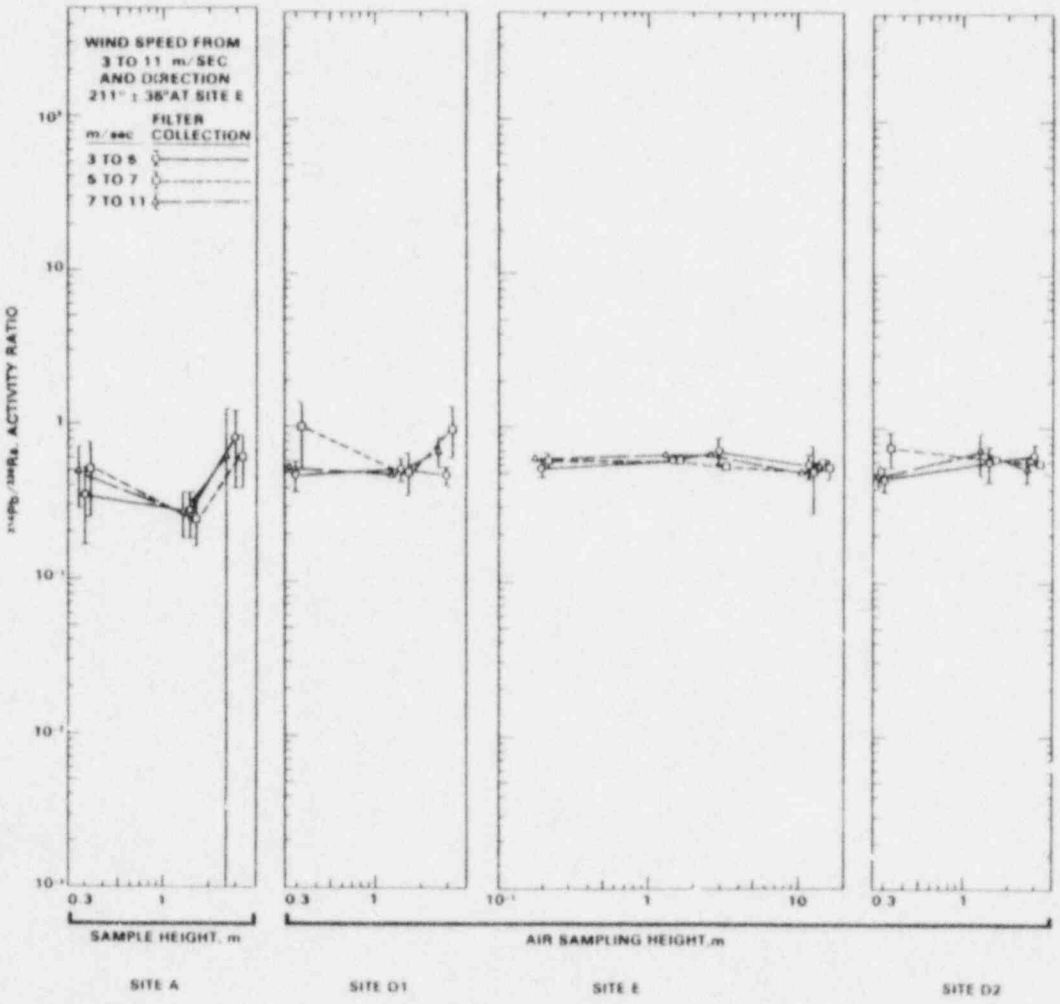

FIGURE 89. Airborne ^{214}Pb Activity Normalized to ^{226}Ra Activity at Each Site During May 15 to July 9, 1979 (data symbols for 5 to 7 and 7 to 11 m/sec offset from sampling height to show the 1σ counting limits) (80B318-67)

radon release at sites D-1, E, and D-2 may be a function of the relative larger particles collected and also the greater relative resistance to radon gas diffusion within these larger particles.

March 30 to April 17, 1978

North Dike

Crosswind variations in airborne radionuclide source strengths were investigated by using airborne samples collected along the north bank retaining dike. Samplers were placed adjacent to the maintenance road along the top of the dike. These were inertial impaction collectors from which relative horizontal mass fluxes were calculated. Mass fluxes were previously reported in the interim report (Figure 43) and are again shown for reference in Figure 90. For latter comparison to activity densities, the mass flux data of interest is the fifth subfigure described by the subtitle "North Dike." Airborne mass fluxes are shown for sampling heights of 0.3 and 1.5 m. Attention is called to the observation that mass fluxes showed a rapid decrease at the 175-m east sampling site. This decrease also occurs for some airborne radionuclide activity densities.

Sufficient airborne solids were collected in these inertial impaction collectors to allow solids to be sieved into size fractions (see size distributions shown in Figure 105) including the < 20-, 44- to 74-, and >420-μm particle-diameter ranges. Selected size fractions were analyzed for radionuclide content. All three size fractions collected at the 0.3-m height were analyzed while only the 44- to 74-μm-diameter size fraction at the 1.5-m height was analyzed for radionuclide content.

In the interpretation and discussion of activity densities and particle size fractions, it should be kept in mind that the inertial collectors are not 100% efficient and their efficiency will be a function of particle size and wind speed. Their primary use was to obtain relative mass loadings at many locations. The activity density as a function of collector location and particle size fraction must be qualified by the sampling uncertainty to provide a completely unbiased sample. The ability of the dry-sieving process used to separate every particle from another, as in all dry separation processes, could

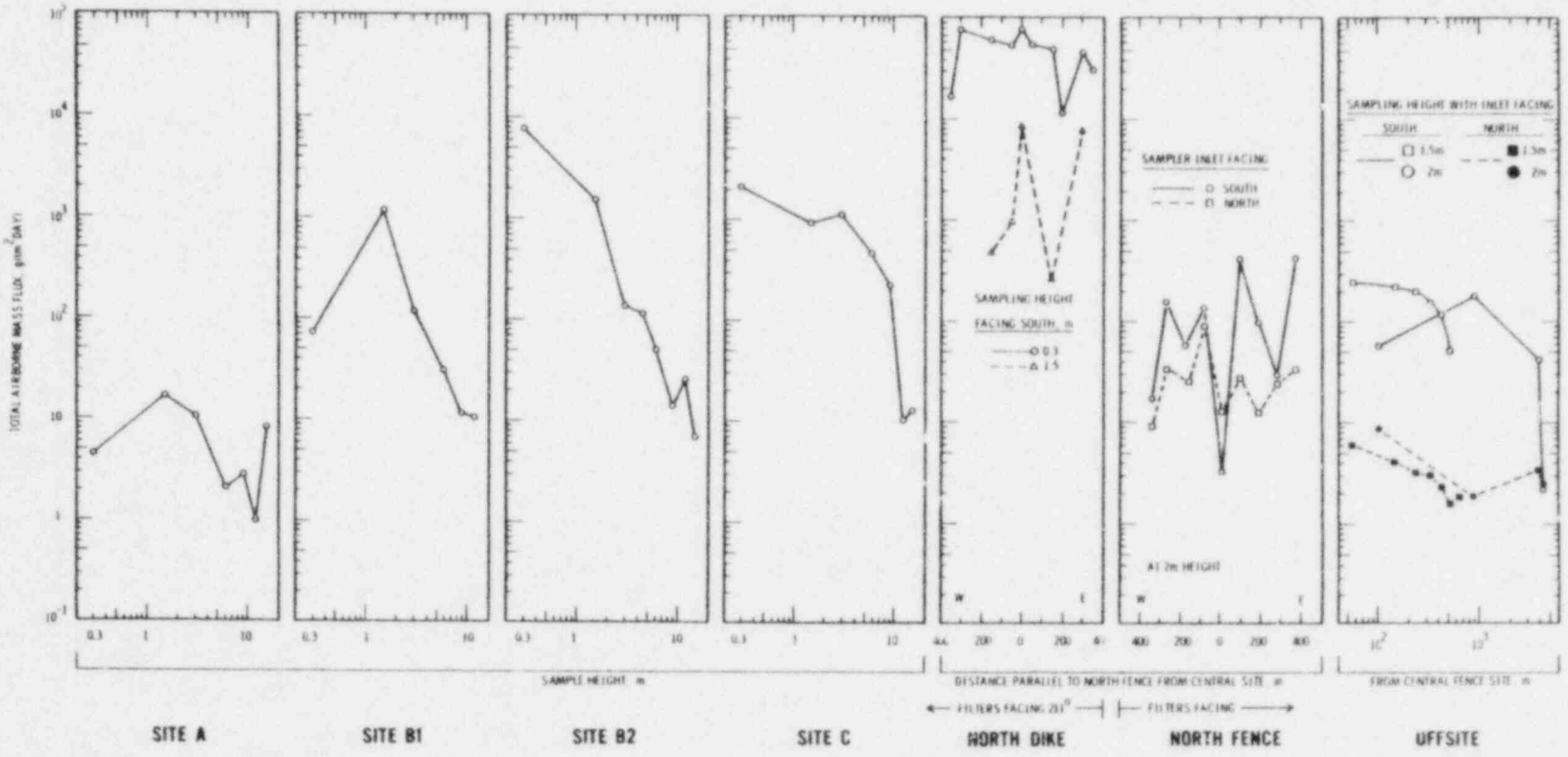

FIGURE 90. Total Airborne Mass Flux from Air Impact Flow Particle Collectors During March 30 to April 17, 1978 (7814185-7)

have resulted in incomplete detachment of some small particles from larger particles. These sampling and sizing observations should also be recognized in the discussion to follow.

Uranium-235, dpm/g. Activity densities for ^{235}U are shown in Figure 91. Activity densities range from 1 to 40 dpm/g and are a function of particle diameter. Activity densities are consistent with results shown in the interim report (Schwendiman et al. 1979). Activity densities are largest for the <20-μm-diameter particle size increment. Activity densities for the two larger diameter increments show an unclear activity density decrease with increasing particle diameter.

Activity densities are also a function of sampling position. Activity densities for the <20-μm-diameter increment show a general increase with sampling position from west to east. However, any change in activity density as a function of the two sampling heights is unclear from these data.

Uranium-238, dpm/g. Activity densities for ^{238}U are shown in Figure 92. Activity densities range from 20 to 900 dpm/g. The precise radiochemical confidence limits for this data set are not shown since confidence limits would be within the data symbols as plotted. Activity densities are non-uniform across the pile for all particle diameter increments. Activity density variations are up to 1 order of magnitude. The largest activity densities are for the <20-μm-diameter particles. At the 0.3-m height, activity densities decrease, with one exception shown as the 150-m east site, with increasing particle diameter. For 44- to 74-μm-diameter particles, activity densities for particles collected at the 1.5-m height are greater than activity densities for particles collected at the 0.3-m height. This increased activity density with increased height may represent an artifact in this instance since other radionuclides did not show such a recognizable difference in activity density with height. If not an artifact, this increased activity density with increased height may reflect differences in the areal source of the collected airborne material. A possible explanation of the increased activity density with increasing height is that 1) particles collected at the 0.3-m height were wind eroded from the north bank, a bank consisting of coarse sands of low-activity density, and 2) airborne particles collected at the 1.5-m height were

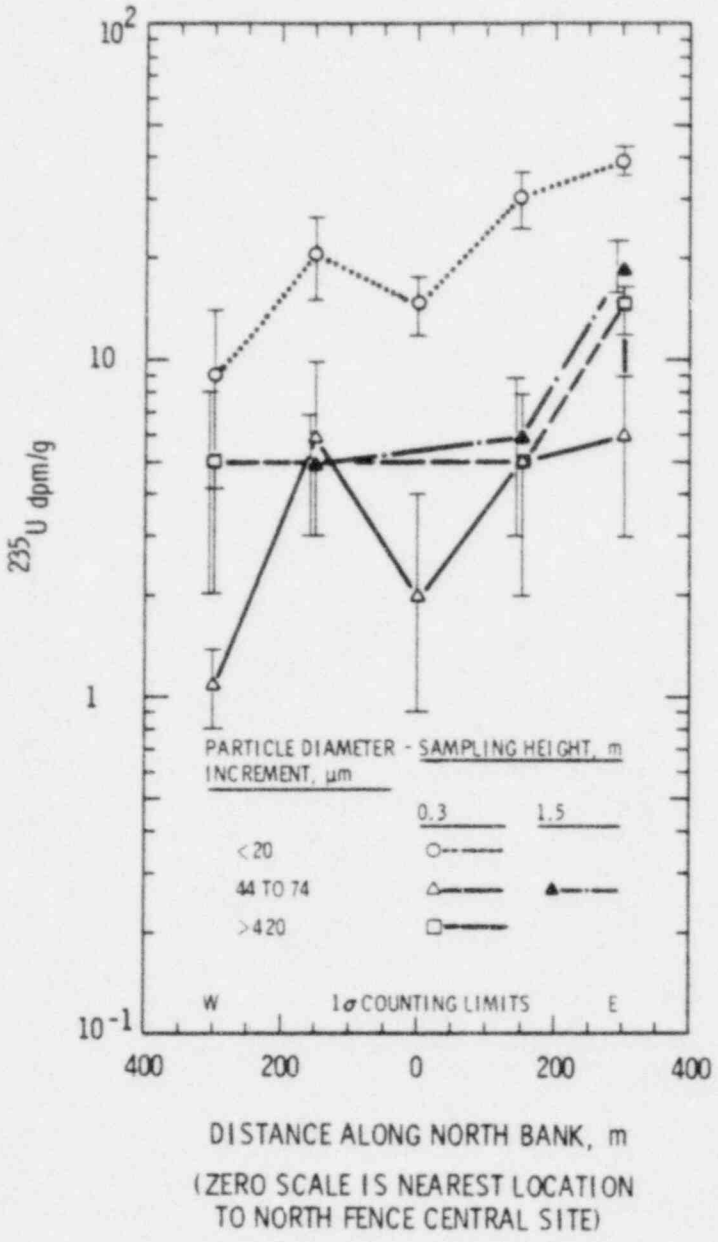

FIGURE 91. ^{235}U Concentration on Airborne Solids as a Function of Nonrespirable Particle Diameter During March 30 to April 17, 1978 (80B236-54)

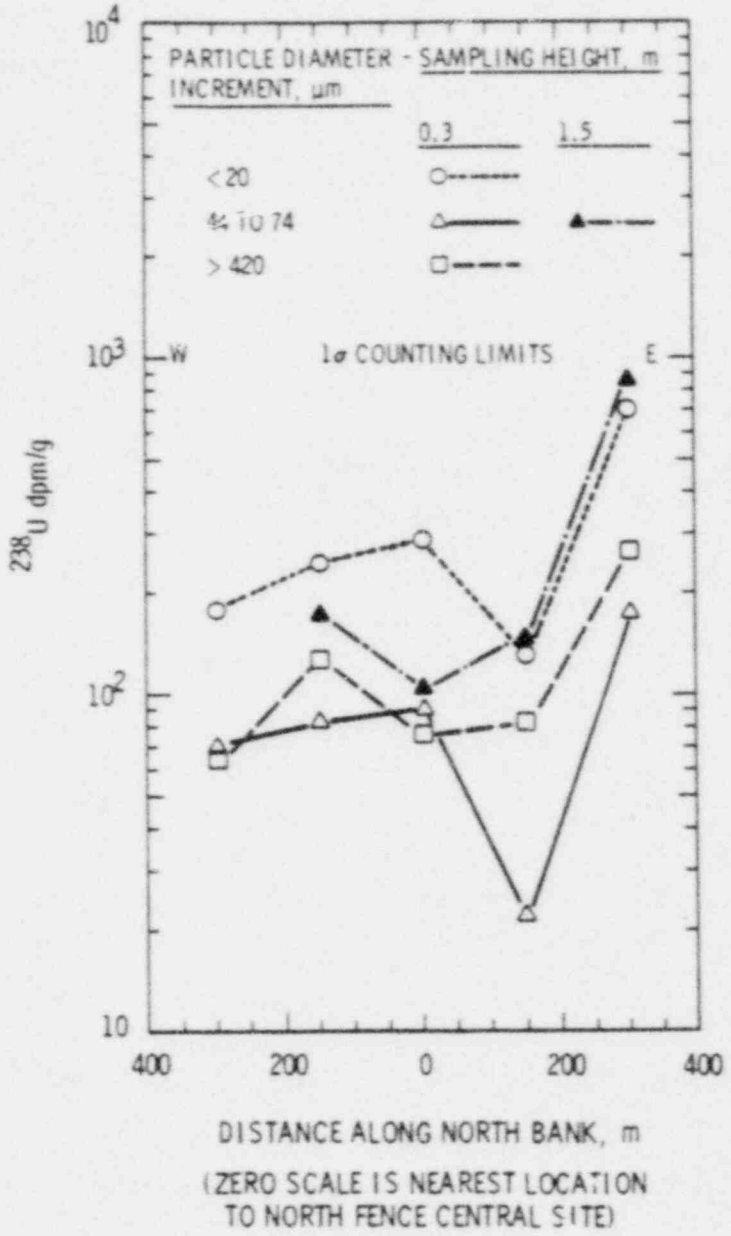

FIGURE 92. ^{238}U Concentration on Airborne Solids as a Function of Nonrespirable Particle Diameter During March 30 to April 17, 1978 (79H891-51)

wind eroded from the central portions of the mill tailings area, a flat area consisting of slimes with greater activity densities.

A further particle-size anomaly is noted at the 150-m east sampling site. Activity densities for the <20-μm and 44- to 74-μm-diameter particles were less than activity densities at other north dike sites. In contrast to this activity density decrease for small particles, activity densities for particles >420-μm-diameter did not show any such decrease. An explanation was not found. However, at this time the cyclone separator that deposited effluents onto the mill tailings pile was approximately in the region of the 150-m east sampling site. Cyclone discharges may have had some influence on the erosion source area because of the immediate upwind wetted dike and "beach" area. Consequently, radionuclide particle sources may have been from more distant portions of the tailings pile. This anomaly was not present for other radionuclides.

Thorium-230, dpm/g. Activity densities for ^{230}Th are shown in Figure 93. Activity densities range from 300 to 2000 dpm/g. The precise radiochemical confidence limits for this data set are not shown since confidence limits would be within the data symbols are plotted. Activity densities are non-uniform across the pile for all particle diameter increments. The largest activity densities are for the <20-μm-diameter particles. For 44- to 74-μm-diameter particles, activity densities for particles collected at the 1.5-m height are greater, with one exception, than activity densities for particles collected at the 0.3-m height.

Radium-226, dpm/g. Activity densities for airborne ^{226}Ra are shown in Figure 94. Activities ranged from about 200 to 3000 dpm/g. Activity densities were greatest for <20-μm-diameter particles and smallest for >420-μm-diameter particles. There are differences between airborne ^{226}Ra activity densities and ^{230}Th activity densities discussed in the previous figure. Radium-226 activity densities were nearly uniform as a function of crosswind distance. Even at the 150-m east sampling location, ^{226}Ra activity densities were uniform and did not show any significant decrease as was observed for ^{230}Th.

A wet beach from cyclone discharge may have affected activity densities for airborne samples collected along the north dike, considering the following facts: 1) the beach was wet, 2) ^{226}Ra activity densities for 44- to

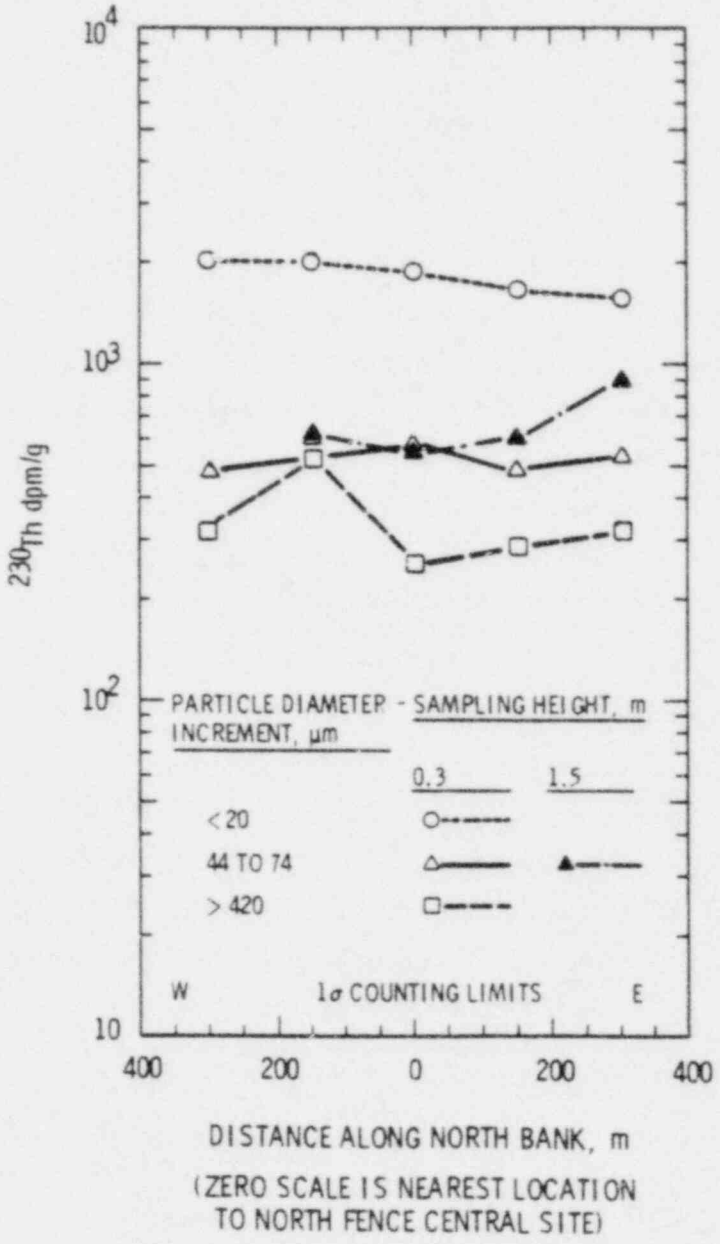

FIGURE 93. ^{230}Th Concentration on Airborne Solids as a Function of Nonrespirable Particle Diameter During March 30 to April 17, 1978 (79H891-49)

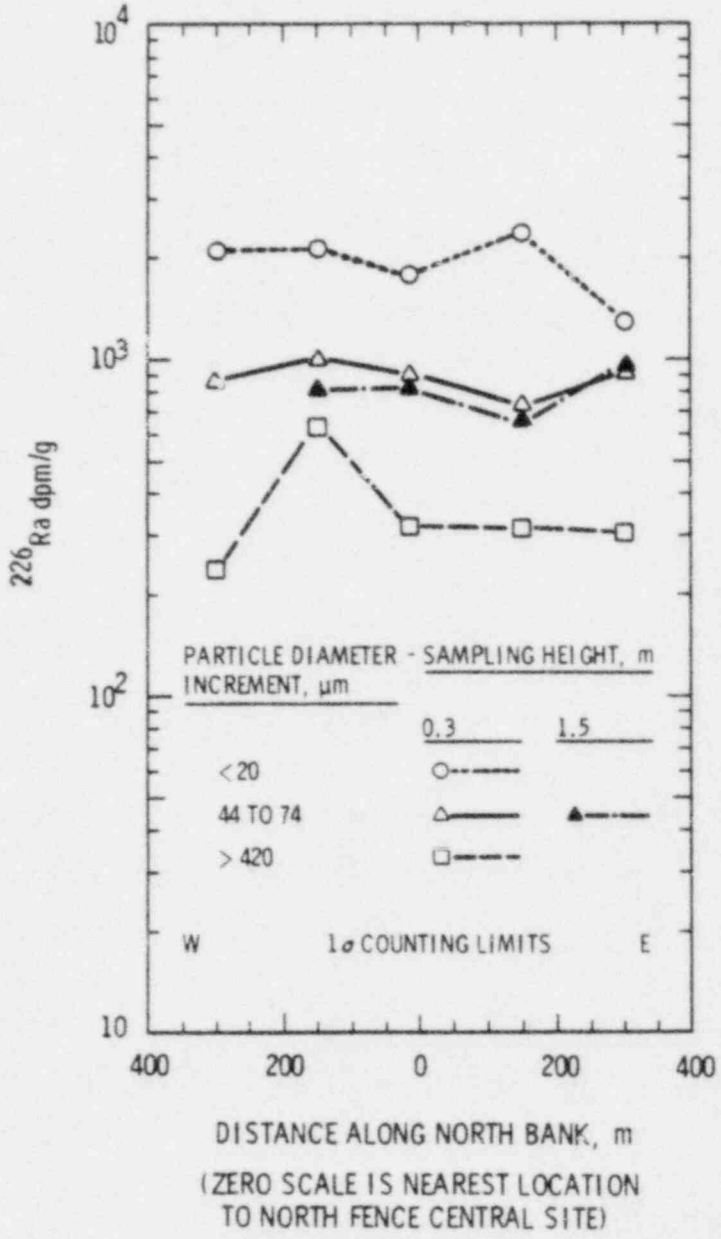

FIGURE 94. ^{226}Ra Concentration on Airborne Solids as a Function of Nonrespirable Particle Diameter During March 30 to April 17, 1978 (80B236-53)

77-μm-diameter particles were less at the 1.5 m height than at the 0.3-m sampling height, and 3) ^{226}Ra activity densities were nearly uniform from west to east. With constant activity densities, an explanation scenario is that most collected ^{226}Ra particles were wind eroded from the dike rather than from dry beach areas.

Lead-214, dpm/g. Activity densities for ^{214}Pb are shown in Figure 95. Due to ... time duration between sampling and analysis, these ^{214}Pb activity densities could represent radionuclide in-growth and decay after field sampling rather than activity densities while wind eroded. This information is of main interest in comparison to ^{210}Pb activity densities. Lead-214 activity densities are significantly less than activity densities for ^{226}Ra, indicating disequilibrium between ^{226}Ra and ^{214}Pb due to radon escape. Some radon gas escaped from samples before daughter ^{214}Pb was formed.

Lead-210, dpm/g. Lead-210 in-growth occurs as a daughter product of ^{214}Pb. If ^{210}Pb activity densities are greater than ^{214}Pb activity densities, the major portion of reported ^{210}Pb activity densities were measured for field conditions rather than from in-growth while in the laboratory.

Activity densities for airborne ^{210}Pb are shown in Figure 96. Activity densities range from about 300 to 1500 dpm/g. Activity densities were nearly uniform from west to east sampling sites. Activity densities were largest for <20-μm-diameter particles and decreased with increasing particle diameter. The smallest activity densities were associated with >420-μm-diameter particles. Lead-210 activity densities were similar at both sampling heights of 0.3 and 1.5 m.

Normalized Activity Densities. Activity densities can be used to estimate the apparent equilibrium between radioactive decay products on airborne solids. To estimate the apparent equilibrium, activity densities for ^{235}U, ^{238}U, ^{230}Th, ^{226}Ra, and ^{214}Pb were normalized by the corresponding activity densities for ^{210}Pb. Resulting activity density ratios are shown in Figure 97. Statistical analyses have not been done on this data. Nevertheless, estimates of the apparent equilibrium, or nonequilibrium can be made. The activity densities are approximately 10^{-2} for $^{235}U/^{210}Pb$; 10^{-1} for $^{238}U/^{210}Pb$; approximately unity for $^{230}Th/^{210}Pb$ and $^{226}Ra/^{210}Pb$; and less than unity for $^{214}Pb/^{210}Pb$.

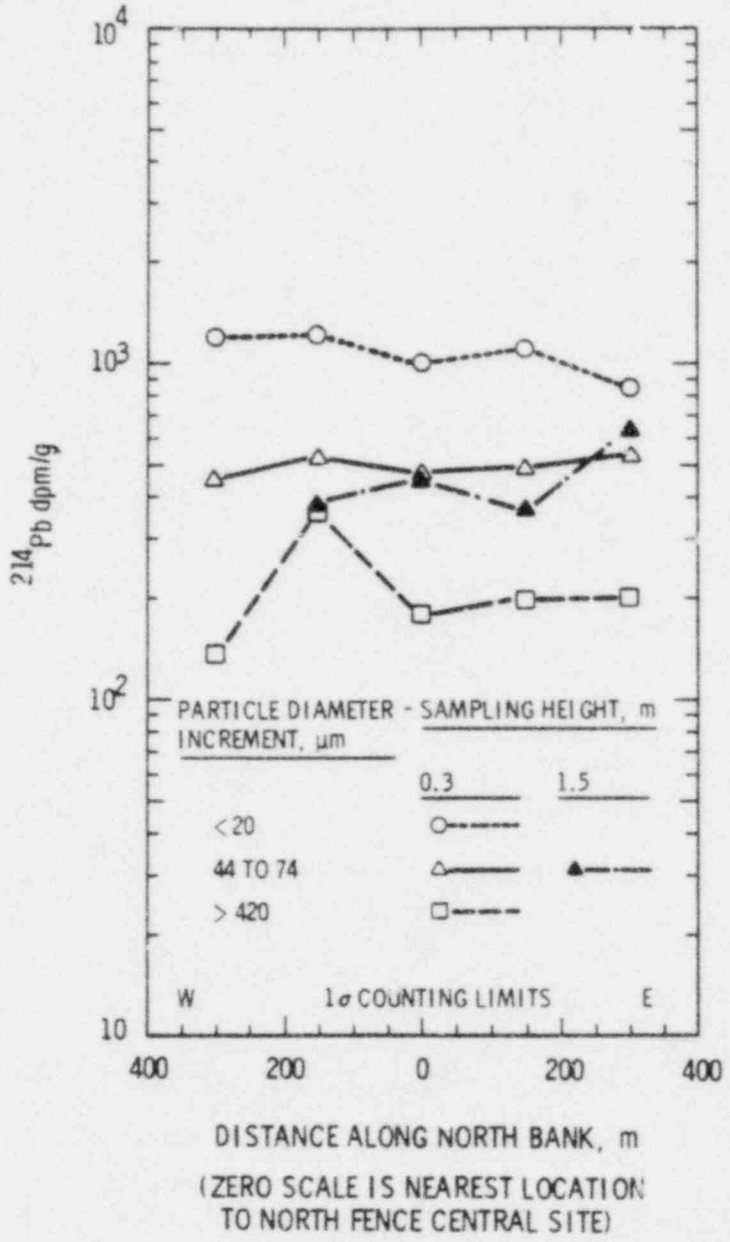

FIGURE 95. ^{214}Pb Concentration on Airborne Solids as a Function of Nonrespirable Particle Diameter During March 30 to April 17, 1978 (79H891-52)

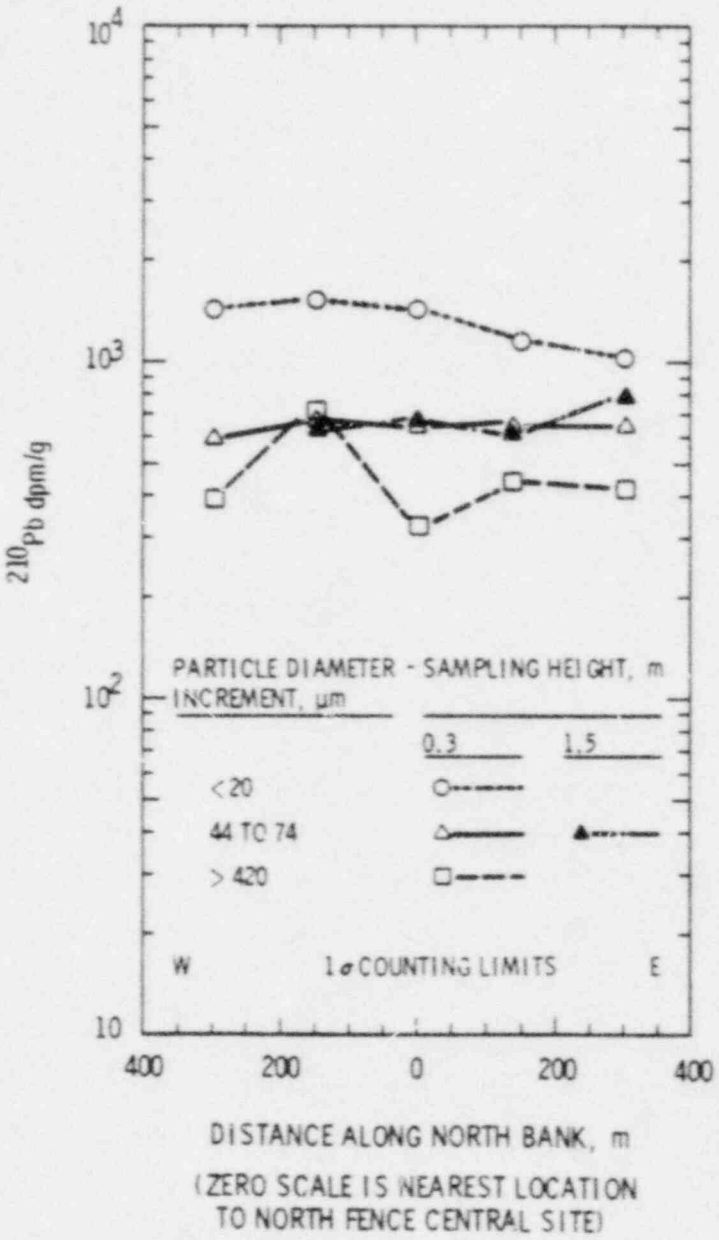

FIGURE 96. ^{210}Pb Concentration on Airborne Solids as a Function of Nonrespirable Particle Diameter During March 30 to April 17, 1978 (79H891-50)

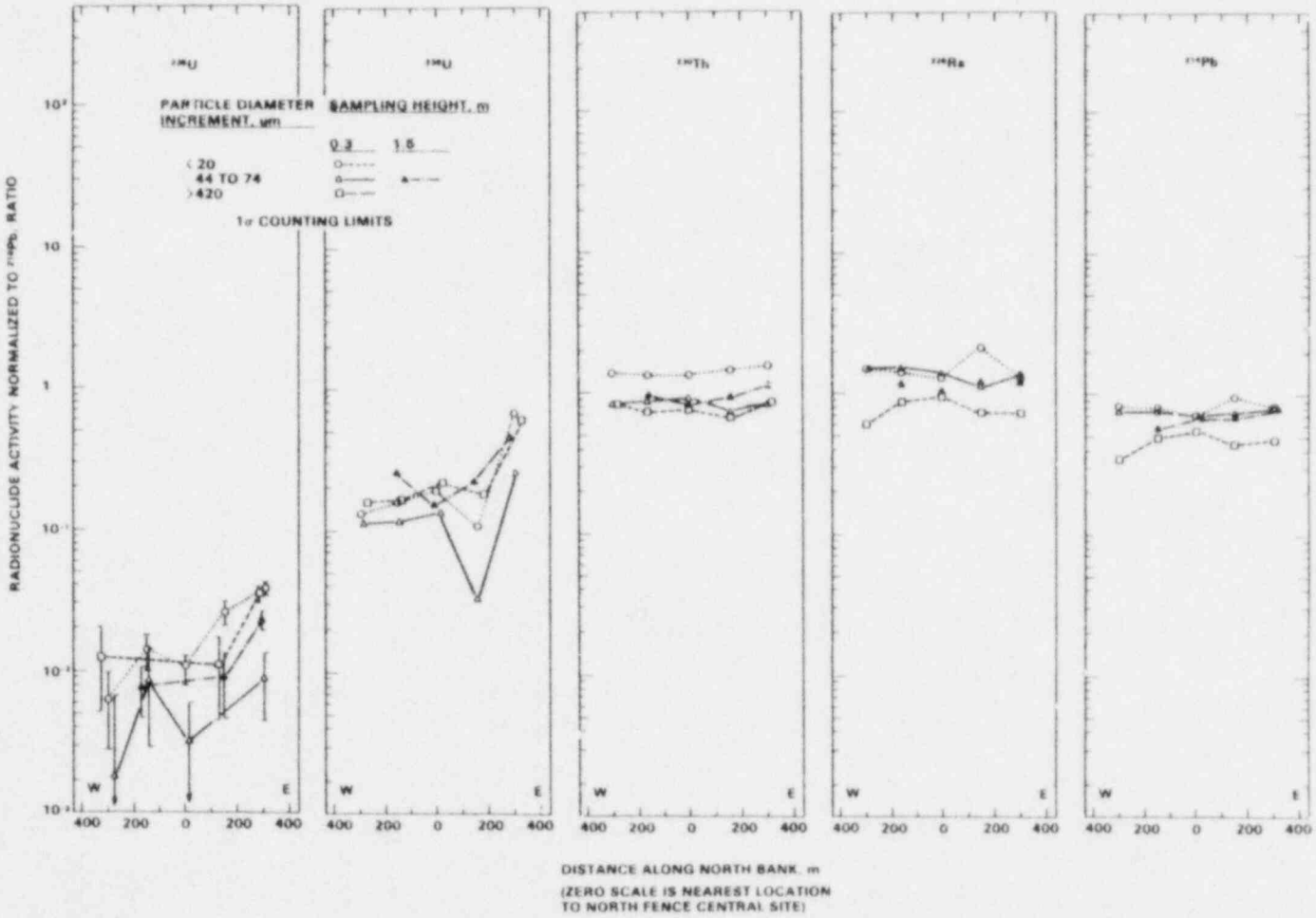

FIGURE 97. Radionuclide Activity Normalized to ^{210}Pb Activity on Airborne Solids Along the North Bank as a Function of Nonrespirable Particle Diameter During March 30 to April 17, 1978 (80B318-78)

February 24 to April 24, 1979

Airborne mass fluxes will be shown for sites previously discussed and in addition, for west array, central array, and east array site locations previously shown in Figure 27. Airborne solids were collected with isokinetic filters, cyclone-preseparators for particle cascade impactors, and air impact flow particle collectors. Airborne mass fluxes were calculated for particles collected within isokinetic sampler inlets and cyclone preseparators. In addition, airborne mass fluxes were calculated from solids collected within air impact flow particle collectors. These two sets of mass flux data need to be interpreted differently. For the isokinetic inlet-determined airborne mass fluxes, these mass fluxes are those which occurred during all wind speeds for a wind direction of 211 $\pm 30^{o}$. Airborne mass fluxes collected from air impact flow collectors are average values for the total time samplers were in the field, rather than only time for which the wind was blowing either from the pile, 211^{o}, or away-from the pile, 31^{o}. A comparison of mass fluxes for 211^{o} and 31^{o} facing collectors can be used as an index of whether or not mass flux sources are from primary mill tailings pile erosion, or from secondary wind erosion from prior tailings deposition (or ambient soil surfaces).

The mass flux as a function of height will be termed the mass flux profile. Mass flux profiles were investigated for heights up to 15 m. At sites A, D-1, E, and D-2, air impact flow collectors were placed at heights from 0.3 to 15 m above ground. This experiment permitted determination of average mass fluxes from 0.3 to 15 m above ground at more sites than was possible with electrically powered isokinetic air samplers.

Mass Fluxes and Loadings

Mass fluxes and airborne mass loadings calculated from isokinetic filter collections are shown in Figure 98. The "inlet" airborne mass fluxes are shown using the lefthand ordinate and the lower portion of the figure. In some cases mass fluxes calculated from filter collection are greater than those calculated from inlet collection. At background site A airborne mass fluxes increased with increasing height. This increase reflects upwind erosion with particle deposition occurring between the erosion area and site A. Along the north

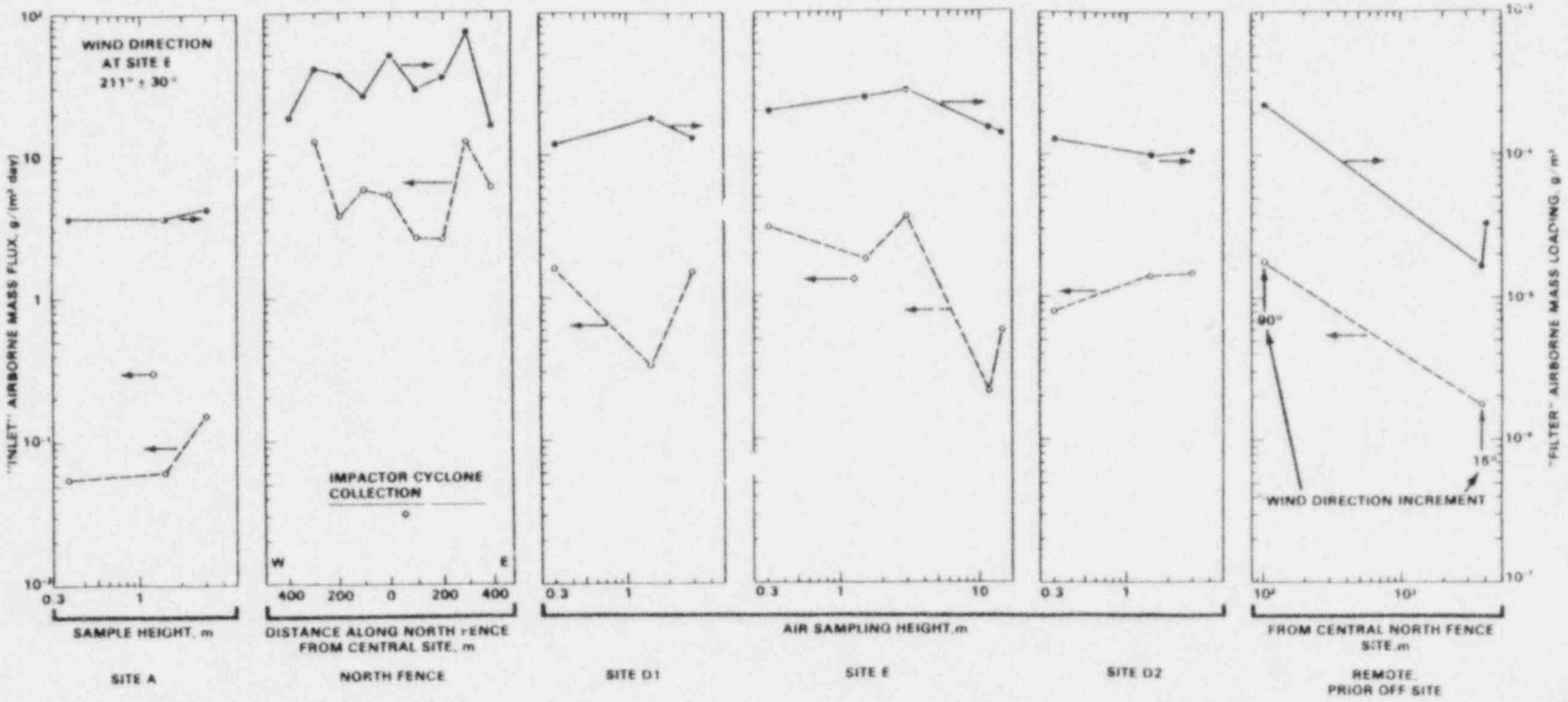

FIGURE 98. Average Airborne Fluxes and Concentrations During February 24 to April 24, 1979 (80B236-9)

fence, mass fluxes increased two orders of magnitude above background. Further downwind, airborne mass fluxes decreased. Mass fluxes were approximately uniform in the crosswind direction at sites D-1, E, and D-2.

Mass fluxes decreased with increasing height at site E. A large flux decrease with increasing height reflects that a significant fraction of the airborne plume of large particles was passing at heights between ground and 15 m, rather than passing over the uppermost sampler as shown for filter airborne mass loadings of smaller particles. Further downwind, airborne mass fluxes decreased with increasing distance. The total flux at the 15^{o} remote site was still above background fluxes measured at site A. Thus, airborne mass fluxes of "large" particles extend beyond approximately 4-km downwind.

Also shown in Figure 98 are inlet airborne mass fluxes determined from solids collections within cyclone preseparators for particle cascade impactors. Mass fluxes calculated from cyclone preseparator inlet collection and from isokinetic sampler inlet collections show some measurements in reasonable agreement and others in total disagreement. The consistencies and inconsistencies may be caused by differences in sampler geometry as well as spatial variations of airborne mass fluxes. The mass flux calculated from the cyclone preseparator collection at site A is about 1 order of magnitude greater than for the mass flux calculated from the isokinetic air sampler inlet. In contrast, at site E, mass fluxes calculated by both methods show agreement within a factor of two.

Mass Fluxes: Air-Impact-Flow Collectors

Airborne mass fluxes were calculated separately for particle collection on the collector inlet and air-exit filter, a 25-μm nylon screen. Airborne mass fluxes are shown in Figure 99.

At site A, mass flux profiles were different for inlet as compared to filter-collected solids. For filter-collected solids, airborne mass fluxes were essentially uniform as a function of height. In comparison, the inlet, i.e., large particles, mass flux profile exhibited a maximum flux at an intermediate sampling height. For the both lowest and highest sampling locations

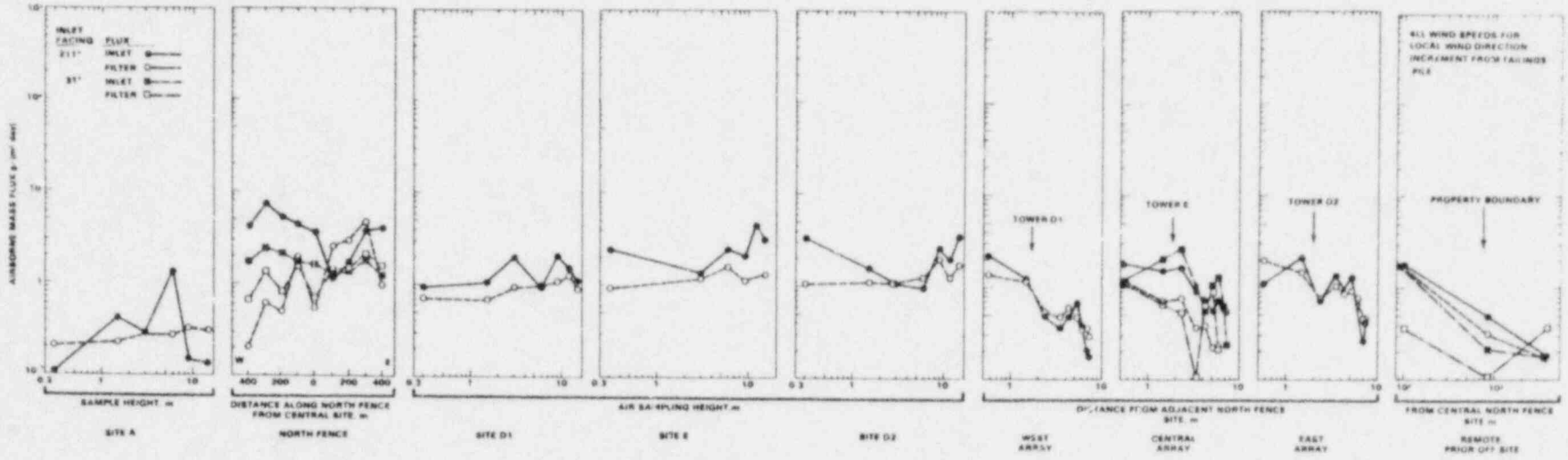

FIGURE 99. Airborne Mass Flux Separated into "Inlet" and "Filter" for Air Impact Flow particle Collectors During February 24 to April 24, 1979 (80B236-11)

the mass fluxes were comparable. This flux profile observation would be consistent with an upwind large particle erosion source producing an airborne plume transported within the lower 15 m, with the plume being depleted by deposition in the 0.3 m adjacent to the ground surface. This explanation is conjectural since these mass fluxes are average fluxes measured for all wind conditions during field sampling.

Airborne mass fluxes determined along the north fence are shown for both collectors facing towards, 211^{o}, and away from, 31^{o}, the pile. Mass fluxes for inlet-collected particles were greater coming from the pile compared to those blowing towards the pile. A fraction of the mass fluxes towards the pile probably reflect road erosion by vehicular traffic along the gravel road immediately north of the north fence. At the western end of the north fence, the mass flux towards, 31^{o}, the pile is greater than the mass flux from, 211^{o}, the pile. In contrast, along the eastern length of the north fence, mass fluxes from the pile, 211^{o}, are greater than mass fluxes towards the pile, 31^{o}.

The downwind airborne plume width and height was investigated with air impact flow collectors located at sampling sites D-1, E, and D-2. At all three sites, airborne mass fluxes tended to be uniform as a function of height. Thus, the airborne plume width is at least 900 m, the distance between sites D-1 and D-2. The airborne plume height extended over 15 m above ground.

Airborne plume width and downwind decrease were investigated with air-impact flow collectors along the west, central, and east arrays. These collectors were faced toward the pile, 211^{o}, along the west and east arrays. Along the central array collectors were faced both towards, 211^{o}, and away from, 31^{o}, the pile. Although there are individual mass-flux differences along each array, the rate of mass-flux decrease with distance is approximately the same for the west, central, and east arrays. However, along the central array, it is surprising that airborne mass fluxes for inlets facing both 211^{o} and 31^{o} are approximately the same. Being nearly the same, these results suggest that secondary erosion from prior-deposited wind-eroded mill tailing particles, or ambient soil, occurs readily and is widespread. Thus, in environmental

impact considerations, both the primary radionuclide source from the mill tailings pile as well as the secondary sources from prior deposition must be considered.

Mass fluxes are shown for distances up to 4,000 m in the last subfigure. Mass fluxes for both inlet- and filter-collected particles are greater for collectors facing toward, 211°, compared to away-from, 31°, the pile. However at 4,000 m the data are inconsistent, but tend to suggest comparable mass fluxes from both directions.

April 27 to July 9, 1979

Airborne mass fluxes were calculated from solids collection within air-impact-flow collectors. All air-impact-flow collectors were faced towards the pile, 211°, except along the north fence and central array in which collectors were faced both towards, 211°, and away from, 31°, the pile. For relative mass flux comparisons during a shorter concurrent time from May 15 to July 9, 1979, airborne mass fluxes determined with isokinetic air samplers were shown in Figures 71 and 72.

Mass Fluxes: Air-Impact-Flow Collectors

Total airborne mass fluxes shown in Figure 100 were calculated from both "inlet" and filter collections within air-impact-flow collectors. At site A, mass fluxes were nearly constant for height between 3 and 15 m. Mass fluxes were greater at lower elevations, suggesting the possibility of local wind erosion upwind of site A. Along the north fence, airborne mass fluxes were greater than background for inlets facing both toward, 211°, and away-from, 31°, the pile. At sites D-1, E, and D-2, airborne mass fluxes were nearly uniform as a function of height. Thus at these sites, the airborne large particle plume extends to heights above the uppermost 15-m collector. In comparing these airborne fluxes with those measured at site A, the plume width extended at least from site E to site D-2. Plume width and heights are comparable for both inlet- and filter-collected particles.

Downwind changes in airborne mass fluxes are indicated by data for the west, central, and east arrays in Figure 100. Downwind changes are comparable for both inlet- and filter-collected particles. The rates of mass flux

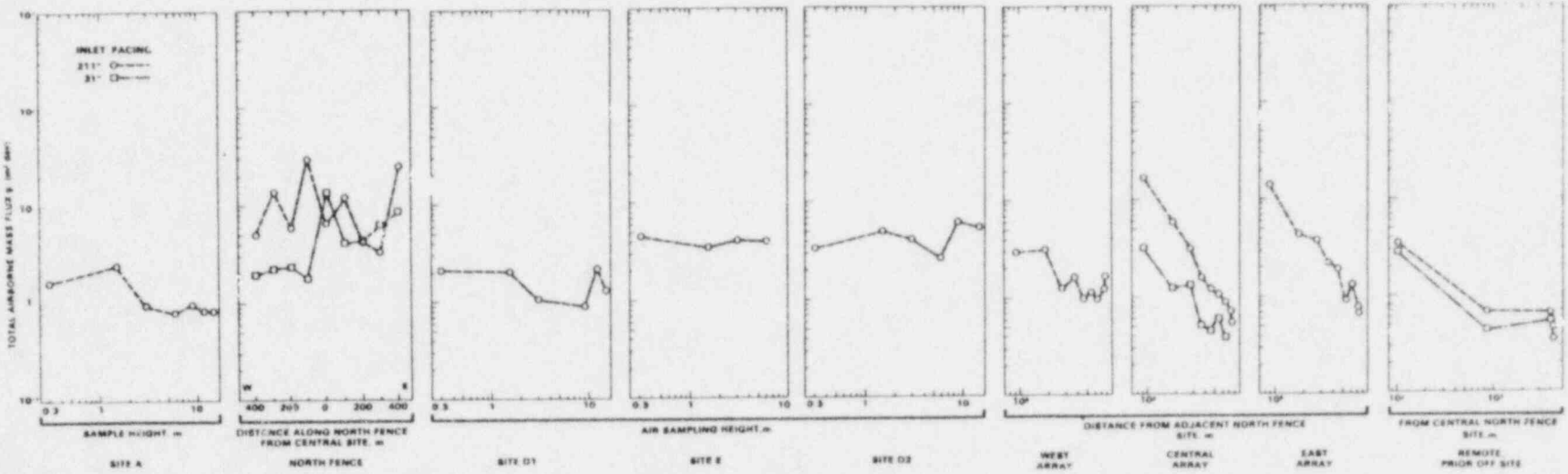

FIGURE 100. Total Airborne Mass Flux from Air Impact Flow Particle Collectors During April 27 to July 9, 1979 (80B236-13)

decrease with distance are more comparable for the central and east arrays, as compared to the rate of mass flux decrease along the west array. At the central array, airborne mass fluxes decreased with distance for inlets facing both toward, 211°, and away-from, 31°, the pile. Again, these data are further confirmatory evidence of a secondary wind-erosion source attributable to prior mill tailings erosion and subsequent deposition in the environs. Additional secondary source evidence is interpreted from the most remote site. Airborne mass fluxes 4-km downwind were less than mass fluxes determined at site A. Since site A mass fluxes are greater, samplers at site A may be measuring secondary wind erosion from upwind sources.

Airborne mass fluxes were also calculated as a function of inlet- and filter-collected solids. These mass fluxes are shown in Figure 101. In cross comparing background data for site A and the 4-km data in the last subfigure, mass fluxes from both filter- and inlet-collection were greater at background site A than 4-km downwind.

Relative Collection Site

Mass fluxes were shown in Figure 101 as a function of particle size, larger particles being collected on the inlet and smaller particles being collected on the filter. An index of the relative mass collection on the filter is shown in Figure 102. Airborne solids collected on the filter are shown as a percent of total solids collection on the inlet plus filter. Solids collected on the filter range from about 6 to over 90%.

June 28 to August 8, 1978

Remote Mass Fluxes as a Function of Particle Diameter

The transport distance of radionuclides on airborne particles from the mill tailings pile is a function of the particle size upon which radionuclides are transported. Airborne mass fluxes as a function of distance and particle diameter were investigated with air-impact particle collectors along the central sampling array (see remote sampler locations shown in Figure 40). After particle collection, particles were subsequently sieved into seven size fractions ranging from <37-μm to >210-μm diameters. Airborne mass fluxes, $g/(m^2\ day)$ were calculated for these size fractions.

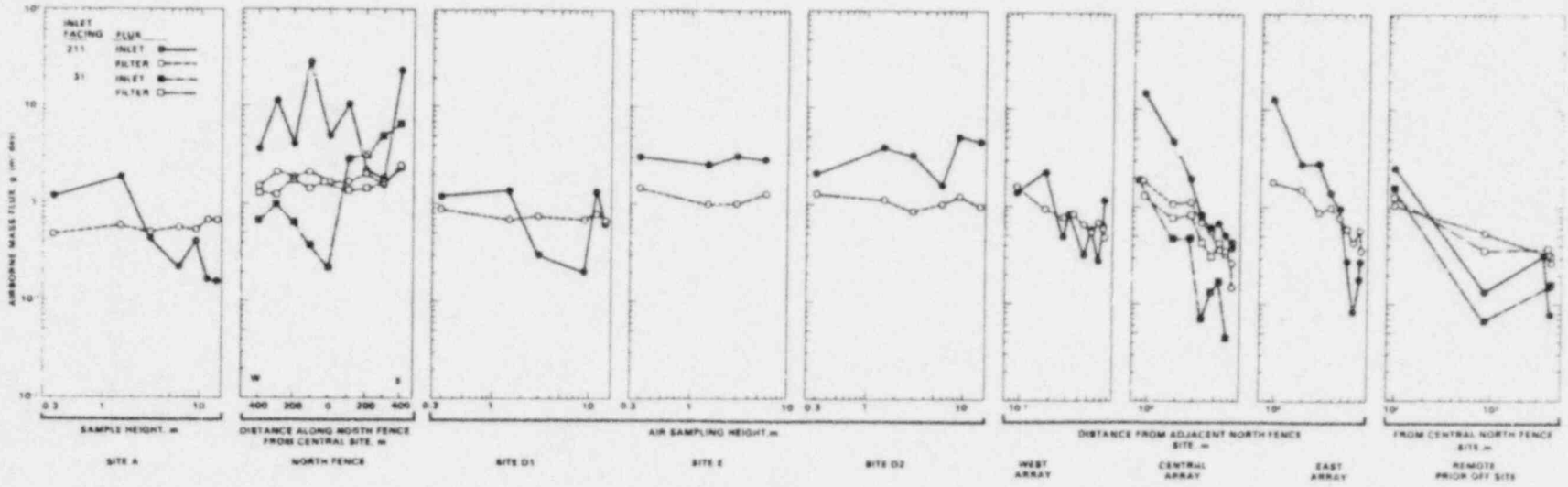

FIGURE 101. Airborne Mass Flux Separated into "Inlet" and "Filter" for Air Impact Flow Particle Collectors During April 27 to July 9, 1979 (80B236-12)

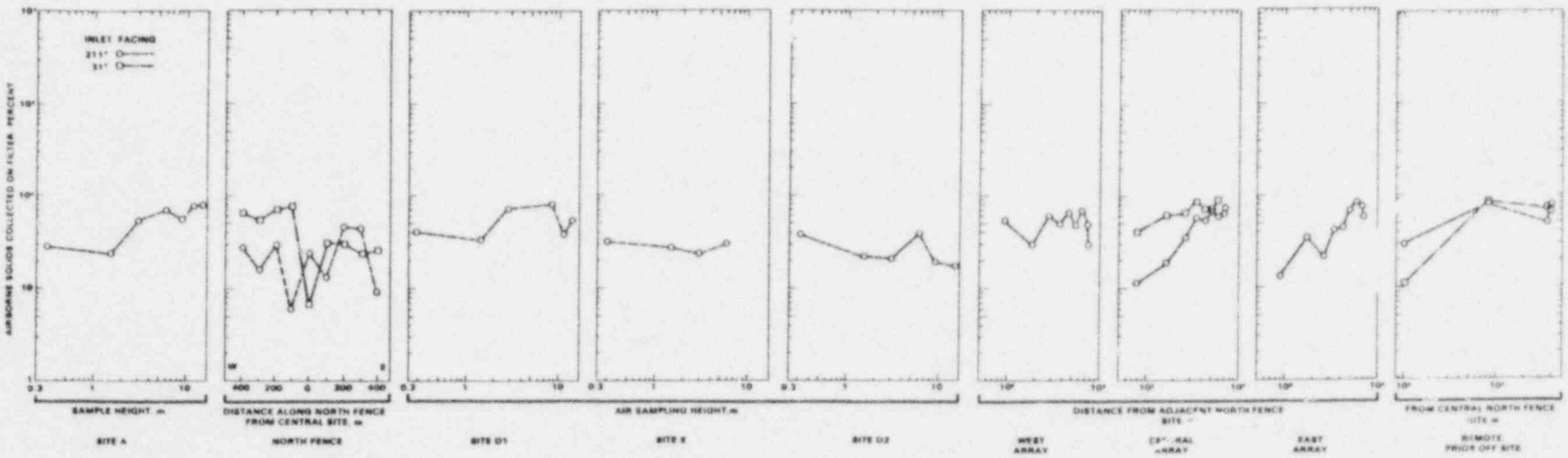

FIGURE 102. Percent Airborne Solids Collected on the Filter in the Air Impact Flow Particle Collectors During April 27 to July 9, 1979 (80B236-10)

Airborne mass fluxes as a function of particle diameter during June 28 to August 8, 1978 are shown in Figure 103. Two subfigures are used to display mass fluxes for the seven particle-diameter increments. Mass fluxes are maximum for an intermediate-diameter increment, 74 to 125 μm. Consequently, mass fluxes for particle diameters <37 μm are shown in the left subfigure while mass fluxes for particle diameters >74 μm are shown in the right subfigure. In both subfigures airborne mass fluxes decrease with increasing distance. In the left subfigure the smallest mass fluxes are for the <37-μm-diameter increment. Mass fluxes increase nonuniformly with particle diameter for the next two particle size ranges. Mass fluxes for the 37- to 53-μm-diameter increment are greater than for the 53- to 74- m-diameter increment. In the right subfigure a consistent trend is shown as a function of particle diameter. Mass fluxes decrease as particle diameter increased. The maximum mass fluxes were for the 74- to 125-μm-diameter increment, and the minimum mass fluxes were for the >210-μm-diameter increment.

The rate at which airborne mass fluxes decrease with increasing distance is a function of particle diameter. The most rapid decrease is for the 74- to 125-μm particle-diameter increment while the least rapid decrease is for the >210-μm-diameter increment. Caution is needed in interpreting these rates. These rates do not represent only one wind-speed increment. The fluxes are average values for all winds occurring during the sampling time period. Consequenty, there is not a one-to-one relationship between these measured mass fluxes and mass fluxes which might be predicted from models using only one wind speed for model predictions. In addition, model predictions are often normalized to a unit strength source, rather than mass fluxes as shown in this figure. Normalized mass fluxes would decrease as a function of distance and increasing particle diameter. This decreased mass flux with increasing particle diameter is caused by preferential dry deposition removal of larger particles.

Airborne Particle Size Distributions

Airborne particle size distributions are a function of site location and are needed for airborne transport model validation. Particle size distributions are reported for three series of experimental results: 1) at the south

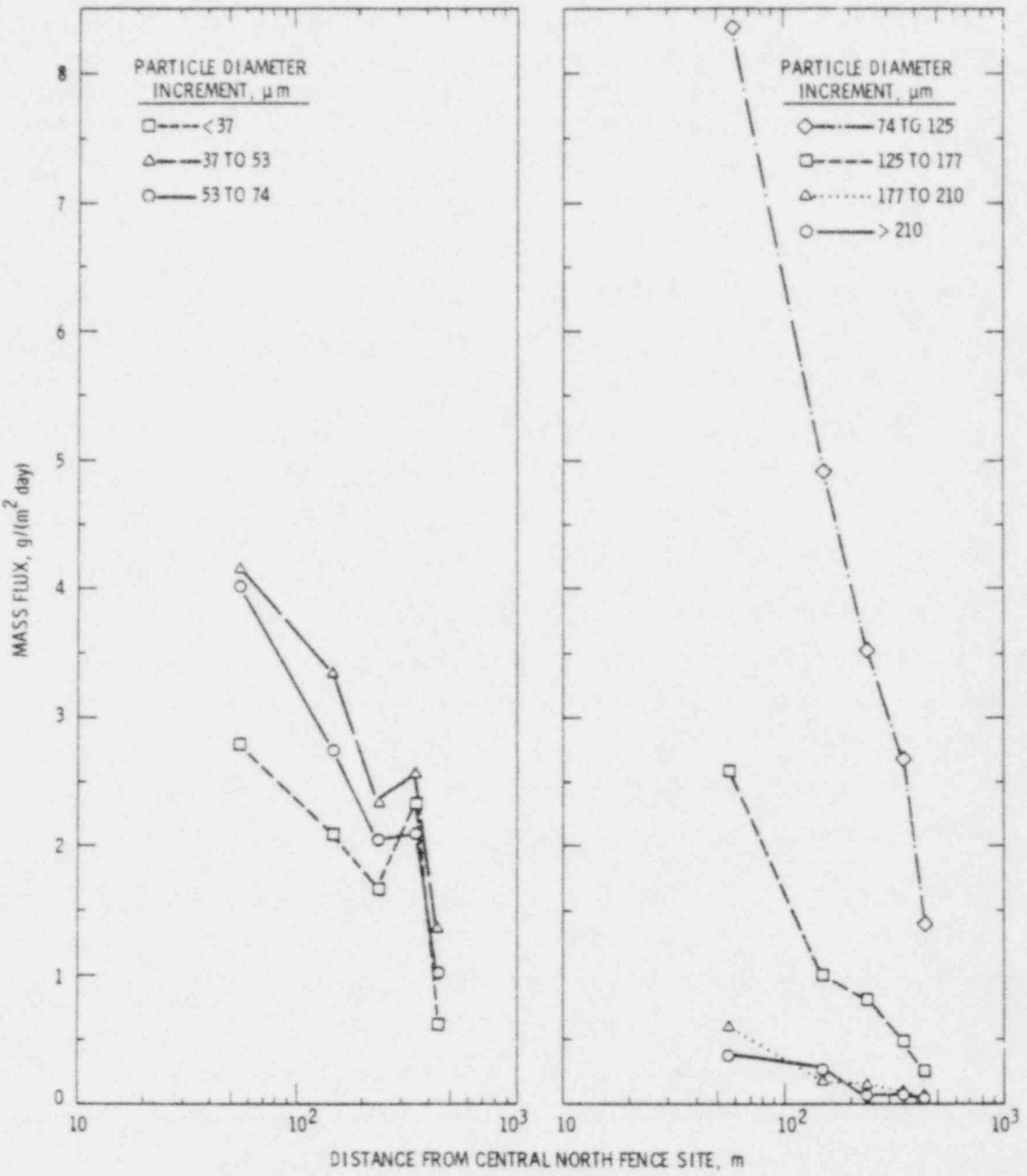

FIGURE 103. Airborne Mass Flux as a Function of Particle Diameter from Air Impact Collectors (1.5-m height) Along the Central Sampling Array During June 28 to August 8, 1978 (80B357-59)

dike site B-2 (see Figure 24 for location), 2) along the north dike, and 3) as a function of distance at remote sites.

Site B-2 Size Distribution. Airborne particle size distributions determined at site B-2 are shown in Figure 104. As shown in Figure 24, site B-2 was on the flat surface of the mill tailings pile immediately north of the south dike. Particle size distributions at this location are indicative of size distributions for particles wind eroded from the sloping banks of the mill tailings pile. Particle size distributions are shown for the three wind-speed increments of 3 to 5, 5 to 7, and 7 to 11 m/sec measured at site A. These particle-size distributions were determined by combining data calculated from particle cascade impactor and cyclone preseparator collections. In this figure the particle cascade impactor data are those for 7-μm diameter and less while the cyclone preseparator data are those for 137-μm diameter and greater.

Size distributions for all wind speeds are similar: 1) the mass median particle diameter was about 120 μm, 2) the respirable mass fraction was less than 5%, and 3) the size distribution is not a simple log-normal distribution. A separate "normal" distribution is indicated for the inhalable particles collected in the particle cascade impactor and also for the nonrespirable particles collected in the cyclone preseparator.

North Dike Size Distribution. Airborne particle size distributions determined with the air-impact-flow collectors along the north dike are shown in Figure 105. Two size distributions are shown, each size distribution being the mass average size distribution for airborne particles collected along the west to east direction. These are the same samples which were analyzed for radionuclide content with activity densities reported in Figures 90 through 97. Only nonrespirable particles were collected. Size distributions were a function of sampling height. At the 0.3-m sampling height, the mass median particle diameter was approximately 190 μm while at the 1.5-m sampling height the mass-median diameter was approximately 130 μm. This rapid decrease in mass median particle diameter (190 to 130 μm) with increasing heights reflects a large particle flux transported near (within about 0.3 m) the ground surface.

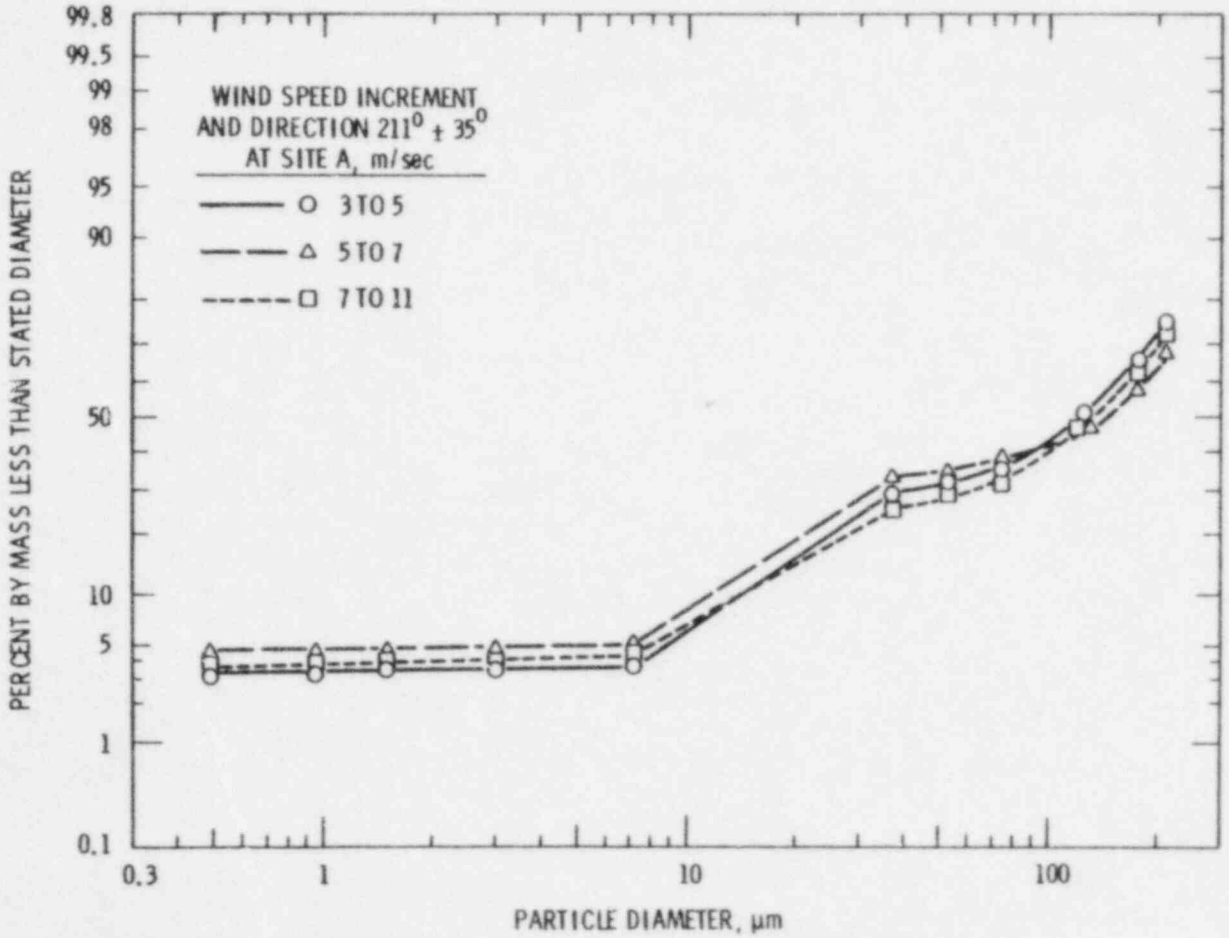

FIGURE 104. Airborne Particle Size Distributions at Site B2 During May 26 to June 16, 1978 (80B378-60)

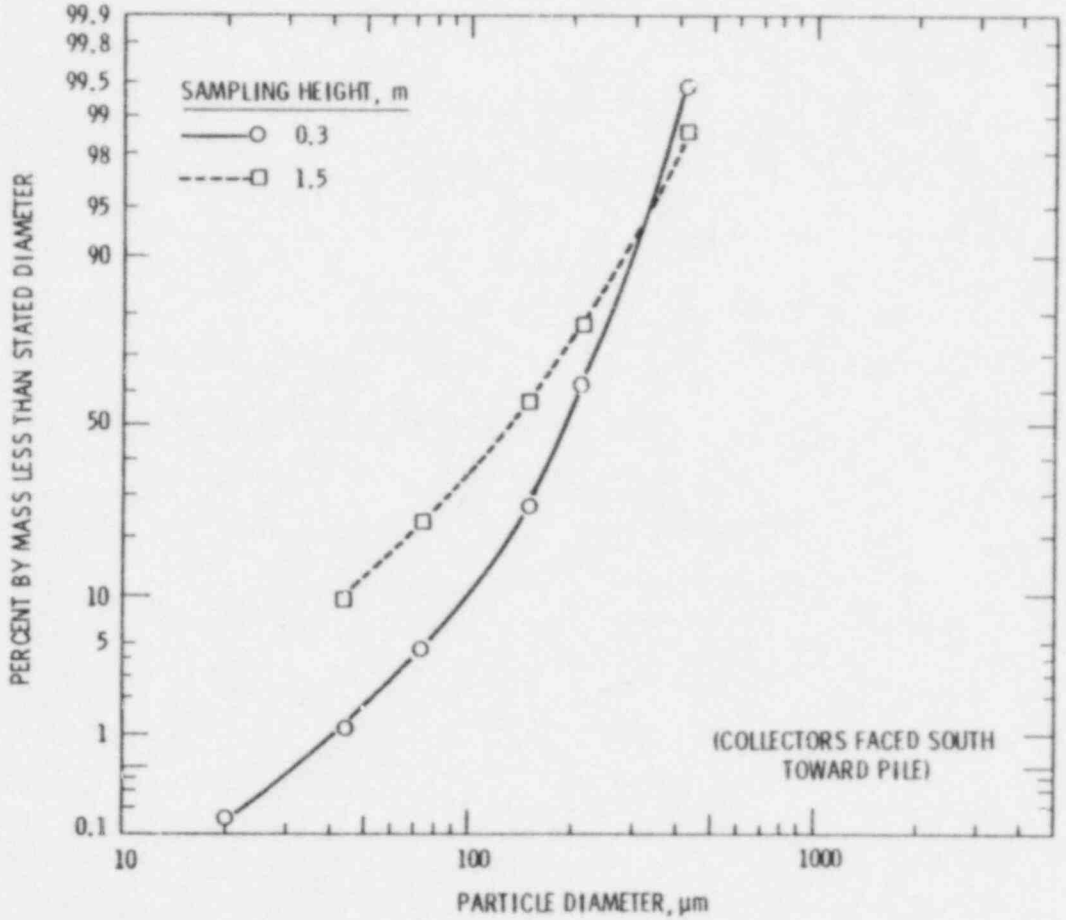

FIGURE 105. Average Crosswind Airborne Particle Size Distributions from Air Impact Flow Collectors Along the North Dike During March 30 to April 17, 1978 (80B378-58)

Remote Particle Size Distributions. Airborne particle size distributions were determined at remote sites using particle cascade impactors and cyclone preseparators. As shown in Figure 25, these remote sites were 100, 870, 3,970, and 4,280 m (i.e., the 90^{o}, 60^{o}, and the two 15^{o} sites) from the central north-fence sampling location.

Airborne particle size distributions shown in Figure 106 were a function of sampling location. A complete size distribution from 0.45- to 210-μm diameter is shown for the 100-m sampling site. The mass median diameter is about 15 μm. This size distribution is not a simple log-normal distribution, but reflects at least two "normal" distributions; i.e., a separate normal distribution for the inhalable particles collected in the cascade impactor and also for the nonrespirable particles collected in cyclone preseparator. At the more distance sites, there was too little solids collection in the cyclone preseparator to permit particle size analysis for nonrespirable particles. At the two 15^{o} sites, these two size distributions reflect large size distribution differences between sites.

Airborne Stable Element Concentrations

Airborne stable element concentrations were initially investigated at site C and subsequently at sites R-2 and R-4.

Site C, August 10 to September 12, 1977

Airborne stable element concentrations determined at site C (see Figure 24 for location) during six time periods between August 10 to September 12, 1977 are shown in Table 18. Sample collection was for all wind speeds during a wind direction from $211^{o} \pm 30^{o}$ at site A. The particulate sampling height was 1 m. Airborne concentrations were calculated for solids collected on the 3.5-μm-diameter virtual cascade impactor stage. For each time period, airborne concentrations are given on the first line and the 1σ chemistry limits are shown on the second line.

Obviously, there is a wide range of airborne concentrations for these 22 stable elements. Larger concentrations may reflect airborne sand and soil rather than stable elements from the mill tailings pile. For instance,

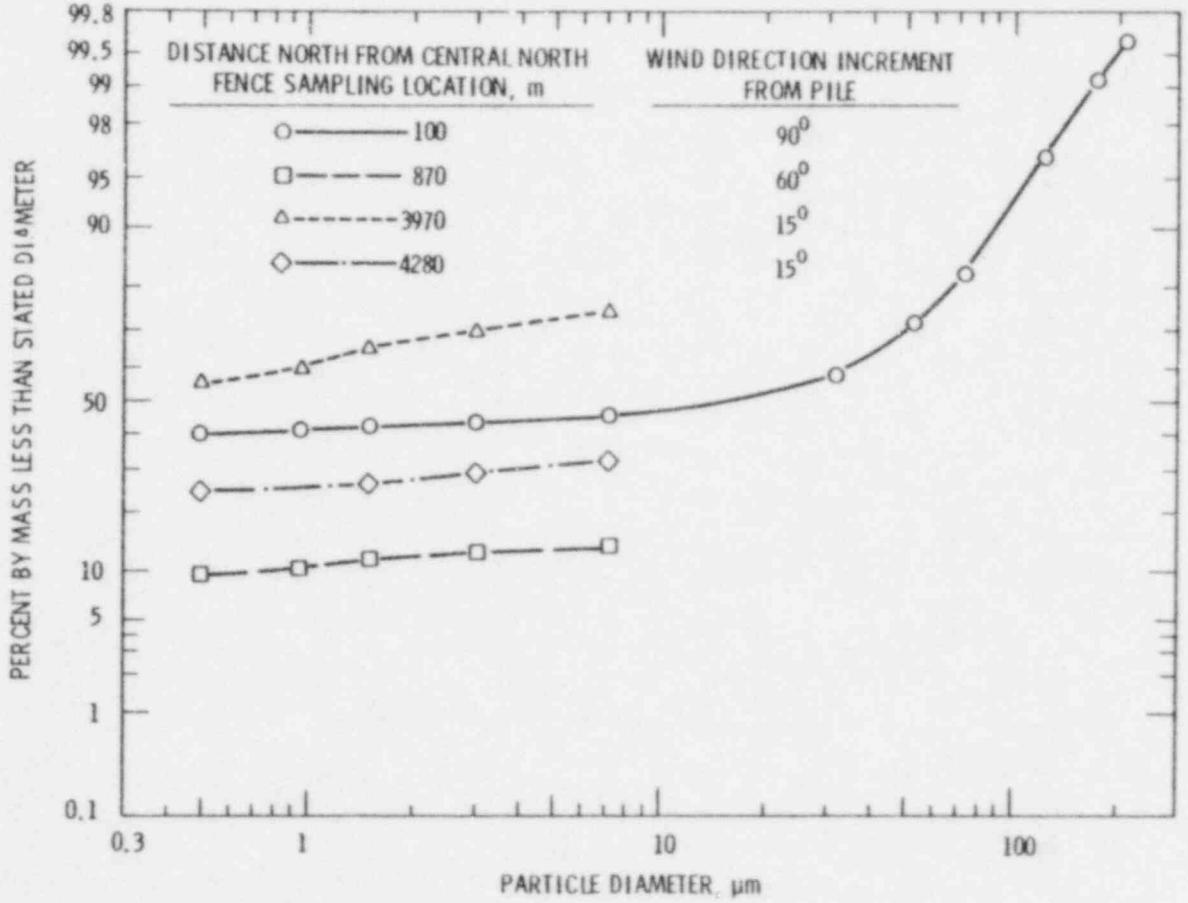

FIGURE 106. Airborne Particle Size Distributions During All Wind Speeds, Particle Collectors Located at 1.5 m Along the Central Off-site Sampling Array During May 27 to June 16, 1978 (80B328-61)

TABLE 18. (1 of 2) Airborne Stable Element Concentrations at Site C During August 10 to October 12, 1977[a]

Sampling Period, 1977	Airborne Concentration, ng/m^3										
	Si	S	Cl	K	Ca	Ti	V	Cr	Mn	Fe	Co
August 10 to 23	<159	636 ±40	<40	21	78 ±8	17 ±3	2 ±2	5 ±12	2 ±1	41 ±2	< 2
August 30 to 31	14700 ±500	7410 ±240	320 ±90	1710 ±70	7600 ±100	510 ±20	140 ±10	15 ±6	50 ±6	3320 ±30	<20
Sept. 9 to 12	1310 ±260	1990 ±130	<93	181 ±23	850 ±30	56 ±7	<9	15 ±3	8 ±2	320 ±10	< 6
Sept. 23 to 29	10700 ±1400	8120 ±600	455	966 ±139	4970 ±190	450 ±51	74 ±28	60 ±19	<28	2024 ±46	<37
Sept. 29 Oct. 4	61500 ±1600	43500 ±600	<300	10390 ±190	63800 ±300	2410 ±50	700 ±30	28 ±17	400 ±20	18600 ±200	<62
Oct. 4 to 12	10300 ±400	3750 ±130	<80	1110 ±40	5300 ±100	260 ±11	70 ±10	11 ±4	38 ±4	1880 ±20	<12

(a) Sampling was with a virtual impactor which operated when the wind direction was 211° ±30° at site A. Sampling height was 1 m. Data shown were calculated from material collected on the 3.5-μm-diameter stage. The 1σ chemistry limits are shown on the second line.

TABLE 18. (2 of 2) Airborne Stable Element Concentrations at Site C During August 10 to October 12, 1977[a]

Sampling Period, 1977	Airborne Concentration, ng/m^3										
	Ni	Cu	Zn	Ga	Hg	Se	Pb	As	Br	Rb	Sr
August 10 to 23	1	8 ±1	10 ±1	<1	< 4	13 ±1	79 ±3	11 ±2	10 ±1	< 1	10
August 30 to 31	5 ±2	16 ±2	18 ±2	3 ±2	11 ±4	104 ±3	38 ±6	15 ±4	10 ±2	< 4	< 27
Sept. 9 to 12	2 ±1	14 ±2	7 ±1	<2	< 7	13 ±1	33 ±5	9 ±3	11 ±2	< 3	< 23
Sept. 23 to 29	<9	42 ±9	28 ±5	<9	<37	93 ±9	42 ±19	14 ±9	37 ±5	<14	<116
Sept. 29 Oct. 4	<9	50 ±5	50 ±5	12 ±3	<19	900 ±20	92 ±16	36 ±9	61 ±5	48 ±5	185 ±29
Oct. 4 to 12	3 ±1	13 ±1	11 ±1	<2	< 5	42 ±1	51 ±4	7 ±2	10 ±1	4 ±1	<17

(a) Sampling was with a virtual impactor which operated when the wind direction was 211° ±30° at site A. Sampling height was 1 m. Data shown were calculated from material collected on the 3.5-μm-diameter stage. The 1σ chemistry limits are shown on the second line.

consider silicon, calcium, and iron concentrations. Airborne silicon concentrations range from <0.159 to 61.5 ng/m^3, calcium concentrations range from 0.078 to 63.8 ng/m^3, and iron concentrations range from 0.041 to 18.6 ng/m^3.

There are reasonable consistencies between ratios of one element concentration to another element concentration. Elemental concentration ratios were calculated for Ca/Si and Fe/Ca. For comparison, ratios for crustal averages will be given in parentheses. Differences between measured and crustal elemental averages may reflect both local geology and chemical separations occurring during uranium milling.

The Ca/Si elemental concentration ratios range from 0.049 to 1.04 (0.13) and the Fe/Ca elemental concentration ratios range from 0.29 to 0.53 (1.38). These concentration ratios, however, are significantly different from ratios of average amounts of elements in the earth's crust.

Other elements than silicon, calcium and iron are potentially of more interest. We have selected selenium, lead, and arsenic for further discussion. Airborne Se concentrations range from 0.042 to 0.104 ng/m^3; airborne Pb concentrations range from 0.033 to 0.79 ng/m^3; and airborne As concentrations range from 0.007 to 0.036 ng/m^3. Ratios of airborne concentrations of these elements compared to airborne Si concentrations were also calculated and compared to crustal abundances shown in parentheses. Airborne Se/Si ratios range from 0.004 to 0.02 (4×10^{-8}); airborne Pb/Si ratios range from 0.001 to 0.02 (4×10^{-8}); and airborne As/Si ratios range from 0.001 to 0.07 (2×10^{-5}). Elemental ratios for crustal abundances are orders of magnitude smaller than ratios determined from site C samples. Obviously, Se, Pb, and As are wind eroded from the uranium mill tailings pile. Airborne concentrations are less than the time-weighted average threshold limit value, TLVs. The 8-hr TLV for airborne Se is 2×10^5 ng/m^3; the TLV for airborne Pb is 1.5×10^5 ng/m^3; and the TLV for As is 5×10^5 ng/m^3.

Sites R-2 and R-4, May 15 to July 9, 1979

Airborne particulate samples collected at remote sites R-2 and R-4 during May 15 to July 9, 1979 were analyzed for stable elements. At each site there were four sampling systems, each a cyclone preseparator and a particle cascade

impactor. Four cyclone-particle cascade-impactor systems were used to determine sampling reproducibility. Each of the four sampling systems were designed to operate simultaneously. However, due to equipment problems each sampler operated for different sampling times. Differences in sampling duration and nonuniform erosion with time qualifies data interpretation. Nevertheless, there are three data groups that are comparable.

At sampling site R-2, the first two samplers operated for 10,852 and 10,940 min, respectively. The third and fourth sampler operated for 8,447 and 8,935 min, respectively. Similarly, at site R-4 systems 1, 2, and 3 operated for 7,199, 7,310, and 7,311 min, respectively. The fourth system operated for a much shorter time period of 2,816 min. Thus, in comparing data from sampling site R-2, data from samplers 1 and 2 should be consistent sets. Likewise, data from samplers 3 and 4 should be consistent data sets. Similarly, at sampling site R-4, data from samplers 1, 2, and 3 should be comparable data sets while data from sampler 4 may show significant differences.

Elemental Composition

Stable element concentrations, percent or ppm, were determined for solids collected in the cyclone preseparator. Concentration and reproducibility results for sites R-2 and R-4 are shown in Tables 19 and 20. For these tables, concentrations of Se, Pb, As, and U are selected for discussion. At sampling site R-2, Se concentrations were 75.0, 48.2, 88.0, and 66.1 ppm, all significantly above the average crustal abundance of 0.09 ppm. In addition to determining absolute concentrations, these data are also an index of sampling reproducibility. It is obvious these four samples all indicate different airborne concentrations, even when the 1σ chemistry limits are considered. The source of these differences is unknown. However, differences may be a function of:

- real spatial variations between samplers of airborne concentrations,
- potential differences due to nonsimultaneous sampling, or
- due to chemistry sampling problems associated with analyzing only a small fraction of, rather than the total of, each collected sample.

TABLE 19. Elemental Composition of Airborne Solids Collected at Sampling Site R-2 Within Cyclone Preseparators During May 15 to July 9, 1979 (All wind speeds were sampled for a 60° wind direction from the Tailings Pile)

Element	Concentration Units	Average Crustal Abundance	Sampler No. 1		Sampler No. 2		Sampler No. 3		Sampler No. 4	
			Units	1σ	Units	1σ	Units	1σ	Units	1σ
Si	%	27.72	19.9	1.1	21.6	1.2	19.3	1.1	14.3	0.8
P	%	0.118	0.420	0.148	<0.25		0.529	0.159	0.319	0.124
S	%	0.052	0.900	0.071	0.465	0.051	0.896	0.075	0.682	0.060
Cl	%	0.032	0.079	0.021	0.040	0.016	0.126	0.023	0.090	0.019
K	%	2.59	1.27	0.07	0.944	0.050	1.36	0.07	0.999	0.052
Ca	%	3.63	7.72	0.39	4.33	0.22	9.49	0.48	5.82	0.29
Ti	%	0.44	0.134	0.010	0.105	0.006	0.223	0.012	0.134	0.007
V	ppm	150	118	16	58.7	10.7	177	20	87.1	12.6
Cr	ppm	200	263	16	117	8	147	11	144	10
Mn	ppm	1000	365	20	216	12	407	22	282	16
Fe	%	5.0	1.38	0.07	0.675	0.03	1.28	0.06	1.38	0.07
Ni	ppm	80	72.5	4.5	28.7	2.4	38.6	2.9	46.6	3.2
Cu	ppm	70	154	8	29.6	1.9	61.3	3.4	94.2	5.0
Zn	ppm	132	254	13	159	8	202	10	291	15
Ga	ppm	15	4.55	0.71	3.38	0.58	5.44	0.64	1.90	0.60
Hg	ppm	0.5	<3.0		<2.6		2.7		<2.6	
Se	ppm	0.09	75.0	3.9	48.2	2.6	88.0	4.5	66.1	3.4
Pb	ppm	0.01	52.3	3.4	32.1	2.6	45.9	3.0	48.8	3.1
As	ppm	5	14.2	1.1	11.1	1.0	15.6	1.1	11.4	1.0
Br	ppm	1.6	8.66	.62	3.87	0.47	7.28	0.53	11.4	0.7
Rb	ppm	310	46.0	2.4	46.4	2.5	48.6	2.5	39.4	2.1
U	ppm	4	127	9	40.8	3.9	128	10	91.0	6.9
Sr	ppm	300	178	12	118	8	196	14	140	10
Y	ppm	28	16.6	1.4	10.7	1.0	18.2	1.4	13.3	1.1
Zr	ppm	220	168	12	265	19	213	15	210	15
Nb	ppm	24	8.38	0.91	5.67	0.78	7.76	0.81	7.34	0.79
Mo	ppm	15	42.8	3.2	17.2	1.57	59.2	4.24	52.9	3.8

TABLE 20. Elemental Composition of Airborne Solids Collected at Sampling Site R-4 Within the Cyclone Preseparators During May 15 to July 9, 1979 (All wind speeds were sampled for a 15° wind direction from the Tailings Pile)

Element	Concentration Units	Average Crustal Abundance	Sampler No. 1		Sampler No. 2		Sampler No. 3		Sampler No. 4	
			Units	1σ	Units	1σ	Units	1σ	Units	1σ
Si	%	27.72	19.3	1.0	16.6	0.9	5.29	0.32	22.2	0.32
P	%	0.118	0.331	0.115	0.246	0.061	0.388	0.058	0.190	0.058
S	%	0.052	0.547	0.052	0.192	0.024	0.319	0.028	0.223	028
Cl	%	0.032	0.134	0.020	0.037	0.009	0.053	0.009	0.067	.009
K	%	2.59	1.29	0.07	0.797	0.042	0.544	0.028	1.05	0.028
Ca	%	3.63	3.25	0.16	0.706	0.037	0.967	0.049	1.00	0.049
Ti	%	0.44	0.168	0.009	0.083	0.005	0.065	0.004	0.092	0.004
V	ppm	150	79.5	12.0	31.2	10.8	29.8	5.7	34.8	5.7
Cr	ppm	200	427	23	19.3	5.7	64.8	4.8	12.1	4.8
Mn	ppm	1000	286	16	128	9	94.0	5.8	117	5.8
Fe	%	5.0	1.16	0.058	0.722	0.036	0.470	0.024	0.632	0.024
Ni	ppm	80	90.7	5.2	10.3	2.6	20.4	1.7	5.81	1.7
Cu	ppm	70	74.6	4.1	33.4	2.7	31.0	1.9	22.4	1.9
Zn	ppm	132	429	22	274	15	146	8	56.9	8
Ga	ppm	15	5.36	0.75	3.68	1.11	2.85	0.47	4.63	0.47
Hg	ppm	0.5	3.0		5.2		2.2		2.4	
Se	ppm	0.09	25.9	1.5	12.9	1.2	17.9	1.0	18.3	1.0
Pb	ppm	0.01	117	6	26.9	3.4	26.6	2.0	27.9	2.0
As	ppm	5	12.1	1.2	5.61	1.21	5.85	0.67	9.00	0.67
Br	ppm	1.6	26.5	1.5	7.5	0.9	8.6	0.6	21.4	0.6
Rb	ppm	310	53.0	2.8	40.9	2.5	27.0	1.5	53.8	1.5
U	ppm	4	70.4	5.8	16.3	4.8	24.2	2.7	18.5	2.7
Sr	ppm	300	129	9.1	54.7	4.1	52.8	3.8	76.6	3.8
Y	ppm	28	15.5	1.3	8.4	1.3	7.3	0.8	11.7	0.8
Zr	ppm	220	187	13	127	9	72.2	5.1	181	5.1
Nb	ppm	24	9.38	0.94	4.64	1.29	6.00	0.74	8.84	0.74
Mo	ppm	15	25.5	2.0	7.86	1.84	10.8	1.08	15.9	1.08

Similar statements can be made about Pb, As, and U concentrations. Uranium concentrations are greater than the average crustal abundance, but are significantly lower than uranium ore grades, approximately 0.2% or 2000 ppm.

Similar observations can also be made about airborne Se, Pb, As, and U concentrations at sampling site R-4. Additionally, the data in Table 20 indicate either 1) particles eroded from the tailings pile were sampled in R-4 sampler inlets, or 2) ambient airborne concentrations of the four elements may be comparable to concentrations measured at site R-4. It is unknown which of these two statements is more correct since a background stable element sample was not collected at site A.

Airborne Elemental Concentrations

Airborne stable element concentrations were also determined as a function of airborne particle diameter for these two data sets at sites R-2 and R-4. Airborne concentrations, ng/m^3, were calculted for five aerodynamic particle diameters as determined with cascade impactors, and also for total collection within each cascade impactor. These concentration data are shown in Tables 21 and 22. For each element, concentration data are presented on successive lines for the four sampling systems: 1, 2, 3, and 4 at each sampling site. As previously mentioned, sampling times for these sampling systems were comparable for only selected sampling systems at each site. At sampling site R-2, data are comparable for systems 1 and 2. Similarly, data are comparable for systems 3 and 4. For sampling site R-4, data are comparable for systems 1, 2, and 3. The operating time for the fourth site was of a much shorter duration.

These data show that stable elements are distributed on all particle diameter ranges as determined by the cascade impactor. In addition, for Se, Pb, As, and U, airborne concentrations tend to be greatest for particles collected on the backup filter.

Data cross-comparison between sampling systems indicate a considerable stable element variation between samples from different sampling systems. Causes for these variations are unknown; nevertheless, it is believed that some variation could possibly be attributed to the sampling technique for x-ray fluorescence.

TABLE 21. (1 of 5) Airborne Trace Element Concentrations and Reproducibility as a Function of Cascade Impactor Collection Site. Samples were collected at site R-2 for all wind speeds and a 60° wind-direction sector from the pile during May 15 to July 19, 1979

Cascade Impactor 50% Stage Efficiency, Diameter		Airborne Concentration, ng/m^3 (* Less than value)											
		>7.2 μm		3.0 μm		1.5 μm		0.95 μm		0.49 μm		Backup Filter	
Element	Sample	ng/m^3	1σ	ng/m^3	1σ	ng/m^3	1σ	ng/m^3	1σ	ng/m^3	1σ	ng/m^3	1σ
Al	1	*80		*90		*90		*95		*80		*400	
	2	*70		*85		*76		*87		106	± 37.0	1115	± 235
	3	*100		*130		*94		*103		*94		925	± 212
	4	160	±9	*82		*87		*105		180	± 50	660	± 230
Si	1	280	± 30	370	30	390	± 30	380	± 30	270	± 30	2900	± 140
	2	317	± 26	472	32	348	± 28	415	± 32	194	± 25	4571	± 173
	3	464.9	± 36.8	567.6	41.2	370	± 330	393	± 36.2	309	± 33.9	2753	± 151
	4	340	± 30	390	± 30	290	± 30	390	± 30	260	± 30	2930	± 150
S	1	22.0	± 6.6	38.9	± 6.6	46.6	± 7.0	49.3	± 7.5	88.4	± 7.9	150	± 30
	2	22.9	± 6.2	42.4	± 6.7	34.0	± 6.7	52.2	± 7.5	86.9	± 7.8	726	± 34.0
	3	36.8	± 9.0	54.3	± 9.2	55.6	± 8.3	71.5	± 8.8	121	± 10.2	577	± 35.4
	4	26	± 8	41	± 8	45	± 8	68	± 9	121	± 10	567	± 34
Cl	1	*5.7		10.4	± 2.8	9.14	± 3.00	*6.2		*6.2		21.8	± 10.8
	2	6.45	± 2.7	8.1	± 2.9	6.5	± 2.9	7.0	± 3.2	*6.3		*25	
	3	27.4	± 8.0	27.4	± 7.2	24.3	± 6.1	*7.5		*8.12		*27.1	
	4	*7.0		*6.9		8.1		8.6	± 3.5	*7.9		*25.8	
K	1	19.2	± 3.1	31.4	± 3.4	31.7	± 3.5	28.9	± 3.3	29.0	± 3.2	191	± 10
	2	20.2	± 2.9	35.3	± 3.2	27.8	± 3.1	32.2	± 3.5	20.2	± 3.03	266	± 10.9
	3	25.6	± 3.8	40.3	± 4.1	35.9	± 4.0	36.0	± 4.2	32.5	± 3.9	199	± 12.0
	4	16.8	± 1.1	220	± 1.2	26.9	± 1.2	31.8	± 1.2	27.9	± 1.2	199	± 5
Ca	1	152	± 2.7	209	± 3.1	177	± 2.9	160	± 1.8	140	± 2.5	1150	± 10
	2	157	± 2.7	224	± 3.2	154	± 2.7	174	± 2.8	93.7	± 2.0	1672	± 12.0
	3	184	± 3.2	254	± 3.8	186	± 3.3	188	± 3.4	143	± 2.8	1056	± 11
	4	152	± 2	161	± 2	161	± 2	163	± 2	131	± 2	1289	± 8

TABLE 21. R-2 (2 of 5)

Cascade Impactor 50% Stage Efficiency, Diameter Element	Sample	Airborne Concentration, ng/m^3 (* Less than value)											
		>7.2 µm		3.0 µm		1.5 µm		0.95 µm		0.49 µm		Backup Filter	
		ng/m^3	1σ	ng/m^3	1σ	ng/m^3	1σ	ng/m^3	1σ	ng/m^3	1σ	ng/m^3	1σ
Ti	1	4.78	± 0.50	6.99	± 0.57	7.13	± 0.54	5.63	± 0.54	6.21	± 0.49	35.4	± 1.6
	2	4.89	± 0.48	7.20	± 0.56	5.05	± 0.53	7.4	± 0.57	4.45	± 0.47	44.8	± 1.89
	3	4.75	± 0.6	6.79	± 0.70	7.06	± 0.61	8.55	± 0.68	5.82	± 0.59	32.6	± 2.0
	4	6.11	± 0.32	6.57	± 0.33	6.70	± 0.35	6.17	± 0.33	5.08	± 0.30	33.9	± 1.1
V	1	0.49	± 0.14	0.88	± 0.35	0.92	± 0.17	0.71	0.33	0.59	± 0.15	4.5	± 1.0
	2	0.38	± 0.15	0.94	± 0.32	0.47	± 0.15	0.97	± 0.18	0.530	± 0.14	4.96	± 1.12
	3	0.34	± 0.20	0.62	± 0.21	1.32	± 0.41	0.71	± 0.21	0.64	± 0.18	4.1	± 1.2
	4	0.44	± 0.17	0.74	± 0.18	0.52	± 0.18	0.52	± 0.18	0.65	± 0.17	3.46	± 0.64
Cr	1	0.66	± 0.25	0.68	± 0.11	0.72	± 0.11	0.63	± 0.25	0.65	± 0.10	3.4	± 0.76
	2	0.92	± 0.24	0.66	± 0.11	0.37	± 0.09	0.50	± 0.25	0.43	± 0.21	3.38	± 0.772
	3	0.53	± 0.30	0.48	± 0.12	0.36	± 0.12	0.39	± 0.12	0.39	± 0.11	1.2	± 0.36
	4	0.87	± 0.13	0.57	± 0.12	0.47	± 0.12	0.68	± 0.12	0.45	± 0.11	3.78	± 0.41
Th	1	*0.40		*0.42		*0.40		*0.37		*0.37		*1.19	
	2	*0.33		*0.36		*0.37		*0.41		*0.40		*1.2	
	3	*0.49		*0.47		*0.47		*0.49		*0.46		*1.5	
	4	*0.49		*0.49		*0.50		*0.47		*0.45		4.64	
Mn	1	0.920	± 0.089	1.55	± 0.24	1.60	± 0.23	1.33	± 0.23	1.28	± 0.21	6.9	± 0.65
	2	0.914	± 0.198	1.49	± 0.216	1.31	± 0.20	1.28	± 0.228	1.03	± 0.11	9.84	± 0.732
	3	0.874	± 0.25	1.53	± 0.28	1.38	± 0.25	1.32	± 0.280	1.02	± 0.263	6.60	± 0.749
	4	1.04	± 0.10	1.24	± 0.11	1.29	± 0.12	1.44	± 0.12	1.34	± 0.10	7.61	± 0.40
Fe	1	41.0	± 0.68	70.9	± 0.87	73.0	± 0.87	66.6	± 0.85	74.1	± 0.79	359.1	± 2.0
	2	35.8	± 0.629	64.5	± 0.817	53.6	± 0.754	65.0	± 0.824	47.7	± 0.677	440	± 3.15
	3	44.2	± 0.80	74.5	± 0.99	70.9	± 0.97	77.5	± 1.02	62.9	± 0.878	330	± 3.12
	4	45.4	± 0.4	57.5	± 0.5	62.6	± 0.5	73.5	± 0.5	65.1	± 0.5	403	± 2

TABLE 21. R-2 (3 of 5)

Cascade Impactor 50% Stage Efficiency, Diameter / Element	Sample	Airborne Concentration, ng/m^3 (* Less than value)											
		>7.2 µm		3.0 µm		1.5 µm		0.95 µm		0.49 µm		Backup Filter	
		ng/m^3	1σ	ng/m^3	1σ	ng/m^3	1σ	ng/m^3	1σ	ng/m^3	1σ	ng/m^3	1σ
Co	1	*0.28		*0.33		*0.34		*0.34		0.38	± 0.15	*1.19	
	2	*0.25		*0.34		*0.31		*0.33		*0.28		*1.3	
	3	*0.32		*0.39		*0.38		*0.42		*0.36		*1.3	
	4	*0.31		*0.35		*0.37		*0.38		*0.35		*1.37	
Ni	1	0.29	± 0.10	0.38	± 0.12	0.32	± 0.043	0.370	± 0.047	0.352	± 0.104	1.39	± 0.36
	2	0.369	± 0.114	0.319	± 0.04	0.165	± 0.032	0.229	± 0.036	0.554	± 0.119	1.39	± 0.380
	3	*0.92		0.21	± 0.05	0.15	± 0.04	0.22	± 0.04	0.22	± 0.05	0.845	± 0.127
	4	0.65	± 0.06	0.72	± 0.06	0.75	± 0.06	1.11	± 0.07	0.86	± 0.06	5.02	± 0.20
Cu	1	0.40	± 0.043	0.82	± 0.12	0.83	± 0.13	1.09	± 0.13	1.55	± 0.13	4.37	± 0.33
	2	0.436	± 0.09	0.876	± 0.116	1.26	± 0.130	2.10	± 0.143	22.8	± 0.143	4.50	± 0.430
	3	0.92	± 0.15	1.50	± 0.72	2.23	± 0.17	3.45	± 0.19	4.35	± 0.21	11.5	± 0.525
	4	0.58	± 0.05	0.76	± 0.07	1.24	± 0.07	2.06	± 0.09	3.07	± 0.09	8.31	± 0.23
Zn	1	0.387	± 0.040	0.799	± 0.108	1.04	± 0.11	1.46	± 0.11	2.69	± 0.14	7.10	± 0.35
	2	0.403	± 0.09	0.523	± 0.098	0.527	± 0.103	1.34	± 0.130	2.70	± 0.150	11.0	± 0.420
	3	0.63	± 0.13	0.74	± 0.12	0.999	± 0.13	2.14	± 0.16	3.73	± 0.19	11.7	± 0.489
	4	0.81	± 0.05	0.58	± 0.05	0.77	± 0.06	1.85	± 0.07	3.76	± 0.09	11.1	± 0.23
Ga	1	*0.063		*0.064		*0.064		*0.070		*0.070		*0.21	
	2	*0.58		*0.06		*0.07		*0.07		*0.07		*0.22	
	3	*0.80		*0.80		*0.08		*0.09		*0.09		*0.267	
	4	*0.08		*0.07		*0.02		*0.08		*0.08		*0.25	
Hg	1	*0.23		*0.21		*0.21		*0.23		*0.22		*1.92	
	2	*0.20		*0.20		*0.20		*0.06		*0.20		*0.60	
	3	*0.28		*0.27		*0.27		*0.28		*0.27		*0.727	
	4	*0.26		*0.25		*0.25		*0.24		*0.24		*0.66	

TABLE 21. R-2 (4 of 5)

Cascade Impactor 50% Stage Efficiency, Diameter		Airborne Concentration, ng/m^3 (* Less than value)											
		>7.2 μm		3.0 μm		1.5 μm		0.95 μm		0.49 μm		Backup Filter	
Element	Sample	ng/m^3	1σ	ng/m^3	1σ	ng/m^3	1σ	ng/m^3	1σ	ng/m^3	1σ	ng/m^3	1σ
Se	1	0.422	± 0.094	0.742		0.765	± 0.041	0.794	± 0.085	1.51	± 0.089	3.27	± 0.18
	2	0.462	± 0.072	0.756	± 0.082	0.672	± 0.084	0.526	± 0.094	1.25	± 0.093	8.35	± 0.292
	3	0.53	± 0.01	0.923	± 0.102	0.841	± 0.103	1.04	± 0.112	1.77	± 0.117	7.26	± 0.335
	4	0.41	± 0.04	0.50	± 0.04	0.68	± 0.05	1.08	± 0.05	1.95	± 0.06	7.44	± 0.17
Pb	1	0.293	± 0.120	0.738	± 0.251	0.736	± 0.254	1.03	± 0.26	1.51	± 0.26	11.5	± 0.79
	2	*0.224		0.621	± 0.116	0.446	± 0.246	1.03	± 0.257	2.01	± 0.267	13.5	± 0.836
	3	0.446	±0.151	0.694	± 0.156	0.940	± 0.281	1.20	± 0.339	2.40	± 0.321	13.8	± 1.02
	4	*0.29		0.47	± 0.14	0.71	± 0.15	1.62	± 0.15	2.65	± 0.16	15.2	± 0.5
As	1	*0.080		0.134	± 0.041	0.191	± 0.044	0.191	± 0.047	0.473	± 0.26	1.59	± 0.42
	2	0.159	± 0.105	0.121	± 0.041	0.213	± 0.043	0.328	± 0.049	0.406	± 0.052	2.41	± 0.190
	3	*0.98		0.141	± 0.054	0.154	± 0.054	0.333	± 0.167	0.640	± 0.167	1.82	± 0.531
	4	*0.099		*0.096		*0.103		0.19	± 0.06	0.56	± 0.07	2.23	± 0.21
Br	1	0.104	± 0.033	0.223	± 0.086	0.369	± 0.034	0.340	± 0.079	0.708	± 0.082	1.35	± 0.23
	2	0.116	± 0.031	0.261	± 0.081	0.320	± 0.081	0.426	± 0.090	0.716	± 0.088	4.63	± 0.257
	3	0.144	± 0.041	0.241	± 0.042	0.396	± 0.094	0.567	± 0.104	1.02	± 0.101	4.95	± 0.327
	4	0.13	± 0.04	0.15	± 0.04	0.26	± 0.04	0.46	± 0.04	1.06	± 0.05	4.77	± 0.14
Rb	1	*0.20		*0.19		*0.20		*0.21		*0.20		0.79	± 0.27
	2	*0.18		*0.19		0.20	± 0.10	*0.22		*0.20		0.740	± 0.321
	3	*0.22		*0.25		*0.255		*0.275		*0.257		*0.738	
	4	*0.11		*0.11		*0.11		*0.11		*0.11		0.60	± 0.16
U	1	0.622	± 0.239	0.770	± 0.246	0.816	± 0.255	1.08	± 0.25	1.52	± 0.24	5.05	± 0.60
	2	*0.44		0.876	± 0.233	1.11	± 0.242	1.53	± 0.269	1.46	± 0.242	7.47	± 0.769
	3	0.676	± 0.200	1.07	± 0.31	1.46	± 0.307	2.04	± 0.329	2.09	± 0.293	5.19	± 0.885
	4	*0.58		0.67	± 0.21	*0.57		1.61	± 0.21	1.77	± 0.29	*1.3	

TABLE 21. R-2 (5 of 5)

Cascade Impactor 50% Stage Efficiency, Diameter		Airborne Concentration, ng/m^3 (* Less than value)											
		7.2 μm		3.0 μm		1.5 μm		0.95 μm		0.49 μm		Backup Filter	
Element	Sample	ng/m^3	1σ	ng/m^3	1σ	ng/m^3	1σ	ng/m^3	1σ	ng/m^3	1σ	ng/m^3	1σ
Sr	1	0.476	± 0.083	0.719	± 0.085	0.701	± 0.083	0.425	± 0.084	0.554	± 0.080	3.21	± 0.23
	2	0.243	± 0.079	0.803	± 0.083	0.490	± 0.087	0.705	± 0.090	0.472	± 0.076	4.40	± 0.256
	3	0.323	± 0.104	0.726	± 0.116	0.645	± 0.101	0.775	± 0.111	0.552	± 0.096	2.99	± 0.279
	4	*0.20		0.70	± 0.10	*0.21		0.59	± 0.10	0.51	± 0.10	*0.62	
Y	1	*0.16		0.16	± 0.075	*0.15		*0.17		*0.15		*0.46	
	2	*0.15		*0.14		*0.17		*0.15		*0.15		0.70	± 0.222
	3	*0.19		*0.20		*0.18		*0.21		*0.18		*0.52	
	4	*0.23		*0.19		*0.21		*0.19		*0.19		*0.72	
Zr	1	*0.20		0.32	± 0.095	0.20	± 0.093	*0.19		0.27	± 0.090	1.95	± 0.28
	2	*0.187		0.298	± 0.09	0.31	± 0.09	0.25	± 0.10	0.34	± 0.09	1.5	± 0.27
	3	*0.25		0.41	± 0.12	0.39	± 0.12	0.42	± 0.12	0.28	± 0.11	1.6	± 0.33
	4	*0.25		0.37	± 0.12	*0.23		*0.22		*0.22		0.95	± 0.41
Nb	1	*0.21		*0.19		*0.19		*0.20		*0.18		*0.57	
	2	0.19		*0.20		*0.20		*0.21		*0.19		*0.56	
	3	*0.26		*0.25		*0.25		*0.25		*0.24		*0.68	
	4	*0.28		*0.26		*0.25		0.24	± 0.11	*0.23		*0.90	
Mo	1	0.23		0.29	± 0.14	*0.24		0.44	± 0.11	*0.21		*0.62	
	2	*0.21		0.30	± 0.11	*0.22		0.50	± 0.1'	0.27	± 0.11	1.9	± 0.32
	3	*0.29		0.38	± 0.14	0.29	± 0.14	0.38	± 0.14	0.38	± 0.13	2.3	± 0.38
	4	*0.29		*0.27		*0.27		0.60	± 0.13	*0.26		1.04	

TABLE 22. (1 of 5) Airborne Trace Element Concentrations and Reproducibility as a Function of Cascade Impactor Collection Site. Samples were collected at site R-4 for all wind speeds and a 60° wind-direction sector from the pile during May 15 to July 9, 1979.

Cascade Impactor 50% Stage Efficiency, Diameter		Airborne Concentration, ng/m^3 (* Less than value)											
		>7.2 μm		3.0 μm		1.5 μm		0.95 μm		0.49 μm		Backup Filter	
Element	Sample	ng/m^3	1σ	ng/m^3	1σ	ng/m^3	1σ	ng/m^3	1σ	ng/m^3	1σ	ng/m^3	1σ
Al	1	270	± 80	120		*110		*102		*90		1080	± 200
	2	*260		260		250		290		280	140	1500	± 500
	3	100		120		*97		*110		*89		*400	
	4	*110		100		*100		*100		*100		710	± 200
Si	1	330	± 40	340	± 40	270	± 30	260	± 30	190	± 30	950	± 100
	2	470	± 70	530	± 80	390	± 70	500	± 80	450	± 70	2000	± 300
	3	260	± 30	350	± 40	220	± 30	310	± 30	120	± 30	1530	± 120
	4	320	± 30	330	± 40	260	± 30	230	± 30	138		940	± 100
S	1	30	± 12	41	± 11	37	± 11	43	± 11	110	± 10	380	± 50
	2	50		76	± 26	53	± 24	73	± 28	230	± 30	860	± 120
	3	24	± 10	44	± 11	34	± 10	49	± 11	75	± 11	*91	
	4	31	± 10	35	± 10	34	± 10	42	± 11	109	± 12	401	± 52
Cl	1	18.6	± 5.1	23.8	± 4.7	14.7	± 4.8	12.5	± 4.9	*9.7		*42	
	2	21.7	±10.6	26.1	±11.1	27.1	±10.4	23		23		95	
	3	15.4	± 4.3	10.9	± 4.8	14.3	± 4.2	10.23	± 4.7	*9.0		*37	
	4	11.4	± 4.4	13.6	± 4.5	11.9	± 4.5	*9.0		9.0		*41	
K	1	18.0	± 4.8	22.3	± 4.5	25.3	± 4.5	20.9	± 4.4	16.8	± 4.1	65.2	± 13.0
	2	35.1	± 9.7	42.8	±10.7	34.8	±10.2	45.3	±10.6	43.7	± 9.8	207	± 31
	3	22.5	± 4.5	29.0	± 4.6	21.1	± 1.2	27.3	± 4.5	19.1	± 4.2	94.4	± 11.6
	4	20.2	± 4.1	25.8	± 4.2	21.1	± 4.3	23.6	± 4.2	18.1	± 4.0	76.6	± 12.8
Ca	1	74.1	± 2.5	110	± 3	93.9	± 2.8	73.0	± 2.4	47.6	± 2.0	202	± 6.2
	2	145	± 5.6	185	± 6.4	140	± 5.9	154	± 5.7	123	± 5.0	611	± 17
	3	91.5	± 2.8	125	± 3.0	89.8	± 2.6	100	± 2.8	56.8	± 2.1	266	± 6.6
	4	83.9	± 2.6	100	± 2.9	76.6	± 2.4	79.1	± 2.5	42.3	± 1.9	252	± 6.8

TABLE 22. R-4 (2 of 5)

Cascade Impactor 50% Stage Efficiency, Diameter Element	Sample	Airborne Concentration, ng/m^3 (* Less than value)											
		>7.2 μm		3.0 μm		1.5 μm		0.95 μm		0.49 μm		Backup Filter	
		ng/m^3	1σ	ng/m^3	1σ	ng/m^3	1σ	ng/m^3	1σ	ng/m^3	1σ	ng/m^3	1σ
Ti	1	4.19	± 0.71	5.35	± 0.68	4.41	± 0.69	3.60	± 0.69	4.00	± 0.62	11.6	± 1.7
	2	9.97	± 1.4	11.3	± 1.5	8.06	± 1.51	7.33	± 1.53	6.99	± 1.38	26.5	± 4.0
	3	5.29	± 0.64	5.36	± 0.70	4.22	± 0.67	5.46	± 0.66	3.45	± 0.58	16.2	± 1.8
	4	4.00	± 0.62	4.63	± 0.65	3.43	± 0.64	4.84	± 0.64	3.47	± 0.59	14.9	± 0.87
V	1	*0.33		*0.37		0.38	± 0.19	*0.36		*0.29		*0.93	
	2	*0.84		*0.86		*0.83		*0.87		0.87	± 0.41	2.6	± 1.2
	3	*0.38		0.60	± 1.9	*0.34		*0.38		*0.33		2.60	± 1.17
	4	*0.36		*0.35		*0.33		*0.34		0.29		*0.93	
Cr	1	0.22	± 0.12	*0.22		0.30	± 0.13	*0.23		0.26	± 0.10	*0.62	
	2	0.59	± 0.28	1.48	± 0.72	*0.52		*0.57		*0.54		*1.5	
	3	1.56	± 0.37	2.07	± 0.40	2.31	± 0.41	2.98	± 0.43	2.51	± 0.35	6.61	± 1.02
	4	0.42	± 0.11	0.32	± 0.11	*0.22		*0.24		0.44	± 0.28	1.01	± 0.32
Th	1	*0.67		*0.61		*0.62		*0.63		*0.65		*2.5	
	2	*1.4		*1.4		*1.5		*1.4		*1.5		*5.5	
	3	*0.62		*0.66		*0.64		*0.60		*0.68		*2.2	
	4	*0.57		*0.53		*0.62		*0.60		*0.63		*2.4	
Mn	1	1.17	± 0.28	1.28	± 0.29	1.14	± 0.30	1.06	± 0.284	0.839	± 0.256	3.38	± 0.71
	2	0.834	± 0.259	2.20	± 0.27	1.45	± 0.26	2.65	± 0.62	1.48	± 0.64	6.81	± 1.84
	3	1.00	± 0.29	1.33	± 0.31	1.26	± 0.30	1.38	± 0.31	0.902	± 0.118	3.84	± 0.81
	4	0.82	± 0.11	1.17	± 0.29	0.88	± 0.29	0.82	± 0.29	0.76	± 0.23	2.54	± 0.71
Fe	1	30.0	± 0.73	45.8	± 0.86	49.3	± 0.91	43.1	± 0.85	31.2	± 0.72	105	± 2.0
	2	56.7	± 1.6	84.6	± 1.9	70.2	± 1.8	80.0	± 1.8	72.7	± 1.7	286	± 5.3
	3	42.6	± 0.84	61.2	± 1.0	53.2	± 0.92	63.9	± 1.0	44.8	± 0.81	206	± 2.7
	4	34.0	± 0.77	45.0	± 0.86	39.9	± 0.81	46.0	± 0.85	30.6	± 0.69	132	± 2.2

TABLE 22. R-4 (3 of 5)

Cascade Impactor 50% Stage Efficiency, Diameter Element	Sample	Airborne Concentration, ng/m^3 (* Less than value)											
		>7.2 µm		3.0 µm		1.5 µm		0.95 µm		0.49 µm		Backup Filter	
		ng/m^3	1σ	ng/m^3	1σ	ng/m^3	1σ	ng/m^3	1σ	ng/m^3	1σ	ng/m^3	1σ
Co	1	*0.29		*0.34		*0.35		*0.32		*0.27		*0.82	
	2	*0.63		*0.73		*0.67		*0.74		*0.67		*2.2	
	3	0.74	± 0.33	*0.39		*0.36		*0.39		*0.31		*1.0	
	4	0.64		*0.68		*0.62		*0.65		*0.58		*1.7	
Ni	1	*0.082		*0.10		0.183	± 0.044	*0.078		0.124	0.042	*0.22	
	2	0.26	± 0.11	*0.23		*0.20		0.26	± 0.11	0.31	± 0.097	*0.65	
	3	0.47	± 0.18	1.00	± 0.18	1.24	± 0.18	1.77	± 0.19	1.40	± 0.17	3.25	± 0.48
	4	0.16	± 0.046	0.093	± 0.039	0.099	± 0.038	0.19	± 0.050	0.19	± 0.049	0.88	± 0.39
Cu	1	0.863	± 0.183	1.99	± 0.20	2.49	± 0.22	4.22	± 0.24	5.07	± 0.24	8.72	± 0.57
	2	2.77	± 0.44	4.48	± 0.48	6.03	± 0.53	10.1	± 0.56	13.1	± 0.63	28.5	± 1.5
	3	1.21	± 0.19	3.39	± 0.22	3.91	± 0.23	6.30	± 0.27	7.05	± 0.27	11.2	± 0.61
	4	1.19	± 0.071	1.87	± 0.19	2.64	± 0.20	4.30	± 0.24	4.70	± 0.12	9.19	± 0.56
Zn	1	0.384	± 0.051	0.460	± 0.156	0.557	± 0.154	0.840	± 0.157	1.19	± 0.17	3.38	± 0.46
	2	1.04	± 0.37	1.41	± 0.34	1.28	± 0.34	1.69	± 0.37	2.76	± 0.37	10.5	± 1.0
	3	0.63	± 0.14	0.80	± 0.15	0.64	± 0.16	1.14	± 0.17	1.53	± 0.16	4.09	± 0.42
	4	0.63	± 0.053	0.58	± 0.14	0.69	± 0.15	0.099	± 0.15	1.53	± 0.16	3.87	± 0.45
Ga	1	*0.098		*0.098		*0.10		*0.10		*0.10		*0.35	
	2	*0.24		*0.24		*0.24		*0.26		*0.25		*0.88	
	3	*0.096		*0.10		*0.099		*0.11		*0.10		*0.33	
	4	*0.093		*0.092		*0.098		*0.10		*0.10		*0.35	
Hg	1	*0.36		*0.32		*0.34		*0.32		*0 31		*0.88	
	2	*0.83		*0.82		*0.80		*0.84		*0.77		*2.3	
	3	*0.33		*0.32		*0.31		*0.31		*0.30		*0.88	
	4	*0.31		*0.32		*0.33		*0.32		*0.30		*0.90	

TABLE 22. R-4 (4 of 5)

Cascade Impactor 50% Stage Efficiency, Diameter Element	Sample	Airborne Concentration, ng/m^3 (* Less than value)											
		>7.2 μm		3.0 μm		1.5 μm		0.95 μm		0.49 μm		Backup Filter	
		ng/m^3	1σ	ng/m^3	1σ	ng/m^3	1σ	ng/m^3	1σ	ng/m^3	1σ	ng/m^3	1σ
Se	1	0.169	± 0.051	0.153	± 0.047	0.362	± 0.111	0.308	± 0.122	0.468	± 0.048	1.55	± 0.36
	2	*0.23		0.522	± 0.280	0.465	± 0.262	0.764	± 0.123	0.790	± 0.258	4.03	± 0.85
	3	0.167	± 0.048	0.286	± 0.048	0.298	± 0.108	0.398	± 0.049	0.523	± 0.114	0.887	± 0.32
	4	0.162	± 0.047	0.206	± 0.046	0.284	± 0.046	0.403	± 0.047	0.690	± 0.111	1.68	± 0.35
Pb	1	1.56	± 0.20	3.01	± 0.41	3.45	± 0.42	4.41	± 0.42	5.97	± 0.40	70.6	± 1.7
	2	2.35	± 0.86	4.30	± 0.94	5.16	± 0.90	9.13	± 0.96	10.3	± 0.92	128	± 3.8
	3	1.81	± 0.37	2.99	± 0.39	3.27	± 0.29	4.61	± 0.14	5.93	± 0.42	58.1	± 1.6
	4	1.44	± 0.36	2.40	± 0.36	3.33	± 0.38	4.70	± 0.39	6.50	± 0.42	73.3	± 0.89
As	1	0.175	± 0.073	0.300	± 0.079	0.452	± 0.084	0.749	± 0.089	1.13	± 0.095	9.66	± 0.44
	2	0.349	± 0.166	1.01	± 0.17	0.593	± 0.174	0.948	± 0.203	1.98	± 0.21	17.4	± 0.96
	3	0.168	± 0.070	0.552	± 0.077	0.385	± 0.076	0.627	± 0.089	1.08	± 0.091	7.20	± 0.39
	4	0.226	± 0.069	0.354	± 0.074	0.403	± 0.077	0.763	± 0.086	0.952	± 0.093	9.43	± 0.44
Br	1	0.71	± 0.14	1.29	± 0.14	1.23	± 0.13	1.43	± 0.14	2.29	± 0.14	29.5	± 0.63
	2	1.31	± 0.29	2.11	± 0.30	1.87	± 0.29	2.79	± 0.33	3.98	± 0.31	57.6	± 1.4
	3	1.06	± 0.13	1.33	± 0.13	1.20	± 0.13	1.74	± 0.14	2.36	± 0.14	4.30	± 0.38
	4	0.79	± 0.054	1.00	± 0.12	1.18	± 0.13	1.67	± 0.13	2.35	± 0.066	30.7	± 0.60
Rb	1	0.31	± 0.15	*0.28		*0.23		*0.29		0.36	± 0.14	*0.88	
	2	*0.64		*0.67		*0.61		*0.67		*0.61		*2.0	
	3	*0.26		*0.28		*0.27		*0.27		*0.25		*0.73	
	4	*0.27		*0.25		*0.26		*0.27		*0.26		*0.87	
U	1	*0.76		*0.45		*0.70		0.719	± 0.243	*0.66		*2.15	
	2	*1.6		*1.7		*1.6		*1.2		*1.1		5.04	± 2.53
	3	*0.68		*0.69		*0.46		0.690	± 0.338	*0.65		1.35	± 0.63
	4	*0.66		*0.63		*0.66		*0.16		0.567	± 0.220	*2.1	

TABLE 22. R-4 (5 of 5)

Cascade Impactor 50% Stage Efficiency, Diameter Element	Sample	Airborne Concentration, ng/m³ (* Less than value)											
		>7.2 μm		3.0 μm		1.5 μm		0.95 μm		0.49 μm		Backup Filter	
		ng/m³	1σ	ng/m³	1σ	ng/m³	1σ	ng/m³	1σ	ng/m³	1σ	ng/m³	1σ
Sr	1	*0.58		1.04	± 0.31	0.98	± 0.28	1.19	± 0.30	*0.54		3.40	± 0.82
	2	*0.28		1.01	± 0.12	0.71	± 0.13	0.86	± 0.12	0.53	± 0.11	1.77	± 0.32
	3	0.31	± 0.12	0.90	± 0.12	0.77	± 0.12	0.76	± 0.12	*0.65		1.34	± 0.32
	4	0.41	± 0.12	1.03	± 0.11	0.72	± 0.12	0.78	± 0.11	0.50	± 0.11	1.89	± 0.31
Y	1	*0.28		*0.24		*0.27		*0.24		*0.24		*0.80	
	2	*0.59		*0.60		*0.59		*0.51		*0.54		*1.7	
	3	*0.23		*0.24		*0.22		*0.24		*0.22		*0.67	
	4	*0.23		*0.23		*0.22		*0.23		*0.22		*0.74	
Zr	1	*0.33		*0.29		*0.30		*0.29		*0.27		*0.78	
	2	*0.71		*0.74		*0.66		*0.72		0.75	± 0.30	*2.0	
	3	*0.26		*0.27		0.43	± 0.13	0.31	± 0.14	*0.24		*0.72	
	4	*0.29		*0.28		0.41	± 0.13	*0.27		*0.24		*0.76	
Mo	1	*0.38		*0.33		0.40	± 0.16	*0.34		*0.31		*0.90	
	2	*0.74		*0.76		*0.73		*0.76		*0.69		*2.1	
	3	*0.28		*0.30		*0.30		*0.29		*0.25		*0.80	
	4	*0.30		*0.29		*0.27		*0.28		*0.28		*0.81	
Nb	1	*0.35		*0.30		*0.30		*0.30		*0.29		*0.82	
	2	*0.79		0.89	± 0.41	*0.80		*0.82		*0.74		*2.2	
	3	*0.35		*0.33		0.44	± 0.15	*0.32		*0.31		1.25	± 0.43
	4	*0.32		*0.31		*0.33		*0.31		*0.29		*0.87	

However, data nonreproducibility between systems could also be real. The variations could reflect nonuniform airborne particulate concentrations between sampling systems.

Airborne Radionuclide Source-Strength Calculations

There are at least two different conceptual approaches in estimating the airborne source strengths of radionuclides released from a uranium mill tailings pile. The first is a "mass loading" approach; the second is an "airborne radionuclide" approach.

In applying these two source-strength calculational approaches, accuracies required for prediction may be the controlling parameter for selecting the approach used. If rather large uncertainties are permissible, the mass loading approach may be adequate. However, if greater predictive accuracy is desired for estimating radionuclide source strengths, direct measurements of airborne radionuclides are required. In either approach, considerations must include airborne source strengths as a function of respirable, inhalable, and nonrespirable particle diameter.

A "mass loading" approach is based on the assumption that airborne radionuclide release is simply related to airborne solids release from the tailings pile. In this approach, the radionuclide source strength is calculated from the solids release rate multiplied by an average radionuclide activity density, dpm/g, on airborne solids. In this case, activity densities are assumed equal to activity densities determined from pile surface samples. The "airborne radionuclide" approach considers more fully variabilities in source release strengths as a function of crosswind variations, particle size, activity densities and apparent nonequilibrium of eroded radioactive decay products. Equations describing each calculational approach are developed in the following section.

Mass Loading Approach

The three-step calculational procedure in the mass loading approach is to measure or to first assume 1) airborne mass loadings, g/m^3, and mass fluxes, $g/(m^2\ day)$, and then subsequently to assume 2) that the radionuclide activity

density, dpm/g, on those airborne solids is equal to the activity density determined from pile surface samples. If airborne mass loadings, g/m^3, are used in this approach, mass fluxes, $g/(m^2\ day)$, are subsequently calculated by multiplying the airborne mass loading by wind speed. Finally, in either calculational approach, the total source strength estimation requires 3) the total cross-sectional area ($A = \iint dydz$) at the distance through which the radionuclide fluxes pass.

The mass loading approach will be described analytically. Since mass fluxes are a function of position coordinates y and z, the total mass loading source strength of airborne solids, Q, estimated at distance x is Q_x:

$$Q_x = \iint M(y,z)\ dydz \tag{1}$$

where M(y,z) is the airborne mass flux $g/(m^2\ day)$. The airborne mass fluxes are directly measured, or calculated from the expression

$$M(y,z) = \iint \overline{X}(y,z)\ \overline{u}\ (y,z)\ dydz$$

where $\overline{X}(y,z)$ is the average airborne mass loading, g/m^3, and $\overline{u}\ (y,z)$ is the average air velocity at position coordinates x,y. In this report, the overbars on $\overline{X}$ and $\overline{u}$ refer in principle to average values for each of the three wind-speed increments used for sampling airborne particulates. After the total source of solids is estimated, the average pile-surface radionuclide activity density, dpm/g, must subsequently be assumed. Finally, the total radionuclide source strength, Q'_x, is calculated from the expression

$$Q'_x = Q_x \overline{R} \tag{2}$$

where $\overline{R}$ is this average pile-surface radionuclide activity density.

Airborne Radionuclide Approach

The second calculational approach will be called the airborne radionuclide approach, as opposed to the mass loading approach. The airborne radionuclide

approach is based on measurements of airborne radionuclides, rather than only airborne solids, and thus more accurately describes the actual airborne effects of wind erosion. In addition, radionuclide activity densities for airborne, not surface, solids are used. In this case the total radionuclide source strength, Q'_x is estimated from either

$$Q'_x = \iint M'(y,z)\ dydz \tag{3}$$

where $M'(y,z)$ is the airborne radionuclide flux, $\mu Ci/(m^2\ day)$, or from

$$Q'_x = \iint \bar{\chi}'(y,z)\ \bar{u}(y,z)\ dydz \tag{4}$$

where $\bar{\chi}'(y,z)$ is the average airborne radionuclide concentration, $\mu Ci/cm^3$.

Calculational Approach Validity

In order to compare the validity of the "mass loading" and "airborne radionuclide" approaches for estimating airborne radionuclide source strengths, activity density data were needed for airborne solids. One uncertainty in using the "mass loading" approach was that either an apparent equilibrium between radionuclide decay products must be assumed or actual values used. Data were presented to show the variability of activity densities on airborne solids. Results show that the mass loading approach probably entails more uncertainties than the "airborne radionuclide" approach and that activity densities and activity density ratios support the "airborne radionuclide" rather than the "mass loading" calculational approach.

SUMMARY: TASK C

The data in this task have been presented as a series of graphs and an accompanying discussion. The consolidation of the data into a descriptive statement of the relationship of mass fluxes, airborne particle sizes, activity densities of the various radionuclides and association with particle sizes, and the primary variables of wind speed and direction, remains yet to

be achieved. The extreme complexity of the interfaces among these dependent and independent variables, coupled with truncation of the study, have not permitted the sought-for relationships to be developed in a data analysis. At present, the more important conclusions drawn from data are the following:

- A rational relationship between wind speed and flux was not disclosed. The tailings pile is nonhomogeneous in surface texture, moisture content, and particle size distribution (see Task A), which, along with spatial variations in meteorology, results in variable resuspendability from one location to another. Thus, in some time periods, fairly systematic changes, an order of magnitude, in airborne flux and activity of particles occur from one side of the tailings pile to the other (crosswind).
- For the range of wind speeds prevailing over a period of about 1 yr, airborne particles identified as originating from the tailings pile were detected at the most distant sampling stations of 4 km. Particle concentrations at 4 km were often essentially the same or greater than concentrations measured at the upwind station.
- Airborne particle concentration increased about 1 to 2 orders of magnitude from the upwind to the downwind side of the tailings pile during winds ranging up to about 11 m/sec, the range studied.
- Airborne concentrations of particles at downwind sampling points, a distance of a few hundred meters, varied with sampling elevation. In most cases, the airborne particle plume was not bounded by the maximum height of 15 m.
- Radionuclide activity densities varied greatly with particle size and corresponded roughly to observations of tailings surface materials--activity densities increasing with the smaller particle size fractions.
- Radioactive equilibrium was shown in most samples for ^{226}Ra, ^{210}Pb, and ^{230}Th. In comparison, ^{238}U showed depletion because of removal during milling.
- Suspension occurs from both primary and secondary sources. Tailings particles deposited in the environment over many years of operation are

secondary resuspension sources which contribute to particles moving directly from the primary tailings pile source. Contributions from this secondary source need investigation.

- Size distributions of airborne particles are variable depending on wind speed and distance from the tailings pile. Assessment of the radiological significance of airborne particles must be based on samples collected to provide the respirable fraction and associated radionuclides.
- When related to guidance levels for airborne concentrations, ^{230}Th appears to be the radionuclide of most radiological interest. Thorium-230 concentrations often exceeded guidance level concentrations.
- Several stable elements in airborne particles identified these particles as originating from the tailings pile. Notable stable elements were selenium and lead.
- Additional analysis is needed, and was originally planned, with the reported observations to relate observations with atmospheric processes. Estimates of integrated particle and radionuclide fluxes as a function of particle size should be possible, notwithstanding the large uncertainties in the data. The reported flux data could be more quantitatively used to investigate whether suspension and transport models are of value in such complex situations.

TASK D. PREDICTION OF ATMOSPHERIC TRANSPORT AND DEPOSITION

Principal Investigator: T. W. Horst

INTRODUCTION

An atmospheric transport, diffusion, and deposition model has been applied to the tailings material suspended by the wind at the carbonate leach mill under study. The model predicts the annual-average airborne concentration and deposition of tailings material, based on the measured particle size distribution of suspended material and on the diffusion climatology at the mill site. Since the field measurements have proven inadequate to specify the suspension of tailings material on a year-round basis, the model predictions assume a suspension flux proportional to u_*^3 with the friction velocity u_* determined from wind-speed measurements at the mill. The resulting predictions are normalized to an annual-average source strength of unity.

ATMOSPHERIC DISPERSION MODEL

The annual-average results to be presented here were computed from a revised version of the diffusion-deposition model used for the sensitivity studies discussed in Schwendiman et al. (1979). The major revision is to use Briggs' (1973) version of the Pasquill-Gifford diffusion curves to estimate the vertical dispersion coefficient σ_z, rather than computing σ_z from Lagrangian similarity theory. The similarity theory predictions are limited to short transport distances and the empirical Pasquill-Gifford curves are more realistic at distances of 5 miles from the tailings pile.

It was decided to continue using a point-source model, even though at distances less than 3 km from the tailings pile the spatial distribution of the source requires an area-source model for best accuracy. The added complexity of an area-source model is not justified at this time because, in addition to uncertainty in the total suspension flux as a function of time, the field measurements are inadequate to specify the spatial distribution of the suspension flux. Thus, the predicted spatial distribution of airborne contamination close to the tailings pile must be considered approximate.

The model predicts the annual-average, ground-level airborne contamination as the sum of contributions for each combination of wind speed u, wind direction θ, atmospheric stability s, and particle diameter D,

$$C(u,\theta,s,D) = p\,Q\,\frac{\overline{D}^{y}p}{x\Delta\theta} \tag{5}$$

Here p is the climatological probability for each possible combination of u, θ, and s, x is the distance from the tailings pile and $\Delta\theta$ is the resolution of the wind direction data (commonly $\pi/8$ for climatological purposes). $\overline{D}^{y}$ describes the vertical diffusion and is here specified by the Gaussian model,

$$\overline{D}^{y} = \frac{2}{\sqrt{2\pi}u\sigma_z}\exp\left(-h^2/2\sigma_z^2\right). \tag{6}$$

Briggs' equations for σ_z as a function of x and s are shown in Table 23. The source height h is assumed here to be equal to the nominal height of the tailings pile, 30 m, and for particles with a finite settling speed v_s, h is replaced by

$$h' = h - v_s\,x/u. \tag{7}$$

The source strength Q is a function of the friction velocity u_* and particle size and, to account for dry deposition of the particles, is a decreasing function of distance from the tailings pile.

$$Q = (u_*^3/\overline{u_*^3})\,f(D)\exp\left\{-\int_0^x v_d(z_*)\,\overline{D}^{y}(x')\,P(x',z_*)\,dx'\right\}. \tag{8}$$

Here u_* is calculated from the wind speed u measured at 10 m, using the relations of Businger et al. (1971) and $\overline{u_*^3}$ is the annual average value of u_*^3; f(D) is the fraction of the mass suspended by the wind associated with

TABLE 23. Formulas for the Determination of σ_z (x and σ_z in meters)

Stability Class	σ_z
A	$0.2x$
B	$0.12x$
C	$0.08x(1 + 2 \cdot 10^{-4}x)^{-1/2}$
D	$0.06x(1 + 1.5 \cdot 10^{-3}x)^{-1/2}$
E	$0.03x(1 + 3 \cdot 10^{-4}x)^{-1}$
F	$0.016x(1 + 3 \cdot 10^{-4}x)^{-1}$
G	$0.01x(1 + 3 \cdot 10^{-4}x)^{-1}$

each particle diameter D; and the exponential factor is the reduction of the source strength to account for deposition as derived in Schwendiman et al. (1979). The latter is a function of the deposition velocity v_d estimated from Sehmel and Hodgson (1976) for each particle size and for a reference height $z_\star$ = 3 cm.

The profile function $P(x,z_\star)$ accounts for the vertical gradient of airborne contamination near the ground caused by deposition. As derived in Schwendiman et al. (1979),

$$P(x,z_\star)=\left[1 + \frac{v_d(z_\star)}{\Delta z} \int_0^{\Delta z} R(z,z_\star)dz\right]^{-1} \tag{9}$$

where $\Delta z = \sqrt{\pi/2}\sigma_z$ and $R(z,z_\star)$ is the atmospheric resistance to vertical transport between z and $z_\star$. For the Gaussian plume model (Horst 1980)

$$R(z,z_\star) = \frac{1}{u}\sqrt{\frac{2}{\pi}} \int_{x(z_\star)}^{x(z)} \frac{dx'}{\sigma_{z(x')}} \tag{10}$$

Model Input Data

The predictions of the model described above are strongly dependent on two major data inputs. These are the particle size distribution f(D) and the diffusion climatology p(u,θ,s). The particle size distribution, shown in Table 24, has been constructed from sieving data on sand collected in air samplers along the north dike of the plant A tailings pile. The diffusion climatology, Table 25, is estimated from a combination of onsite measurements of wind speed, wind direction, and precipitation and from observations of cloud cover and ceiling height from Gallup, New Mexico, 80 km WNW of the mill.

Atmospheric diffusion estimates require data on wind speed, wind direction and atmospheric stability. The distribution of wind speed and direction is based on data collected near the mill from May 1977 to September 1978. It was shown in Schwendiman et al. (1979) that due to topographical influences on the wind, onsite measurements are essential. Unfortunately, a 17-mo period of record is too short to assure that the resulting climatology is representative of a longer period, such as the lifetime of the tailings pile.

TABLE 24. Suspended Particle Size Distribution

Particle Diameter (μm)	% by Mass
10	0.03
16	0.27
25	1.53
40	5.81
63	14.72
100	23.66
158	25.21
251	17.65
398	8.18
631	2.40
1000	0.47
1580	0.07

TABLE 25. Joint Frequency Distribution of Wind-Speed Direction and Atmospheric Stability

Wind Speed (kts)	Atmospheric Stability	Direction From Which Wind Blows															
		NNE	NE	ENE	E	ESE	SE	SSE	S	SSW	SW	WSW	W	WNW	NW	NNW	N
1-3	A	0.093	--	--	--	--	--	--	--	--	--	--	--	--	--	--	--
	B	1.087	0.328	0.423	0.216	0.086	0.078	0.095	0.173	0.112	0.017	0.060	0.190	0.233	0.112	0.414	0.690
	C	0.650	0.400	0.417	0.192	0.158	0.033	0.083	0.033	0.075	0.025	0.092	0.117	0.175	0.033	0.183	0.450
	D	0.117	0.109	0.187	0.023	0.086	0.047	0.109	0.241	0.132	0.016	0.062	0.078	0.093	0.078	0.202	0.187
	F	0.532	0.133	0.332	0.258	0.199	0.100	0.125	0.116	0.100	0.083	0.158	0.274	0.224	0.116	0.141	0.391
	G	2.087	0.738	1.106	0.816	0.416	0.086	0.235	0.267	0.212	0.078	0.204	0.494	0.573	0.141	0.306	0.738
4-6	A	0.019	--	0.019	0.037	0.019	--	0.019	--	0.019	--	0.019	0.056	0.019	--	--	0.037
	B	0.257	0.078	0.022	0.056	0.022	0.101	0.078	0.224	0.022	0.011	0.112	0.134	0.101	0.011	0.123	0.448
	C	0.203	0.051	0.093	0.025	0.042	--	0.034	0.093	0.008	0.008	0.093	0.085	0.102	0.025	0.152	0.237
	D	0.457	0.195	0.220	0.335	0.144	0.102	0.305	0.237	0.102	0.017	0.228	0.322	0.271	0.051	0.161	0.322
	E	0.982	0.351	0.459	0.387	0.252	0.036	0.198	0.153	0.135	0.045	0.036	0.315	0.306	0.144	0.117	0.297
	F	2.615	1.321	1.676	0.754	0.381	0.044	0.115	0.310	0.168	0.089	0.293	0.408	0.337	0.098	0.275	0.496
7-9	B	0.063	0.038	0.013	--	0.050	0.025	0.138	0.100	0.013	--	0.063	0.226	0.100	--	0.088	0.176
	C	0.166	0.017	0.035	0.009	0.070	0.105	0.210	0.087	0.044	--	0.096	0.140	0.166	0.017	0.279	0.306
	D	0.656	0.213	0.435	0.237	0.229	0.206	0.514	0.545	0.340	0.126	0.379	0.490	0.372	0.150	0.435	0.324
	E	0.791	0.366	0.754	0.343	0.104	0.142	0.291	0.291	0.254	0.052	0.157	0.209	0.463	0.157	0.425	0.343
10-15	C	0.087	--	--	0.035	0.070	0.122	0.402	0.175	0.096	0.026	0.105	0.324	0.122	0.052	0.245	0.297
	D	1.216	0.074	0.121	0.181	0.450	0.833	2.431	1.088	0.685	0.423	1.464	1.357	1.249	0.551	1.840	1.605
	E	0.327	0.055	0.102	0.014	0.048	0.041	0.170	0.123	0.061	0.020	0.143	0.102	0.184	0.095	0.259	0.279
16-22	C	--	--	--	0.027	0.068	0.122	0.210	0.095	0.122	0.074	0.243	0.061	0.081	0.020	0.108	0.047
	D	0.380	0.045	0.045	0.122	0.606	0.780	2.159	0.447	0.631	0.651	2.049	1.495	1.250	0.548	1.334	0.541
23-30	C	--	--	--	--	0.032	0.019	0.019	0.025	0.076	0.044	0.234	0.082	0.006	--	0.013	--
	D	0.044	0.013	0.019	0.069	0.328	0.441	0.681	0.290	0.340	0.435	1.393	0.618	0.952	0.542	0.353	0.057
GE.31	C	--	--	--	--	--	0.013	--	0.051	0.038	0.013	0.089	0.013	0.038	--	--	0.006
	D	--	--	--	--	0.062	0.080	0.204	0.142	0.204	0.340	0.334	0.136	0.384	0.025	0.012	0.006

Table specifies percent of time for occurrence of each condition; total equals 98.49%.
Calms and/or precipitation occur 1.51% of time.

The stability is estimated from the wind speed and the net radiation, which is a function of solar altitude and coverage of the sky by clouds (Turner 1964). Since the mill data do not include observations of cloud cover, data were used from Gallup, New Mexico. The correlation of cloud cover at Gallup with that at Milan was investigated by comparing simultaneous observations for June and December 1953. The net radiation at the two locations was found to have a correlation coefficient of 0.89 for June and 0.72 for December.

Model Predictions

Figure 107 shows the contribution to the annual-average ground level airborne contamination for several particle sizes. These values are averages over all wind directions and are shown as a function of r, the distance from the tailings pile. Recall also that these predictions are for an annual-average source of unity, e.g., 1 g/sec. The smaller particles are carried to the surface principally by turbulent diffusion, and thus their peak contributions are found at the same distance, about 400 m from the pile. The larger particles, however, are carried to the surface more quickly by gravitational settling, the peak contribution of the largest particles occurring closest to the pile.

Figure 108 shows the annual-average ground level airborne contamination for all particle sizes. The peak ground-level concentration occurs about 100 m from the pile, corresponding to the 100- to 250-μm-diameter particles which account for about two-thirds of the suspended mass flux from the pile. Also shown in Figure 108 is the fraction of the suspended mass which has been deposited within a given distance from the pile; 10% is deposited within the first 150 m, 50% within 600 m, and 90% within 10 km.

Figure 109 shows the annual-average deposition flux, again normalized to a unit annual-average source, as a function of both distance and direction from the tailings pile. This may be compared to Figures 12 and 14 which show isopleths of ^{226}Ra and ^{210}Pb soil concentration in the vicinity of the tailings pile. Except for a prominent peak in the ^{226}Ra to the north of the pile, the distributions are in good qualitative agreement. This substantiates the use of a suspension flux which increases with wind speed since, as shown

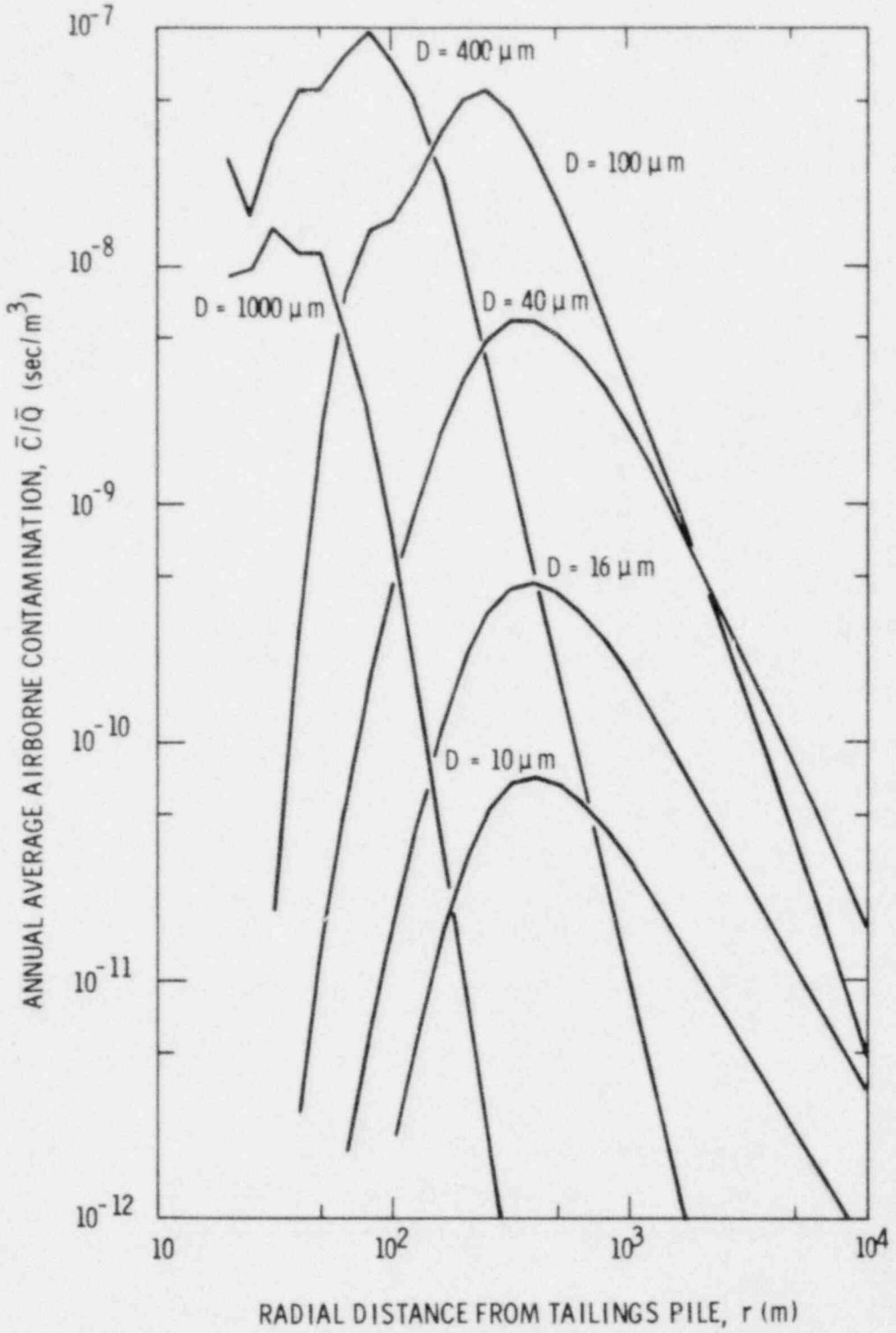

FIGURE 107. Airborne Contamination, Modeled as a Function of Particle Size and Distance from the Source

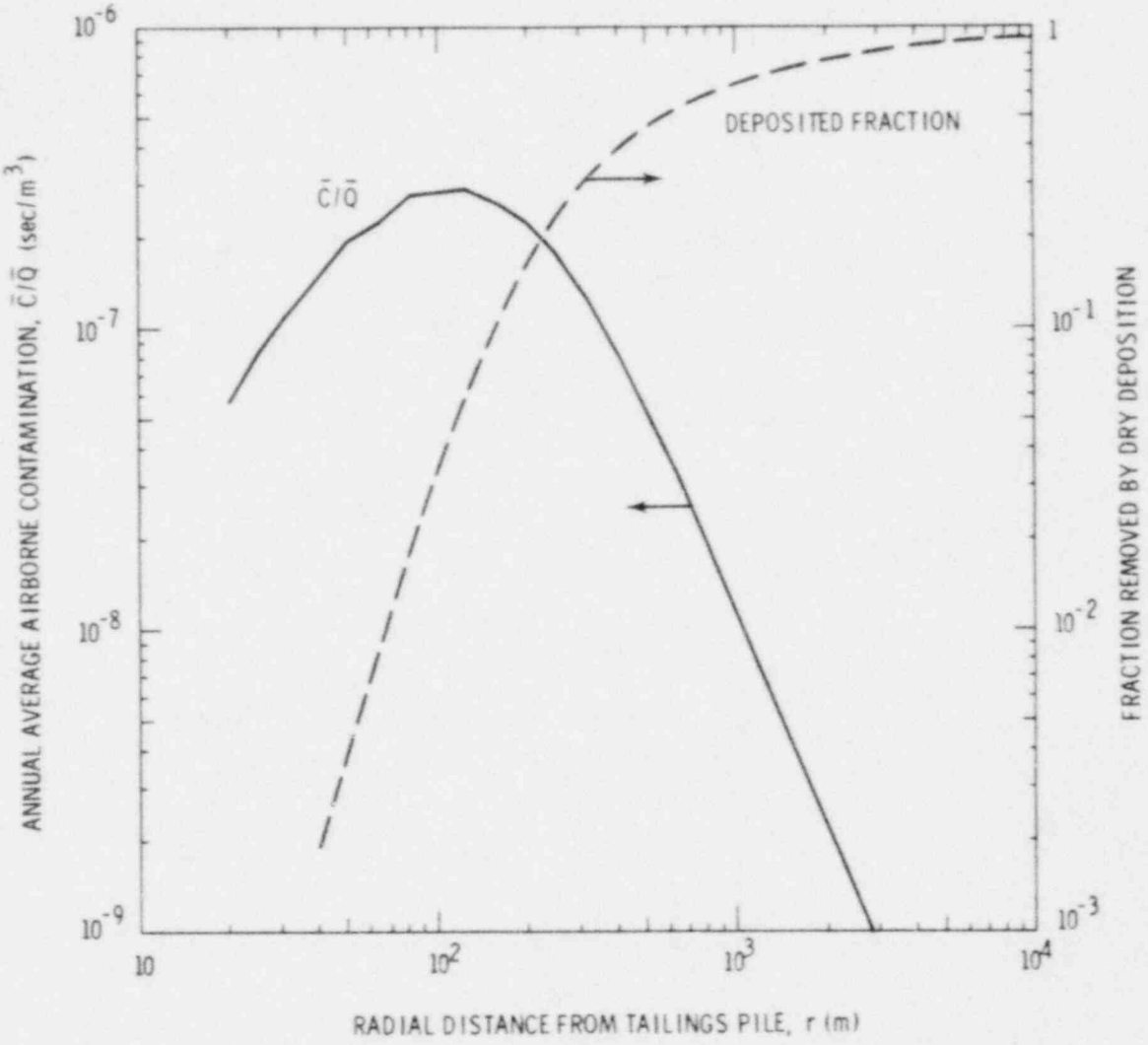

FIGURE 108. Modeled Airborne Contamination and Deposition for all Particle Sizes

in Figure 55 of Schwendiman et al. (1979), a suspension flux independent of wind speed produces a dramatically different azimuthal distribution.

CONCLUSIONS: TASK D

The development of a transport and deposition model has provided a framework for prediction of ground deposition and the airborne concentrations of particles from a source of airborne particles. The model, when applied to

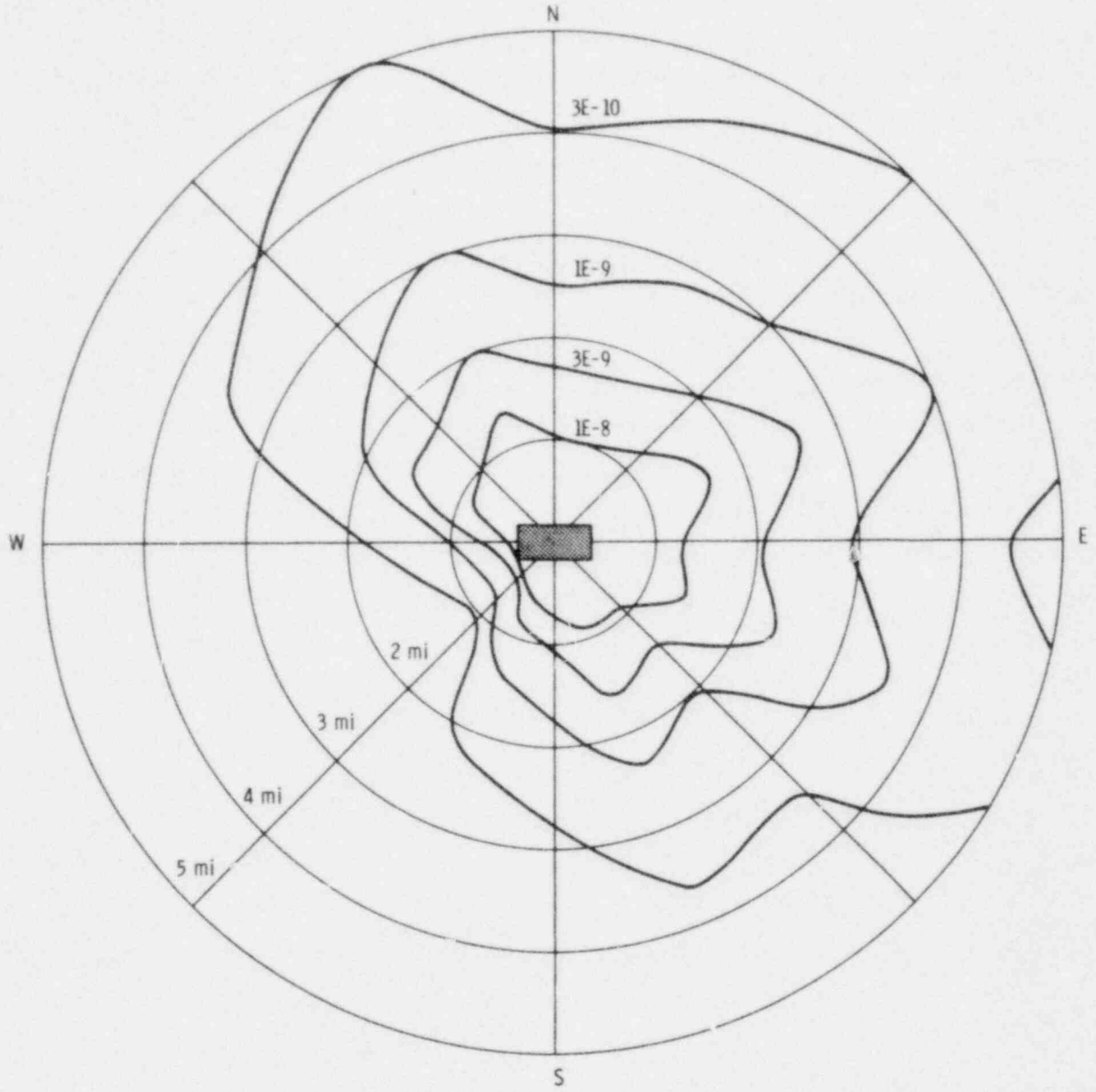

FIGURE 109. Annual Average Deposition, Modeled as a Function of Distance and Direction from the Source

particles whose size distribution was determined from sizing particles airborne at the downwind rim of the tailings pile, gave relative ground deposition patterns similar to those found in the field study. Clear-cut definition of airborne particle size and associated radionuclide composition leaving the pile as a function of wind speed is needed to constructively exercise the model under many conditions. Although many field studies have been made to obtain the necessary detailed source-term information, the application of the model using the field data for source term has not been possible at this writing. Furthermore, the field data on airborne particles has not disclosed the consistent relationships between the source term and variables which had been anticipated in the scope of the study. We recommend that the modeling effort be continued to a point that all observations from field sampling be reconciled with model assumptions, or to a point at which a decision would be made that the problem is one of such complexity that further work would not be justified.

REFERENCES

Briggs, G. A. 1973. Diffusion Estimation for Small Emissions. ATDL Contribution 79, Air Resources Atmospheric Turbulence and Diffusion Laboratory, Oak Ridge, Tennessee.

Businger, J. A., et al. 1971. "Flux-Profile Relationships in the Atmospheric Surface Layer." J. Atmos. Sci. 28:181-189.

Code of Federal Regulations. 1979. 10 CFR 20, Appendix B. Office of Federal Register, Washington, DC 20402.

Horst, T. W. 1980. "Application of the Modified Source Depletion Model." Pacific Northwest Laboratory Annual Report for 1979 to the DOE Assistant Secretary for Environment, Part 3, Atmospheric Sciences. PNL-3300, Part 3, Pacific Northwest Laboratory, Richland, Washington. **

Kelley, W. D. 1979. "Threshold Limit Values for Chemical Substances in Workroom Air." National Safety News, pp. 80-84.

Mercer, T. T. 1977. "Matching Sampler Penetration Curves to Definition of Respirable Fraction." Health Physics 33:3.

Schwendiman, L. C. et al. 1979. A Field and Modeling Study of Windblown Particles from a Uranium Mill Tailings Pile (Interim Report). NUREG/CR-0629, PNL-2890, Pacific Northwest Laboratory, Richland, Washington 99352. *

Sehmel, G. A. 1978. "Airborne Particulate Concentrations and Fluxes at an Active Uranium Mill Tailings Site." In Proceedings of the Seminar on Management, Stabilization and Environmental Impact of Uranium Mill Tailings, Albuquerque, New Mexico, pp. 65-84. (Organized by the OECD Nuclear Energy Agency at the Invitation of the Nuclear Regulatory Commission.)

Sehmel, G. A., and W. H. Hodgson. 1976. "Predicted Dry Deposition Velocities." In Proceedings of Atmosphere-Surface Exchange of Particulate and Gaseous Pollutants Symposium, Richland, Washington, pp. 399-419. NTIS-CONF-740921. **

Silker, W. B., and P. G. Heasler. 1979. Diffusion and Exhalation of Radon from Uranium Tailings. NUREG/CR-1138, PNL-3207, Pacific Northwest Laboratory, Richland, Washington 99352. *

Turner, D. B. 1964. "A Diffusion Model for an Urban Area." J. Appl. Met. 3:83-91.

Weast, R. C., and S. M. Selby, eds. 1966. Handbook of Chemistry and Physics. 47th edition. The Chemical Rubber Co., Cleveland, Ohio.

*Available for purchase from the NRC/GPO Sales Program, U.S. Nuclear Regulatory Commission, Washington, D.C. 20555, and the National Technical Information Service, Springfield, VA 22161

**Available for purchase from the National Technical Information Service, Springfield, VA 22161

APPENDIX A

METHODS OF SAMPLING AND INSTRUMENTAL TECHNIQUE FOR THE MEASUREMENT OF URANIUM AND URANIUM DAUGHTERS

METHODS OF SAMPLING AND INSTRUMENTAL TECHNIQUE FOR THE MEASUREMENT OF URANIUM AND URANIUM DAUGHTERS

The 5-cm core samples were taken by using a specially designed coring device. This device is constructed of stainless steel and contains four tracks positioned 1/2 cm, 1 cm, 2 cm, and 5 cm from the top of the device (see Figure A.1). By driving the coring device into the ground and digging away at each end, a stainless steel blade can be forced along each track to reach the desired sampling depth. The deeper cores were obtained by digging a trench and inserting a stainless steel flat scoop with 5-cm high walls. The large area sample was obtained by scraping a 1-m^2 section to a depth of 1 cm.

The measurement of uranium and daughter radionuclides for each sample was obtained by first preparing a perfectly flat homogeneously mixed pellet. Fifteen grams of the sample matrix was homogenized with two grams of cellulose binder and formed under 30 tons of pressure into a 1/4-in. x 2-in. pellet in a pressing chamber. The pellet was then placed in Saran wrap and analyzed with a high-resolution intrinsic germanium diode that measured the concentration of ^{238}U, ^{235}U, and uranium daughters. (Uranium-238 is actually determined from analysis of its ^{234}Th daughter; therefore, one must be certain that the parent-daughter equilibrium exists in making this measurement.)

The following table lists the radionuclides, photon energies, and the abundance of each of these photons.

TABLE A.1. Radionuclides, Photon Energies, and Abundance of Photons

Radionuclide	Photon Energies (keV)	% Abundance
^{226}Ra	186	4.0
^{214}Pb	295	18.9
^{235}U	205	5.0
^{210}Pb	47	4.0
^{230}Th	67	0.4
^{227}Th	236	10.4
^{234}Th (^{238}U)	63	5.7

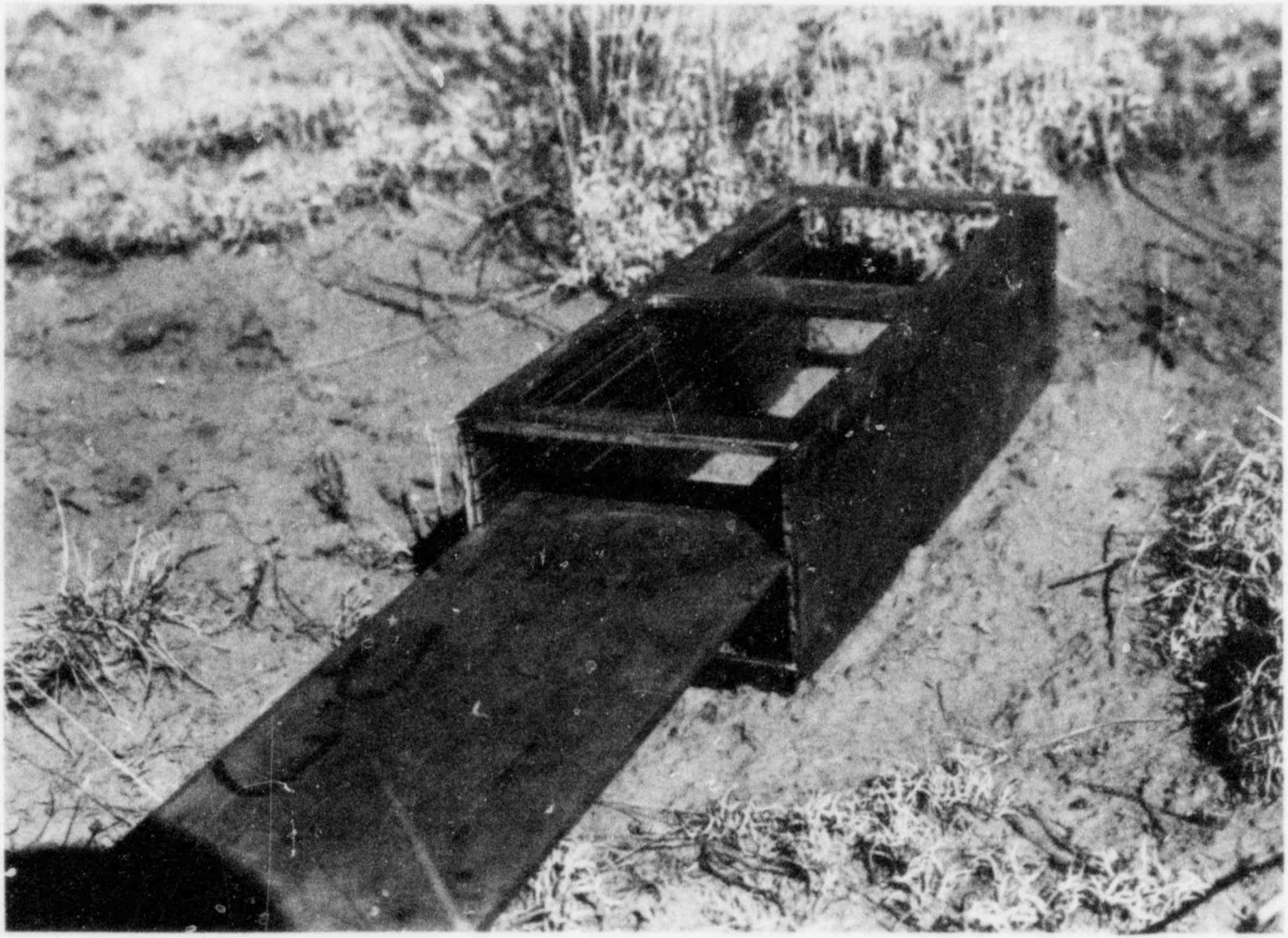

FIGURE A.1. Coring Device for Five-Centimeter Core Samples (Neg. 775832-27)

No. of Copies

OFFSITE

A. A. Churm
DOE Patent Division
9800 So. Cass Avenue
Argonne, IL 60439

343 U.S. Nuclear Regulatory Commission
Division of Technical Information and Document Control
7920 Norfolk Avenue
Bethesda, MD 20014

2 DOE Technical Information Center
Washington, D.C. 20545

Robert C. Bates
Spokane Mining Research Center
E. 315 Montgomery Avenue
Spokane, WA 99207

J. E. Cleveland
Environmental Engineer
Kerr-McGee Nuclear Corporation
P. O. Box 218
Grants, NM 87020

Betty L. Perkins
Los Alamos Scientific Laboratory
P. O. Box 1663
Los Alamos, NM 87545

25 Laura Santos
Office of Nuclear Regulatory Research
Division of Safeguards, Fuel Cycle and Environmental Research
Mail Stop 1130-SS
Washington, D.C. 20555

No. of Copies

ONSITE

50 Pacific Northwest Laboratory

C.E. Elderkin
T.W. Horst (3)
G.B. Long
J. Mishima
R.W. Perkins (8)
L.C. Schwendiman (8)
G.A. Sehmel (15)
C.W. Thomas (5)
N.A. Wogman
Technical Information (5)
Publishing Coordination (2)

NRC FORM 335 (7-77)

U.S. NUCLEAR REGULATORY COMMISSION

BIBLIOGRAPHIC DATA SHEET

1. REPORT NUMBER (Assigned by DDC)
NUREG/CR-1407
PNL-3345

4. TITLE AND SUBTITLE (Add Volume No., if appropriate)
Final Report: A Field and Modeling Study of Windblown Particles from a Uranium Mill Tailings Pile

2. (Leave blank)

3. RECIPIENT'S ACCESSION NO.

7. AUTHOR(S)
L.C, Schwendiman and others

5. DATE REPORT COMPLETED
MONTH: May YEAR: 1980

9. PERFORMING ORGANIZATION NAME AND MAILING ADDRESS (Include Zip Code)
Pacific Northwest Laboratory
P.O. Box 999,
Richland, WA 99353

DATE REPORT ISSUED
MONTH: June YEAR: 1980

6. (Leave blank)

8. (Leave blank)

12. SPONSORING ORGANIZATION NAME AND MAILING ADDRESS (Include Zip Code)
Laura Santos
Office of Nuclear Regulatory Research
U.S. Nuclear REgulatory Commission
Wash. D.C. 20555 Mail Stop 1130SS

10. PROJECT/TASK/WORK UNIT NO.

11. CONTRACT NO.
Fin No. B2095-9

13. TYPE OF REPORT

PERIOD COVERED (Inclusive dates)

15. SUPPLEMENTARY NOTES

14. (Leave blank)

16. ABSTRACT (200 words or less)

An extensive field study whose primary objective was to obtain knowledge and understanding of the nature and quantity of windblown particles from uranium mill tailings piles was conducted in the Ambrosia Lake District of New Mexico.

The following major field tasks were undertaken: determination of physical, chemical, & radioactivity characteristics of mill tailings particles; an investigation of the nature & quantity of tailings particles in soil in the vicinity of tailings piles; and the determination of the nature and flux of particles being transported by wind as a function of wind speed and height. Results of the field study are presented. Particle size distributions & associated radioactivity were measured. Radioactivity relationships showed uranium daughters in mill tailings to be in essential radioactive equilibrium for the carbonate leach process but thorium-230 tends to be leached into the slurry water for the acid process mill tailings. One objective of the study was to relate windblown particle concentrations, fluxes, and particle sizes to wind speed. Hundreds of samples were taken & analyses were performed, but relationships between wind speed, airborne particle sizes and concentrations were found to be vague & inconclusive. A resuspension, deposition, and transport model was developed and applied using site meteorology. Ground deposition patterns predicted were similar to those found.

17. KEY WORDS AND DOCUMENT ANALYSIS

17a. DESCRIPTORS

Particle Resuspension

Tailings Particle Characterization

Transport Model

17b. IDENTIFIERS/OPEN-ENDED TERMS

18. AVAILABILITY STATEMENT
Unlimited

19. SECURITY CLASS (This report)
Unclassified

21. NO. OF PAGES

20. SECURITY CLASS (This page)
Unclassified

22. PRICE
$

NRC FORM 335 (7-77)